



PRIMATE GENOMES

Phylogenomic analyses provide insights into primate evolution

Yong Shao^{1†}, Long Zhou^{2†}, Fang Li^{3,4}, Lan Zhao⁵, Bao-Lin Zhang¹, Feng Shao⁶, Jia-Wei Chen⁷, Chun-Yan Chen⁸, Xupeng Bi², Xiao-Lin Zhuang^{1,9}, Hong-Liang Zhu⁷, Jiang Hu¹⁰, Zongyi Sun¹⁰, Xin Li¹⁰, Depeng Wang¹⁰, Iker Rivas-González¹¹, Sheng Wang¹, Yun-Mei Wang¹, Wu Chen¹², Gang Li¹³, Hui-Meng Lu¹⁴, Yang Liu¹³, Lukas F. K. Kuderna^{15,16}, Kyle Kai-How Farh¹⁶, Peng-Fei Fan¹⁷, Li Yu¹⁸, Ming Li¹⁹, Zhi-Jin Liu²⁰, George P. Tiley²¹, Anne D. Yoder²¹, Christian Roos²², Takashi Hayakawa^{23,24}, Tomas Marques-Bonet^{15,25,33,34}, Jeffrey Rogers²⁶, Peter D. Stenson²⁷, David N. Cooper²⁷, Mikkel Heide Schierup¹¹, Yong-Gang Yao^{9,28,29,30}, Ya-Ping Zhang^{1,29,30}, Wen Wang^{1,8,29}, Xiao-Guang Qi^{5*}, Guojie Zhang^{1,2,3,31*}, Dong-Dong Wu^{1,29,30,32*}

Comparative analysis of primate genomes within a phylogenetic context is essential for understanding the evolution of human genetic architecture and primate diversity. We present such a study of 50 primate species spanning 38 genera and 14 families, including 27 genomes first reported here, with many from previously less well represented groups, the New World monkeys and the Strepsirrhini. Our analyses reveal heterogeneous rates of genomic rearrangement and gene evolution across primate lineages. Thousands of genes under positive selection in different lineages play roles in the nervous, skeletal, and digestive systems and may have contributed to primate innovations and adaptations. Our study reveals that many key genomic innovations occurred in the Simiiformes ancestral node and may have had an impact on the adaptive radiation of the Simiiformes and human evolution.

The order Primate contains >500 species from 79 genera and 16 families (1), with new species continuing to be discovered (2–5), making primates the third most speciose order of living mammals after bats (Chiroptera) and rodents (Rodentia). As our closest living relatives, nonhuman primates play important roles in the cultures and religions of human societies (1). Many nonhuman primate species have been widely used as animal models because of their genetic, physiological, and anatomical similarities to humans, allowing the efficacy and safety of newly developed drugs and vaccines to be tested (6). For example, since the emergence of COVID-19, macaques have served as important models in the research and development of vaccines (7–16). Primates display considerable morphological, behavioral, and physiological diversity and

hold the key to understanding the evolution of our own species, particularly the evolution of human phenotypes such as high-level cognition (17, 18).

Nonhuman primates occupy a wide range of diverse habitats in the tropical forest, savanna, semidesert, and subtropical regions of Asia, Central and South America, and Africa, and humans have spread across much of the earth's surface. Nevertheless, according to the International Union for Conservation of Nature (IUCN) Red Lists, >33% of primate species are critically endangered or vulnerable, ~60% are threatened with extinction, and ~75% are experiencing population decline (1). With global climate change and increasing anthropogenic interference, the conservation status of primates has attracted global scientific and public awareness.

Despite the importance of nonhuman primates, reference genomes have been sequenced in <10% of species (19–27), which both impedes research and hampers conservation efforts. Here, we present high-quality reference genomes for 27 primate species with long-read sequencing generated from our first-phase program of the Primate Genome Project.

Assembly and annotation of 27 new primate reference genomes

We applied long-read genome-sequencing technologies, including Pacbio and Nanopore, to sequence the genomes of 27 nonhuman primate species from 26 genera of 11 families (table S1). Long reads were self-polished and assembled, and the genome assemblies were further corrected and polished by paired-end short reads sequenced from the same individuals (tables S2 to S4). We also used sequencing data generated by high-throughput chromosome conformation capture technology (28) to anchor assembled contigs into chromosomes for four species (fig. S1 and table S4). The sizes of the new genome assemblies of the primate species under study ranged from $\sim 2.4 \times 10^9$ base pairs (Gbp) (*Daubentonia madagascariensis*) to ~ 3.1 Gbp (*Erythrocebus patas*), which were mostly consistent with the k-mer-based estimations (fig. S2 and table S5), with a high average contig N50 length of $\sim 15.9 \times 10^6$ base pairs (Mbp) (table S6). All of the genome assemblies yielded BUSCO complete scores >92% (table S6). A method that integrates de novo and homology-based strategies was applied to annotate all genomes with protein sequences from human, chimpanzee, gorilla, orangutan, and mouse as references for homology-based gene model prediction. Between 20,066 and 21,468 protein-coding genes were predicted in these genome assemblies (table S7). Further, we also identified ~ 24.2 Mbp of primate-specific highly conserved elements by using whole-genome alignments between all primates and nine other mammals (fig. S3).

¹State Key Laboratory of Genetic Resources and Evolution, Kunming Natural History Museum of Zoology, Kunming Institute of Zoology, Chinese Academy of Sciences, Kunming 650201, China.

²Center of Evolutionary & Organismal Biology, and Women's Hospital at Zhejiang University School of Medicine, Hangzhou 310058, China. ³Section for Ecology and Evolution, Department of Biology, University of Copenhagen, DK-2100 Copenhagen, Denmark. ⁴Institute of Animal Sex and Development, Zhejiang Wanli University, Ningbo 315100, China. ⁵Shaanxi Key Laboratory for Animal Conservation, College of Life Sciences, Northwest University, Xi'an 710069, China. ⁶Key Laboratory of Freshwater Fish Reproduction and Development (Ministry of Education), Southwest University School of Life Sciences, Chongqing 400715, China. ⁷BGI-Shenzhen, Shenzhen 518083, China. ⁸School of Ecology and Environment, Northwestern Polytechnical University, Xi'an 710072, China. ⁹Kunming College of Life Science, University of the Chinese Academy of Sciences, Kunming 650204, China. ¹⁰Grindomics Biosciences, Beijing 102206, China. ¹¹Bioinformatics Research Centre, Aarhus University, DK-8000 Aarhus, Denmark. ¹²Guangzhou Zoo & Guangzhou Wildlife Research Center, Guangzhou 510070, China. ¹³College of Life Sciences, Shaanxi Normal University, Xi'an 710119, China. ¹⁴School of Life Sciences, Northwestern Polytechnical University, Xi'an 710072, China. ¹⁵Institute of Evolutionary Biology (UPF-CSIC), PRBB, 08003 Barcelona, Spain. ¹⁶Illumina Artificial Intelligence Laboratory, Illumina Inc, San Diego, CA 92122, USA. ¹⁷School of Life Sciences, Sun Yat-sen University, Guangzhou, Guangdong 510275, China. ¹⁸CAS Key Laboratory for Conservation and Utilization of Bio-Resources in Yunnan, School of Life Sciences, Yunnan University, Kunming 650091, China. ¹⁹CAS Key Laboratory of Animal Ecology and Conservation Biology, Institute of Zoology, Chinese Academy of Sciences, Beijing 100101, China. ²⁰College of Life Sciences, Capital Normal University, Beijing 100048, China. ²¹Department of Biology, Duke University, Durham, NC 27708, USA. ²²Gene Bank of Primates and Primate Genetics Laboratory, German Primate Center Leibniz Institute for Primate Research, 37077 Göttingen, Germany. ²³Faculty of Environmental Earth Science, Hokkaido University, Sapporo, Hokkaido 060-0810, Japan. ²⁴Japan Monkey Centre, Inuyama, Aichi 484-0081, Japan. ²⁵Catalan Institution of Research and Advanced Studies (ICREA), Passeig de Lluís Companys, 23, 08010 Barcelona, Spain. ²⁶Human Genome Sequencing Center, Department of Molecular and Human Genetics, Baylor College of Medicine, Houston, TX 77030, USA. ²⁷Institute of Medical Genetics, School of Medicine, Cardiff University, Cardiff CF14 4XN, UK. ²⁸Key Laboratory of Animal Models and Human Disease Mechanisms of Chinese Academy of Sciences & Yunnan Province, Kunming Institute of Zoology, Chinese Academy of Sciences, Kunming 650201, China. ²⁹Center for Excellence in Animal Evolution and Genetics, Chinese Academy of Sciences, Kunming 650201, China. ³⁰National Resource Center for Non-Human Primates, Kunming Primate Research Center, and National Research Facility for Phenotypic & Genetic Analysis of Model Animals (Primate Facility), Kunming Institute of Zoology, Chinese Academy of Sciences, Kunming 650107, China. ³¹Liangzhu Laboratory, Zhejiang University Medical Center, Hangzhou 311121, China. ³²KIZ-CUHK Joint Laboratory of Bioresources and Molecular Research in Common Diseases, Kunming Institute of Zoology, Chinese Academy of Sciences, Kunming 650204, China. ³³CNAG-CRG, Centre for Genomic Regulation (CRG), Barcelona Institute of Science and Technology (BIST), 08028 Barcelona, Spain. ³⁴Institut Català de Paleontologia Miquel Crusafont, Universitat Autònoma de Barcelona, Edifici ICTA-ICP, c/ Columnes s/n, 08193 Cerdanyola del Vallès, Barcelona, Spain.

*Corresponding author. Email: wudongdong@mail.kiz.ac.cn (D.-D.W.); guojiezhang@zjhu.edu.cn (G.Z.); qixg@nwu.edu.cn (X.-G.Q.) †These authors contributed equally to this work.

The Primate Genome Project also generated high-quality reference genomes for another 16 primate species that were used in the accompanying papers to reveal hybrid speciation during the rapid radiation of the macaques (29), the homoploid hybrid speciation in the snub-nosed monkey *Rhinopithecus* genus (30), social evolution in the Asian colobines driven by cold adaptation (31), and the evolutionary adaptations of slow lorises (32). All genomic

data have been published openly and can be freely accessed in the National Center for Biotechnology Information (NCBI) Assembly Database under the accession information described in this study.

A genomic phylogeny of living primates

We next performed phylogenomic analyses comprising the 27 newly generated genomes, another 22 published primate genomes, one

long-read genome from *Nycticebus pygmaeus* reported in an accompanying paper (32), and two close relatives of primates, the Sunda flying lemur (*Galeopterus variegatus*) and the Chinese tree shrew (*Tupaia belangeri chinensis*) (33), as outgroups (table S8). We constructed whole-genome-wide phylogenetic trees using ExaML under a GTR+GAMMA model (34). Altogether, ~433.5 Mbp of gap-free data for synteny orthologous sequences were retrieved

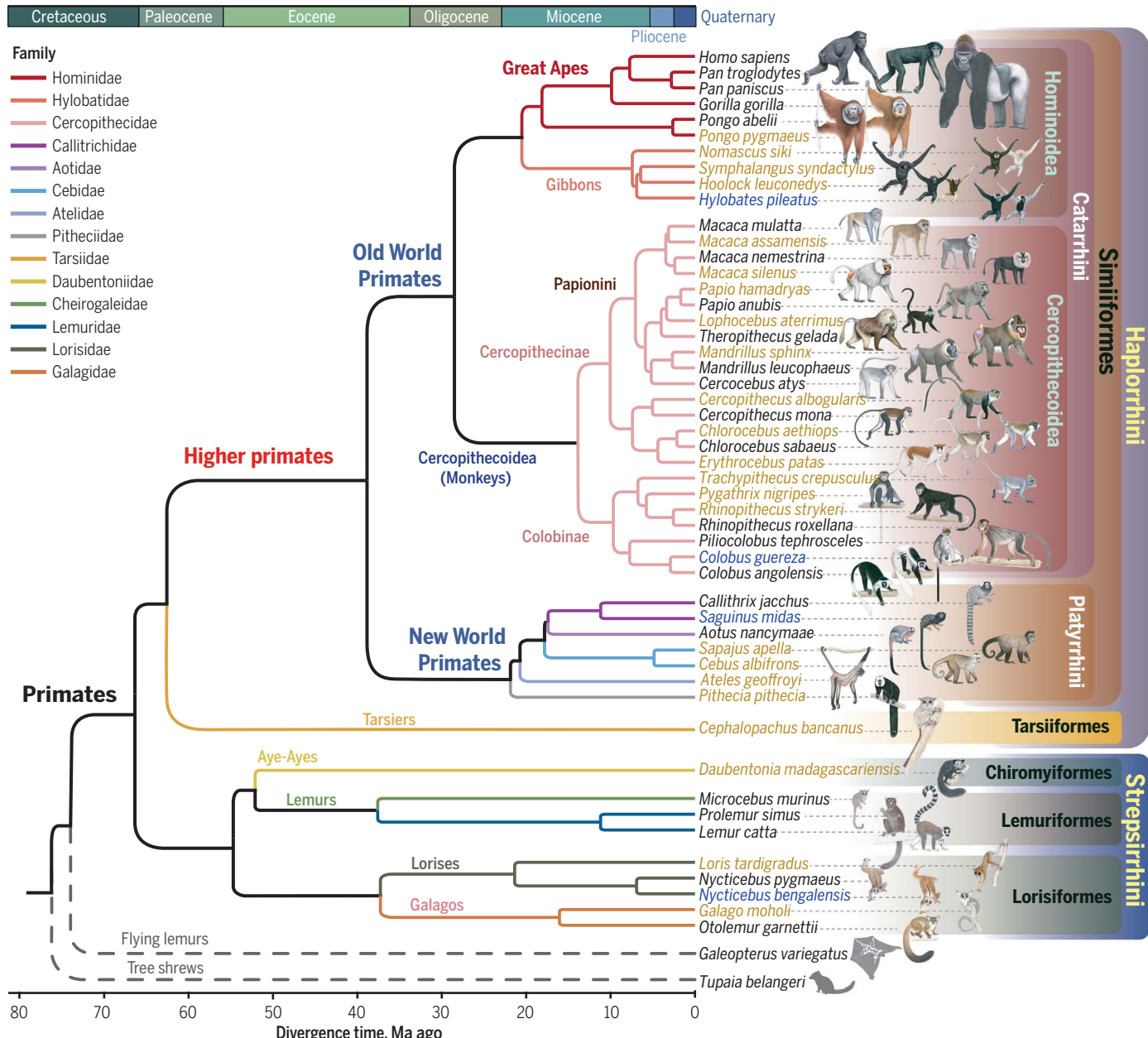


Fig. 1. Genomic phylogeny of primates. The maximum likelihood method was used to infer the primate species tree from whole-genome sequences across 52 species, including 50 primate species and two outgroup species (the Sunda flying lemur and the Chinese tree shrew) with 100 bootstraps under a GTR+GAMMA model. The divergence time was estimated using fossil calibrations (fig. S11) and the MCMCTree algorithm. The yellow and blue species names represent

those genomes newly produced in this study. The genomes of the species marked in blue were assembled at the chromosome level. The genomes of the species marked in black were downloaded from the NCBI and Ensembl databases (table S8). Monkey pictures are copyrighted by Stephen D. Nash/IUCN/SSC Primate Specialist Group and are used in this study with their permission.

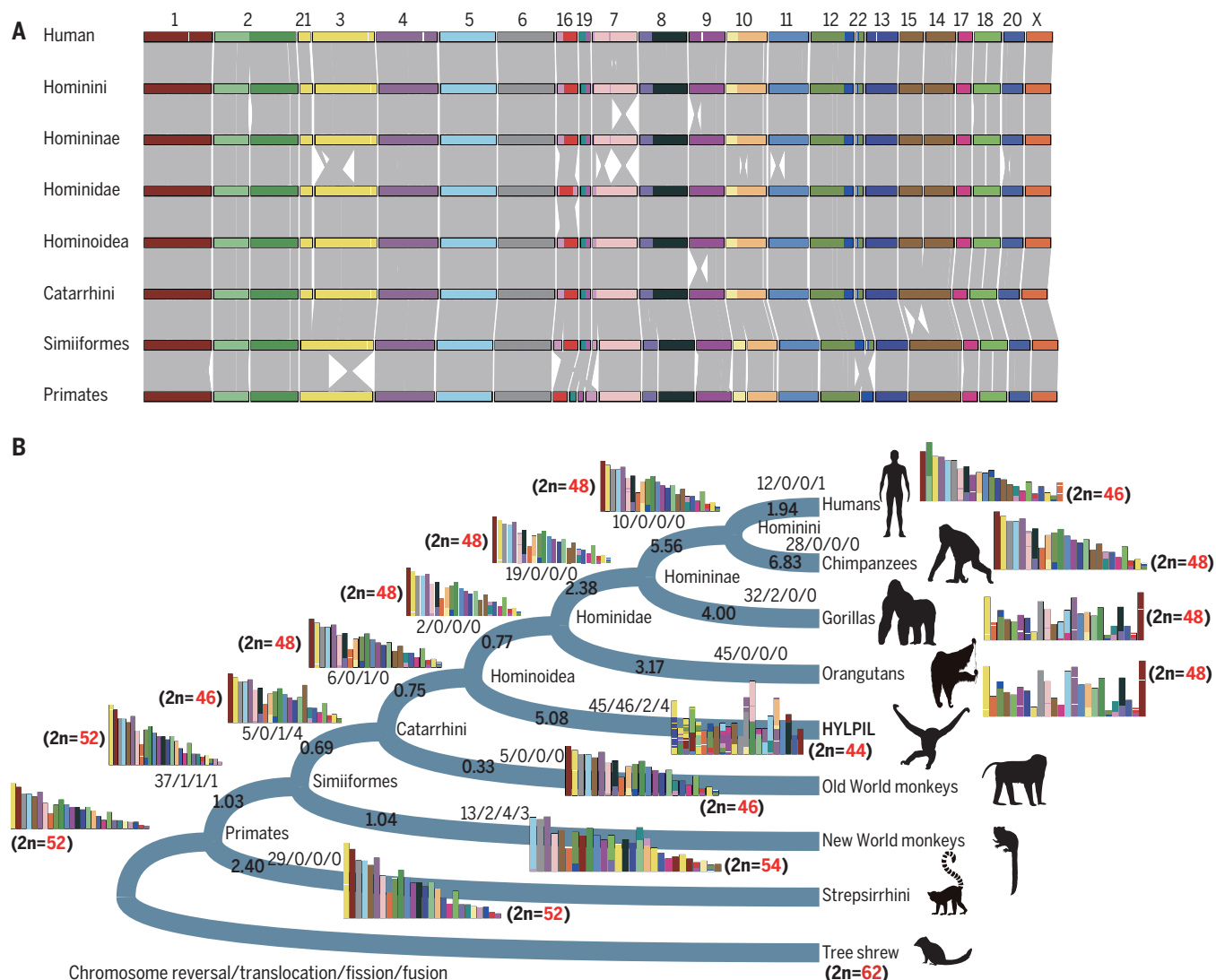


Fig. 2. Reconstruction of primate ancestral chromosomes. (A) Chromosome evolution patterns from the primate common ancestral lineage leading to the human lineage. Chromosomes are colored on the basis of human homologies. (B) Karyotype evolution and genome rearrangement. The rates of genomic rearrangement are highlighted in black bold font. Chromosome variations from ancestral nodes to derived branches are shown by pathways including chromosome reversal, translocation, and fission and fusion events, which are shown by number, e.g., reversal, translocation, fission, and fusion. "HYLPIL" represents the gibbon *Hylobates pileatus*, the genome of which was assembled at the chromosome level.

from the whole-genome alignments (table S9) and used to infer the primate phylogeny, yielding a high-resolution whole-genome nucleotide evidence tree with identical topology to a previous tree derived from 54 nuclear gene regions from 186 living primates (35). This tree has 100% bootstrap support for all evolutionary nodes, with the exception of the node (*(Symphalangus syndactylus, Hoolock leuconedys, Hylobates pileatus)*) among gibbon genera with 90% bootstrap support (Fig. 1 and figs. S4 and S5). The evolution of gibbons has been characterized by their rapid karyotypic changes and remains controversial in primate phylogeny at the genus level (24, 35, 36). To confirm the phylogeny of this node, we also

generated partitioned trees with orthologous protein-coding genes, exon codons with first and second positions, fourfold degenerate sites, and conserved nonexonic elements (figs. S6 to S9). The tree from conserved nonexonic elements yielded the identical topologies for the gibbon lineages with the whole-genome nucleotide evidence trees (fig. S9). However, the trees from orthologous protein-coding genes and exon codons with first and second positions and fourfold degenerate sites, respectively, supported the alternative topologies, ((*Nomascus*, *Hylobates*), (*Sympthalangus*, *Hoolock*)) and ((*Nomascus*, (*Sympthalangus*, *Hoolock*)), *Hylobates*) (figs. S6 to S8). The two topologies were shown in previous studies based on var-

iants called by mapping short reads to the reference genome of *Nomascus leucogenys* (24, 36).

Our analyses again confirmed the phylogenetic challenge within the gibbon lineage, which has experienced pronounced adaptive radiation within an extremely short evolutionary time period (24, 35). Consistently, we observed extremely short internal branches in this lineage on the phylogeny. A comparative analysis using CoalHMM (37) across primate lineages showed that the gibbon lineage represents one of the lineages with the highest frequency of incomplete lineage sorting (38), supporting a previous study based on population data (24). Specifically, the two gibbon branches showed incomplete lineage-sorting

proportions of 57 and 61%, respectively, but the species topology inferred from incomplete lineage-sorting analyses was identical to those presented herein (figs. S4 and S10).

Using the whole-genome nucleotide evidence tree and fossil calibration data (35, 39) (Fig. 1 and fig. S11), the divergence dating of living primates was estimated by means of the MCMCTree algorithm (40) (Fig. 1 and fig. S12). We estimated that the most recent common ancestor of all primates evolved between 64.95 and 68.29 million years (Ma) ago, which is close to the estimate given in the latest phylogenetic study across mammals (41), suggesting that the origin of the primate group was near the Cretaceous–Tertiary boundary at 66 Ma ago. We also estimated that the most recent common ancestor of Strepsirrhini appeared between 52.57 and 56.56 Ma ago, and that of the Simiiformes emerged between 35.65 and 42.55 Ma ago (Fig. 1 and fig. S12).

Genomic structure and evolution of primates

Karyotype evolution and genome rearrangement

The speciation process is often accompanied by karyotypic evolution, which also affects genome evolution and gene function (42–44). We reconstructed the ancestral karyotype evolutionary process across primate lineages (table S10) and observed an overall conserved pattern of chromosome-level synteny (Fig. 2A). The numbers of ancestral karyotypes of Catarrhini ($2n = 46$) and Hominoidea ($2n = 48$) were consistent with previous inferences derived from the fluorescence in situ hybridization data of bacterial artificial chromosomes (45) (Fig. 2A). However, we deduced that both of the ancestral karyotypes of primates and Simiiformes had a diploid number of $2n = 52$ (Fig. 2A) rather than $2n = 50$ as previously suggested (45), recovering a fission event in chromosome 8 that was observed in the common ancestor of primates (Fig. 2A and fig. S13). Fusion and fission are the most common mechanisms of karyotype evolution in primates, as exemplified by the fusion of chromosome 2, which occurred specifically in the human lineage (45). Our analyses further identified at least one fission and one fusion during the emergence of the Simiiformes, as well as one fission and four fusions associated with the Catarrhini node (Fig. 2B and fig. S13), resulting in the contemporary karyotype structure of our own. The rapid change of karyotypes in the Simiiformes also led to an increased chromosome number in New World monkeys, which have the largest number of chromosomes across primates. We further estimated the rate of genome rearrangement by taking into account all large-scale genomic rearrangement events, including reversions, translocations, fusions, and fissions, in key evolutionary nodes from the primate common ancestral lineage leading to the human lineage. We observed an increasing rate of

rearrangement in the Homininae (*Gorilla–Homo–Pan*) (~2.38/Ma) and particularly in the Hominini (*Homo–Pan*) (~5.56/Ma) (Fig. 2B), which contradicts the Hominini slowdown hypothesis on the nucleotide substitution rates (35).

Lineage-specific segmental duplication

We next compiled segmental duplication maps (segmental duplication length ≥ 5 kbp) for primates and five outgroup species (fig. S14 and table S11). Compared with other primate lineages, we observed a marked increase in the number of lineage-specific segmental duplications ($n = 221$) in the great ape genomes (Fig. 3A and table S12), consistent with previous findings describing a burst of segmental duplications in the great ape ancestor (46). These specific segmental duplications in great apes overlapped with 57 protein-coding genes (table S13), 20 of which were highly expressed in the human brain (fig. S15). We also observed lineage-specific segmental duplications in other primate groups producing lineage-specific new genes that might have contributed to the evolution of these lineages (table S13). We further explored the functions of all genes overlapping segmental duplications in primate genomes (table S13) against the Human Gene Mutation Database (47), and found that a high proportion of these genes (52.8%) have been reported to be associated with inherited conditions including autism, intellectual disabilities, and other developmental disorders (Fig. 3B and table S14).

Evolution of genome size and transposable elements

Compared with other mammalian groups, the primates on average have a relatively large genome size (48, 49). Among primates, the lemurs (Lemuriformes and Chiromyiformes) were found to be characterized by a significantly smaller genome size (~2.36 Gbp) than other groups such as the lorisoids (Lorisiformes: Lorisidae and Galagidae, ~2.70 Gbp), New World monkeys (~2.82 Gbp), Old World monkeys (~2.91 Gbp), and Hominoidea (~2.96 Gbp) ($P < 0.05$, Mann-Whitney U test) (fig. S16). The increase of genome size in the Simiiformes can be attributed to the expansion of transposable elements (figs. S16 to S18 and table S15), especially *Alu* elements, ~300 nucleotide short interspersed sequence elements (SINEs) that make up ~11% of the human genome (50–54). We observed that the genomes of lemurs exhibited a relative paucity of SINEs, especially *Alu* (~3.87%), which is less than one-third of the proportion noted in other lineages (figs. S16 to S18). By contrast, the *Alu* elements in both Simiiformes and Lorisiformes experienced major bursts of retrotranspositional activity at ~40 to 45 and ~34 to 39 Ma ago independently (fig. S19). Specifically, we noticed a

substantial expansion of the *AluS*-related subclasses, especially *AluSx* in the Simiiformes, whereas the *AluJ*-related subclasses (especially *AluJb*) were the dominant subclasses of *Alu* in the Lorisiformes (fig. S20).

Variation in the nucleotide substitution rate

We estimated the overall nucleotide substitution rate in primates to be $\sim 1.1 \times 10^{-3}$ substitutions per site per million years (Fig. 3C, fig. S21, and table S16), which is much lower than the average rate for mammals ($\sim 2.7 \times 10^{-3}$) and birds ($\sim 1.9 \times 10^{-3}$) (55). However, the nucleotide substitution rate exhibited a high degree of heterogeneity between primate lineages, potentially caused by differences with respect to life history traits (56–58). The New World monkeys evolved the fastest at $\sim 1.4 \times 10^{-3}$ substitutions per site per million years (Fig. 3C and fig. S21). We confirmed the hominoid “slowdown” (35, 59–61) hypothesis by detecting a reduced substitution rate in hominoids ($\sim 0.8 \times 10^{-3}$ substitutions per site per million years) (fig. S21). Our analysis and a previous study (62) suggested that tarsiers, as the most basal haplorrhines, potentially evolved with a rapid substitution rate compared with other primates (fig. S21).

Evolution of protein-coding genes

We obtained a high-confidence orthologous gene set comprising 10,185 orthologs across 50 primate species, along with the Sunda flying lemur and the Chinese tree shrew. On the basis of the whole-genome nucleotide evidence tree topology of primates, we calculated the ratio of the rates of nonsynonymous (d_N) to synonymous (d_S) substitutions for each ortholog to explore the evolutionary constraints operating on coding regions. We estimated the evolutionary rate of tissue-specific expressed genes for different tissues across evolutionary clades in primates based on the observation that tissue-specific expressed genes are generally conserved across diverse species (63, 64), and observed that testis- and spleen-specific expressed genes generally displayed higher values of d_N/d_S (Fig. 3D and figs. S22 and S23) than other tissue-specific expressed genes, corroborating the rapid evolution of the reproductive and immune systems in primates (65, 66). By contrast, brain-specific expressed genes generally showed a high degree of conservation with lower d_N/d_S values, as previously reported, despite the rapid evolution of primate cognitive functions (67).

Next, we detected 82 positively selected genes in the common ancestral lineage of primates by comparison with other mammalian species (table S17) using the codeml algorithm under the branch-site model with a likelihood rate test in PAML4 (40, 68). We found that these positively selected genes were significantly enriched in genes exhibiting high-level

expression in brain, bone marrow, and testis (table S18). In particular, close to 37% (30 genes) of positively selected genes exhibited biased expression in the brain (tables S18 and S19), and we found that some of them (e.g., *SPTAN1*, *MYT1L*, and *SHMT1*) could have important roles in brain function, because deleterious mutations of these genes have been reported to cause brain disorders (69–71) such as epilepsy and schizophrenia. These genes may be important candidates for involvement in the evolution of the primate brain because of their functional importance. Our results suggest that some positively selected genes in the primate

ancestral lineage may have been involved in the rapid evolution of their brain functions despite the general conservation of brain-specific expressed genes. In addition, several immune-related genes (e.g., *XRCC6* and *CD2*) (table S17) also experienced positive selection in the primate ancestor, suggesting that the adaptive immune system might also have contributed to primate evolution.

An increased level of genomic change in the ancestor of the Simiiformes

To provide new insights into the genetic underpinnings of primate phenotypic evolu-

tion, we performed various comparative genomic analyses, including the identification of positively selected genes, genes having conserved noncoding regions that have been subject to lineage-specific accelerated evolution (72), and expanded gene families in different primate lineages (68). An increased level of genomic evolutionary changes, as reflected by the high numbers of positively selected genes, lineage-specific accelerated regions, and expanded gene families, was observed in the Simiiformes ancestor (Fig. 4A). Consistently, the Simiiformes have also experienced rapid evolution of a series of complex traits, unlike

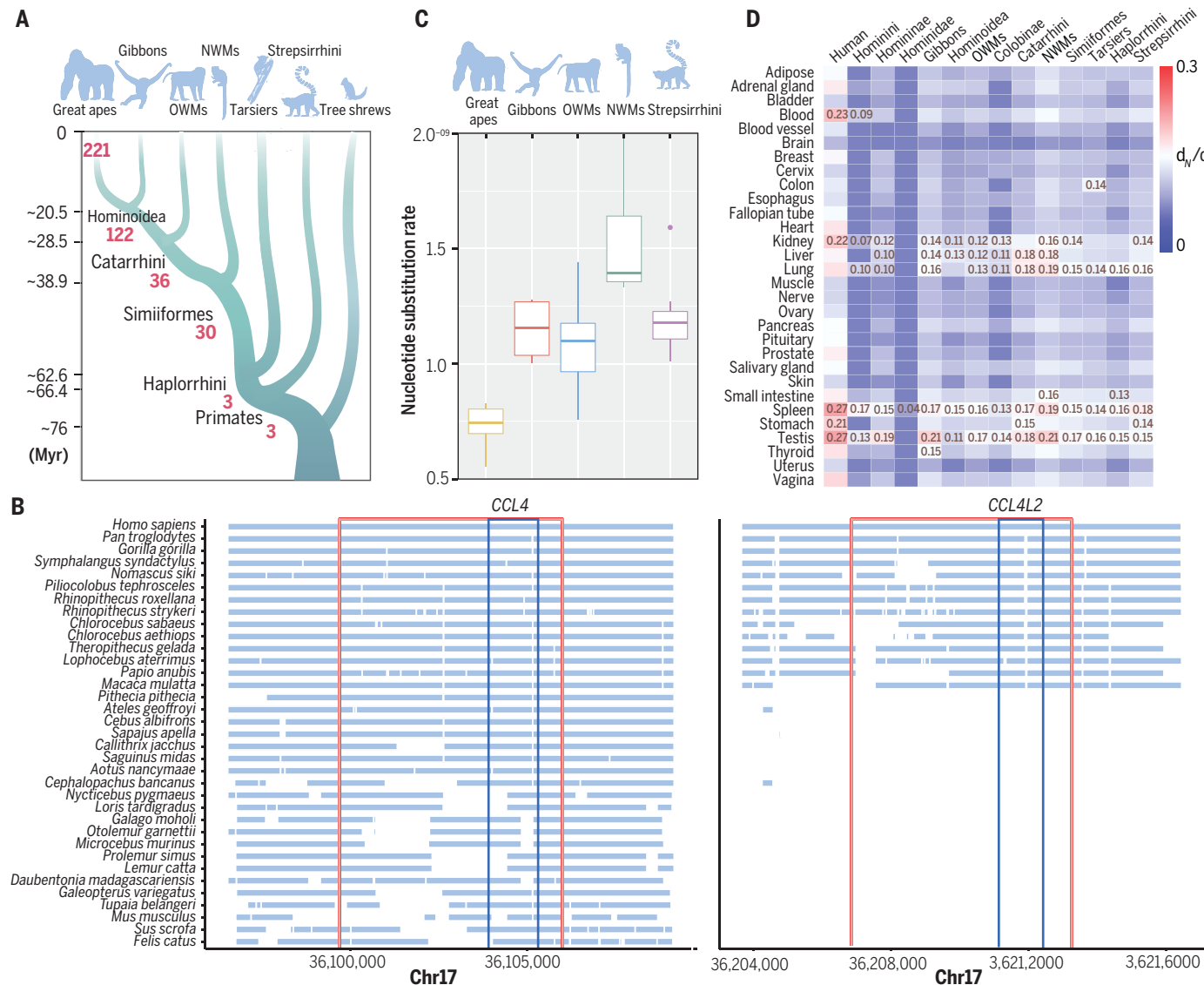


Fig. 3. Structural evolution in primate genomes. (A) Evolutionary pattern of lineage-specific segmental duplications in primates. The numbers of lineage-specific segmental duplications are shown in red. The largest number of segmental duplications was found in the great ape lineage. OWMs, Old World monkeys; NWMS, New World monkeys. (B) Example of specific segmental duplications during evolution of the genome in Catarrhini. A gene pair overlapping the segmental duplication (left, *CCL4*; right, *CCL4L2*) is associated

with HIV susceptibility. The red and green boxes represent the segmental duplication region and the overlapping gene pair, respectively. (C) Substitution rates across five evolutionary branches in primates. (D) Evolutionary constraints of tissues across diverse lineages in primates. The evolutionary constraints of tissues are shown by the d_N/d_S median of tissue-specific expressed genes in different evolutionary nodes among primates.

the Strepsirrhini and Tarsiiformes. For example, the Simiiformes generally exhibit a larger brain volume and body mass than the Strepsirrhini and Tarsiiformes (Fig. 4B) (73, 74). Functional enrichment analyses showed that the associated genes relevant to these rapid genomic changes in the Simiiformes ancestor (tables S20 to S22) were overrepresented in functions related to the nervous system and development, such as postsynaptic density, synapses, and the negative regulation of the canonical Wnt signaling pathway (table S23).

Additional analyses indicated that various candidate genes in the Simiiformes ancestral lineage, comprising 168 positively selected genes, 273 genes associated with lineage-specific ac-

celerated regions, and 14 expanded gene families, were enriched in central nervous system terms, i.e., brain, cerebrum, cerebellum, hippocampus, and cerebral cortex (table S24). More specifically, five genes participated in pathway axon guidance (Fig. 4C), being expressed in the human brain at a high level (table S25). Axon guidance represents a key stage in the formation of a neural network (75, 76) and may have been an important influence on brain volume. In this pathway, two semaphorin genes, *SEMA3B* and *SEMA3D*, which are critical for central nervous system patterning (77, 78), experienced positive selection and served as a gene associated with the lineage-specific accelerated region, respectively. These

two genes, together with another three genes associated with the lineage-specific accelerated regions, *EPHA3*, *RAC1*, and *NTNG2*, are known to be important for brain development (79–81). Furthermore, eight genes were assigned under the term “Hippo signaling pathway” (Fig. 4D), an evolutionarily conserved signaling pathway that controls organ or body size by regulating cell growth, proliferation, and apoptosis in a range of animals from flies to humans (82–84). Genes involved in neuronal network formation and the control of organ size appear to have undergone adaptive evolution in the Simiiformes ancestral lineage and may have been responsible for specific phenotypic changes, particularly the progressive

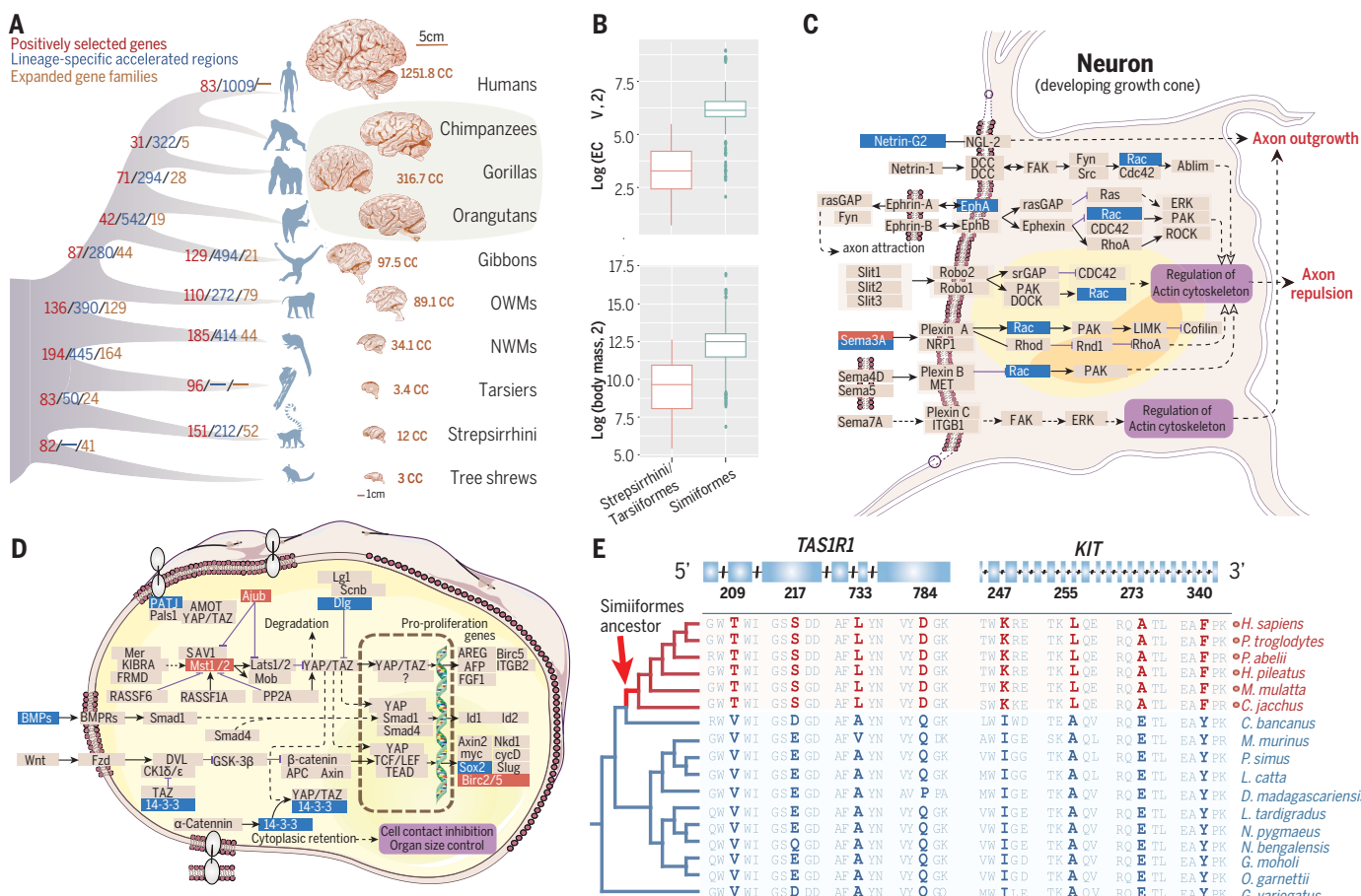


Fig. 4. Genomic changes and phenotype evolution in the ancestor of the Simiiformes. (A) Increased level of genomic evolutionary change, including positively selected genes, lineage-specific accelerated regions, and significantly expanded gene families, seen in the Simiiformes ancestral lineage. The brain sizes and brain structures are shown in representative evolutionary groups of primates. The brain sizes across primate and outgroup species are derived from previous studies (156, 157). Brain images are from the Michigan State University Comparative Mammalian Brain Collections (www.brainmuseum.org). (B) Representative phenotype variations, including brain size and body mass, between the Strepsirrhini and Tarsiiformes and the Simiiformes. Statistical significance was assessed by the Mann-Whitney *U* test as $P < 0.05$. (C) Candidate genes involved in the axon guidance KEGG pathway (hsa04360). Genes relating to genomic changes in the Simiiformes ancestral lineage are shown in this pathway. The

protein product of the positively selected gene in the Simiiformes ancestral lineage, *SEMA3B*, is shown in red. The protein products of genes associated with lineage-specific accelerated regions, *EPHA3*, *RAC1*, *NTNG2*, and *SEMA3D*, are shown in blue. (D) The Hippo signaling pathway (hsa04390), which is involved in organ size and body size, with candidates including positively selected genes and genes associated with lineage-specific accelerated regions (*PATJ*, *SOX2*, *BMP2*, *DLG2*, and *YWHAQ*) in the Simiiformes ancestral lineage are shown in red, and the products of genes associated with lineage-specific accelerated regions (*SEMA3B*, *SEMA3D*, *SEMA3A*, *SEMA4D*, *SEMA5*, *SEMA7A*, *ITGB1*, *YAP1*, *YAP2*, *TAZ1*, *TAZ2*, *PP2A*, *SMAD1*, *SMAD4*, *SMAD6*, *SMAD7*, *SMAD9*, *SMAD10*, *SMAD11*, *SMAD12*, *SMAD13*, *SMAD14*, *SMAD15*, *SMAD16*, *SMAD17*, *SMAD18*, *SMAD19*, *SMAD20*, *SMAD21*, *SMAD22*, *SMAD23*, *SMAD24*, *SMAD25*, *SMAD26*, *SMAD27*, *SMAD28*, *SMAD29*, *SMAD30*, *SMAD31*, *SMAD32*, *SMAD33*, *SMAD34*, *SMAD35*, *SMAD36*, *SMAD37*, *SMAD38*, *SMAD39*, *SMAD40*, *SMAD41*, *SMAD42*, *SMAD43*, *SMAD44*, *SMAD45*, *SMAD46*, *SMAD47*, *SMAD48*, *SMAD49*, *SMAD50*, *SMAD51*, *SMAD52*, *SMAD53*, *SMAD54*, *SMAD55*, *SMAD56*, *SMAD57*, *SMAD58*, *SMAD59*, *SMAD60*, *SMAD61*, *SMAD62*, *SMAD63*, *SMAD64*, *SMAD65*, *SMAD66*, *SMAD67*, *SMAD68*, *SMAD69*, *SMAD70*, *SMAD71*, *SMAD72*, *SMAD73*, *SMAD74*, *SMAD75*, *SMAD76*, *SMAD77*, *SMAD78*, *SMAD79*, *SMAD80*, *SMAD81*, *SMAD82*, *SMAD83*, *SMAD84*, *SMAD85*, *SMAD86*, *SMAD87*, *SMAD88*, *SMAD89*, *SMAD90*, *SMAD91*, *SMAD92*, *SMAD93*, *SMAD94*, *SMAD95*, *SMAD96*, *SMAD97*, *SMAD98*, *SMAD99*, *SMAD100*, *SMAD101*, *SMAD102*, *SMAD103*, *SMAD104*, *SMAD105*, *SMAD106*, *SMAD107*, *SMAD108*, *SMAD109*, *SMAD110*, *SMAD111*, *SMAD112*, *SMAD113*, *SMAD114*, *SMAD115*, *SMAD116*, *SMAD117*, *SMAD118*, *SMAD119*, *SMAD120*, *SMAD121*, *SMAD122*, *SMAD123*, *SMAD124*, *SMAD125*, *SMAD126*, *SMAD127*, *SMAD128*, *SMAD129*, *SMAD130*, *SMAD131*, *SMAD132*, *SMAD133*, *SMAD134*, *SMAD135*, *SMAD136*, *SMAD137*, *SMAD138*, *SMAD139*, *SMAD140*, *SMAD141*, *SMAD142*, *SMAD143*, *SMAD144*, *SMAD145*, *SMAD146*, *SMAD147*, *SMAD148*, *SMAD149*, *SMAD150*, *SMAD151*, *SMAD152*, *SMAD153*, *SMAD154*, *SMAD155*, *SMAD156*, *SMAD157*, *SMAD158*, *SMAD159*, *SMAD160*, *SMAD161*, *SMAD162*, *SMAD163*, *SMAD164*, *SMAD165*, *SMAD166*, *SMAD167*, *SMAD168*, *SMAD169*, *SMAD170*, *SMAD171*, *SMAD172*, *SMAD173*, *SMAD174*, *SMAD175*, *SMAD176*, *SMAD177*, *SMAD178*, *SMAD179*, *SMAD180*, *SMAD181*, *SMAD182*, *SMAD183*, *SMAD184*, *SMAD185*, *SMAD186*, *SMAD187*, *SMAD188*, *SMAD189*, *SMAD190*, *SMAD191*, *SMAD192*, *SMAD193*, *SMAD194*, *SMAD195*, *SMAD196*, *SMAD197*, *SMAD198*, *SMAD199*, *SMAD200*, *SMAD201*, *SMAD202*, *SMAD203*, *SMAD204*, *SMAD205*, *SMAD206*, *SMAD207*, *SMAD208*, *SMAD209*, *SMAD210*, *SMAD211*, *SMAD212*, *SMAD213*, *SMAD214*, *SMAD215*, *SMAD216*, *SMAD217*, *SMAD218*, *SMAD219*, *SMAD220*, *SMAD221*, *SMAD222*, *SMAD223*, *SMAD224*, *SMAD225*, *SMAD226*, *SMAD227*, *SMAD228*, *SMAD229*, *SMAD230*, *SMAD231*, *SMAD232*, *SMAD233*, *SMAD234*, *SMAD235*, *SMAD236*, *SMAD237*, *SMAD238*, *SMAD239*, *SMAD240*, *SMAD241*, *SMAD242*, *SMAD243*, *SMAD244*, *SMAD245*, *SMAD246*, *SMAD247*, *SMAD248*, *SMAD249*, *SMAD250*, *SMAD251*, *SMAD252*, *SMAD253*, *SMAD254*, *SMAD255*, *SMAD256*, *SMAD257*, *SMAD258*, *SMAD259*, *SMAD260*, *SMAD261*, *SMAD262*, *SMAD263*, *SMAD264*, *SMAD265*, *SMAD266*, *SMAD267*, *SMAD268*, *SMAD269*, *SMAD270*, *SMAD271*, *SMAD272*, *SMAD273*, *SMAD274*, *SMAD275*, *SMAD276*, *SMAD277*, *SMAD278*, *SMAD279*, *SMAD280*, *SMAD281*, *SMAD282*, *SMAD283*, *SMAD284*, *SMAD285*, *SMAD286*, *SMAD287*, *SMAD288*, *SMAD289*, *SMAD290*, *SMAD291*, *SMAD292*, *SMAD293*, *SMAD294*, *SMAD295*, *SMAD296*, *SMAD297*, *SMAD298*, *SMAD299*, *SMAD300*, *SMAD301*, *SMAD302*, *SMAD303*, *SMAD304*, *SMAD305*, *SMAD306*, *SMAD307*, *SMAD308*, *SMAD309*, *SMAD310*, *SMAD311*, *SMAD312*, *SMAD313*, *SMAD314*, *SMAD315*, *SMAD316*, *SMAD317*, *SMAD318*, *SMAD319*, *SMAD320*, *SMAD321*, *SMAD322*, *SMAD323*, *SMAD324*, *SMAD325*, *SMAD326*, *SMAD327*, *SMAD328*, *SMAD329*, *SMAD330*, *SMAD331*, *SMAD332*, *SMAD333*, *SMAD334*, *SMAD335*, *SMAD336*, *SMAD337*, *SMAD338*, *SMAD339*, *SMAD340*, *SMAD341*, *SMAD342*, *SMAD343*, *SMAD344*, *SMAD345*, *SMAD346*, *SMAD347*, *SMAD348*, *SMAD349*, *SMAD350*, *SMAD351*, *SMAD352*, *SMAD353*, *SMAD354*, *SMAD355*, *SMAD356*, *SMAD357*, *SMAD358*, *SMAD359*, *SMAD360*, *SMAD361*, *SMAD362*, *SMAD363*, *SMAD364*, *SMAD365*, *SMAD366*, *SMAD367*, *SMAD368*, *SMAD369*, *SMAD370*, *SMAD371*, *SMAD372*, *SMAD373*, *SMAD374*, *SMAD375*, *SMAD376*, *SMAD377*, *SMAD378*, *SMAD379*, *SMAD380*, *SMAD381*, *SMAD382*, *SMAD383*, *SMAD384*, *SMAD385*, *SMAD386*, *SMAD387*, *SMAD388*, *SMAD389*, *SMAD390*, *SMAD391*, *SMAD392*, *SMAD393*, *SMAD394*, *SMAD395*, *SMAD396*, *SMAD397*, *SMAD398*, *SMAD399*, *SMAD400*, *SMAD401*, *SMAD402*, *SMAD403*, *SMAD404*, *SMAD405*, *SMAD406*, *SMAD407*, *SMAD408*, *SMAD409*, *SMAD410*, *SMAD411*, *SMAD412*, *SMAD413*, *SMAD414*, *SMAD415*, *SMAD416*, *SMAD417*, *SMAD418*, *SMAD419*, *SMAD420*, *SMAD421*, *SMAD422*, *SMAD423*, *SMAD424*, *SMAD425*, *SMAD426*, *SMAD427*, *SMAD428*, *SMAD429*, *SMAD430*, *SMAD431*, *SMAD432*, *SMAD433*, *SMAD434*, *SMAD435*, *SMAD436*, *SMAD437*, *SMAD438*, *SMAD439*, *SMAD440*, *SMAD441*, *SMAD442*, *SMAD443*, *SMAD444*, *SMAD445*, *SMAD446*, *SMAD447*, *SMAD448*, *SMAD449*, *SMAD450*, *SMAD451*, *SMAD452*, *SMAD453*, *SMAD454*, *SMAD455*, *SMAD456*, *SMAD457*, *SMAD458*, *SMAD459*, *SMAD460*, *SMAD461*, *SMAD462*, *SMAD463*, *SMAD464*, *SMAD465*, *SMAD466*, *SMAD467*, *SMAD468*, *SMAD469*, *SMAD470*, *SMAD471*, *SMAD472*, *SMAD473*, *SMAD474*, *SMAD475*, *SMAD476*, *SMAD477*, *SMAD478*, *SMAD479*, *SMAD480*, *SMAD481*, *SMAD482*, *SMAD483*, *SMAD484*, *SMAD485*, *SMAD486*, *SMAD487*, *SMAD488*, *SMAD489*, *SMAD490*, *SMAD491*, *SMAD492*, *SMAD493*, *SMAD494*, *SMAD495*, *SMAD496*, *SMAD497*, *SMAD498*, *SMAD499*, *SMAD500*, *SMAD501*, *SMAD502*, *SMAD503*, *SMAD504*, *SMAD505*, *SMAD506*, *SMAD507*, *SMAD508*, *SMAD509*, *SMAD510*, *SMAD511*, *SMAD512*, *SMAD513*, *SMAD514*, *SMAD515*, *SMAD516*, *SMAD517*, *SMAD518*, *SMAD519*, *SMAD520*, *SMAD521*, *SMAD522*, *SMAD523*, *SMAD524*, *SMAD525*, *SMAD526*, *SMAD527*, *SMAD528*, *SMAD529*, *SMAD530*, *SMAD531*, *SMAD532*, *SMAD533*, *SMAD534*, *SMAD535*, *SMAD536*, *SMAD537*, *SMAD538*, *SMAD539*, *SMAD540*, *SMAD541*, *SMAD542*, *SMAD543*, *SMAD544*, *SMAD545*, *SMAD546*, *SMAD547*, *SMAD548*, *SMAD549*, *SMAD550*, *SMAD551*, *SMAD552*, *SMAD553*, *SMAD554*, *SMAD555*, *SMAD556*, *SMAD557*, *SMAD558*, *SMAD559*, *SMAD560*, *SMAD561*, *SMAD562*, *SMAD563*, *SMAD564*, *SMAD565*, *SMAD566*, *SMAD567*, *SMAD568*, *SMAD569*, *SMAD570*, *SMAD571*, *SMAD572*, *SMAD573*, *SMAD574*, *SMAD575*, *SMAD576*, *SMAD577*, *SMAD578*, *SMAD579*, *SMAD580*, *SMAD581*, *SMAD582*, *SMAD583*, *SMAD584*, *SMAD585*, *SMAD586*, *SMAD587*, *SMAD588*, *SMAD589*, *SMAD590*, *SMAD591*, *SMAD592*, *SMAD593*, *SMAD594*, *SMAD595*, *SMAD596*, *SMAD597*, *SMAD598*, *SMAD599*, *SMAD600*, *SMAD601*, *SMAD602*, *SMAD603*, *SMAD604*, *SMAD605*, *SMAD606*, *SMAD607*, *SMAD608*, *SMAD609*, *SMAD610*, *SMAD611*, *SMAD612*, *SMAD613*, *SMAD614*, *SMAD615*, *SMAD616*, *SMAD617*, *SMAD618*, *SMAD619*, *SMAD620*, *SMAD621*, *SMAD622*, *SMAD623*, *SMAD624*, *SMAD625*, *SMAD626*, *SMAD627*, *SMAD628*, *SMAD629*, *SMAD630*, *SMAD631*, *SMAD632*, *SMAD633*, *SMAD634*, *SMAD635*, *SMAD636*, *SMAD637*, *SMAD638*, *SMAD639*, *SMAD640*, *SMAD641*, *SMAD642*, *SMAD643*, *SMAD644*, *SMAD645*, *SMAD646*, *SMAD647*, *SMAD648*, *SMAD649*, *SMAD650*, *SMAD651*, *SMAD652*, *SMAD653*, *SMAD654*, *SMAD655*, *SMAD656*, *SMAD657*, *SMAD658*, *SMAD659*, *SMAD660*, *SMAD661*, *SMAD662*, *SMAD663*, *SMAD664*, *SMAD665*, *SMAD666*, *SMAD667*, *SMAD668*, *SMAD669*, *SMAD670*, *SMAD671*, *SMAD672*, *SMAD673*, *SMAD674*, *SMAD675*, *SMAD676*, *SMAD677*, *SMAD678*, *SMAD679*, *SMAD680*, *SMAD681*, *SMAD682*, *SMAD683*, *SMAD684*, *SMAD685*, *SMAD686*, *SMAD687*, *SMAD688*, *SMAD689*, *SMAD690*, *SMAD691*, *SMAD692*, *SMAD693*, *SMAD694*, *SMAD695*, *SMAD696*, *SMAD697*, *SMAD698*, *SMAD699*, *SMAD700*, *SMAD701*, *SMAD702*, *SMAD703*, *SMAD704*, *SMAD705*, *SMAD706*, *SMAD707*, *SMAD708</*

increase in brain volumes and body sizes compared with the Tarsiiformes and Strepsirrhini.

A major phenotypic difference between the Strepsirrhini and Tarsiiformes and the Simiiformes is nocturnal versus diurnal life history. The visual system has diverged substantially between the Strepsirrhini and Tarsiiformes and the Simiiformes such that the diurnal Simiiformes have much smaller corneal sizes (relative to their eyes) and higher visual acuity than the Strepsirrhini and Tarsiiformes (85). Consistent with this phenotypic difference, we detected positive selection signals in three genes, *NPHP4*, *GRHL2*, and *SLC39A5*, which are associated with eye development (Gene Ontology identifier: 0001654) in the Simiiformes ancestral lineage. An intragenic deletion in *NPHP4* causes recessive cone-rod dystrophy with a predominant loss of cone function in the dachshund (86). *GRHL2* encodes a transcription factor that suppresses epithelial-to-mesenchymal transition; ectopic *GRHL2* expression caused by mutation accelerates cell state transition and leads to posterior polymorphous corneal dystrophy and vision function disruption (87). The *GRHL2* gene has the highest number of positively selected sites in the Simiiformes ancestor compared with the other genes involved in eye development (fig. S24). *TAS1R1* encodes a taste receptor that can form a heterodimer with *TAS1R3* to elicit the umami taste (88). We found that *TAS1R1* also experienced positive selection with four positively selected sites in the Simiiformes ancestor (Fig. 4E). The rapid and concerted evolution of taste receptors and vision could have helped the diurnal Simiiformes to locate and identify food. The detailed functional consequences of these amino acid changes might be worthy of further study.

Compared with the Strepsirrhini and Tarsiiformes, the Simiiformes generally exhibit darker skin pigmentation and a less bright coat color (fig. S25) (89). We identified two pigmentation-related genes, *KIT* and *CREB3L4*, that participate in the melanogenesis pathway that evolved under positive selection (detected by the branch-site model) in the Simiiformes ancestor (Fig. 4E). Melanocytes play an important role during the formation of skin and coat colors in mammals by regulating melanin-related genes (90). *KIT*, a proto-oncogene, encodes a receptor tyrosine kinase that regulates cell migration, proliferation, and differentiation in melanocytes and plays a key role in melanin deposition (91, 92). *KIT* also communicates with *MITF*, a key gene in the formation of melanin that regulates the development of melanocytes (93–95).

Genetic mechanisms underlying primate phenotype evolution

Primates have evolved diverse phenotypic traits to adapt to their challenging environ-

ments. Here, we sought to investigate the evolution of complex phenotypes in the brain, skeletal system, digestive system, and sense organs, as well as body size, in primates.

Brain evolution

In primates, brain volumes range from ~ 2 cm³ in the mouse lemur to ~ 1300 cm³ in human (73). To reveal the genetic changes that might underlie brain evolution in primates, we detected signals of positive selection in brain development genes using a branch-site model in PAML in key evolutionary nodes in the primate phylogeny. A total of 34 brain genes were found to be under positive selection in one of the primate evolutionary nodes (table S26) (68). Four of them, *SLC6A4*, *NR2E1*, *NIPBL*, and *XRCC6*, were under positive selection in the common ancestor of all primates, whereas 30 were under positive selection in other primate ancestral nodes leading to the evolution of humans (table S26). These results appear to suggest that primates underwent continuous brain evolution over an extended period of evolutionary time. Knockout experiments in mice on many of these positively selected genes have shown brain function impairment. For instance, the *NIPBL* gene interacts with *ZFP609* to regulate the migration of cortical neurons, and its mutations are frequently involved in brain neurological defects encompassing intellectual disability and seizures (96). We identified two amino acid residues in the *NIPBL* protein that experienced adaptive change in the common ancestor of all primate lineages (fig. S26).

Microcephaly is characterized by severe neurological defects, the small brain size being caused by a disturbance of the proliferation of nerve cells (97). Some genes involved in microcephaly have been proposed as candidates for involvement in the evolution of brain size (98–100). We also searched for positive selection signals in the I113 coding genes involved in microcephaly (g:Profiler identifier HP:0000252). In total, 65 positively selected genes with functional roles in microcephaly were identified, along with the primate ancestor leading to the human lineage (table S27), suggesting that microcephaly genes may have been involved in the marked evolutionary expansion of brain size that characterizes primates, especially in those crucial evolutionary nodes characterized by a sharp increase in the degree of cortical folding (gyrification) and brain volume (101).

We next sought to investigate the roles of regulatory elements in the evolution of primate brain size. We first identified noncoding regions that were highly conserved and under strong purifying selection across all primates and detected signals of accelerated evolution in four lineages: the Simiiformes ancestor (table S21), the Catarrhini ancestor (table S28), the ancestor of great apes (table S29), and the

human lineage (table S30), representing crucial evolutionary nodes for the enlargement of primate brain size (101) (fig. S27). These lineage-specific accelerated regions should be under strong positive selection specifically in the targeted lineages and might contribute to the adaptation or innovation of these lineages (72). We found 15 genes associated with lineage-specific accelerated regions in the common ancestor of the great apes that showed particularly high expression in the human fetal brain (fig. S27 and table S31) ($P = 0.023$, modified Fisher's exact test). More than half of these genes have been reported to have roles in brain development and function (102–109). For example, knockout of the transcription factor-encoding *MEF2C* in a mouse model resulted in impaired neuronal differentiation and smaller somal size among neural progenitor cells (108). Coincidentally, the lineage-specific accelerated region of this gene was detected in the great ape ancestral lineage. The *DLG5* gene, which is required for the polarization of citron kinase in mitotic neural precursors, also contains a lineage-specific accelerated region in the great ape lineage, and *DLG5*^{-/-} mice have smaller brains and thinner neocortices (109, 110).

We further investigated the evolution of neurotransmitters, which mediate the neurogenesis process (111, 112) and also play a role in the regulation of brain size (111). We detected 12 positively selected genes and 39 genes associated with lineage-specific accelerated regions in the ancestral nodes leading to the human lineage that were found to be involved in the release, transportation, and reception of neurotransmitter signals (Fig. 5A and fig. S28). These genes participate in diverse neurotransmitter systems: glutamatergic, dopaminergic, cholinergic, and GABAergic synapses and the synaptic vesicle cycle. Among these, five positively selected genes and 33 genes associated with lineage-specific accelerated regions are highly expressed in the human brain (table S32). It is likely that at least some of these genomic changes affecting the neurotransmitter signaling pathway might have played a role in primate brain evolution.

Evolution of the skeletal system and limbs

The arboreal lifestyle coevolved with adaptive changes of the skeletal system and limb development. Genes functioning in bone development are likely to have been especially important for the adaptive radiation of the primates. We identified four positively selected genes, *PIEZ01*, *EGFR*, *BMPER*, and *NOTCH2*, that were involved in bone development (113–116) in the ancestral lineage of primates (table S17). Bone development requires the recruitment of osteoclast precursors from the surrounding mesenchyme, thereby actuating the key events of bone growth, such as marrow cavity formation, capillary

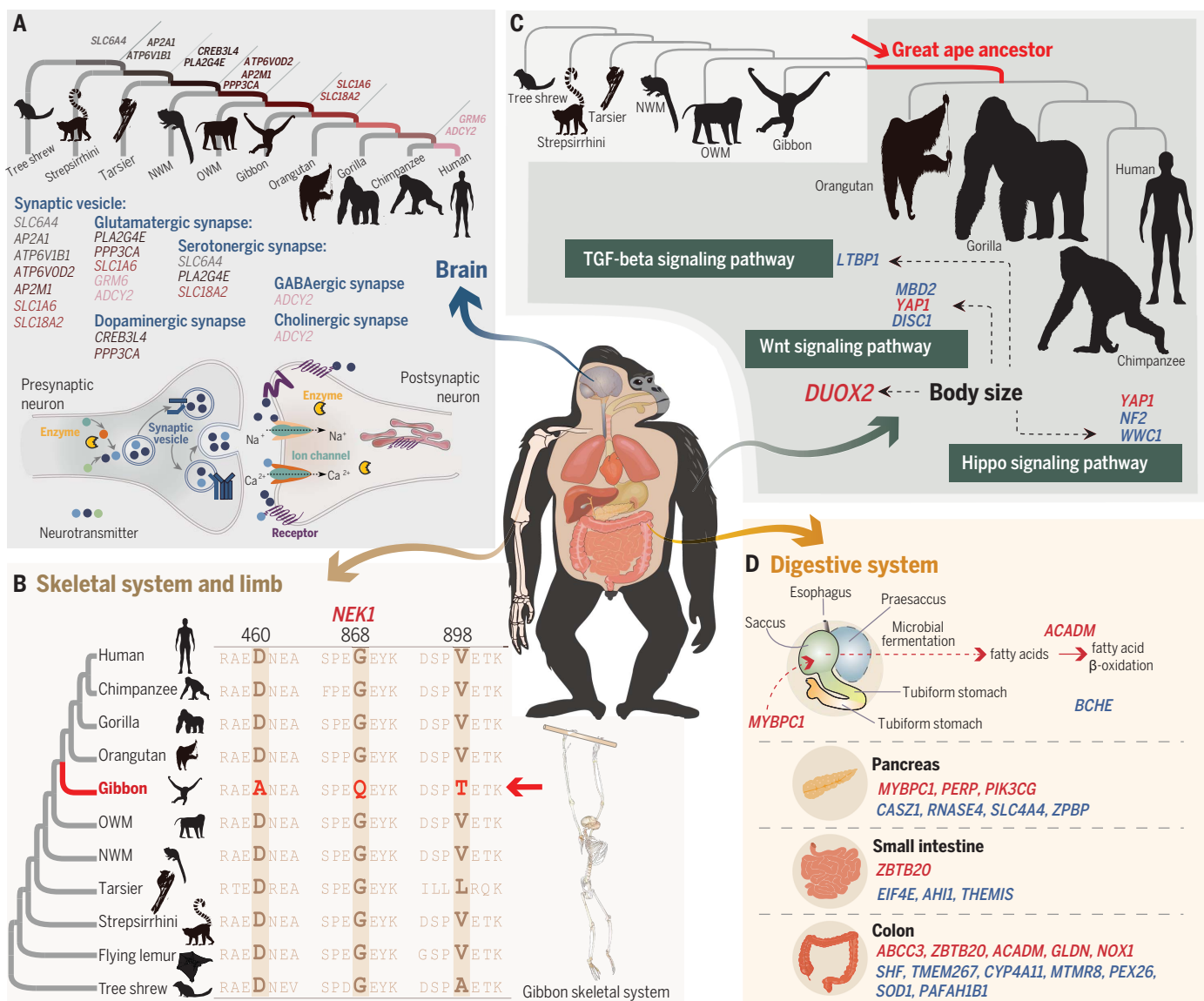


Fig. 5. Associations between genomic evolutionary characteristics and phenotypic traits in primates. (A) Positively selected genes and genes associated with lineage-specific accelerated regions from the primate ancestral lineage leading to the human lineage that are involved in transport, release, and receptors in neurotransmitter signaling. (B) The *NEK1* gene, which is involved in upper limb bone development, was under positive selection with three positively selected sites in the gibbon ancestral lineage. The gibbon ancestor is

shown in red. (C) Eight positively selected genes and genes associated with lineage-specific accelerated regions from the great ape ancestral lineage involved in the TGF- β , Wnt, and Hippo signaling pathways. (D) Positively selected genes and genes associated with lineage-specific accelerated regions involved in the evolution of the digestive system in the Colobinae ancestral lineage. Genes marked in red and blue represent positively selected genes and genes associated with lineage-specific accelerated regions, respectively, in this lineage.

invasion, and matrix remodelling. The mechanical sensing protein *PIEZO1* accommodates bone homeostasis through osteoclast-osteoblast cross-talk (113). Osteoclasts then influence osteoblast formation and differentiation through the secretion of some soluble factors (117). *EGFR* negatively regulates mTOR signaling during osteoblast differentiation to control bone development (114). The *NOTCH2* gene regulates cancellous bone volume and microarchitecture in osteoblast precursors (116, 118).

Although tails vary in length and shape across the primates, they generally play key

roles in relation to locomotion (119). This notwithstanding, the tail was lost in some primate lineages, including the common ancestor of the apes (120, 121). We retrieved 151 genes associated with lineage-specific accelerated regions in the common ancestral lineage of the apes (table S33), including *KIAA1217* (sickle tail protein homolog) (figs. S29 and S30). Mutations in *KIAA1217* are associated with malformations of the notochord and caudal vertebrae in humans, and in mice they affect the development of the vertebral column, leading to a characteristic short tail due to a

reduced number of caudal vertebrae (122, 123). Thus, the lineage-specific accelerated region may serve as a regulator of the expression of *KIAA1217*, because this lineage-specific accelerated region, residing in the vicinity of *KIAA1217* in the ape lineage, overlaps with the enhancer EH38E1455433 (pELS) (fig. S31). High-throughput chromosome conformation capture data (fig. S32) also showed that this lineage-specific accelerated region is located in the same topologically associated domain as *KIAA1217*, suggesting that they may physically interact with each other. Furthermore, the

lesser apes (gibbons) are of particular interest because of their dominant locomotor style, brachiation (124, 125). This locomotor adaptation was accompanied by the acquisition of distinct morphological characteristics, particularly the elongated forelimb, representing

one of the most intriguing phenotypic traits in gibbons that enables them to travel through the canopy at high speed (126). We found that positive selection has operated on four genes related to upper limb bone morphology in the gibbon ancestral lineage (table S34). Of these,

NEK1, which encodes a serine or threonine kinase, contains the most positively selected sites (Fig. 5B). Functional studies have shown that genetic variants in this gene can influence bone length and shorten the humerus and femur in humans (127, 128). Therefore,

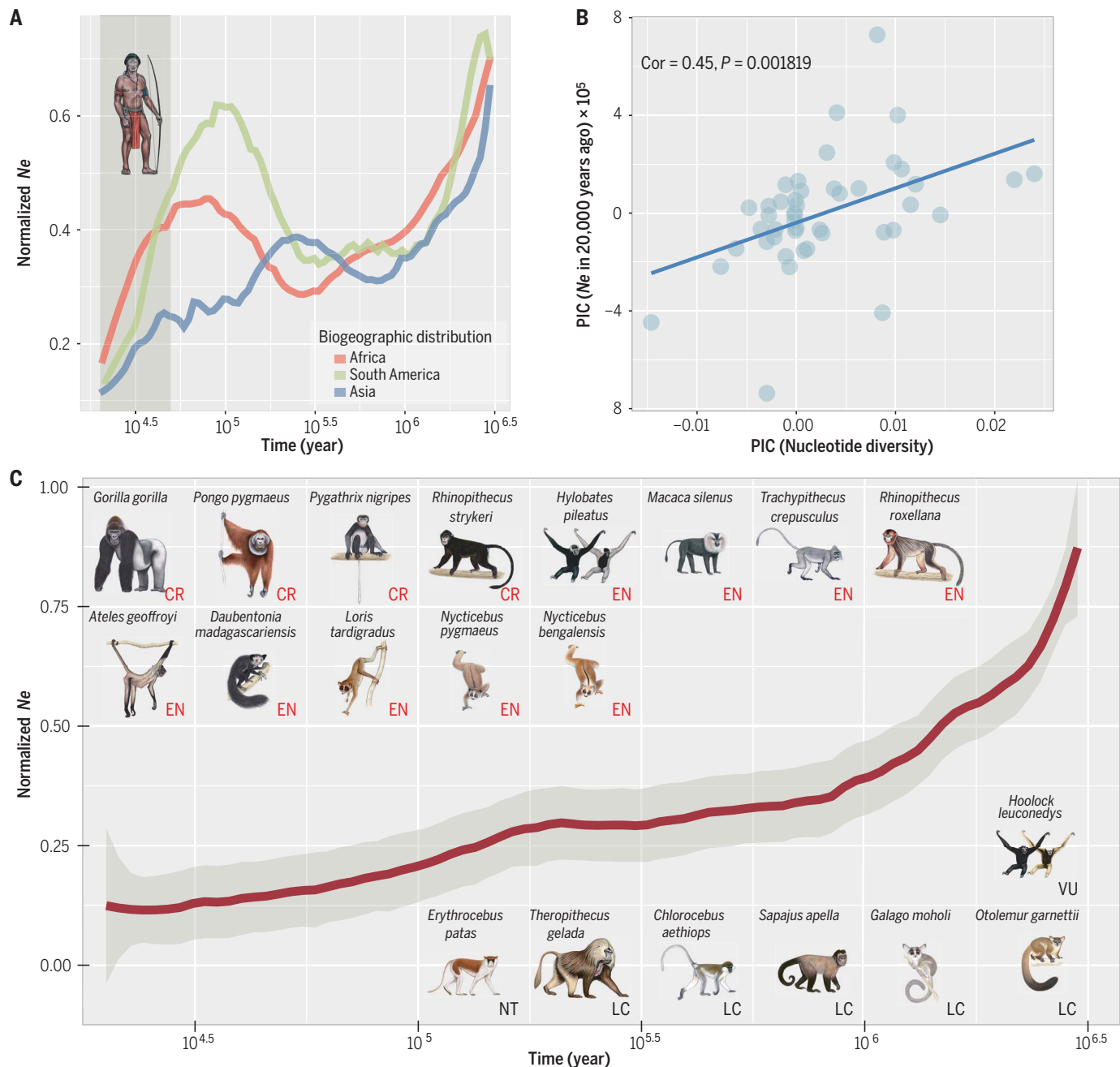


Fig. 6. Demographic history of nonhuman primates. (A) Primate species grouped according to their biogeographic distribution (Africa, Asia, or South America). The plot shows the normalized demographic history of all species within each biogeographic region. The normalized N_e was inferred by dividing the estimated value of N_e for each species at each time point by its maximum value. *Callithrix jacchus* was removed from this analysis because the genome was derived from an inbred individual. The time period from 50,000 to 20,000 years ago (late Pleistocene) is indicated by a gray background. (B) Correlation

analysis between nucleotide diversity and N_e after phylogenetic corection using the Ape library in R (<http://ape-package.ird.fr>). N_e represents the median value of effective population size for each species 20,000 years ago. (C) Nearly half ($n = 20$) of all nonhuman primate species experienced a continual decline in N_e over the past 3 million years. These include the 13 critically endangered or endangered species shown in red. The IUCN Red List status is shown for each species in the inserted plot: CR, critically endangered; EN, endangered; VU, vulnerable; NT, near threatened; and LC, least concern.

positive selection acting on genes related to upper limb bone morphology may have been important in the acquisition of the elongated forelimb, a key adaptive trait for the unique brachiating locomotion style of gibbons.

Evolution of body size in primates

Like other mammalian groups (129, 130), extant primate species exhibit a large range of body sizes, from dwarf galagos and mouse lemurs (~60 to 70 g) at one end of the spectrum to male gorillas (>200 kg in some individuals) at the other (131). Thus, primate body size has experienced significant divergence, particularly for the great apes with their substantial enlargement in body size. We detected several positively selected genes in the common ancestors of the great apes that might have contributed to the evolution of this trait. *DUOX2* encodes a protein involved in a critical step of thyroid hormone synthesis, and mutations in *DUOX2* are known to cause decreased body size in mouse and panda (132, 133). This gene experienced strong positive selection in the great ape ancestral lineage ($P = 0.018$, χ^2 test) (Fig. 5C and table S35). Additionally, we found several genes involved in the transforming growth factor- β (TGF- β) signaling pathway (e.g., *LTBP1*) or the Wnt signaling pathway (e.g., *MBD2*, *YAPI*, and *DISC1*), two of the best known pathways participating in bone development and body size (48), that were either under strong positive selection in the great apes or had lineage-specific accelerated regions in this lineage (Fig. 5C and tables S29 and S35).

Several positively selected genes and genes associated with lineage-specific accelerated regions in the great ape ancestor were also significantly overrepresented in the Hippo signaling pathway ($P = 0.045$, modified Fisher's exact test) (table S36), which has been implicated in the determination of organ and body size (82). When combining all positively selected genes, genes associated with lineage-specific accelerated regions, and expanded gene families in the Simiiformes ancestral lineage, which markedly increased their body size compared with non-Simiiformes lineages (Fig. 4B), we also detected diverse candidate genes with adaptive changes in the Hippo signaling pathway. These results indicate potentially important roles for the Hippo pathway in body size changes in these two nodes during primate evolution.

Evolution of the digestive system

Primate lineages have evolved diverse dietary habits and specialized digestive functions (134). In particular, leaf-eating colobines, an African and Asian subfamily (Colobinae) of Old World monkeys, have evolved a uniquely specialized and compartmentalized foregut in which there are discrete alkaline and acidic sections to cope with their folivorous diet

and microbial fermentation can take place (135, 136). Although colobines eat leaves, fruits, flowers, and seeds, they typically focus much of their feeding time on leaves (estimated range: ~34 to 81% of their annual diet) (135). Accordingly, these leaf-eaters are well adapted in terms of meeting their energy metabolism requirements and balancing micronutrients and protein intake while also dealing with the toxins contained in their food plants (137).

In the ancestor of the Colobinae, we identified a number of pivotal digestive genes that underwent positive selection (table S37). Acyl-CoA dehydrogenase, encoded by the *ACADM* gene, is an important lipolytic enzyme that catalyzes the initial step in each cycle of mitochondrial fatty acid β -oxidation and plays a key role in metabolizing fatty acids derived from ingested foods (138). Energy-rich short-chain volatile fatty acids are produced by the microbial fermentation process and absorbed by the host, thus making an important contribution to the energy budget of colobines (135). Therefore, rapid evolution of this gene, with two positively selected sites (V75M and A138C), may have been important for the absorption of fatty acids by colobines (Fig. 5D and fig. S33). *NOX1*, which is highly expressed in the colon, was identified as being under positive selection in the ancestor of the Colobinae (Fig. 5D and tables S37 and S38). *NOX1*-dependent reactive oxygen species production can further regulate microorganism homeostasis in the ileum of mice (139). The rumens of ruminants and the saccus stomachs of colobines have developed a similar adaptive strategy to allow the microbial fermentation of high-fiber foods, and therefore are an example of convergent evolution. We found that *MYBPC1*, which has been shown to contribute to morphological and functional differences in the bovine rumen (140), also underwent positive selection in the ancestor of the Colobinae (Fig. 5D and table S37). In addition, 100 genes associated with lineage-specific accelerated regions were identified in the ancestral lineage of the Colobinae (table S39). Several of these genes were also highly expressed in the stomach, colon, pancreas, and small intestine (Fig. 5D and table S38). Of these, *RNASE4* encodes a vital digestive enzyme, pancreatic ribonuclease 4, and is a paralog of *RNASE1*, which is known to have undergone adaptive evolution by gene duplication in leaf-eating colobines and howler monkeys (26, 141). Colobines may therefore have acquired adaptations to allow them to digest fatty acids and ribonucleic acids, and their unique foregut and intestinal microbiota enabled them to cope with their folivorous diet.

Evolution of sensory organs

In many mammals, olfaction is the dominant sense and provides much of the sensory information

upon which animals rely to navigate, forage, and avoid predators or for social behavior and courtship (134). Most Strepsirrhini species are nocturnal, whereas most Simiiformes are diurnal with well-developed color vision systems attuned to their priorities in diurnal activity (142–145). By contrast, olfactory sensitivity appears to have decreased in the Simiiformes compared with the Strepsirrhini (134, 146, 147). Consistent with these findings, we found that the copy number of several specific olfactory receptor gene families was significantly reduced in the Simiiformes. For example, the olfactory receptor gene family *OR52A* underwent a significant contraction in the Simiiformes (40 species), with only ~0.7 copies on average, in contrast to the ~3.4 average copies in the Strepsirrhini (nine species) (figs. S34 and S35) ($P = 4.072 \times 10^{-5}$, Mann-Whitney *U* test). Anatomically, Strepsirrhini are characterized by the presence of a rhinarium, a moist and naked surface around the tip of the nose that is present in most mammals, including dogs and cats, but has been lost in the Simiiformes (134, 147). Olfactory bulb volume, which correlates with olfactory receptor neuron population size, is also larger in the Strepsirrhini than in the Simiiformes (146, 148). The *LHX2* gene, which participates in olfactory bulb development (149, 150), experienced positive selection in the ancestor of the Strepsirrhini ($P = 0.03$, χ^2 test; table S40).

Demographic history of nonhuman primates

The IUCN lists more than one-third of primates as critically endangered or vulnerable (1). To evaluate the effects of climate change and human activity on the recent population declines in these primates, we inferred their demographic histories over the past million years by using the pairwise sequentially Markovian coalescent model (151) for each species in this study (fig. S36 and tables S16 and S41). Our data showed that most nonhuman primate species experienced rapid population declines during the late Pleistocene (Fig. 6A and fig. S37), consistent with the record of a large mass extinction of mammals during this period (48, 152). Although we did not observe a significant difference between endangered species and other species in terms of nucleotide diversity (fig. S38 and table S42), we did detect a significant positive correlation between the median effective population size (N_e) over the past ~20,000 years and nucleotide diversity ($P = 0.002$, Pearson's product-moment correlation after phylogenetic correction) (Fig. 6B and table S42), indicating a long-term effect of N_e decline on the loss of genetic diversity. According to the historical demographic patterns, we further clustered all nonhuman primate species with similar trends of historical N_e and found that 20 species experienced a

continual N_e decline over the past 3 million years (Fig. 6C). Sixty-five percent of these species are now listed as endangered or critically endangered (Fig. 6C and fig. S39). This ratio is twice that of the remaining species, suggesting that the prehistoric environmental effects (e.g., habitat fragmentation) (26) may also have driven population decline and contributed to the current endangered status of these species well before human interference in the modern era.

Conclusions

Understanding the evolution and genetic basis of human-specific traits requires a systematic comparison of genomes along the primate lineages. Previous studies of primate genomes have focused on genomic changes in the human lineage that influenced brain functions and other traits (120, 153–155). Our comparative phylogenomic analyses across primate lineages have revealed some of the accumulated genomic changes at different primate ancestral nodes that may have contributed to the evolution of unique human traits. Of particular interest, we report a hitherto unreported increase in the rate of genomic change in the Simiiformes common ancestor that may have played a role in the later diversification of Simiiformes and the evolution of humans. Our comparative genomic analyses also yielded insights into the genetic basis of phenotypic diversity across primate lineages. With the rich diversity of morphology and physiology among nonhuman primates, further genomic analyses covering all primate species will provide an indispensable resource for comparative studies allowing expansion of the scope of biomedical research programs using primates as model systems. Further, increased knowledge of the genomic makeup and variations of nonhuman primates should help to identify risk factors for genetic disorders and enhance wildlife health management in both wild and captive members of these species.

REFERENCES AND NOTES

- A. Estrada et al., *Sci. Adv.* **3**, e1600946 (2017).
- C. Roos et al., *Zool. Res.* **41**, 656–669 (2020).
- A. Nater et al., *Curr. Biol.* **27**, 3487–3498.e10 (2017).
- P. F. Fan et al., *Am. J. Primatol.* **79**, e22631 (2017).
- C. Li, C. Zhao, P. F. Fan, *Am. J. Primatol.* **77**, 753–766 (2015).
- J. Rogers, R. A. Gibbs, *Nat. Rev. Genet.* **15**, 347–359 (2014).
- B. Rockx et al., *Science* **368**, 1012–1015 (2020).
- A. Chandrasekhar et al., *Science* **369**, 812–817 (2020).
- Q. Gao et al., *Science* **369**, 77–81 (2020).
- J. Yu et al., *Science* **369**, 806–811 (2020).
- V. J. Munster et al., *Nature* **585**, 268–272 (2020).
- N. B. Mercado et al., *Nature* **586**, 583–588 (2020).
- K. S. Corbett et al., *N. Engl. J. Med.* **383**, 1544–1555 (2020).
- N. van Doremalen et al., *Nature* **586**, 578–582 (2020).
- B. N. Williamson et al., *Nature* **585**, 273–276 (2020).
- T. Z. Song et al., *Zool. Res.* **41**, 503–516 (2020).
- W. Enard, S. Pääbo, *Annu. Rev. Genomics Hum. Genet.* **5**, 351–378 (2004).
- Z. N. Kronenberg et al., *Science* **360**, eaar6343 (2018).
- Chimpanzee Sequencing and Analysis Consortium, *Nature* **437**, 69–87 (2005).
- R. A. Gibbs et al., *Science* **316**, 222–234 (2007).
- A. Scally et al., *Nature* **483**, 169–175 (2012).
- Marmoset Genome Sequencing and Analysis Consortium, *Nat. Genet.* **46**, 850–857 (2014).
- D. P. Locke et al., *Nature* **469**, 529–533 (2011).
- L. Carbone et al., *Nature* **513**, 195–201 (2014).
- L. Yu et al., *Nat. Genet.* **48**, 947–952 (2016).
- X. Zhou et al., *Nat. Genet.* **46**, 1303–1310 (2014).
- A. O. Ayoola et al., *Mol. Biol. Evol.* **38**, 876–890 (2021).
- D. M. Bickhart et al., *Nat. Genet.* **49**, 643–650 (2017).
- B.-L. Zhang et al., *Sci. Adv.* **9**, eadd3580 (2023).
- H. Wu et al., *Science* **380**, eabl4997 (2023).
- X.-G. Qi et al., *Science* **380**, eabl8621 (2023).
- M.-L. Li et al., *Proc. Natl. Acad. Sci. U. S. A.* **119**, e2123030119 (2022).
- M. S. Ye et al., *Zool. Res.* **42**, 692–709 (2021).
- A. M. Kozlov, A. J. Aberer, A. Stamatakis, *Bioinformatics* **31**, 2577–2579 (2015).
- P. Perelman et al., *PLOS Genet.* **7**, e1001342 (2011).
- C. M. Shi, Z. Yang, *Mol. Biol. Evol.* **35**, 159–179 (2018).
- A. Hobolth, O. F. Christensen, T. Mailund, M. H. Schierup, *PLOS Genet.* **3**, e7 (2007).
- I. Rivas-González et al., *Science* **380**, eabn4409 (2022).
- D. Vanderpool et al., *PLOS Biol.* **18**, e3000954 (2020).
- Z. Yang, *Mol. Biol. Evol.* **20**, 1586–1591 (2007).
- S. Álvarez-Carretero et al., *Nature* **602**, 263–267 (2022).
- C. Liu et al., *Sci. Adv.* **7**, eabe9459 (2021).
- E. E. Eichler, D. Sankoff, *Science* **301**, 793–797 (2003).
- Y. Yin et al., *Nat. Commun.* **12**, 6858 (2021).
- R. Stanyon et al., *Chromosome Res.* **16**, 17–39 (2008).
- T. Marques-Bonet et al., *Nature* **457**, 877–881 (2009).
- P. D. Stenson et al., *Hum. Genet.* **139**, 1197–1207 (2020).
- L. Chen et al., *Science* **364**, eaav6202 (2019).
- J. D. Smith, J. W. Bickham, T. R. Gregory, *Genome* **56**, 457–472 (2013).
- S. Shen et al., *Proc. Natl. Acad. Sci. U.S.A.* **108**, 2837–2842 (2011).
- G. E. Liu, C. Alkan, L. Jiang, S. Zhao, E. E. Eichler, *Genome Res.* **19**, 876–885 (2009).
- T. Hayakawa, Y. Satta, P. Gagneux, A. Varki, N. Takahata, *Proc. Natl. Acad. Sci. U.S.A.* **98**, 11399–11404 (2001).
- P. Kuehnen et al., *PLOS Genet.* **8**, e1002543 (2012).
- J. Jurka, *Curr. Opin. Genet. Dev.* **14**, 603–608 (2004).
- G. Zhang et al., *Science* **346**, 1311–1320 (2014).
- P. Moorjani, C. E. Amorim, P. F. Arndt, M. Przeworski, *Proc. Natl. Acad. Sci. U.S.A.* **113**, 10607–10612 (2016).
- E. Fontanillas, J. J. Welch, J. A. Thomas, L. Bromham, *BMC Evol. Biol.* **7**, 95 (2007).
- A. Wong, *Mol. Biol. Evol.* **31**, 1432–1436 (2014).
- W. H. Li, M. Tanimura, *Nature* **326**, 93–96 (1987).
- M. E. Steiper, N. M. Young, *Mol. Phylogenet. Evol.* **41**, 384–394 (2006).
- S. H. Kim, N. Elango, C. Warden, E. Vigoda, S. V. Yi, *PLOS Genet.* **2**, e163 (2006).
- J. Schmitz et al., *Nat. Commun.* **7**, 12997 (2016).
- L. Fang et al., *Genome Res.* **30**, 790–801 (2020).
- B. Y. Liao, J. Zhang, *Mol. Biol. Evol.* **23**, 1119–1128 (2006).
- G. J. Wyckoff, W. Wang, C. I. Wu, *Nature* **403**, 304–309 (2000).
- T. Boehm, *Curr. Biol.* **22**, R722–R732 (2012).
- H. Y. Wang et al., *PLOS Biol.* **5**, e13 (2007).
- Materials and methods are available as supplementary materials.
- J. Tohyama et al., *J. Hum. Genet.* **60**, 167–173 (2015).
- P. Mansfield, J. N. Constantino, D. Baldwin, *Am. J. Med. Genet. B. Neuropsychiatr. Genet.* **183**, 227–233 (2020).
- M. Maekawa et al., *J. Neurochem.* **115**, 1374–1385 (2010).
- X. Bi et al., *Sci. Adv.* 10.1126/sciadv.95057 (2023).
- J. K. Rilling, T. R. Insel, *Neuroreport* **10**, 1453–1459 (1999).
- K. Isler et al., *J. Hum. Evol.* **55**, 967–978 (2008).
- C. Plachez, L. J. Richards, *Curr. Top. Dev. Biol.* **69**, 267–346 (2005).
- M. A. Robichaux, C. W. Cowan, *Curr. Top. Behav. Neurosci.* **16**, 19–48 (2014).
- J. Falk et al., *Neuron* **48**, 63–75 (2005).
- M. A. Wolman, Y. Liu, H. Tawarayama, W. Shoji, M. C. Halloran, *J. Neurosci.* **24**, 8428–8435 (2004).
- C. Kudo, I. Ajioka, Y. Hirata, K. Nakajima, *J. Comp. Neurol.* **487**, 255–269 (2005).
- M. V. Tejada-Simon, *J. Neurochem.* **133**, 767–779 (2015).
- S. L. Eastwood, P. J. Harrison, *Neuropsychopharmacology* **33**, 933–945 (2008).
- D. Pan, *Genes Dev.* **21**, 886–897 (2007).
- S. H. Patel, F. D. Camargo, D. Yilmaz, *Gastroenterology* **152**, 533–545 (2017).
- R. H. Gokhale, A. W. Shingleton, *Wiley Interdiscip. Rev. Dev. Biol.* **4**, 335–356 (2015).
- E. C. Kirk, *Anat. Rec. A Discov. Mol. Cell. Evol. Biol.* **281**, 1095–1103 (2004).
- A. C. Wilk et al., *Genome Res.* **18**, 1415–1421 (2008).
- P. Liskova et al., *Am. J. Hum. Genet.* **102**, 447–459 (2018).
- Y. Toda et al., *Curr. Biol.* **31**, 4641–4649.e5 (2021).
- J. M. Kamilar, B. J. Bradley, *J. Biogeogr.* **38**, 2270–2277 (2011).
- S. Hu et al., *PeerJ* **8**, e9402 (2020).
- M. C. Garrido, B. C. Bastian, *J. Invest. Dermatol.* **130**, 20–27 (2010).
- J. M. Grichnik, *J. Invest. Dermatol.* **126**, 945–947 (2006).
- Y. Mizutani, N. Hayashi, M. Kawashima, G. Imokawa, *Arch. Dermatol. Res.* **302**, 283–294 (2010).
- R. Kitamura et al., *J. Pathol.* **202**, 463–475 (2004).
- B. Wen et al., *Pigment Cell Melanoma Res.* **23**, 441–447 (2010).
- D. L. C. van den Berg et al., *Neuron* **93**, 348–361 (2017).
- G. H. Mochida, C. A. Walsh, *Curr. Opin. Neurol.* **14**, 151–156 (2001).
- S. H. Montgomery, I. Capellini, C. Venditti, R. A. Barton, N. I. Mundy, *Mol. Biol. Evol.* **28**, 625–638 (2011).
- L. Shi, M. Li, Q. Lin, X. Qi, B. Su, *BMC Biol.* **11**, 62 (2013).
- L. Shi, B. Su, *Zool. Res.* **40**, 236–238 (2019).
- J. Rogers et al., *Neuroimage* **53**, 1103–1108 (2010).
- S. V. Puram et al., *Genes Dev.* **25**, 2659–2673 (2011).
- A. Yamada et al., *Mol. Cell. Neurosci.* **56**, 234–243 (2013).
- R. Kusano et al., *FEBS Lett.* **590**, 3606–3615 (2016).
- M. Talarowska, J. Szemraj, M. Kowalczyk, P. Gafecki, *Med. Sci. Monit.* **22**, 152–160 (2016).
- A. K. Pandey, L. Lu, X. Wang, R. Homayouni, R. W. Williams, *PLOS ONE* **9**, e88889 (2014).
- A. Graziano, G. Foffani, E. B. Knudsen, J. Shumsky, K. A. Moxon, *PLOS ONE* **8**, e54350 (2013).
- H. Li et al., *Proc. Natl. Acad. Sci. U.S.A.* **105**, 9397–9402 (2008).
- Y. Chang, O. Klezovitch, R. S. Walikonis, V. Vasioukhin, J. J. LoTurco, *Cell Cycle* **9**, 1990–1997 (2010).
- M. R. Sarkisian, *Cell Cycle* **9**, 1876 (2010).
- D. A. Berg, L. Belnoue, H. Song, A. Simon, *Development* **140**, 2548–2561 (2013).
- P. Levitt, J. A. Harvey, E. Friedman, K. Simansky, E. H. Murphy, *Trends Neurosci.* **20**, 269–274 (1997).
- L. Wang et al., *Nat. Commun.* **11**, 282 (2020).
- M. Lindner et al., *Cell Death Differ.* **25**, 1094–1106 (2018).
- F. Xiao et al., *Cell. Physiol. Biochem.* **45**, 1927–1939 (2018).
- S. Zanotti, E. Canalis, *Bone* **62**, 22–28 (2014).
- J. M. Kim, C. Lin, Z. Stavre, M. B. Greenblatt, J. H. Shim, *Cells* **9**, 2073 (2020).
- S. Zanotti, E. Canalis, *Endocr. Rev.* **37**, 223–253 (2016).
- M. Schmidt, *Adv. Sci. Res.* **5**, 23–39 (2011).
- Y. He et al., *Nat. Commun.* **10**, 4233 (2019).
- S. A. Williams, G. A. Russo, *Evol. Anthropol.* **24**, 15–32 (2015).
- K. Semba et al., *Genetics* **172**, 445–456 (2006).
- N. Al Dhaheri et al., *Am. J. Med. Genet. A* **182**, 1664–1672 (2020).
- J. R. Usherwood, J. E. Bertram, *J. Exp. Biol.* **206**, 1631–1642 (2003).
- J. R. Usherwood, S. G. Larson, J. E. Bertram, *Am. J. Phys. Anthropol.* **120**, 364–372 (2003).
- S. M. Cheyne, in *Primate Locomotion: Linking Field and Laboratory Research*, K. D'Août, E. E. Vereecke, Eds. (Springer, NY, 2011), pp. 201–213.
- C. Thiel et al., *Am. J. Hum. Genet.* **88**, 106–114 (2011).
- J. El Hokayem et al., *J. Med. Genet.* **49**, 227–233 (2012).
- J. M. Vasquez, V. J. Lynch, *eLife* **10**, e65041 (2021).
- J. G. M. Thewissen, L. N. Cooper, J. C. George, S. Bajpai, *Evolution (N. Y.)* **2**, 272–288 (2009).
- W. L. Jungers, in *Size and Scaling in Primate Biology*, W. L. Jungers, Ed. (Springer, 1985), pp. 345–381.
- A. M. Rudolf et al., *Natl. Sci. Rev.* **9**, nwab125 (2021).
- K. R. Johnson et al., *Mol. Endocrinol.* **21**, 1593–1602 (2007).
- J. G. Fleagle, *Primate Adaptation and Evolution* (Academic, 2013).
- K. Milton, *Int. J. Primatol.* **19**, 513–548 (1998).
- I. Matsuda, C. A. Chapman, M. Clauss, *J. Morphol.* **280**, 1608–1616 (2019).
- M. C. Janiak, *Evol. Anthropol.* **25**, 253–266 (2016).
- J. J. Kim, R. Miura, *Eur. J. Biochem.* **271**, 483–493 (2004).

139. C. Matziouridou *et al.*, *Mucosal Immunol.* **11**, 774–784 (2018).
140. C.-J. Li, R. W. Li, R. L. Baldwin Vi, *Agric. Sci.* **9**, 619–638 (2018).
141. M. C. Janiak, A. S. Burrell, J. D. Orkin, T. R. Disotell, *Sci. Rep.* **9**, 20366 (2019).
142. P. Pontarotti, *Evolutionary Biology: Mechanisms and Trends* (Springer, 2012).
143. N. J. Dominy, P. W. Lucas, *Nature* **410**, 363–366 (2001).
144. N. G. Caine, N. I. Mundy, *Proc. Biol. Sci.* **267**, 439–444 (2000).
145. A. C. Smith, H. M. Buchanan-Smith, A. K. Surridge, D. Osorio, N. I. Mundy, *J. Exp. Biol.* **206**, 3159–3165 (2003).
146. S. Heritage, *PLOS ONE* **9**, e113904 (2014).
147. A. Matsui, Y. Go, Y. Niimura, *Mol. Biol. Evol.* **27**, 1192–1200 (2010).
148. T. D. Smith, K. P. Bhatnagar, *Anat. Rec. B New Anat.* **279**, 24–31 (2004).
149. A. Berglund, A. C. Häggblund, S. Bohm, L. Carlsson, *FASEB J.* **26**, 3464–3472 (2012).
150. J. Hirota, P. Mombaerts, *Proc. Natl. Acad. Sci. U.S.A.* **101**, 8751–8755 (2004).
151. H. Li, R. Durbin, *Nature* **475**, 493–496 (2011).
152. A. D. Barnosky, P. L. Koch, R. S. Feranec, S. L. Wing, A. B. Shabel, *Science* **306**, 70–75 (2004).
153. X. Luo *et al.*, *Cell* **184**, 723–740.e21 (2021).
154. C. Yang *et al.*, *Nature* **594**, 227–233 (2021).
155. G. Dumas, S. Malesys, T. Bourgeron, *Genome Res.* **31**, 484–496 (2021).
156. J. K. Rilling, *Evol. Anthropol.* **15**, 65–77 (2006).
157. H. Stephan, H. Frahm, G. Baron, *Folia Primatol. (Basel)* **35**, 1–29 (1981).
158. Genome annotation GFF files at Mendeley Data for: Y. Shao *et al.*, Phylogenomic analyses provide insights into primate evolution, Mendeley (2023).
159. Genome annotation GFF files at Figshare for: Y. Shao *et al.*, Phylogenomic analyses provide insights into primate evolution, Figshare (2023); <https://doi.org/10.5061/dryad.8w9ghx3qj>.
160. Gene sequences for: Y. Shao *et al.*, Phylogenomic analyses provide insights into primate evolution, Dryad (2023).

ACKNOWLEDGMENTS

We are grateful to the many individuals in our host institutions who provided support for this project. **Funding:** This work was supported by the Strategic Priority Research Program of the Chinese Academy of Sciences (grants XDPB17 and XDB31020000); the National Natural Science Foundation of China (grants 31822048 and 32270500); the CAS Light of West China Program (grant xbzg-zdssys-202213); the Yunnan Fundamental Research Project (grant 2019FJ010); the Animal Branch of the Germplasm Bank of Wild Species of Chinese Academy of Science (Large Research Infrastructure Funding); the International Partnership Program of Chinese Academy of Sciences (grant 152453KYSB20170002); a Villum Investigator Grant (25900 to G.Z.); the Japan Society for the Promotion of Science (JSPS) KAKENHI grants 16K18630, 19K16241, 20H04987, 21H04919, and 21KK0106; Hokkaido University Sousei Tokutei Research; and JSPS Bilateral Joint Research Project (JPJSBP grant 120219902 to T.H.). T.M.B. was supported by funding from the European Research Council (ERC) under the European Union's Horizon 2020 research and innovation programme (grant 864203), PID2021-126004NB-100 (MICIIN/FEDER, UE), and Secretaria d'Universitats i Recerca and CERCA Programme del Departament d'Economia i Coneixement de la Generalitat de Catalunya (GRC 2021 SGR 00177). **Author contributions:** D.D.W. and G.J.Z. led the project. D.D.W., G.J.Z., and X.G.Q. conceived and designed the research. Y.S., L.Z., F.L., L.Z., B.L.Z., F.S., J.W.C., C.Y.C., X.P.B., X.L.Z., H.L.Z., I.R.G., S.W., Y.M.W., L.K., G.L., H.M.L., Y.L., and P.D.S. performed comparative genomics analysis. L.Z., J.H., Z.Y.S., X.L., D.P.W., and K.F. contributed genome sequencing, assembly, and annotation. P.F.F., M.L., Z.J.L., G.P.T., A.D.Y., C.R., T.H., T.M.B., and J.R. collected samples. J.R. and T.M.B. generated

some genome assemblies for comparative genomics analysis. C.R., G.P.T., J.R., L.Y., M.H.S., D.N.C., Y.G.Y., Y.P.Z., W.W., and X.G.Q. provided comments for improving the manuscript. Y.S., X.G.Q., and L.Z. plotted and revised the figures. Y.S. drafted the manuscript. D.D.W., G.J.Z., and Y.S. wrote the manuscript. D.N.C. edited the manuscript. All authors approved the final manuscript.

Competing interests: J.R. is also a core scientist at the Wisconsin National Primate Research Center, University of Wisconsin, Madison. Employees of Illumina, Inc., are indicated in the list of author affiliations. The authors declare no competing financial interests.

Data and materials availability: All 27 primate genome assemblies and the raw genome long- and short-read sequencing data have been deposited at the NCBI Assembly Database (<https://www.ncbi.nlm.nih.gov/assembly/>) and the Sequence Read Archive Database (<https://www.ncbi.nlm.nih.gov/sra/>) under accessible BioProject accession codes PRJNA785018 and PRJNA911016. All genome annotation GFF files have been uploaded to the Mendeley Data database (158) and the Figshare database (159). The positively selected genes and their sequence alignments have been uploaded to a public Dryad dataset (160). **License information:** Copyright © 2023 the authors, some rights reserved; exclusive licensee American Association for the Advancement of Science. No claim to original US government works. <https://www.science.org/about/science-licenses-journal-article-reuse>

SUPPLEMENTARY MATERIALS

science.org/doi/10.1126/science.abn6919

Materials and Methods

Figs. S1 to S39

Tables S1 to S42

References (161–237)

MDAR Reproducibility Checklist

Submitted 16 December 2021; accepted 26 January 2023
10.1126/science.abn6919

Phylogenomic analyses provide insights into primate evolution

Yong Shao, Long Zhou, Fang Li, Lan Zhao, Bao-Lin Zhang, Feng Shao, Jia-Wei Chen, Chun-Yan Chen, Xupeng Bi, Xiao-Lin Zhuang, Hong-Liang Zhu, Jiang Hu, Zongyi Sun, Xin Li, Depeng Wang, Iker Rivas-Gonzlez, Sheng Wang, Yun-Mei Wang, Wu Chen, Gang Li, Hui-Meng Lu, Yang Liu, Lukas F. K. Kuderna, Kyle Kai-How Farh, Peng-Fei Fan, Li Yu, Ming Li, Zhi-Jin Liu, George P. Tiley, Anne D. Yoder, Christian Roos, Takashi Hayakawa, Tomas Marques-Bonet, Jeffrey Rogers, Peter D. Stenson, David N. Cooper, Mikkel Heide Schierup, Yong-Gang Yao, Ya-Ping Zhang, Wen Wang, Xiao-Guang Qi, Guojie Zhang, and Dong-Dong Wu

Science, **380** (6648), .
DOI: 10.1126/science.abn6919

View the article online

<https://www.science.org/doi/10.1126/science.abn6919>

Permissions

<https://www.science.org/help/reprints-and-permissions>



Supplementary Materials for

Phylogenomic analyses provide insights into primate evolution

Yong Shao *et al.*

Corresponding authors: Xiao-Guang Qi, qixg@nwu.edu.cn; Guojie Zhang, guojiezhang@zju.edu.cn; Dong-Dong Wu, wudongdong@mail.kiz.ac.cn

Science **380**, 913 (2023)
DOI: 10.1126/science.abn6919

The PDF file includes:

Materials and Methods

Figs. S1 to S39

Tables S1 to S20, S23 to S27, S31, S32, S34 to S38, S40 to S42

References

Other Supplementary Material for this manuscript includes the following:

Tables S21, S22, S28 to S30, S33, and S39

MDAR Reproducibility Checklist

Materials and Methods

SM Text 1 Species and sample information

The complete set of primate genomes used in our project encompassed a total of 50 species, including 27 newly assembled genomes (tables S1–S4), one genome (for *Nycticebus pygmaeus*, the *pygmy slow loris*) from our accompanying paper (32), and 22 previously published genomes (table S8).

Sample collection strictly followed the rules of CITES (the Convention on International Trade in Endangered Species of Wild Fauna and Flora). The blood samples from each species for 25 primate species were obtained from zoos in China, during physical examination. The frozen liver tissue for the species including *Daubentonia madagascariensis* and *Galago moholi* were obtained from the Duke Lemur Center (<https://lemur.duke.edu/>), and sequenced by RTL Genomics, Marsha Sharp Fwy, USA. All animal specimens were obtained legally and in accordance with the code of ethics for the Care and Use of Animals of the Kunming Institute of Zoology, Chinese Academy of Sciences, China (Approval ID: SMKX-20180701-01), which conforms to the regulatory standards for the human care and treatment of animals in research.

SM Text 2 Genome sequencing, assembly and annotation

DNA sample collection

Genomic DNA from 27 primate species (table S1) was extracted from fresh blood or frozen tissues according to the protocol of the DNAeasy Blood & Tissue kit (Qiagen, USA). Briefly, 20 µl proteinase K and 220 µl anticoagulated blood were added to 200 µl Buffer AL in a 2 ml microcentrifuge tube. The solution was then mixed thoroughly by vortexing before being incubated at 56°C for 10 min. Next, 200 µl ethanol was added to the solution, and the sample mixed fully by vortexing. The mixture was further pipetted into a DNeasy Mini spin column and centrifuged at 8,000 rpm for 1 min. The DNeasy Mini spin column was placed in a new 2 ml collection tube with 500 µl Buffer AW1, and the mixture was centrifuged for 1 min at 8,000 rpm. Around 500 µl Buffer AW2 was added to the spin column and was centrifuged for 3 min at 14,000 rpm to dry the DNeasy membrane. Finally, 50 µl Buffer AE was placed directly onto the DNeasy membrane and centrifuged for 2 min at 8,000 rpm prior to elution after incubation at room temperature for 5 min.

DNA library construction and sequencing

A NanoDrop spectrophotometer, a Qubit fluorometer and gel electrophoresis were used to evaluate the DNA purity, concentration and integrity.

13 DNA libraries (representing 12 primate species, namely *Pongo pygmaeus*, *Nomascus siki*, *Sympalangus syndactylus*, *Lophocebus aterrimus*, *Cercopithecus albogularis*, *Chlorocebus aethiops*, *Sapajus apella*, *Ateles geoffroyi*, *Pithecia pithecia*, *Cephalopachus bancanus*, *Daubentonia madagascariensis*, *Loris tardigradus* and

Galago moholi) were constructed for PacBio SMRT sequencing following the Pacific Biosciences recommended protocols (28). Subsequently, 20 kbp libraries were sequenced on a PacBio RS II platform (Pacific Biosciences, USA). On average, ~147.50 Gbp (~53.81X) of clean subread bases was generated for each of 13 primate species for downstream analyses (table S1).

14 DNA libraries (representing 15 primate species, specifically *Hoolock leuconedys*, *Hylobates pileatus*, *Macaca assamensis*, *Macaca silenus*, *Papio hamadryas*, *Mandrillus sphinx*, *Erythrocebus patas*, *Trachypithecus crepusculus*, *Pygathrix nigripes*, *Rhinopithecus strykeri*, *Colobus guereza*, *Saguinus midas*, *Cebus albifrons* and *Nycticebus bengalensis*) were constructed for Oxford Nanopore Technology sequencing following the manufacturer's instructions. Subsequently, libraries were sequenced on a Nanopore PromethION platform. On average, ~148.53 Gbp (~51.32X) of clean subread bases were generated for each of 14 primate species for downstream analyses (table S1).

Four Hi-C libraries for 4 species including *Hylobates pileatus* (in Hominoidea), *Colobus guereza* (in Old World monkeys [OWMs]), *Saguinus midas* (in New World monkeys [NWMs]) and *Nycticebus bengalensis* (in Strepsirrhini) were constructed and sequenced according to the manufacturer's instructions to link contigs into scaffolds. On average, ~332.61 Gb (~114.15X) clean Hi-C data were generated for each of the 4 species (table S4).

For 4 newly sequenced primate species, namely *Nomascus siki*, *Sympalangus syndactylus*, *Ateles geoffroyi* and *Pithecia pithecia*, we generated 10X Genomics Chromium sequencing data to link contigs into scaffolds and to further polish sequencing errors from the long-read sequencing platforms (PacBio RS II and Nanopore PromethION) (table S3). For the remaining 23 newly sequenced primate species, we additionally produced Illumina clean short-read sequencing data to correct sequencing errors from the long-read platforms (table S3). A total of ~4.91 tera base-pairs (Tbp) sequencing data [on average ~189.04 Gbp (~67.11X) per species] were generated during this study (table S3).

Genome assembly

In order to obtain an optimal assembly for each species, we adopted diverse assembly strategies and ultimately selected the best assembly version (table S2). We generated optimal assemblies using wtdbg2 (161) for 15 species (*Pongo pygmaeus*, *Nomascus siki*, *Hoolock leuconedys*, *Lophocebus aterrimus*, *Cercopithecus albogularis*, *Chlorocebus aethiops*, *Trachypithecus crepusculus*, *Pygathrix nigripes*, *Rhinopithecus strykeri*, *Ateles geoffroyi*, *Cephalopachus bancanus*, *Daubentonia madagascariensis*, *Loris tardigradus*, *Nycticebus bengalensis* and *Galago moholi*), NextDenovo (<https://github.com/Nextomics/NextDenovo>) for 10 species (*Hylobates pileatus*, *Macaca assamensis*, *Macaca silenus*, *Papio hamadryas*, *Mandrillus sphinx*, *Erythrocebus patas*, *Colobus guereza*, *Saguinus midas*, *Sapajus paella*, and *Cebus albifrons*), and FALCON (162) for two species (*Sympalangus syndactylus* and

Pithecia pithecia) (table S2).

For the 15 genome assemblies derived by using wtdbg2 (161), the short-read sequencing data for each species were aligned back to their assembled contigs using BWA (v0.7.12) (163) in order to correct sequencing errors from long-read sequencing platforms; an additional polish was performed by means of wtdbgcns from wtdbg2 (161). For the 10 genome assemblies derived by using NextDenovo (<https://github.com/Nextomics/NextDenovo>), we first performed self-error correction for subreads using NextDenovo with parameters “read_cutoff= 1k; seed_cutoff= 25k”. Then the self-error corrected reads were assembled into contigs using wtdbg (v1.2.8) (<https://github.com/ruanjue/wtdbg>) with parameters “wtdbg -k 0 -p 17 -S 2; wtdbg-cns -c 0 -k 15; kbm-1.2.8 -k 0 -p 15 -S 2 -O 0”. We utilized the short-read sequencing data for each species aligned to their assembled contigs using BWA (v0.7.12) (163); nextpolish (<https://github.com/Nextomics/NextPolish>) was utilized to polish each assembly three times. For the two genome assemblies derived by using FALCON (162), the ARROW program in SMRTLink (v5.1.0.26412) (resequencing pipeline) was employed to polish assemblies using the default parameters.

For 4 newly sequenced primate species (specifically *Nomascus siki*, *Sympalangus syndactylus*, *Ateles geoffroyi* and *Pithecia pithecia*), we generated scaffolds by 10X Chromium barcoded linked reads through two rounds of scaffolding with Scaff10x (v2.1) (<https://github.com/wtsi-hpag/Scaff10X>) (table S3). The 10X Chromium barcoded linked reads were mapped to the contigs using BWA (v0.7.12) (163). The output of the first round of Scaff10x (v2.1) was used as input for the second round. For 4 new sequenced species (specifically *Hylobates pileatus*, *Colobus guereza*, *Saguinus midas* and *Nycticebus bengalensis*), the Hi-C read pair data were aligned to the genome (table S4); both duplicates and near-duplicates were removed, and read pairs that aligned to three or more locations were set aside. The Hi-C contacts were listed as input for 3d-dna. Then 3d-dna were used to correct misassemblies, serving to anchor, order and orient fragments of DNA based on Hi-C contacts to generate high quality scaffolds.

Genome completeness evaluation

The completeness of the newly assembled primate genomes was evaluated by Benchmarking Universal Single-Copy Orthologs (BUSCO, v3.0.2) (164) based on the mammalian single-copy orthologs (mammalia_odb9). In this study, >92% of BUSCO genes were completely annotated in each newly assembled genome, indicating that the genome sequence assemblies were of the highest quality (table S6).

Genome annotation

We performed repeat sequence and gene annotation for each *de novo* assembled genome. To further standardize the annotation results, we utilized the same method to re-annotate the downloaded primate assemblies except for human (*Homo sapiens*).

Repeat annotation

Transposable elements (TEs) were identified in each genome by means of an integration of homology-based and *de novo* approaches. We used RepeatMasker (v4.0.6) (<http://www.repeatmasker.org/>), TRF (v4.07) (165), and RepeatModeler (v1.0.8) (<http://www.repeatmasker.org/RepeatModeler/>) to identify repetitive sequences for each genome. Genome sequences were aligned to RepBase (v21.11) (<https://www.girinst.org/repbase/>) through RepeatMasker (v4.0.6), and then each hit was further subclassified into a specific category. Tandem repeats, which are defined as DNA sequences containing >2 adjacent copies, were identified using TRF (v4.07) (165) using the default parameters. At the protein level, RepeatProteinMask, an updated program in RepeatMasker (v4.0.6), was used to perform RMBlast against the TE protein database. In addition, RepeatModeler (v1.0.8) was employed to build a *de novo* repeat library based on each genome. Using this library as a database, RepeatMasker (v4.0.6) was run to identify repeats in each genome. All identified repeat elements were classified into diverse categories (DNA, LINE, SINE, LTR and Unknown) according to the classification generally employed in repeat databases. Repeat annotations were combined into a non-redundant repeat annotation for each genome. In total, we predicted that ~40.55% of bases in each primate genome are derived from TEs (table S15).

Protein-coding gene annotation

In order to predict a gene set for each genome, we employed a number of different methods and integrated the diverse results obtained. In total, we obtained ~20,000 genes for each species (table S7). Homologous proteins from well-annotated mammalian genomes including mouse (*Mus musculus*, GRCm38), human (*Homo sapiens*, GRCh38), chimpanzee (*Pan troglodytes*, GCF_002880755.1), gorilla (*Gorilla gorilla*, GCA_900006655.3) and orangutan (*Pongo abelii*, GCA_002880775.3) were mapped to each primate genome using TBLASTN (v.2.2.26) (<https://blast.ncbi.nlm.nih.gov/Blast.cgi>) (166) with an E-value cutoff of 1e-5. In addition to human (*Homo sapiens*, GRCh38) and mouse (*Mus musculus*, GRCm38), these great ape species with high genome assembly and annotation quality were often used as reference annotation resources applied for the annotation of genomes of other different primate groups [e.g., the Chinese rhesus macaque (*Macaca mulatta*) (120) and African mico monkey (*Cercopithecus mico*) (27) in Old World monkeys]. Together with a relatively small divergence time for Crown Primates (appearing at ~66.36 million years ago), gene annotations should be largely conserved across primate species. Therefore, we concluded that these species could be used as references for homologous annotations in this study. Multiple adjacent hits from the same protein were then linked together using genBlastA (v1.0.4) (167) in order to obtain the candidate gene boundaries. The aligned sequences as well as their query proteins were filtered and passed to GeneWise (v.2.4.1) (168) to search for accurately spliced alignments. We randomly selected 1,000 high score homology-based genes to train Augustus (v3.0.3) (169) for *de novo* prediction on the repeat N-masked genome with default parameters.

Single CDS genes < 300bp or multiple-CDS genes < 150bp were filtered out. Homology annotation results were first merged to generate a homology gene set. One best gene model was retained for each locus according to the GeneWise score. Finally, results obtained by means of these methods were merged into a non-redundant gene set. In brief, the homologous annotation was first used as a backbone and the *de novo* annotation was merged into it, thereby providing the additional CDS information. Genes from the *de novo* annotation that failed to overlap with genes from the homology annotation were aligned to Swiss-Prot (v2019_03) (<https://www.uniprot.org/>) and InterPro (v68.0) (<http://www.ebi.ac.uk/interpro/>) (170). Only genes that aligned to these databases and had multiple CDS were retained to be merged into the final gene set.

SM Text 3. Primate phylogeny analysis and divergence time

Primate phylogeny analysis

Whole genome alignments

We performed whole genome alignments across all 52 species representing 27 newly assembled primate species (table S1), 22 downloaded primate species (table S8), one long-read genome from *Nycticebus pygmaeus* reported in an accompanying paper (32), and two outgroup species, Sunda flying lemur (*Galeopterus variegatus*) and Chinese tree shrew (*Tupaia belangeri chinensis*) (table S8). First, the pairwise whole genome alignments were obtained between human (*Homo sapiens*) and each of the other species using LASTZ (v1.04.00) (<https://www.geneious.com/plugins/lastz-plugin/>) with the parameter settings ‘--step=19 --hspthresh=2200 --inner=2000 --ydrop=3400 --gappedthresh=10000 --scores=birdMatrix --format=axt’. The Chain/Net was performed by axtChain with parameters ‘-minScore=5000, -linearGap=loose’. Multi-way alignments across all species were generated using MULTIZ (v11.2) (171) by merging MAF files sequentially according to phylogenetic distance. Closely related species in one group were respectively merged, and then MAF files from all groups were merged into one. Segments in the final merged MAF file that were lacking more than five species were discarded; then, all segments were concatenated by means of an in-house script. In total, we generated final alignments containing ~433.51 Mbp for all 52 species (table S9).

Whole genome tree

The whole genome alignments of 50 primate genomes and two outgroup genomes (Sunda flying lemur and Chinese tree shrew) were utilized to construct the whole genome tree. Exascale Maximum Likelihood (ExaML) (v3.0.14) is relatively new code for large-scale phylogenetic analyses on supercomputers, and both addresses and provides generally applicable solutions to several performance bottlenecks in parallel phylogenetic likelihood calculations (34). In total, ~433.51 Mbp of syntenic

orthologous sequences was obtained from whole genome alignments across 52 species. These data were concatenated and used to construct the complete genome trees using ExaML (v3.0.14) (34) (<https://github.com/stamatak/ExaML>) under the GAMMA model run 100 times. The tree with the highest likelihood was selected as the final tree (Figs. 1 and S4).

Coalescent-based genome tree inference

Standard concatenation approaches may do not completely model the discordance among gene trees beyond differences in sequence evolution rates (172). Previous studies have also shown that the incomplete lineage sorting (ILS) could lead to incorrect topology, possibly due to estimation bias in concatenated analyses where the mixture of gene trees represents a model violation (173). These possible limitations can theoretically be overcome with multispecies coalescent methods using e.g., ASTRAL (174).

Therefore, we used IQ-TREE (v1.6.12) (<http://www.iqtree.org/>) to generate 28,034 trees for each 5 kbp window with the window interval of 50 kbp across the whole genome alignments of 52 species. Then all trees were parsed by ASTRAL (v5.5.4) to obtain the coalescent-based consensus species tree (Fig. S5).

Identification of pair-wise orthologous genes

Pair-wise orthologous genes were identified between human (*Homo sapiens*, GRCh38), each of the other primate species and the outgroup species, the Chinese tree shrew (175), based on criteria including reciprocal best blastp hit (RBH), gene synteny and genome synteny.

We first selected syntenic gene pairs and genomic syntenic regions using pair-wise genome alignments between human and other species. For each gene pair, we further calculated the synteny ratio of the two genes respectively (the length of the coding region overlapping with the syntenic region/total length of the coding region). The synteny ratio for each gene should be $\geq 30\%$. The alignment rate for a pair of genes is the length of aligned sequence of the genes/the shortest gene length. The alignment rate should also be $\geq 30\%$. Then, we filtered out those gene pairs without gene synteny. Two gene pairs on an identical chromosome/scaffold should meet the requirement that the number of genes between the two gene pairs is less than 5. Where there was only one gene pair on the chromosome/scaffold, the gene pair was retained for further analyses. Finally, we obtained those pair-wise orthologous genes meeting these criteria including reciprocal best blastp hit (RBH), gene synteny and genome synteny. Orthologous pairs from different comparisons were merged across 52 species including 50 primate species and two outgroup species, the Sunda flying lemur and Chinese tree shrew (175).

In total, 10,185 orthologous genes were identified across 52 species including 50 primate species and two outgroup species, the Sunda flying lemur and Chinese tree shrew (175), when permitting a species-missing threshold of ≤ 5 .

Orthologous protein-coding gene tree

10,185 one-to-one orthologous genes were co-shared among 52 species including 50 primate species, Sunda flying lemur, and the Chinese tree shrew (175) when we permitted a species-missing threshold of ≤ 5 . For each species, a “–” symbol was inserted if the locus could not be aligned to the human genome.

Then, 10,185 one-to-one orthologous genes across 52 species were concatenated to generate a supergene sequence, which was used for the construction of a phylogenetic tree. Orthologous gene trees were constructed using RAxML (v8.2.12) (176) with 100 bootstrap replicates under the GTRGAMMA model. The resulting tree with the highest likelihood score was selected as the best tree (Fig. S6).

Exon codon tree with 1st and 2nd positions

Considering the composition heterogeneity of different codon positions, we further partitioned the orthologous gene sequences into 1st, 2nd and 3rd codon positions. Then, the positions with codon 1st and codon 2nd for 10,185 one-to-one orthologous genes were further concatenated into a super-sequence to generate the exon codon tree with 1st and 2nd positions. The concatenated super-sequence from exon codons with 1st and 2nd positions was employed to generate the exon codon ML tree with 1st and 2nd positions using RAxML (v8.2.12) (176) with 100 bootstrap replicates under the GTRGAMMA model (Fig. S7).

Fourfold degenerate site tree

The 4d-sites of 10,185 one-to-one orthologous genes were extracted using our in-house scripts. All 4d-sites of orthologous genes were obtained and concatenated to construct ML trees based on RAxML (v8.2.12) (176) with 100 replicates for nodal supports under the GTRGAMMA model (Fig. S8).

Conserved non-exonic element tree

We first filtered the 52-way primate genome alignments and at least 90% of the species were presented in the alignments. The 4d-sites were employed to extract MAFs from the 52-way primate genome alignments. We employed the phyloFit program in PHAST (v1.5) (177) to estimate the non-conserved model. Then, we ran the phastCons program in PHAST (v1.5) (177) with the primates’ non-conserved model to create the primates’ conserved models with the option ‘--estimate-rho’. The highly conserved elements were predicted in primates using the phastCons program in PHAST (v1.5) with options ‘--most-conserved –score options’. Eventually, we identified 1,309,699 HCEs with an average length of 147 bp and a total length of 192 Mbp.

We generated the conserved non-exonic elements by excluding exon regions from highly conserved elements and finally obtained 1,118,099 conserved non-exonic elements with a total length of 156.9 Mbp and an average length of 140 bp.

These conserved non-exonic element data, generated across 52 species, were then concatenated and used to construct the conserved non-exonic element tree using

ExaML (v3.0.14) (34) (<https://github.com/stamatak/ExaML>), under the GAMMA model and run 100 times. The tree with the highest likelihood was selected as the final tree (Fig. S9).

Primate divergence time evaluation

To evaluate precisely the divergence times in primates, we added a further two outgroup species genomes, specifically the domestic cat (*Felis catus*; v9.0.97) and the pig (*Sus scrofa*; v11.1.97) from Ensembl 97 (<http://jul2019.archive.ensembl.org/index.html>) to our previous whole genome alignments across 52 species based on the identical pipeline above. Taken together, we obtained whole genome alignments of 54 species including 50 primate species and 4 outgroup species.

Then, our whole genome alignments across 54 species and utilized the MCMCTree program in PAML (v4.9) (<http://abacus.gene.ucl.ac.uk/software/paml.html>) (40) to infer the primate divergence times. Eleven fossils from Vanderpool *et al.* (39) and Perelman *et al.* (35) were used to calibrate the nodal divergence time, and the divergence time (~76-88 Mya) between primates and *Tupaia* was obtained from TimeTree (<http://www.timetree.org/>). The dating of eleven fossils (35, 39) was listed as follows: “(5.7, 10) Mya for the most recent common ancestor (TMRCA) of *Homo-Pan*; (14, 34) Mya for TMRCA of Hominidae; (3.5, 4.5) Mya for TMRCA of the Theropithecus clade; (6, 8) Mya for TMRCA of Papionini; (25, 34) Mya for TMRCA of Catarrhini; (36, 50) Mya for TMRCA of Simiiformes; (20.5, 26.5) Mya for TMRCA of Platyrrhini; (37, 43) Mya for TMRCA of galagids and lorisids; (38, 56) Mya for TMRCA of Strepsirrhini; (55.8, 65.8) Mya for TMRCA of Primate; (61, 165) Mya for TMRCA of Primatomorpha” (Fig. S11).

SM Text 4. Structural evolution of primate genomes

Karyotype evolution

Karyotype evolution is involved in many aspects of biology e.g. speciation and genome evolution (42, 43). In this primate genome project, a mass of species-sampling genomes of high quality (from Pacific Biosciences and Oxford Nanopore Technology platforms) allowed us to accurately explore the evolution of primate karyotypes.

Here, we utilized the human genome (*Homo sapiens*; GRCh38) as a reference to reconstruct the ancestral nodal karyotype in primates. First, we selected 37 primate genomes with scaffold N50 \geq 13 Mbp (table S10) as inputs. Then we used the DESCHRAMBLER algorithm (<https://github.com/jkmlab/DESCHRAMBLER>), Chains and Nets generated by LASTZ (v1.04.00) (178) (<https://www.geneious.com/plugins/lastz-plugin/>) to generate conserved syntenic fragments across 37 species (table S10). Syntenic fragments of length \geq 500 kbp were used to build the conserved syntenic fragments. Finally, the structures of ancestral

genomes were constructed by using ANGES (v1.01) (179) across ancestral nodes in phylogenetic tree: Primates, Strepsirrhini, Simiiformes, Platyrrhini, Catarrhini, Cercopithecoidea, Hominoidea, Hominidae, Hylobatidae, Homininae, *Pongo*, Hominini and *Pan* (Fig. 2). GRIMM (v2.01) (180) was utilized to analyze genome rearrangements (e.g. chromosome reversals, fusions, fissions, translocations) from ancestral genomes to next nodal genomes.

We further investigated the karyotype changes from primate common ancestor to human (*Homo sapiens*; GRCh38). The different colors represent different chromosomes in human (*Homo sapiens*; GRCh38), whilst the gray lines denote the movement of genome markers from ancestral nodes to next nodes (Fig. 2).

Evolution of segmental duplications

Segmental duplications are DNA fragments longer than 1 kbp, distributed within and between chromosomes and sharing more than 90% identity at the DNA sequence level (181-183).

In this study, we considered segmental duplications of length ≥ 5 kbp and identity $>90\%$. We selected 39 well-assembled genomes with a high scaffold N50 and a genome of flying lemur and used ASGART (v2.3) (184) to predict segmental duplications for each species (table S11). Pairwise whole genome alignments with reciprocal best hit using human (*Homo sapiens*; GRCh38) as reference were produced. Then lineage-specific segmental duplications were further grouped according to genome synteny criteria. All segmental duplications were grouped based on their co-shared sequence homology. For lineage-specific SDs, they were required to meet the following conditions: firstly, these segmental duplications had to be found only in species from the identical group although they were missing from other groups; secondly, the number of species in the group had to be greater than a certain threshold (table S12).

Comparative genomics analyses of genome sizes and transposable elements in primates

Genome size analyses in different evolutionary clades of primates

In this study, we integrated 27 newly assembled primate genomes and 23 downloaded genomes. The primate genome sizes ranged from ~2.12 Gbp (*Lemur catta*) to ~3.29 Gbp (*Pan paniscus*, GCA_000258655.2). Thus, we found an average primate genome size of ~2.85 Gbp, which is larger than that of Ruminants (~2.7 Gbp), Chiroptera (~2.35 Gbp) and Carnivora (~2.3 Gbp) (48, 49).

Then, we further compared the heterogeneity of genome sizes for different evolutionary clades of primate including Hominoidea, Old World monkeys, New World monkeys, lemurs [*Microcebus murinus* (GCA_000165445.3), *Prolemur simus* (GCA_003258685.1), *Lemur catta*], and *Daubentonia madagascariensis* (newly assembled genome in this study)], and Lorisiformes [*Loris tardigradus* (newly assembled genome in this study), *Nycticebus pygmaeus* (32), *Nycticebus bengalensis*

(newly assembled genome in this study), *Galago moholi* (newly assembled genome in this study), and *Otolemur garnettii* (GCA_000181295.3)] (Fig. S16A). *P* values for genome size differences of evolutionary clades in primates were calculated by the Mann-Whitney U test.

Evolution of transposable elements

Transposable elements (TEs) have played important roles in the evolution of genomes and phenotypes (185-187). In this study, we found significant differences in genome size between the lemurs and other primate evolutionary clades (e.g. Lorisiformes, New World monkeys, Old World monkeys, Hominoidea) by Mann-Whitney U test (*P* < 0.05), due to differences in the relative representation of TEs in the genomes (Figs. S16 and S17). According to TE annotations, we subdivided TEs into the categories DNA, LINE, SINE, LTR, Other and Unknown classes (table S15). The 67 TEs with highest percentage content in 50 primate genomes and the outgroup species genome are given in Fig. S18. The statistical difference analysis of TE percentage content for different primate clades was performed by the Mann-Whitney U test (*P* < 0.05) (Figs. S16 and S17).

According to the TE annotations for each species [Chinese tree shrew (*Tupaia belangeri chinensis*; <http://www.treeshrewdb.org>) as an outgroup] in this study, we extracted all Alu sequences from the primate and Chinese tree shrew genomes. Next, CD-HIT (188) with parameters “-c 0.8 -n 5 -d 0 -M 16000 -T 10” was used for Alu clustering analysis of each species. Finally, where there were three or more Alu sequences in this cluster, we selected the longest Alu sequence as the consensus sequence. For each species, the Alu consensus sequences obtained above were applied as the library, and RepeatMasker (v4.0.6) (<http://www.repeatmasker.org/>) was used to annotate the Alu transposons in the corresponding species.

We calculated the Alu insertion times for primate (Fig. S19) and tree shrew genomes using the algorithm $T = K/2r$, where K is the Kimura distance-based copy divergence of TEs and r is the nucleic acid substitution rate. The K -value was obtained from RepeatMasker (v4.0.6) (<http://www.repeatmasker.org/>). To estimate r -values for primate and tree shrew, we used the alignments of LASTZ (v1.04.00) (178) and MULTIZ (v11.2) (171) along with genomes in our evolutionary analyses, with the human genome as the reference sequence. With the whole-genome alignments, we used the MSA view tool in PHAST (v1.2.1) (177) to extract 4d-site alignments based on the human gene annotations. The phyloFit program in PHAST (v1.2.1) (177) was used to estimate the phylogenetic model, with tree topology (our primate phylogeny analyses) as an input parameter. The branch length results were represented in units of substitutions per site. We calculated the root-to-tip substitution rates from the most recent common ancestors in clades to each lineage, and then divided the root-to-tip substitution rates by the divergence time between the Chinese tree shrew and the most recent common ancestor of primates in this study.

Comparative analyses of the nucleotide substitution rates in primates

The nucleotide substitution rates determined in different primate lineages have exhibited heterogeneity as a consequence of the limited genomic data available from primates (35, 56). In this study, a considerable number of high-quality primate reference genomes from long-read sequencing platforms (Pacific Biosciences and Nanopore PromethION) allowed us to arrive at a robust assessment of the nucleotide substitution rates along diverse primate lineages on a genome-wide scale.

In this study, the nucleotide substitution rates (in units of substitutions per site per million years) in primate genomes were estimated by comparisons of the fourfold degenerate (4d) sites in coding regions and divergence times between primate species (Figs. 3C, S21 and table S16). Then, the nucleotide substitution rates of different evolutionary primate clades were analyzed comparatively by box plotting (Figs. 3C and S21). Our comparative analyses involved different evolutionary clades of primates including great apes (here representing the Hominidae), gibbons, Old World monkeys, New World monkeys, Strepsirrhini, lorises (Lorisidae) (including *Loris tardigradus*, *Nycticebus pygmaeus* and *Nycticebus bengalensis* in this study), Hominoidea, Catarrhini, Simiiformes, Haplorrhini, lemurs (Chiromyiformes+Lemuriformes) and lorisoids (Lorisiformes) (including *Loris tardigradus*, *Nycticebus pygmaeus*, *Nycticebus bengalensis*, *Galago moholi* and *Otolemur garnettii*).

Evolutionary analyses of protein-coding genes in primates

Based on 10,185 identified orthologous genes across 52 species including 50 primates and two outgroup species, Sunda flying lemur (*Galeopterus variegatus*) and Chinese tree shrew (*Tupaia belangeri chinensis*; TreeshrewDB v2.0; <http://www.treeshrewdb.org>) by methods including RBH, gene synteny and genome synteny (See the section—**SM Text 3. Primate phylogeny analysis and divergence time: Identification of pair-wise orthologous genes**) and primate species tree (Fig. 1) in this study, we explored the evolutionary constraints operating on coding regions for each orthologous gene. To this end, we calculated the dN/dS ratio [rates of nonsynonymous (dN) to synonymous (dS) substitutions] of each orthologue by the codeml program in PAML (v4) (40) under a free-ratio model. Meanwhile, the codeml algorithm under a free-ratio model could also give other evolutionary parameters (i.e., N, S, dN, dS, N*dN, and S*dS) for each orthologous gene along with all branches in primates.

Next, we characterized the evolutionary rates of tissues by following tissue-specific genes in different evolutionary nodal lineages across the primate phylogeny. Previous studies have indicated that the expression patterns of tissue-specific expressed genes are conserved during mammalian evolution (63, 64). Therefore, in this study, we downloaded the gene expression matrix of 30 tissues from 7,862 human samples from the Genotype-Tissue Expression (GTEx) project (189) (<https://commonfund.nih.gov/GTEx/>). We were then able to utilize the tissue-specific expressed genes of human (GRCh38) to infer the evolutionary rates of diverse tissues

across different evolutionary lineages in primates. The evolutionary rate of each tissue for each branch was obtained by the median of the dN/dS values for tissue-specific expressed genes (Fig. 3D).

We identified tissue-specific expressed genes for each tissue based on t-statistics in human (GRCh38) according to a previous study (63). Briefly, we performed t-statistics on single-copy orthologous genes between the target tissue samples and all other samples, and then ranked the t-values from high to low. According to the ranking, the top 5% of genes based on *t*-values were defined as tissue-specific expressed genes in human (GRCh38).

SM Text 5. Genomic features and phenotypic adaptations in primate evolution

Identification of positively selected genes in crucial primate evolutionary nodes

The 10,185 orthologous genes among 52 species, including 50 primates and two outgroup species (Sunda flying lemur and Chinese tree shrew), were identified by a combination of methods including RBH, gene synteny and genome synteny (See the section—**SM Text 3. Primate phylogeny analysis and divergence time: Identification of pair-wise orthologous genes**).

The orthologous gene coding sequences across these species were aligned by MUSCLE (v3.8.31) (190) and the low-quality aligned regions were further trimmed by Gblocks (v0.91b) (191, 192) with the parameters “./Gblocks \$i -t=c -b4=5”. The aligned orthologous genes with CDS length < 100 bp were removed for our downstream evolutionary analyses. Based on our reliably constructed species-guided tree topology (Fig. 1), the branch-site model in PAML (v4) (40) and the likelihood rate test (LRT) between null hypothesis and alternative hypothesis were utilized to detect positively selected genes with $P < 0.05$ (χ^2 test) in crucial evolutionary lineages of primates among the single-copy orthologous genes. The Bayes empirical Bayes algorithm in PAML (v4.4) (40) was applied to calculate the posterior probabilities of inferred positively selected sites. Thus, we inferred the positively selected genes in 14 crucial evolutionary lineages including the ancestral branch of Strepsirrhini, the ancestral branch of Haplorrhini, the Western tarsier lineage, the ancestral branch of Simiiformes, the ancestral branch of New World monkeys (Platyrrhini), the ancestral branch of Catarrhini, the ancestral branch of Old World monkeys (Cercopithecoidea), the ancestral branch of Colobinae, the ancestral branch of Hominoidea, the ancestral branch of Hominidae, the ancestral branch of Hylobatidae, the ancestral branch of Homininae, the ancestral branch of Hominini (*Homo-Pan*), and the Human lineage.

To infer the positively selected genes of the common ancestral branch of Primates, together with Chinese tree shrew, we also added five extra outgroup genomes, namely Sunda flying lemur (*Galeopterus variegatus*, NCBI project id: PRJNA399345), mouse (*Mus musculus*, GRCm38.p6), domestic cat (*Felis catus*; v9.0.97), domestic dog (*Canis lupus familiaris*; CanFam3.1) and pig (*Sus scrofa*; v11.1.97) from Ensembl 97

(<http://jul2019.archive.ensembl.org/index.html>) to the identifications of orthologous genes among 56 species based on the identical pipeline including RBH, gene synteny and genome synteny (See the section—**SM Text 3. Primate phylogeny analysis and divergence time: Identification of pair-wise orthologous genes**). We identified 9,907 orthologous genes among 56 species including 50 primates and 6 outgroup species. According to the consistent pipeline for the identification of positively selected genes, we inferred the potential positively selected genes along with the common ancestral branch of primates.

In total, we inferred the positively selected genes from 15 evolutionary lineages for primates, and these positively selected genes were checked manually for their sequence alignments.

Evolutionary analyses of gene families in primates

Identification of gene families in primates

DNA and protein data for 5 outgroup species, specifically mouse (*Mus musculus*, GRCm38.p6), dog (*Canis lupus familiaris*; CanFam3.1), pig (*Sus scrofa*; v11.1.97), Sunda flying lemur, and Chinese tree shrew, were obtained from the Ensembl (v97) and TreeshrewDB (v2.0) (175) databases. Meanwhile, 27 newly assembled primate genomes (table S1), one long-read genome from *Nycticebus pygmaeus* reported in an accompanying paper (32), and 22 downloaded primate genomes (table S8) were integrated into our analyses of gene families. For those genes with alternative splicing variants, the longest transcripts were selected to represent the genes. In this study, we used the TreeFam algorithm (193) (<http://www.treefam.org>) to define a gene family as a group of genes that descended from a single gene in the last common ancestor of the species considered. The specific screening pipeline was similar to a previous study (194) as follows: 1) Blastp (166) was applied to all protein sequences against a database containing a protein dataset of all species with an e-value of 1e-07 and conjoined fragmental alignments for each gene pair. We assigned a connection (edge) between the two nodes (genes) if more than 1/3 of the region aligned to both genes. An Hscore that ranged from 0 to 100 was used to weigh the similarity (edge). For two genes (G1 and G2), the Hscore was defined as a score $(G1G2)/\max(score(G1G1), score(G2G2))$ (the score here is the raw Blast score). 2) Extraction of gene families (clustered by Hcluster_sg). We utilized the average distance for the hierarchical clustering algorithm requiring the minimum edge weight (Hscore) to be larger than 5, and the minimum edge density (total number of edges/theoretical number of edges) to be larger than 1/3.

In total, we identified 22,174 gene families among 55 species in this study for the downstream analyses.

Expansions of gene families in primates

After using the Treefam algorithm (193) to construct gene families from among 55 species, including 50 primates and 5 outgroup species, we further ascertained the

expansions of gene families for some crucial evolutionary nodes in primates. Computational Analysis of gene Family Evolution (CAFE) is a tool for the statistical analysis of the evolution of gene family size (195). If the copy number of the gene family in the detected branch lineage was higher than that of its most recent common ancestral branch lineage, then the gene family was defined as being substantially expanded in the detected branch lineage, according to the output of the CAFE (195) algorithm.

In order to compare the copy number variations of gene families across different evolutionary clades and to infer the significantly expanded gene families in specific clades, we used an unpaired *t*-test to determine the significance of differences in copy number for different nodes. Each of the target groups (the targeted evolutionary clades) and the contrast groups (all other remaining clades) should contain at least 3 species. Briefly, our identification of significantly expanded gene families in specific nodes had to meet the following rigorous screening procedures:

1) The *P* values of expanded gene families in specific clades using the unpaired *t*-test had to be less than 0.05. Further, the *P* values were corrected by Benjamini-Hochberg false discovery rate (FDR) (196) and had to be ≤ 0.05 .

2) For the targeted evolutionary clade, the average copy number of gene families from all species had to be more than 4 times that of the control clades (other remaining clade species) ($\text{Log}_2(\text{targeted clade}/\text{control clades}) \geq 2$). If the average copy number of the gene families in the control clades was equal to zero while the copy number of the gene families in the targeted clade was greater than zero, then the gene families were regarded as potential candidates for expansion in the specific evolutionary clade.

Thus, we inferred the significantly expanded gene families in the 13 evolutionary nodes for primates. These evolutionary nodes included the ancestral branch of the Primates, the ancestral branch of the Haplorrhini, the ancestral branch of the Strepsirrhini, the ancestral branch of the Simiiformes, the ancestral branch of the New World monkeys, the ancestral branch of the Catarrhini, the ancestral branch of Old World monkeys, the ancestral branch of the Colobinae, the ancestral branch of the Hominoidea, the ancestral branch of the Hominidae, the ancestral branch of the Hylobatidae, the ancestral branch of the Homininae, and the ancestral branch of the Hominini (*Homo-Pan*) (Fig. 4A).

Lineage-specific accelerated regions

Lineage-specific accelerated regions were identified from highly conserved elements in the 52-way primate alignments (See **SM Text 3. Primate phylogeny analysis and divergence time: Conserved non-exonic element tree**).

In order to find accelerated regions specific to certain subgroups, we estimated acceleration scores for the highly conserved elements using the phyloP program in PHAST (v1.5) (177) with the parameters “--method LRT, --branch and --mode ACC” for 12 selected subgroups. The significant acceleration at FDR adjusted p-values ≤ 0.05 was considered in further analyses. Lineage-specific accelerated regions in coding

regions and the Y chromosome were removed. The detailed screening pipeline is to be found in an accompanying paper (72).

Finally, according to gene annotations, we obtained the nearest genes to the lineage-specific accelerated regions (all located within 500kb of these genes) for each crucial evolutionary lineage. In all, we inferred the significant lineage-specific accelerated regions in 13 evolutionary nodes for primates. These evolutionary nodes represented the ancestral branch of the Haplorrhini, the ancestral branch of the Strepsirrhini, the ancestral branch of the Simiiformes, the ancestral branch of the New World monkeys, the ancestral branch of the Catarrhini, the ancestral branch of the Old World monkeys, the ancestral branch of the Colobinae, the ancestral branch of the Hominoidea, the ancestral branch of the Hominidae, the ancestral branch of the Hylobatidae, the ancestral branch of the Homininae, and the ancestral branch of the Hominini (*Homo-Pan*) and human (Fig. 4A).

Gene enrichment analysis

The Database for Annotation, Visualization and Integrated Discovery (DAVID) (v6.8) (197-204) (<https://david.ncifcrf.gov/>) was used to perform the gene function enrichment analysis, including Functional Category (e.g. UP_KEYWORDS), Gene Ontology (e.g. GOTERM BP DIRECT, GOTERM CC DIRECT, GOTERM MF DIRECT), Pathway (e.g., KEGG PATHWAY), and Tissue Expression (e.g., UP_TISSUE) for candidate gene lists under a current background *Homo sapiens* with a two-tailed corrected Fisher's Exact test ($P < 0.05$).

For a gene list (e.g., lineage-specific positively selected genes and genes associated with lineage-specific accelerated regions), the highly expressed genes in specific tissues (or tissue-specific highly expressed genes) were assigned according to the Tissue Expression Database (e.g., UP_TISSUE) in DAVID (v6.8) (197-204) under the annotation background of *Homo sapiens*.

SM Text 6. Primate demographic history analyses

We inferred the demographic history for 48 of 50 primate species by applying the pairwise sequentially Markovian coalescent model (PSMC) (151). For two species, specifically *Chlorocebus sabaeus* and *Piliocolobus tephrosceles*, the demographic history analyses were excluded because of the lack of short-read genome sequencing data for this study. To ensure the quality of consensus sequences, >46.8x clean short-read sequencing data for newly assembled genomes (table S3) and >30x clean short-read data for downloaded genomes (table S41) were used, respectively. For each species, we first excluded the contigs/scaffolds that were only aligned to the sex chromosomes of human, according to the 52-way whole genome alignments.

For each species, the short-read sequencing data were mapped to their reference genomes using BWA-MEM (v0.7.12) (205) with default parameters. Then, SAMtools (v1.3.1) (206) was used to sort and remove PCR duplicates. Alignments around indels

were realigned using the indelRealigner program in GATK (v2.6.5) (207). After obtaining the bam files, the average depth statistics were calculated for each alignment using BEDTools (v2.26.0) (208) and an in-house script. SNPs were identified using BCFtools (v1.9) (<https://samtools.github.io/bcftools/>) and then filtered for proximity to indels (--SnpGap 6) and depth (1/3 average depth \leq DP \leq 2 * average depth) using the BCFtools filter. Indels were removed from the final output (-v snps) using the BCFtools view. A diploid consensus genome sequence was generated using the "vcfutils.pl vcf2fq" function in BCFtools (v1.9). We transformed the format of the consensus sequence by using fq2psmcfa (with the parameters: fq2psmcfa -q20). The generation times (g) of the different species were taken from the summary listing in table S41. The mutation rates per million years were estimated as given in table S16. The mutation rate per generation was estimated by multiplying the per year mutation rates by the generation time. The population size histories of 48 primates were displayed in Fig. S36. The genome-wide diversity for each species was calculated using VCFtools (v0.1.11) (209) (<http://vcftools.sourceforge.net>) with non-overlapping 50-kb (--window-pi 50000) based on the filtered individual SNP files. In order to reveal the dynamic trends of N_e across multiple species, we used a value of normalized N_e . The normalized N_e was calculated by dividing the real value of N_e at each time point by the maximum value for the same species throughout the timescale. Correlation analyses between N_e and nucleotide diversity were estimated by cor.test function (Pearson's product-moment correlation) in R (v3.5.0) after phylogenetic correction [Phylogenetic Independent Contrast (PIC)] using the ape library (<http://ape-package.ird.fr/>) in the R software.

Fig. S1. Hi-C interactions of chromosomes. Strong interactions are indicated in dark red, weak interactions in light red. The genomes of four species including *Hylobates pileatus*, *Colobus guereza*, *Saguinus midas* and *Nycticebus bengalensis* were assembled into chromosome levels in this study according to the previous method (28).

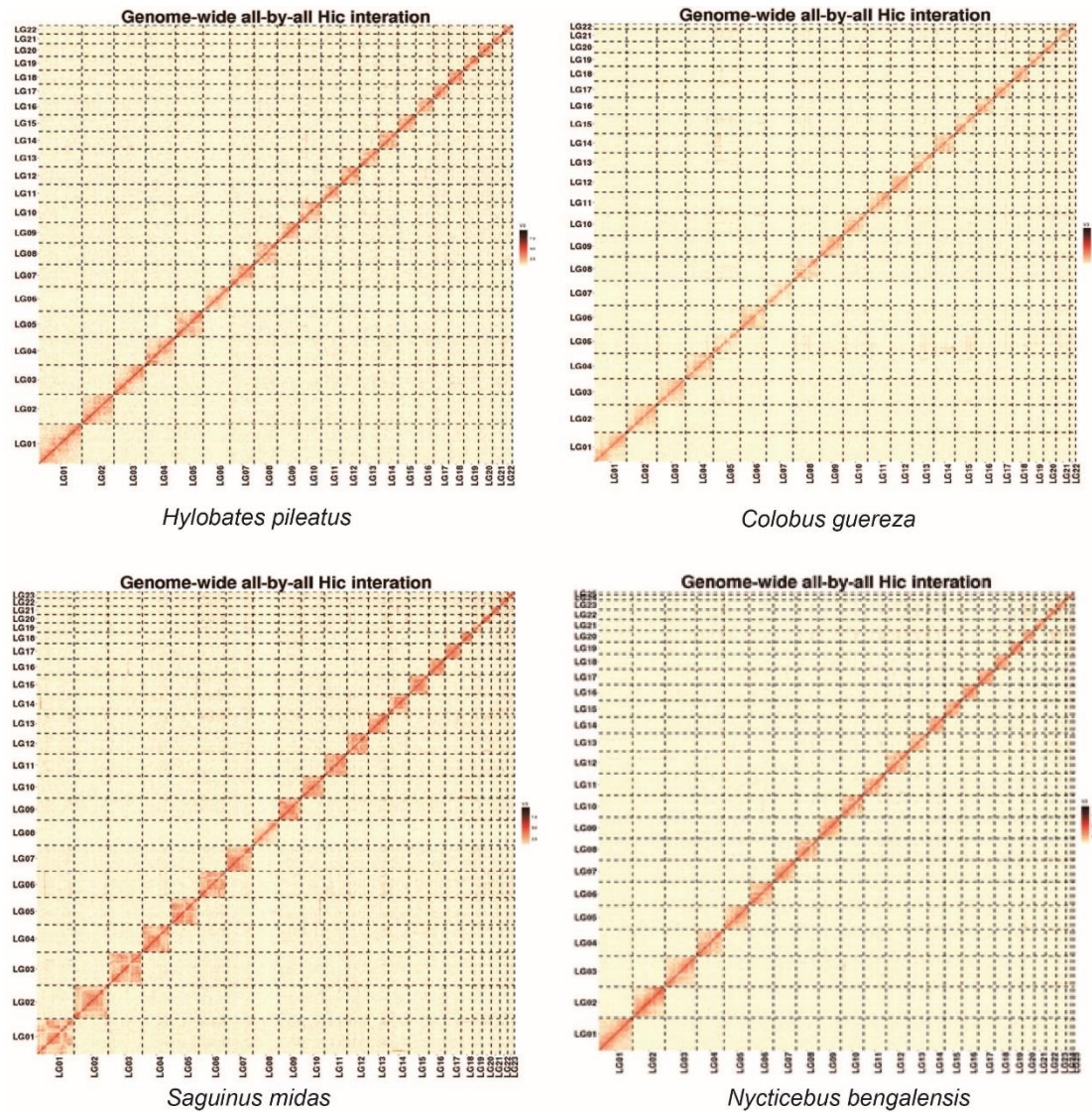


Fig. S2. Evaluation of genome size in primates using 17-Kmer analysis. X-axis represents the depth, whilst the y-axis represents the frequency.

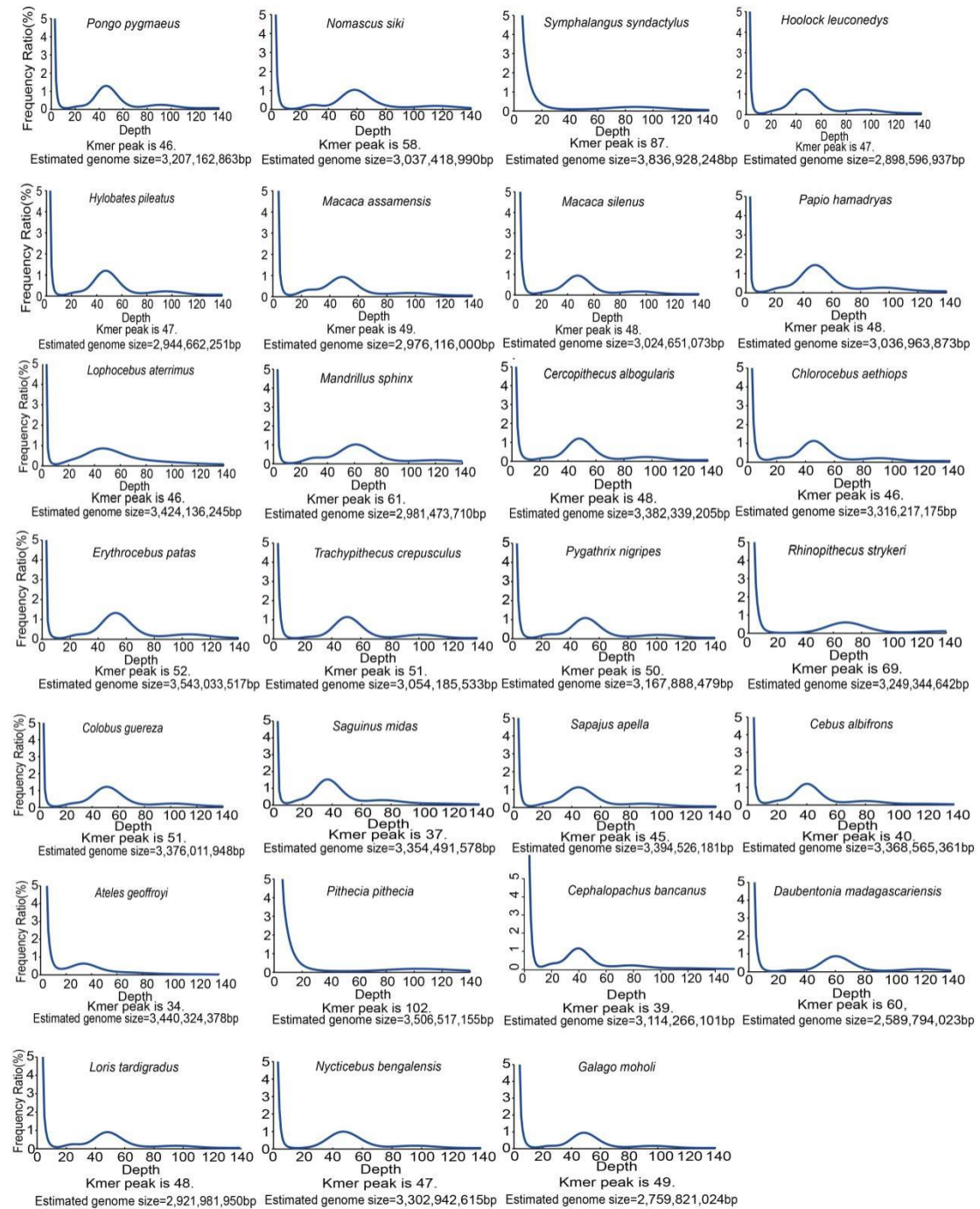


Fig. S3. Summary of primate-specific highly conserved elements. The distribution of primate-specific highly conserved elements is shown by using gene/genomic region partitions. These primate-specific highly conserved elements were divided into two categories (A and B) based on the CONS scores in homologous sequences in the outgroup species. The nine outgroup species were *Galeopterus variegatus*, *Tupaia belangeri*, *Mus musculus*, *Oryctolagus cuniculus*, *Sus scrofa*, *Felis catus*, *Canis familiaris*, *Phascolarctos cinereus* and *Ornithorhynchus anatinus*.

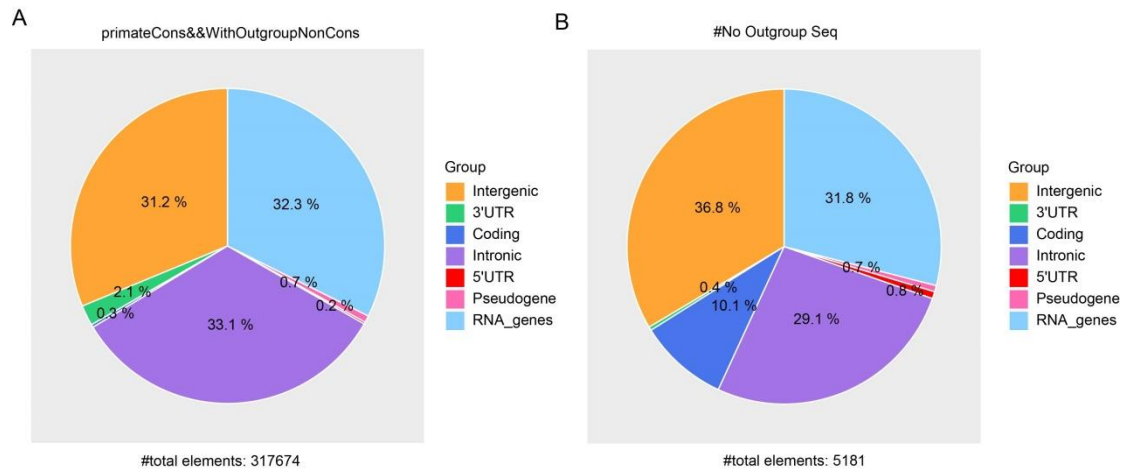


Fig. S4. Maximum likelihood whole-genome nucleotide evidence tree of primates estimated by ExaML. The whole genome alignments (~ 433.5 Mbp) of 52 species (50 primate species + flying lemur [*Galeopterus variegatus*] + tree shrew [*Tupaia belangeri*]) were used to construct a whole genome ML tree under a GTR+GAMMA model. The bootstraps with 100 replicates were applied to produce the nodal supports. The gibbon branches are highlighted by a pink box. The nodal support and branch length are shown respectively. The yellow and blue species names represent those genomes newly produced in this study. The genomes of the species marked in blue were assembled at the chromosome level.

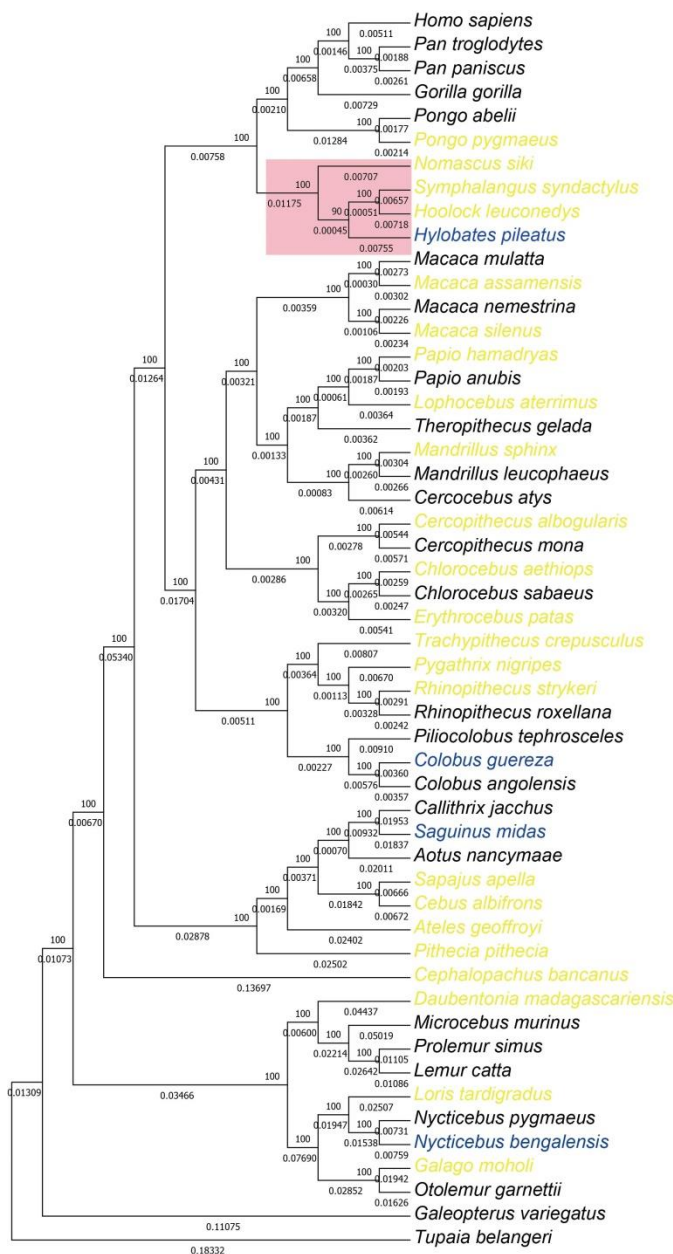


Fig. S5. Coalescent-based whole-genome nucleotide evidence tree estimated by ASTRAL. The whole-genome alignments of 52 species (50 primates+Sunda flying lemur+Chinese tree shrew) were used to construct the whole-genome coalescent-based ASTRAL tree. The bootstrap with 100 replicates was applied to produce nodal supports. The gibbon branches are highlighted by a pink box. The yellow and blue species names represent those genomes newly produced in this study. The genomes of the species marked in blue were assembled at the chromosome level.

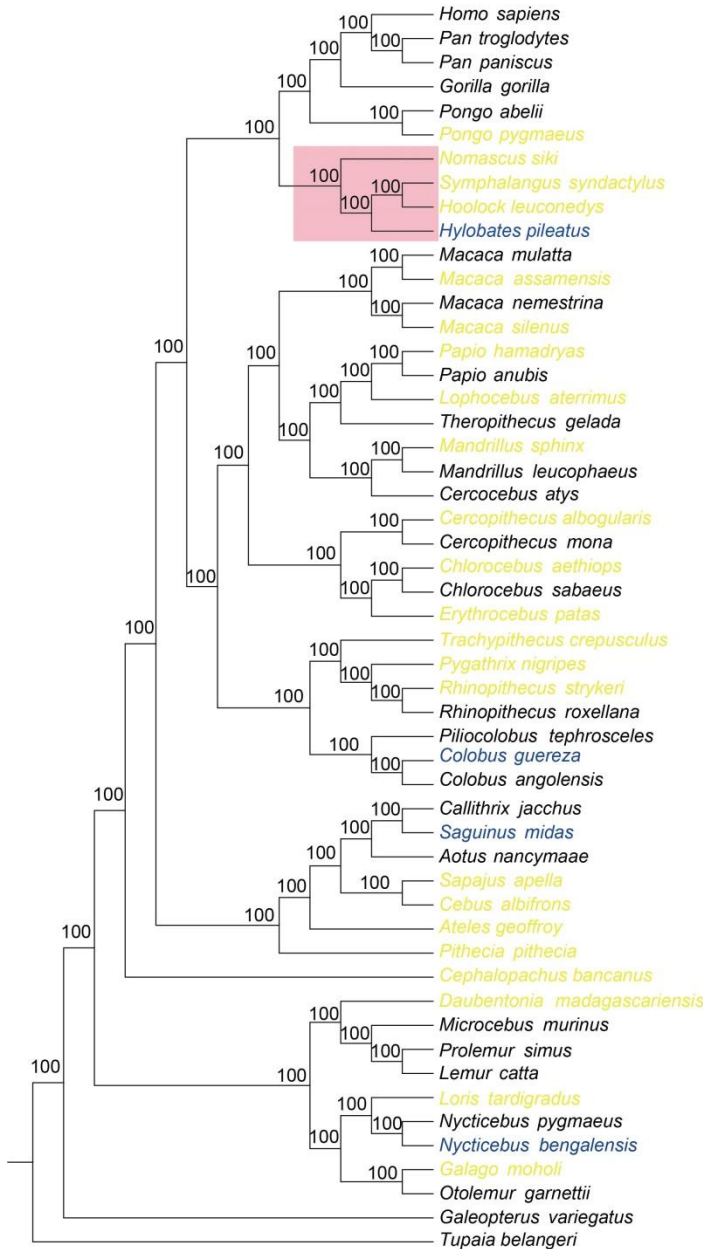


Fig. S6. Maximum likelihood phylogenetic tree of primates estimated using orthologous protein-coding genes. 10,185 orthologous genes among 52 species (50 primate species + flying lemur [*Galeopterus variegatus*] + tree shrew [*Tupaia belangeri*]) were obtained and concatenated into a single super gene to construct a ML tree based on RAxML under a GTR+GAMMA model. The bootstraps with 100 replicates were applied to produce nodal supports. The gibbon branches are highlighted by a pink box. The nodal support and branch length are shown respectively. The yellow and blue species names represent those genomes newly produced in this study. The genomes of the species marked in blue were assembled at the chromosome level.

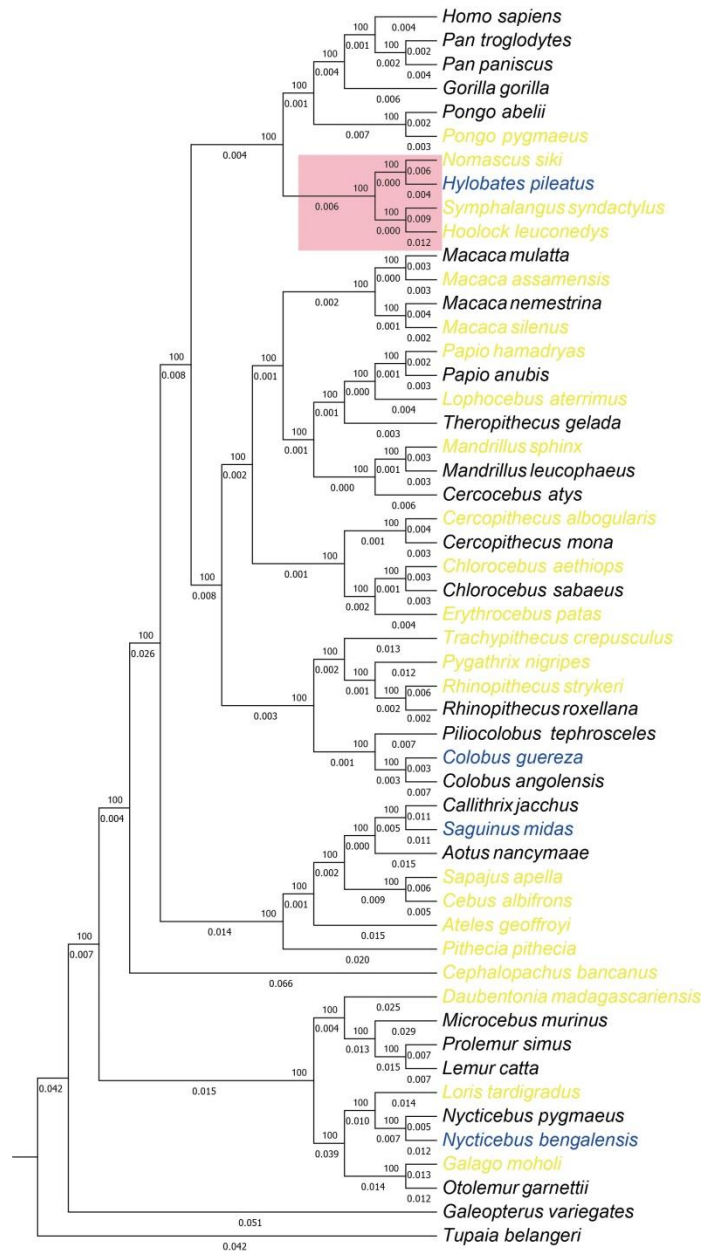


Fig. S7. Maximum likelihood phylogenetic tree of primates estimated using the exon codons with 1st and 2nd positions. The 1st and 2nd codon nucleotides of 10,185 orthologous coding genes were concatenated to construct a ML tree based on RAxML under a GTR+GAMMA model. The bootstraps with 100 replicates were applied to produce the nodal supports. The gibbon branches are highlighted by a pink box. The nodal support and branch length are shown respectively. The yellow and blue species names represent those genomes newly produced in this study. The genomes of the species marked in blue were assembled at the chromosome level.

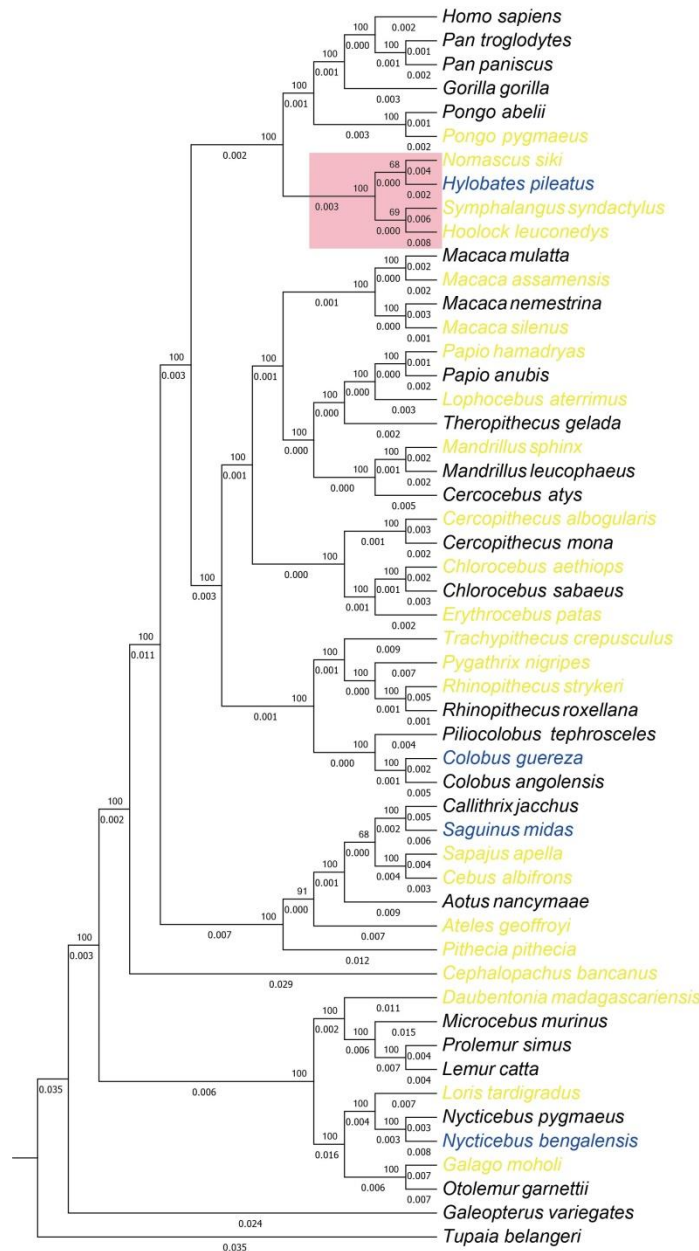


Fig. S8. Maximum likelihood phylogenetic tree of primates estimated using four-fold degenerate sites. The four-fold degenerate sites of 10,185 orthologous coding genes were extracted and concatenated to construct a ML tree based on RAxML with 100 replicates for nodal supports under a GTR+GAMMA model. The gibbon branches are highlighted by a pink box. The nodal support and branch length are shown respectively. The yellow and blue species names represent those genomes newly produced in this study. The genomes of the species marked in blue were assembled at the chromosome level.

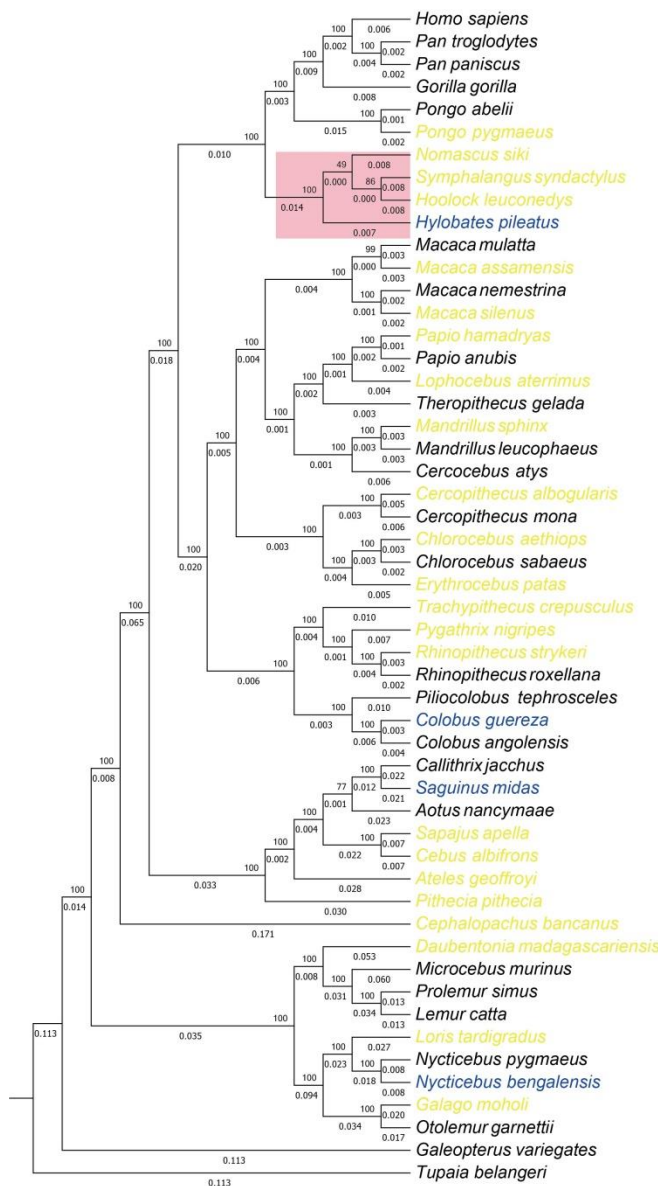


Fig. S9. Maximum likelihood phylogenetic tree of primates estimated using conserved non-exonic elements. The conserved non-exonic elements (~168.3 Mbp) were extracted and concatenated to construct a ML tree based on ExaML with 100 replicates for nodal supports under a GTR+GAMMA model. The gibbon branches are highlighted by a pink box. The nodal support and branch length are shown respectively. The yellow and blue species names represent those genomes newly produced in this study. The genomes of the species marked in blue were assembled at the chromosome level.

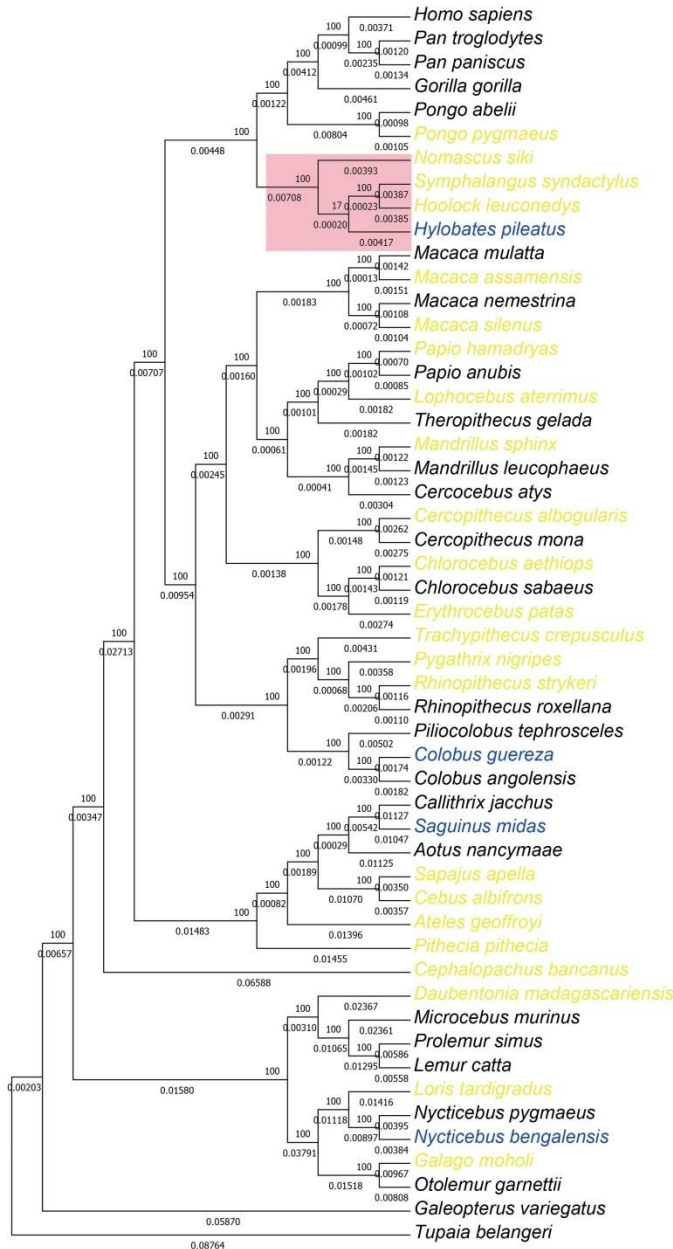


Fig. S10. CoalHMM runs of the two gibbon branches. CoalHMM can be used to infer the proportion of incomplete lineage sorting given three species and an outgroup. CoalHMM requires that the species topology (V0) is specified, so CoalHMM was run for all three possible species topologies as V0 per gibbon branch with human as an outgroup (see Rivas-González et al. for further details) (38). Each site in the alignment was then classified as belonging to V0 or to one of the deep coalescence topologies, namely V1 (which follows the same tree as V0), V2 and V3. V2 and V3 thus correspond to topologies that do not follow the species tree. The proportion of sites belonging to each of the four states is represented as bars in the above figure. The exact topology can be consulted in the color legend in Newick format, where species names have been abbreviated by taking the first three letters of the genus and the first three letters of the species name. The horizontal line and number correspond to the level of incomplete lineage sorting for that CoalHMM run, namely V2+V3. The figure shows that the leftmost panel is the one having the least amount of incomplete lineage sorting for both gibbon branches, which corresponds to specifying V0 as the species topology presented in this paper. Moreover, the incomplete lineage sorting proportion estimated by specifying the other topologies as V0 yields asymmetric V2/V3 proportions, with an excess of sites assigned to the topology presented in the paper (red and light blue respectively). All this indicates that incomplete lineage sorting favors the topologies presented in this paper for the gibbon branches, although we cannot discard ancient introgression completely.

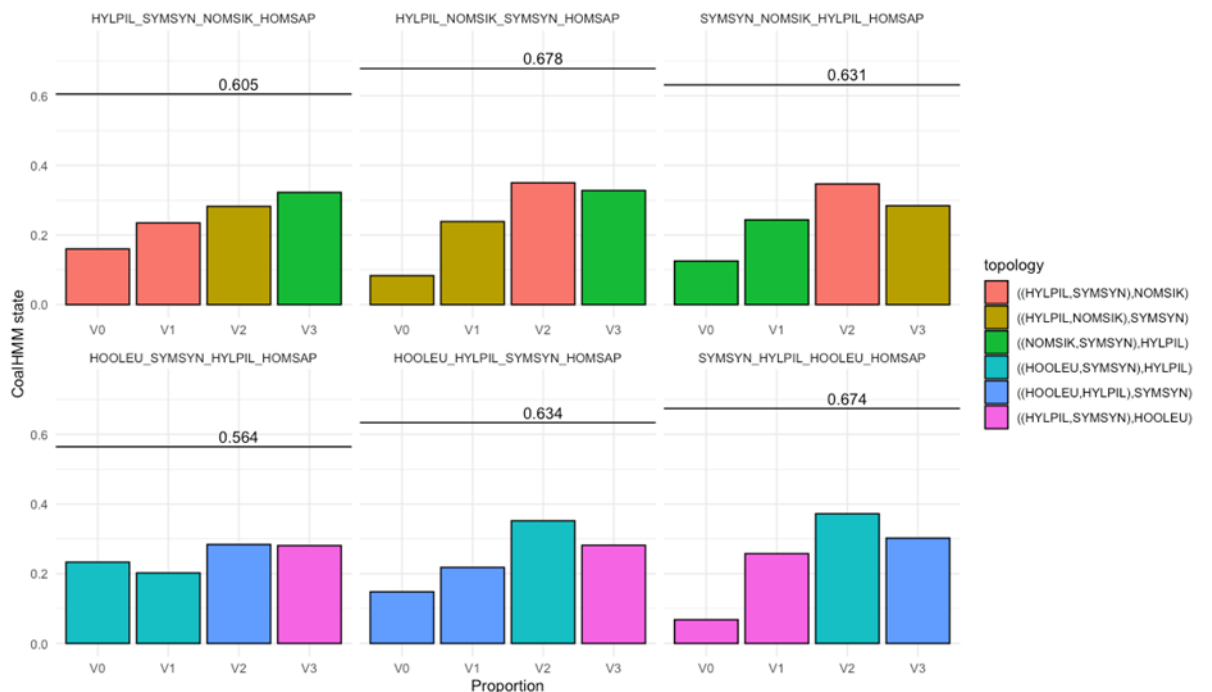


Fig. S11. Information of fossil calibrations in this study. Eleven fossil calibration points (B-L, Mya), colored in purple with confidence intervals provided, were obtained from Vanderpool *et al.* (39) and Perelman *et al.* (35). The nodal divergence dating (A colored in red) with a range (76-88 Mya) was obtained from TimeTree (<http://www.timetree.org/>).

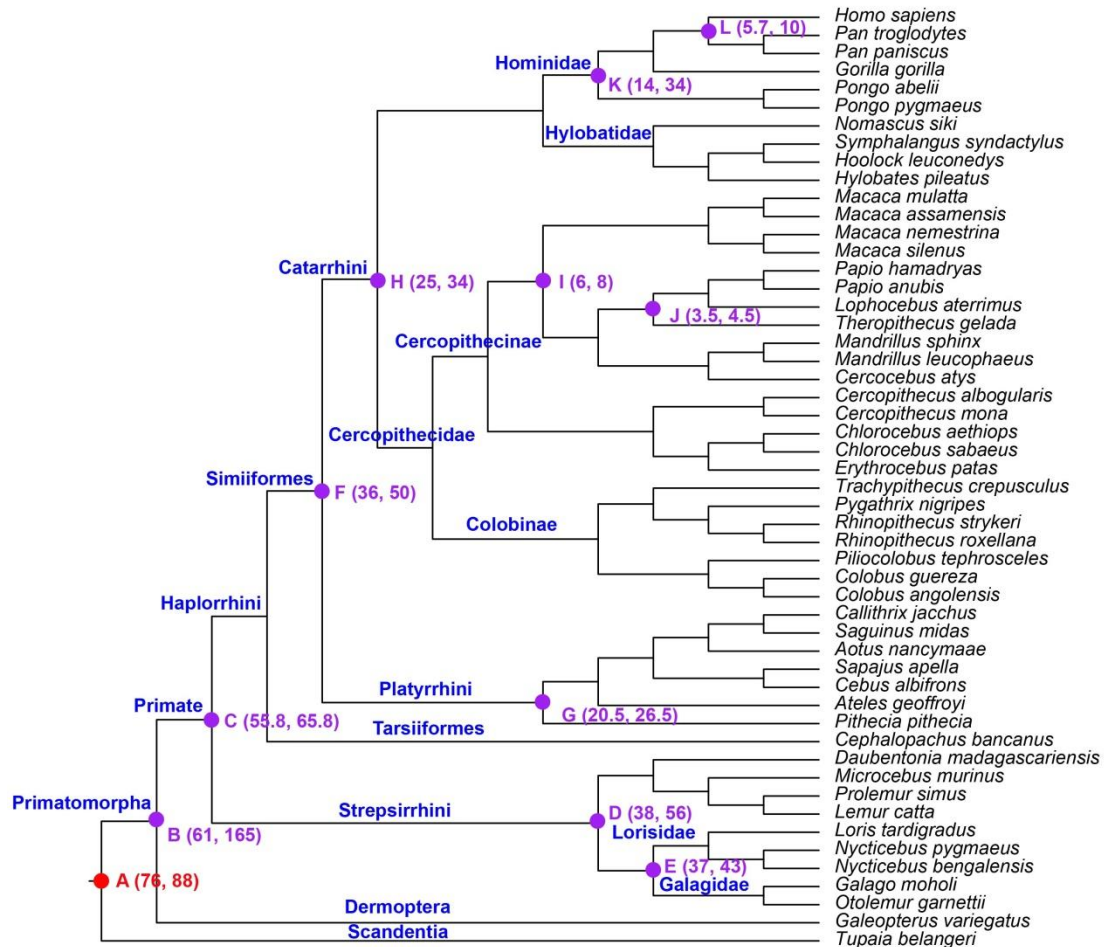


Fig. S12. Divergence dates of primates estimated by the MCMCTree algorithm in PAML4. The blue bars represent 95% credibility intervals. Upper and lower boundaries of 95% credibility intervals are given in parentheses.

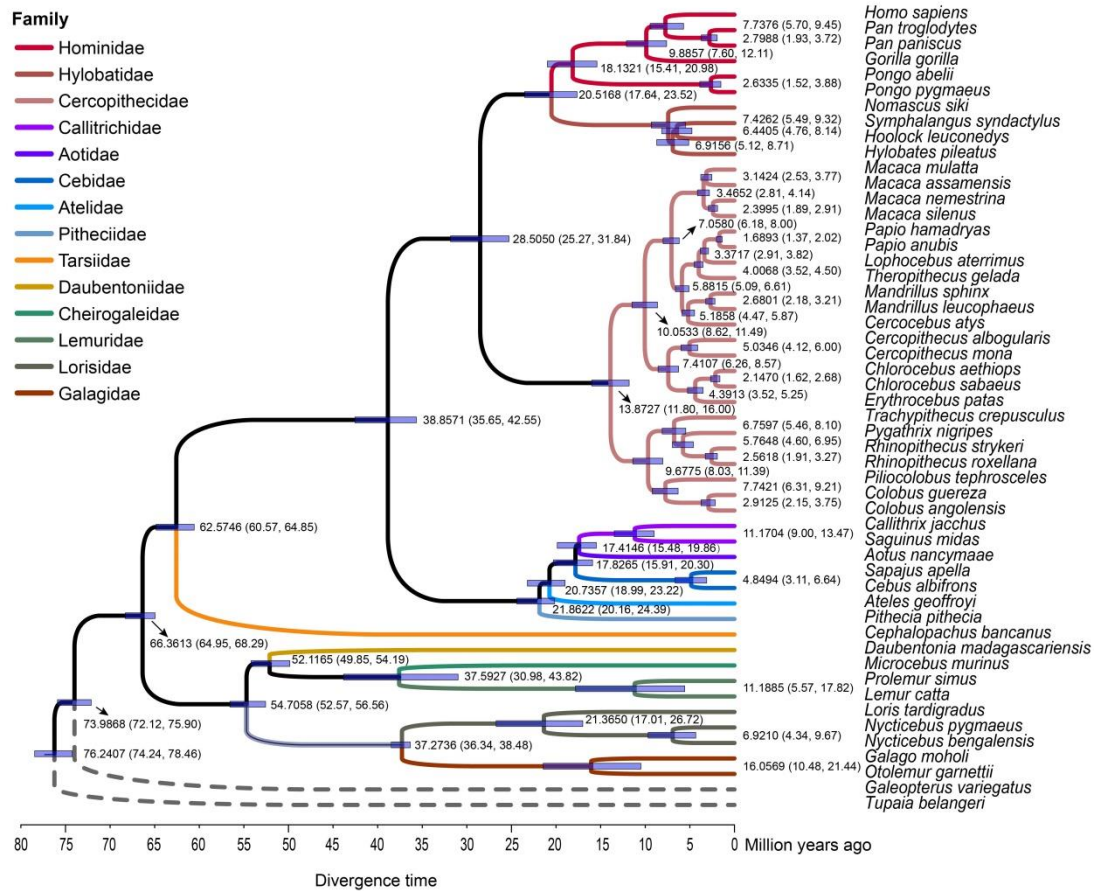


Fig. S13. A fusion event involving chromosome 8 occurred during the emergence of the Catarrhini. (A) Evolutionary pattern of chromosome 8 from the primate common ancestral lineage leading to the human lineage. The ancestral lineage of the Catarrhini is marked by a red asterisk. (B) The evidence for the fusion event involving chromosome 8 from ancestral karyotypes of Simiiformes to ancestral karyotypes of the Catarrhini by synteny alignments. The Chr IDs represent the chromosome numbers of the respective species.

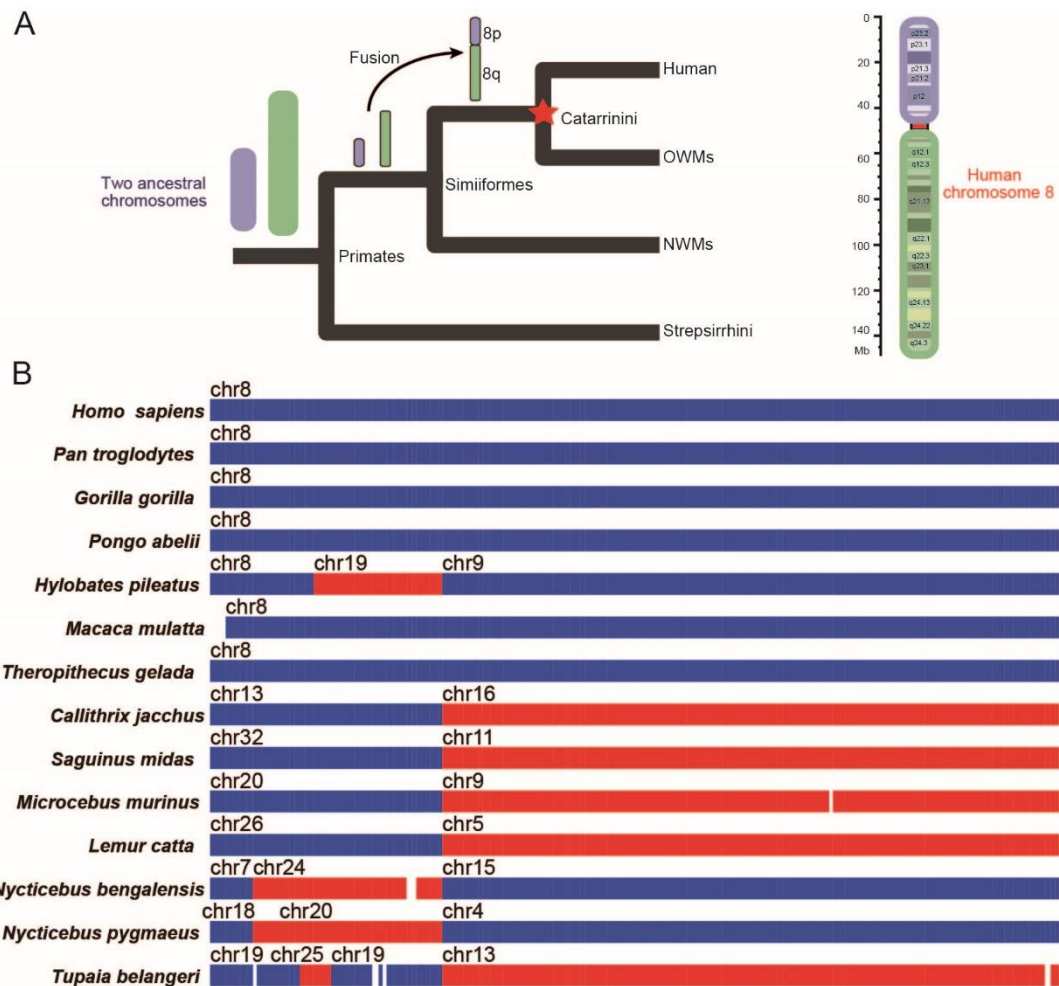


Fig. S14. A sample plot of the identification of segmental duplications for each primate species genome. Here we have used segmental duplications from the *Colobus guereza* genome as an example of a typical plot. LG-number in the outer circle represents the Chromosome number of the species.



Fig. S15. Tissue expression analysis of 57 genes overlapping segmental duplications in the great apes. (A) Proportion of highly expressed genes in tissues. Only those tissues with ≥ 2 highly expressed genes were retained for this statistic. (B) Highly expressed genes by tissue. Brain has the highest number of genes overlapping segmental duplications. The highly expressed genes in tissues were assigned according to the ‘UP_TISSUE’ category of Tissue Expression Database in DAVID (<https://david.ncifcrf.gov/>). SD: segmental duplication.

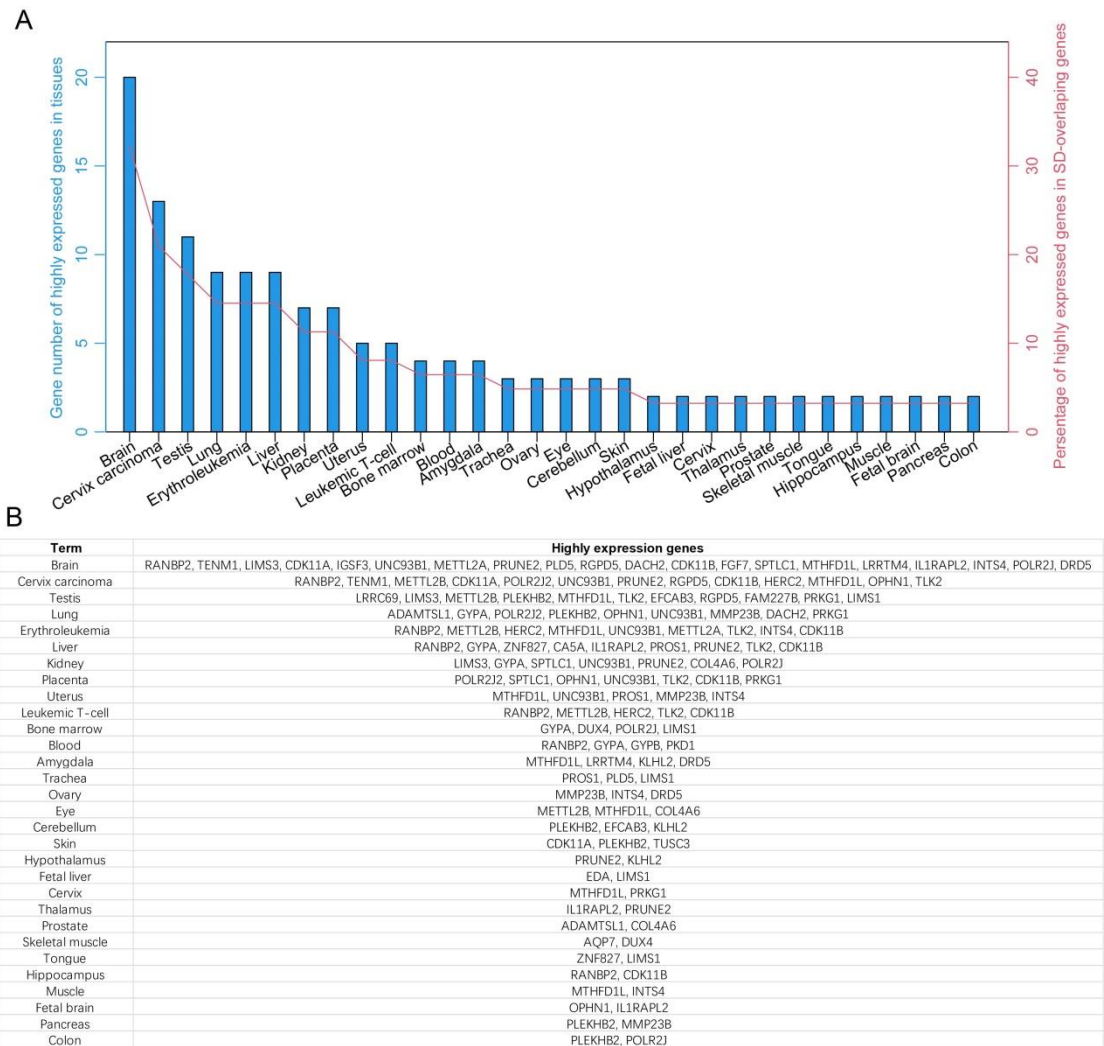


Fig. S16. Comparative analyses of genome sizes and transposable elements in different evolutionary branches among primates. (A) Genome sizes. (B) TE content. (C) *Alu* content. *P* values were calculated by the Mann-Whitney *U* test. The ‘lemurs’ included *Prolemur simus*, *Lemur catta*, *Microcebus murinus* and *Daubentonia madagascariensis*, whereas the ‘lorisoids’ included *Loris tardigradus*, *Nycticebus pygmaeus*, *Nycticebus bengalensis*, *Galago moholi* and *Otolemur garnettii* in this study. OWMs: Old World monkeys. NWMS: New World monkeys. TE: transposable element.

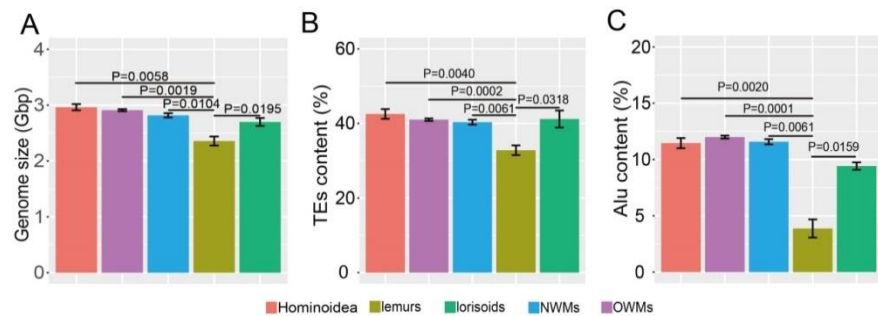


Fig. S17. Transposable elements contributing to variations in primate genome size.
 Lemur genome sizes were significantly lower than other evolutionary clades, e.g., lorisoids (Lorisiformes species), NWMs, OWMs, and Hominoidea (including apes and human). P values were calculated by the Mann-Whitney U test. OWMs: Old World monkeys. NWMs: New World monkeys. TE: transposable element.

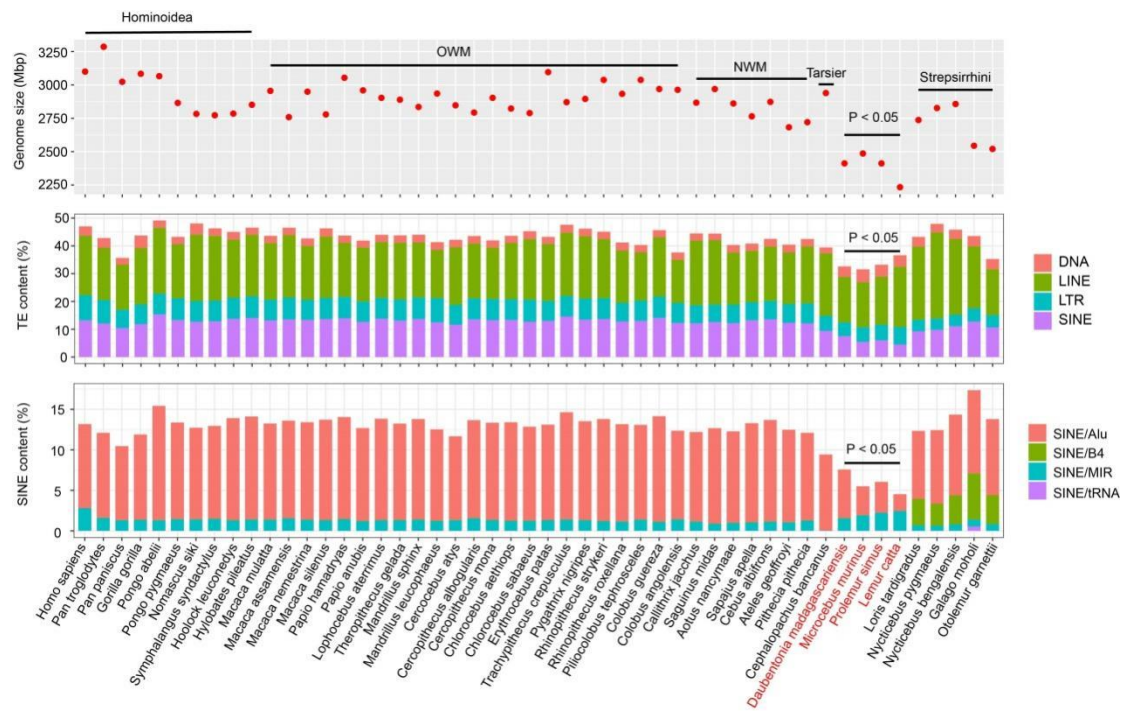


Fig. S18. Comparative analyses of transposable elements with a high proportional genome content in primates. The 67 TE subclasses with the highest genome percentage content in primate genomes are shown. TE: transposable element.

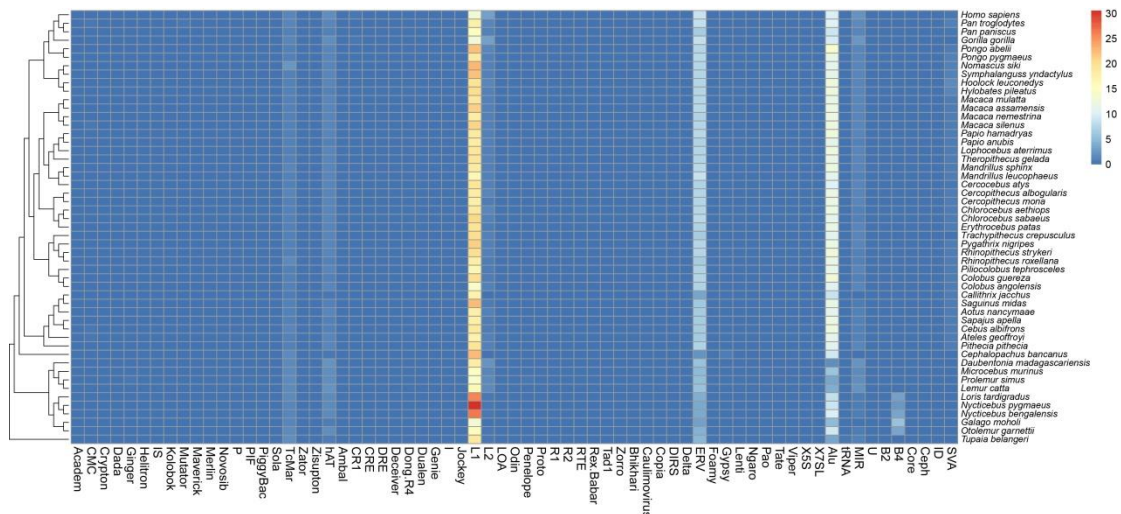


Fig. S19. Comparative analysis of *Alu* insertion times between Simiiformes and lorisoids. (A) *Alu* insertion times in Simiiformes species. (B) *Alu* insertion times in lorisoid species. The insertion time bursts are highlighted by blue bars.

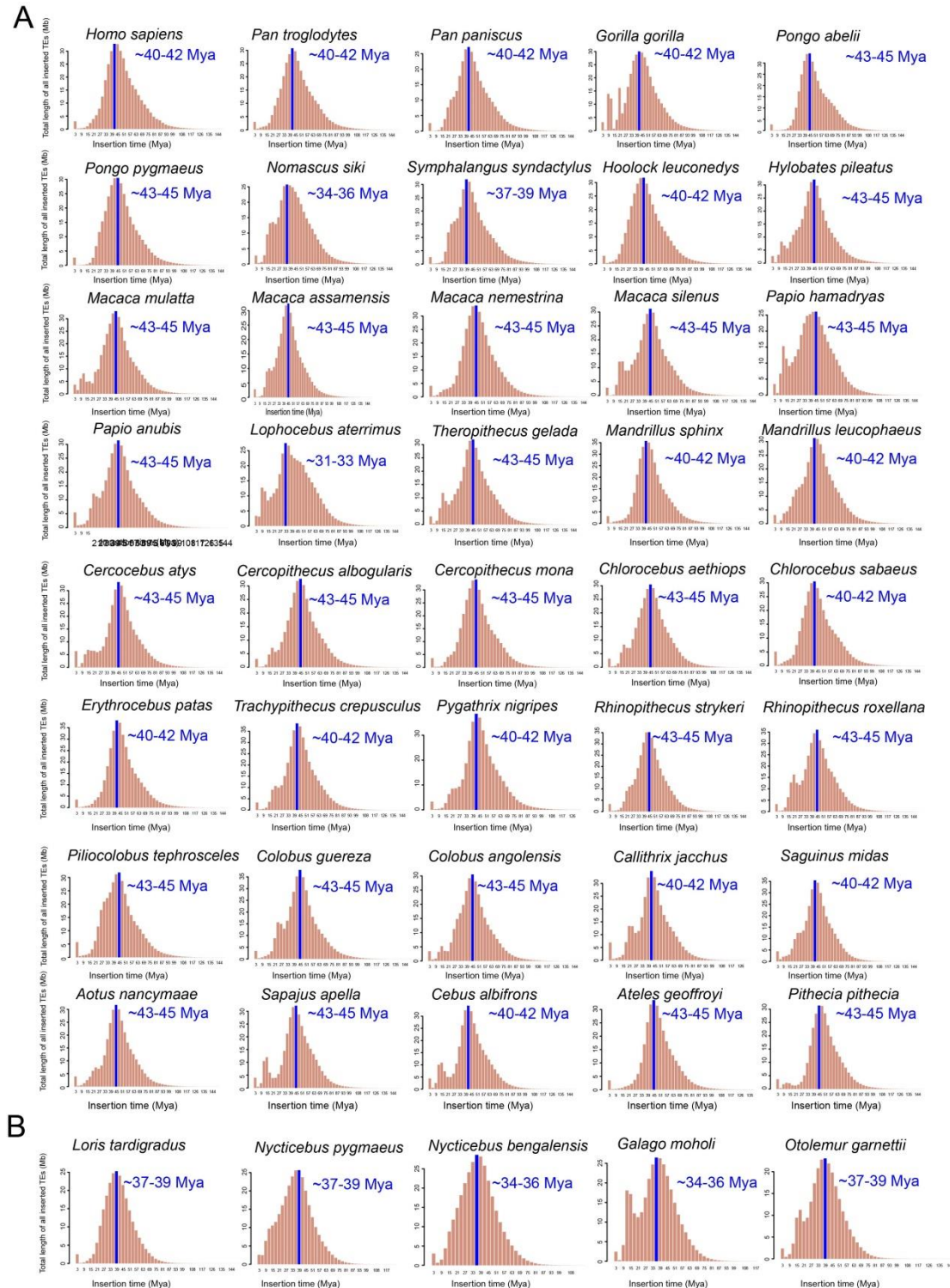


Fig. S20. Proportional analyses of genomic *Alu* subclasses between Simiiformes and Lorisiformes. (A) Proportion of *Alu* subclasses relative to the total length of all *Alu* elements in each Simiiformes species. In the Simiiformes, for each large evolutionary branch (e.g. great apes, gibbons, Cercopithecinae, Colobinae, NWMs), we selected *Homo sapiens*, *Hylobates pileatus*, *Macaca mulatta*, *Colobus guereza*, and *Saguinus midas* as representative species. (B) Proportion of of *Alu* subclasses relative to the total length of all *Alu* elements in each Lorisiformes species. All 5 extant Lorisiformes species were covered in this study. We observed a dramatic expansion of the *AluS*-related subclass, especially *AluSx* in Simiiformes, which was somewhat divergent from the pattern in Lorisiformes which was dominated by the conspicuous expansion of the *AluJ*-related subclass, especially *AluJb*.

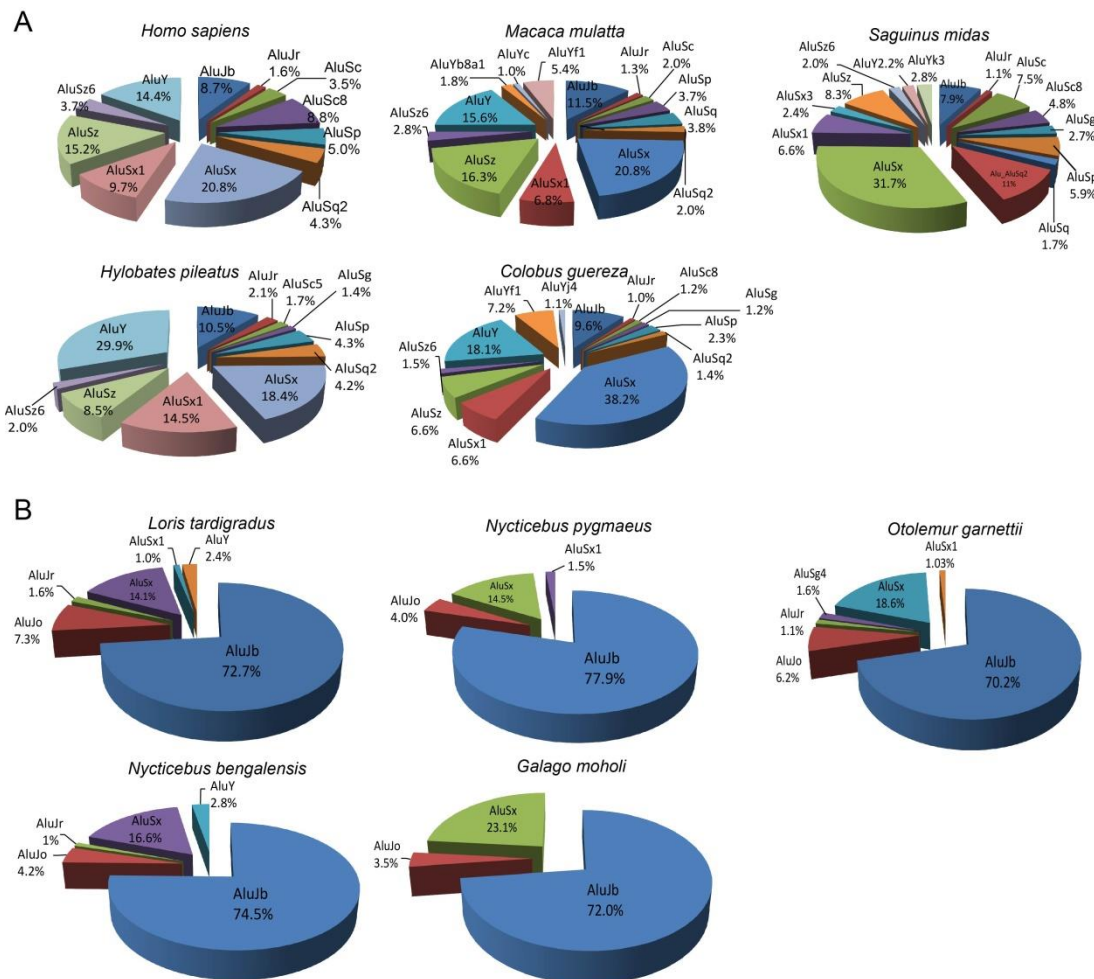


Fig. S21. Nucleotide substitution rates across primate lineages. Substitution rates in lineages were estimated by the comparison of fourfold degenerate (4d) sites in coding regions, in units of substitutions per site per million years. The overall pan-genome background substitution rate in primates is highlighted by a red full line. The nucleotide substitution rate of Western tarsier (*Cephalopachus bancanus*) in Haplorrhini was indicated by a black arrow. OWMs: Old World monkeys. NWMs: New World monkeys.

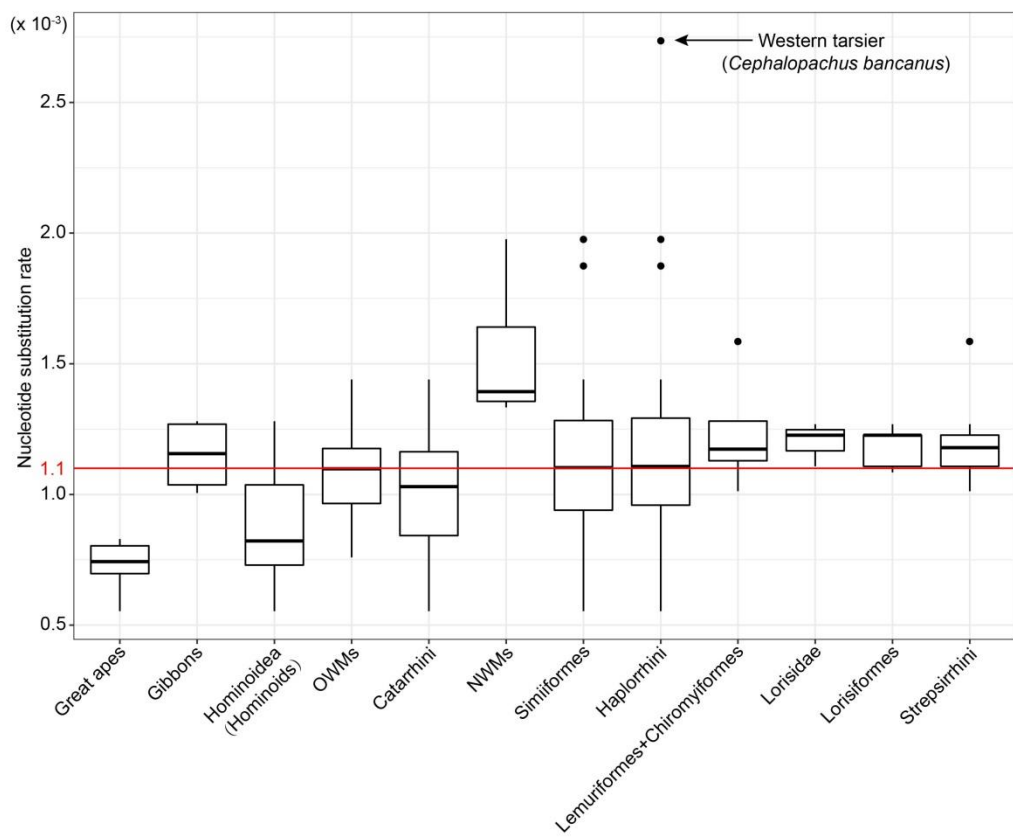


Fig. S22. An example of tissue-specific expressed genes obtained in human. The expression of target adipose samples ($n>3$) was compared with the expression of all other tissues ($n>3$) using t-statistics. The t-values were ranked from high to low. The genes with the top 5% t-values were regarded as human adipose-specific expressed genes. The red dotted line shows the top 5% cutoff of t-values (breaks=200). In total, we downloaded the gene expression matrix of 30 tissues representing 7,862 human samples from GTEx (<https://commonfund.nih.gov/GTEx>) for analyses of tissue-specific expressed genes.

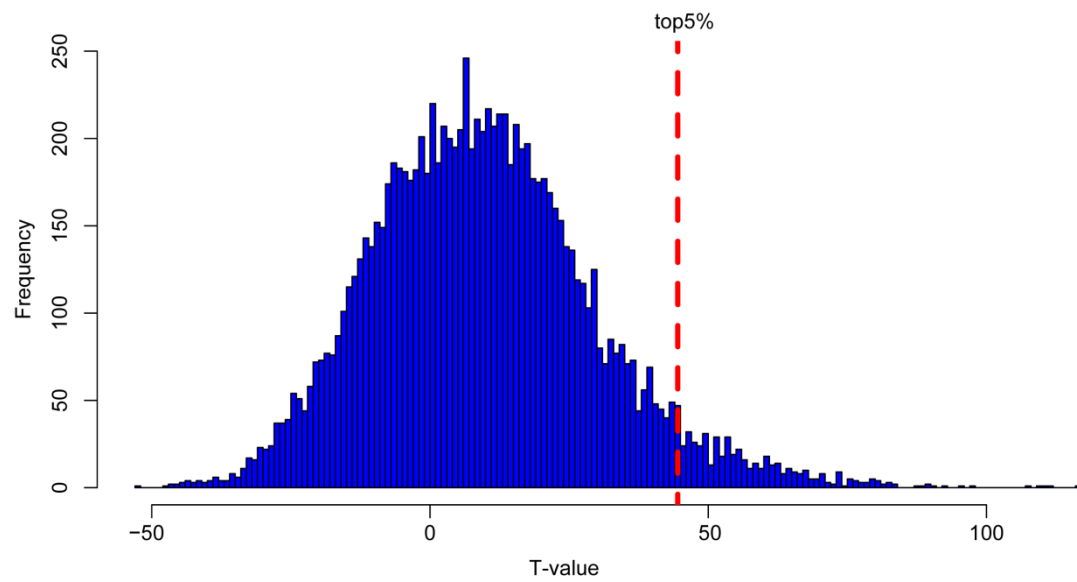


Fig. S23. Comparison of evolutionary constraints in tissues between human and other branches of primates. The X-axis represents d_N/ds for 30 tissues in human, whereas the Y-axis represents d_N/ds for 30 tissues for other ancestral branches in primates. Each circle represents a tissue type. The 30 tissues comprised adipose, adrenal gland, bladder, blood, blood vessel, brain, breast, cervix, colon, esophagus, fallopian tube, heart, kidney, liver, lung, muscle, nerve, ovary, pancreas, pituitary, prostate, salivary gland, skin, small intestine, spleen, stomach, testis, thyroid, uterus and vagina.

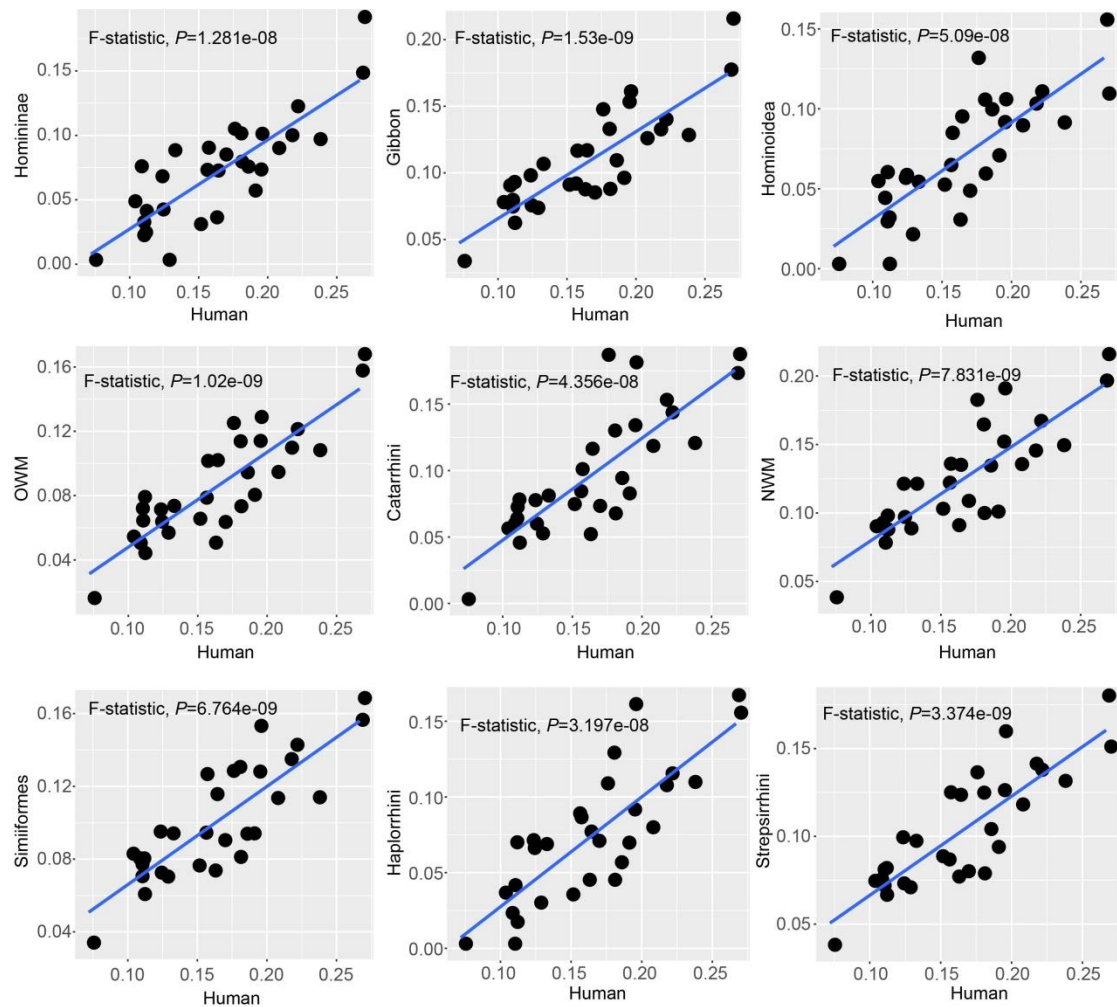


Fig. S24. Sequence alignment analysis of positively selected sites in the *GRHL2* gene in the Simiiformes ancestral lineage. The yellow bar denotes the sequence alignment of positively selected sites. The order of the human protein ENSP00000495564 (Ensembl protein id) is shown as the alignment order in this analysis. The names of the Simiiformes species are highlighted in red.

	141	147	525	535	
QYSISFP	PESSAII	FGPVPSK	EEGTKRV	Homo sapiens	
QYSISFP	PESSAII	FGPVPSK	EEGTKRV	<i>Pan troglodytes</i>	
QYSISFP	PESSAII	FGPVPSK	EEGTKRV	<i>Pan paniscus</i>	
QYSISFP	PESSAII	FGPVPSK	EEGTKRV	<i>Gorilla gorilla</i>	
QYSISFP	PESSAII	FGPVPSK	EEGTKRV	<i>Pongo abelii</i>	
QYSISFP	PESSAII	FGPVPSK	EEGTKRV	<i>Pongo pygmaeus</i>	
QYSISFP	PESSAII	FGPVPSK	EEGTKRV	<i>Nomascus siki</i>	
QYSISFP	PESSAII	FGPVPSK	EEGTKRV	<i>Sympalangus syndactylus</i>	
QYSISFP	PESSAII	FGPVPSK	EEGTKRV	<i>Hoolock leuconedys</i>	
QYSISFP	PESSAII	FGPVPSK	EEGTKRV	<i>Hylobates pileatus</i>	
QYSISFP	PESSAII	FGPVPSK	EEGTKRV	<i>Macaca mulatta</i>	
QYSISFP	PESSAII	FGPVPSK	EEGTKRV	<i>Macaca assamensis</i>	
QYSISFP	PESSAII	FGPVPSK	EEGTKRV	<i>Macaca nemestrina</i>	
QYSISFP	PESSAII	FGPVPSK	EEGTKRV	<i>Macaca silenus</i>	
QYSISFP	PESSAII	FGPVPSK	EEGTKRV	<i>Papio hamadryas</i>	
QYSISFP	PESSAII	FGPVPSK	EEGTKRV	<i>Papio anubis</i>	
QYSISFP	PESSAII	FGPVPSK	EEGTKRV	<i>Lophocebus aterrimus</i>	
QYSISFP	PESSAII	FGPVPSK	EEGTKRV	<i>Theropithecus gelada</i>	
QYSISFP	PESSAII	FGPVPSK	EEGTKRV	<i>Mandrillus sphinx</i>	
QYSISFP	PESSAII	FGPVPSK	EEGTKRV	<i>Mandrillus leucophaeus</i>	
QYSISFP	PESSAII	FGPVPSK	EEGTKRV	<i>Cercacebus atys</i>	
QYSISFP	PESSAII	FGPVPSK	EEGTKRV	<i>Cercopithecus albogularis</i>	
QYSISFP	PESSAII	FGPVPSK	EEGTKRV	<i>Cercopithecus mona</i>	
QYSISFP	PESSAII	FGPVPSK	EEGTKRV	<i>Chlorocebus aethiops</i>	
QYSISFP	PESSAII	FGPVPSK	EEGTKRV	<i>Chlorocebus sabaeus</i>	
QYSISFP	PESSAII	FGPVPSK	EEGTKRV	<i>Erythrocebus patas</i>	
QYSISFP	PESSAII	FGPVPSK	EEGTKRV	<i>Trachypithecus crepusculus</i>	
QYSISFP	PESSAII	FGPVPSK	EEGTKRV	<i>Pygathrix nigripes</i>	
QYSISFP	PESSAII	FGPVPSK	EEGTKRV	<i>Rhinopithecus strykeri</i>	
QYSISFP	PESSAII	FGPVPSK	EEGTKRV	<i>Rhinopithecus roxellana</i>	
QYSISFP	PESSAII	FGPVPSK	EEGTKRV	<i>Piliocolobus tephrosceles</i>	
QYSISFP	PESSAII	FGPVPSK	EEGTKRV	<i>Colobus guereza</i>	
QYSISFP	PESSAII	FGPVPSK	EEGTKRV	<i>Colobus angolensis</i>	
QYSISVP	PESSAII	FGPVPSK	EEGTKRV	<i>Callithrix jacchus</i>	
QYSISVP	PESSAII	FGLPSPSK	EETAKRV	<i>Saguinus midas</i>	
QYSISVP	PESSAII	FGPVPSK	EEGTKRV	<i>Aotus nancymaae</i>	
QYSISVP	PESSAII	FGPVPSK	EEGTKRV	<i>Sapajus apella</i>	
QYSISVP	PESSAII	FGPVPSK	EEGTKRV	<i>Cebus albifrons</i>	
QYSISVP	PESSAII	FGPVPSK	EEGTKRV	<i>Ateles geoffroyi</i>	
QYSISVP	PESSAII	FGPVPSK	EEGTKRV	<i>Pithecia pithecia</i>	
QYSASIP	PESPAII	FGPAPS	EEGMKR	<i>Cephalopachus bancanus</i>	
QYSASVP	PESPAII	FGPAPS	EEGMKR	<i>Daubentonia madagascariensis</i>	
QYAGAVP	PDSPAII	FGPAPS	EEGMKR	<i>Microcebus murinus</i>	
QYSASVP	PESPAII	FGPAPS	EEGMKR	<i>Prolemur simus</i>	
QYSASVP	PESPAII	FGPAPS	EEGMKR	<i>Lemur catta</i>	
QYLTSVP	PESPAII	FGPAPS	EEGVKR	<i>Loris tardigradus</i>	
QYLTSVP	PESPAII	FGPAPS	EEGMKR	<i>Nycticebus pygmaeus</i>	
QYLTSVP	PESPAII	FGPAPS	EEGMKR	<i>Nycticebus bengalensis</i>	
QYLTSVP	PESPAII	FGPAPS	EEVMKR	<i>Galago moholi</i>	
QYLTSVP	PESPAII	FGPAPS	EEVMKR	<i>Otolemur garnettii</i>	
QYSASVP	PESPAVI	FGPAPS	EEGMKR	<i>Galeopterus variegatus</i>	
QYSASVP	PESPAVI	FGPAPS	EEGMKR	<i>Tupaia belangeri</i>	

Fig. S25. Comparative analyses of coat color luminance between Simiiformes and Strepsirrhini/Tarsiiformes. The left hand side represents the comparative analysis of the dorsal luminance between Simiiformes and Strepsirrhini/Tarsiiformes. The right hand side represents comparative analysis of the ventral luminance between Simiiformes and Strepsirrhini/Tarsiiformes. Significance was assessed by means of the Mann-Whitney U test ($P<0.05$). The coat color luminance data of primates were obtained from a previous study (89).

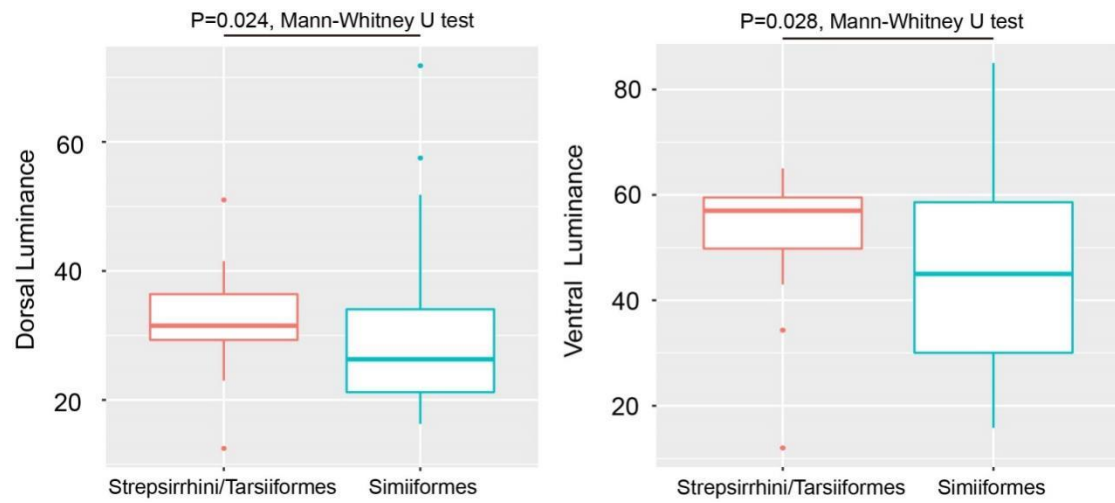


Fig. S26. Sequence alignment analysis of positively selected sites in the *NIPBL* gene in the primate ancestral lineage. The yellow bar denotes the sequence alignment of positively selected sites. The order of the human protein ENSP00000282516 (Ensembl protein id) is shown as the alignment order in this analysis. The names of the primate species are highlighted in red.

638	763	
SSE N KL E	HRH D N R R	<i>Homo sapiens</i>
SSE N KL E	HRH D N R R	<i>Pan troglodytes</i>
SSE N KL E	HRH D N R R	<i>Pan paniscus</i>
SSE N KL E	HRH D N R R	<i>Gorilla gorilla</i>
SSE N KL E	HRH D N R R	<i>Pongo abelii</i>
SSE N KL E	HRH D N R R	<i>Pongo pygmaeus</i>
SSE N KL E	HRH D N R R	<i>Nomascus siki</i>
SSE N KL E	HRH D N R R	<i>Sympalangus syndactylus</i>
SSE N KL E	HRH D N R R	<i>Hoolock leuconedys</i>
SSE N KL E	HRH D N R R	<i>Hylobates pileatus</i>
STE N KL E	HRH D N R R	<i>Macaca mulatta</i>
STE N KL E	HRH D N R R	<i>Macaca assamensis</i>
STE N KL E	HRH D N R R	<i>Macaca nemestrina</i>
STE N KL E	HRH D N R R	<i>Macaca silenus</i>
STE N KL E	HRH D N R R	<i>Papio hamadryas</i>
STE N KL E	HRH D N R R	<i>Papio anubis</i>
STE N KL E	HRH D N R R	<i>Lophocebus aterrimus</i>
STE N KL E	HRH D N R R	<i>Theropithecus gelada</i>
STE N KL E	HRH D N R R	<i>Mandrillus sphinx</i>
STE N KL E	HRH D N R R	<i>Cercocebus atys</i>
STE N KL E	HRH D N R R	<i>Cercopithecus albogularis</i>
STE N KL E	HRH D N R R	<i>Cercopithecus mona</i>
STE N KL E	HRH D N R R	<i>Erythrocebus patas</i>
STE N KL E	HRH D N R R	<i>Trachypithecus crepusculus</i>
STE N KL E	HRH D N R R	<i>Pygathrix nigripes</i>
STE N KL E	HRH D N R R	<i>Rhinopithecus strykeri</i>
STE N KL E	HRH D N R R	<i>Rhinopithecus roxellana</i>
STE N KL E	HRH D N R R	<i>Piliocolobus tephrosceles</i>
STE N KL E	HRH D N R R	<i>Colobus guereza</i>
STE N KL E	HRH D N R R	<i>Colobus angolensis</i>
SSE N KL E	HRH D N R R	<i>Callithrix jacchus</i>
SSE N KL E	HRH D N R R	<i>Saguinus midas</i>
SSE N KL E	HRH D N R R	<i>Aotus nancymaae</i>
SSE N KL E	HRH D N R R	<i>Sapajus apella</i>
SSE N KL E	HRH D N R R	<i>Cebus albifrons</i>
SSE N KL E	HRH D N R R	<i>Ateles geoffroyi</i>
SSE N KL E	HRH D N R R	<i>Pithecia pithecia</i>
SSE N KL E	HRH D N R R	<i>Cephalopachus bancanus</i>
SSE N KL E	HRH D N R R	<i>Daubentonia madagascariensis</i>
SSE N KI E	HRH D N R R	<i>Microcebus murinus</i>
SSE N KI E	HRH D N R R	<i>Prolemur simus</i>
SSE N KTE	HRH D N R R	<i>Lemur catta</i>
SNE N KI E	HRH D N R R	<i>Loris tardigradus</i>
SNE N KI E	HRH D N R R	<i>Nycticebus pygmaeus</i>
SNE N KI E	HRH D N R R	<i>Nycticebus bengalensis</i>
SNE N KL E	HRH D N R R	<i>Galago moholi</i>
SNE N KL E	HRH D N R R	<i>Otolemur garnettii</i>
SSESKL E	HRHEN R R	<i>Galeopterus variegatus</i>
SNESKVE	HKHEN R R	<i>Tupaia belangeri</i>
SNESKL E	HRHEN R R	<i>Mus musculus</i>
SNESKL E	HRHEN R R	<i>Felis catus</i>
SSES KL E	HRHEN R R	<i>Canis lupus familiaris</i>
SSES KL D	HRHEN R R	<i>Sus scrofa</i>

Fig. S27. Tissue enrichment analyses of genes associated with lineage-specific accelerated regions from the Haplorrhini ancestor leading to the human lineage.

Tissue enrichment analyses were performed by DAVID (v6.8) database (<https://david.ncifcrf.gov/tools.jsp>). Statistical significance was assessed by the Modified Fisher's Exact test with $P < 0.05$. * $P < 0.05$; ** $P < 0.01$; *** $P < 0.001$.

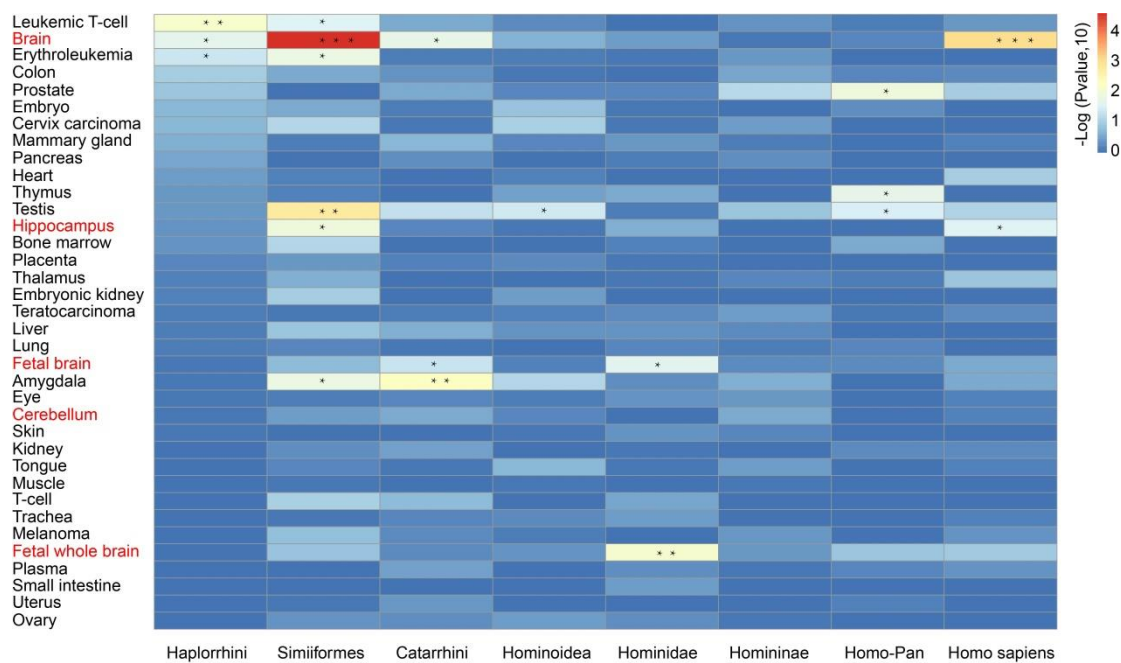


Fig. S28. 39 genes associated with lineage-specific accelerated regions involved in neurotransmitter signaling pathways from the Haplorrhini ancestral lineage leading to the human lineage. The different ancestral lineages are highlighted by different colors. The genes associated with lineage-specific accelerated regions concurrently emerging in different lineages are linked by a solid line.

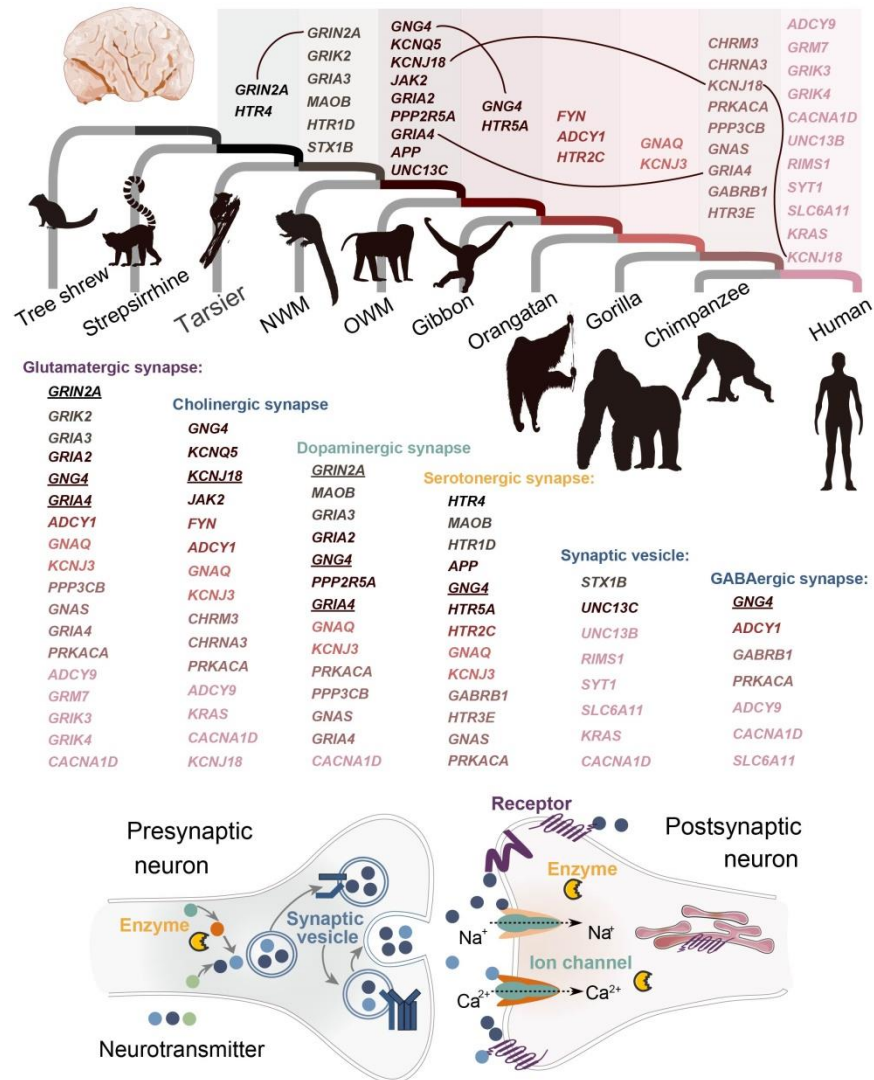


Fig. S29. An ape-specific accelerated region including several highly divergent sites compared to non-ape primate species. The nearest gene (*KIAA1217*) to this ape-specific accelerated region is involved in tail development phenotypes in mouse. The human DNA sequence was used as the reference to determine the sequence order. The names of the great ape (and lesser ape) species are highlighted in red.

24,158,524	24,158,531	24,158,582	24,158,781	(Chr10,hg38)
TTTAGAG	AATTCCAT	GCACTGA	TGTCTGGCCGGT	<i>Homo sapiens</i>
TTTAGAG	AATTCCAT	GCACTGA	TGTCTGGCCGGT	<i>Pan troglodytes</i>
TTTAGAG	AATTCCAT	GCACTGA	TGTCTGGCCGGT	<i>Pan paniscus</i>
TTTAGAG	AATTCCAT	GCACTGA	TGTCTGGCTGGT	<i>Gorilla gorilla</i>
TTTAGAG	AATTCCAT	GCACTGA	TGTCTGGCCAGT	<i>Pongo abelii</i>
TTTAGAG	AATTCCAT	GCACTGA	TGTCTGGCCAGT	<i>Pongo pygmaeus</i>
TTTAGAG	AATTCCAT	GCACTGA	TGTCTGGCCAGT	<i>Hylobates pileatus</i>
TTTAGAG	AATTCCAT	GCACTGA	TGTCTGGCCAGT	<i>Sympalangus syndactylus</i>
TTTAGAG	AATTCCAT	GCACTGA	TGTCTGGCCAGT	<i>Hoolock leuconedys</i>
TTTAGAG	AATTCCAT	GCACTGA	TGTCCGGCCAGT	<i>Nomascus siki</i>
TTTGGAG	AATCCAT	GCAGTGA	TGTTTGGCTGGT	<i>Macaca mulatta</i>
TTTGGAG	AATCCAT	GCAGTGA	TGTTTGGCTGGT	<i>Macaca assamensis</i>
TTTGGAG	AATCCAT	GCAGTGA	TGTTTGGCTGGT	<i>Macaca nemestrina</i>
TTTGGAG	AATCCAT	GCAGTGA	TGTTTGGCTGGT	<i>Macaca silenus</i>
TTTGGAG	AATCCAT	GCAGTGA	TGTTTGGCTGGT	<i>Cercocebus atys</i>
TTTGGAG	AATCCAT	GCAGTGA	TGTTTGGCTGGT	<i>Mandrillus sphinx</i>
TTTGGAG	AATCCAT	GCAGTGA	TGTTTGGCTGGT	<i>Mandrillus leucophaeus</i>
TTTGGAG	AATCCAT	GCAGTGA	TGTTTGGCTGGT	<i>Papio hamadryas</i>
TTTGGAG	AATCCAT	GCAGTGA	TGTTTGGCTGGT	<i>Papio anubis</i>
TTTGGAG	AATCCAT	GCAGTGA	TGTTTGGCTGGT	<i>Lophocebus aterrimus</i>
TTTGGAG	AATCCAT	GCAGTGA	TGTTTGGCTGGT	<i>Theropithecus gelada</i>
TTTGGAG	AATCCAT	GCAGTGA	TGTTTGGCTGGT	<i>Cercopithecus mona</i>
TTTGGAG	AATCCAT	GCAGTGA	TGTTTGGCTGGT	<i>Erythrocebus patas</i>
TTTGGAG	AATCCAT	GCAGTGA	TGTTTGGCTGGT	<i>Chlorocebus sabaeus</i>
TTTGGAG	AATCCAT	GCAGTGA	TGTTTGGCTGGT	<i>Chlorocebus aethiops</i>
TTTGGAG	AATCCAT	GCAGTGA	TGTTTGGCTGGT	<i>Colobus angolensis</i>
TTTGGAG	AATCCAT	GCAGTGA	TGTTTGGCTGGT	<i>Colobus guereza</i>
TTTGGAG	AATCCAT	GCAGTGA	TGTTTGGCTGGT	<i>Piliocolobus tephrosceles</i>
TTTGGAG	AATCAAT	GCAGTGA	TGTTTGGCTGGT	<i>Trachypithecus crepusculus</i>
TTTGGAG	AATCCAT	GCAGTGA	TGTTTGGCTGGT	<i>Pygathrix nigripes</i>
TTTGGAG	AATCCAT	GCAGTGA	TGTTTGGCTGGT	<i>Rhinopithecus strykeri</i>
TTTGGAG	AATCCAT	GCAGTGA	TGTTTGGCTGGT	<i>Rhinopithecus roxellana</i>
TTTGGAG	AATCCAT	GCAGTGA	TGTTTGGCTGGT	<i>Pithecia pithecia</i>
TTTGGAG	AATCCAT	GCAGTGA	TGTTTGGCTGGT	<i>Sapajus apella</i>
TTTGGAG	AATCCAT	GCAGTGA	TGTTTGGCTGGT	<i>Cebus albifrons</i>
TTTGGAG	AATCCAT	--AGTGG	TGTTTGGCTGGT	<i>Callithrix jacchus</i>
TTTGGAG	AATCCAT	GCAGTGA	TGTTTAGCTGGT	<i>Saguinus midas</i>
TTTGGAG	AATCCAT	GCAGTGA	TGTCTGGC--T	<i>Aotus nancymaae</i>
TTTGGAG	AATCCAT	ACAAATGA	TGTTTGGCTGGT	<i>Cephalopachus bancanus</i>
TTTGGAG	AATCCAT	ACAGTGA	TGTTCGGCTGGT	<i>Daubentonia madagascariensis</i>
TTTGGAG	AATCCAT	ACAGTGA	TGTTCGGCTGGT	<i>Lemur catta</i>
TTTGGAG	AATCCAT	ACAGTGA	TGTTCGGCTGGT	<i>Prolemur simus</i>
TTTGGAG	AATCCAT	ACAGTGA	TGTTTGGCTGGT	<i>Microcebus murinus</i>
TTTGGAG	AATCCAT	ACAGTGA	TGTTTGGCTGGT	<i>Otolemur garnettii</i>
TTTGGAG	AATCCAT	ACAGTGA	TGTTTGGCTGGT	<i>Galago moholi</i>
TTTGGAG	AATCCGT	ACAGTGA	TGCTTGGCTGGT	<i>Nycticebus pygmaeus</i>
TTTGGAG	AATCCAT	ACGGTGA	TGTT---CTGGT	<i>Nycticebus bengalensis</i>
TTTGGAG	AATCCAT	ACAGTGA	TGTTTGGCTGGT	<i>Loris tardigradus</i>
TTTGGTG	AATCCAT	ACAGTGA	TGTTCGGCTGGT	<i>Galeopterus variegatus</i>
TTTGGAG	AATCCAT	ATAGTGA	TGTTCGGCTGGT	<i>Tupaia belangeri</i>

Fig. S30. Phylogenetic analysis of an ape-specific accelerated region among primate species. The nearest gene to this ape-specific accelerated region (*KIAA1217*) is involved in tail development phenotypes in mouse. Branches of the ape species are highlighted in red. The evolutionary history was inferred by using the Maximum Likelihood method based on the Hasegawa-Kishino-Yano model (210). The tree is drawn to scale, with branch lengths measured in the number of substitutions per site (next to the branches). Evolutionary analyses were conducted in MEGA7 (211).

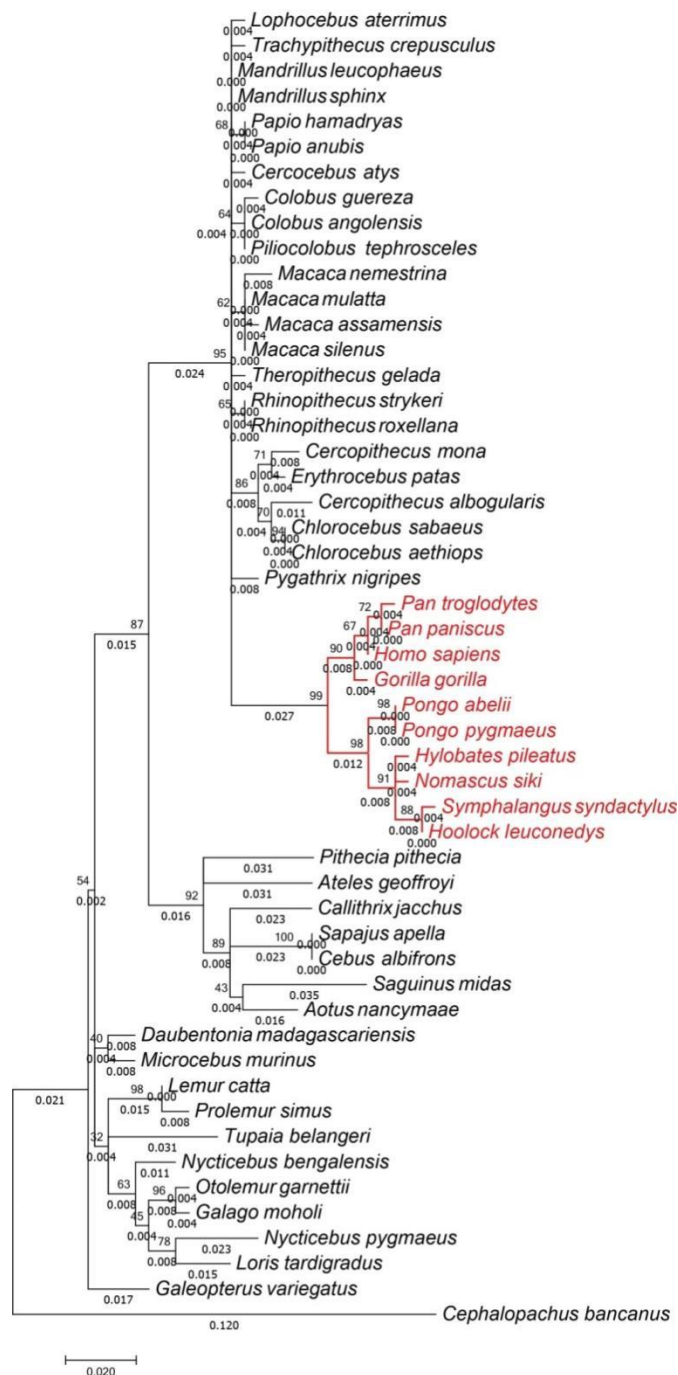


Fig. S31. The lineage-specific accelerated region (Chr10: 24,158,492–24,158,793; total length=301bp) in the great ape lineages overlaps an enhancer EH38E1455433 (pELS). Our analysis suggests that this ape-specific accelerated region may regulate the expression level of *KIAA1217*, the nearest gene to the ape-specific accelerated region.

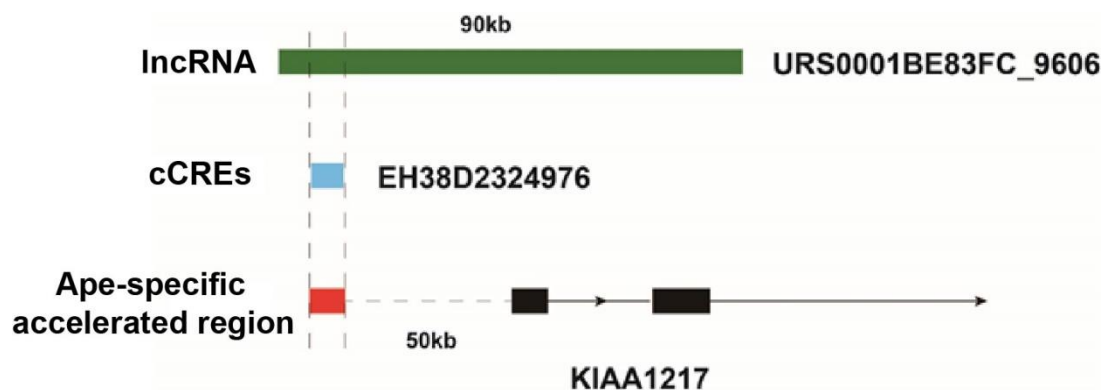


Fig. S32. High-throughput chromosome conformation capture data supporting a strong interaction between the ape-specific accelerated region and its neighboring gene *KIAA1217*. The high-throughput chromosome conformation capture reads for human blood samples were downloaded from Encode (<https://www.encodeproject.org/experiments/ENCSR118YWJ/>). Reads were sampled by ~30X. Sampled reads were mapped to the human genome with juicer (v1.6) (212). The merged_nodups.txt file was used to generate Hi-C contact map employing different levels of resolution (10 Kb, 20 Kb, 50 Kb, 100 Kb, 200 Kb, 500 Kb, 1 Mb, 2 Mb, 5 Mb) with cooler (v0.8.11) (213), converted to h5 format and normalized with KR method with hicexplorer (v3.7.2) (214). Regional high-throughput chromosome conformation capture maps were visualized by hicexplorer package. This lineage-specific accelerated region and its neighboring gene *KIAA1217* are located within the same topologically associating domain.

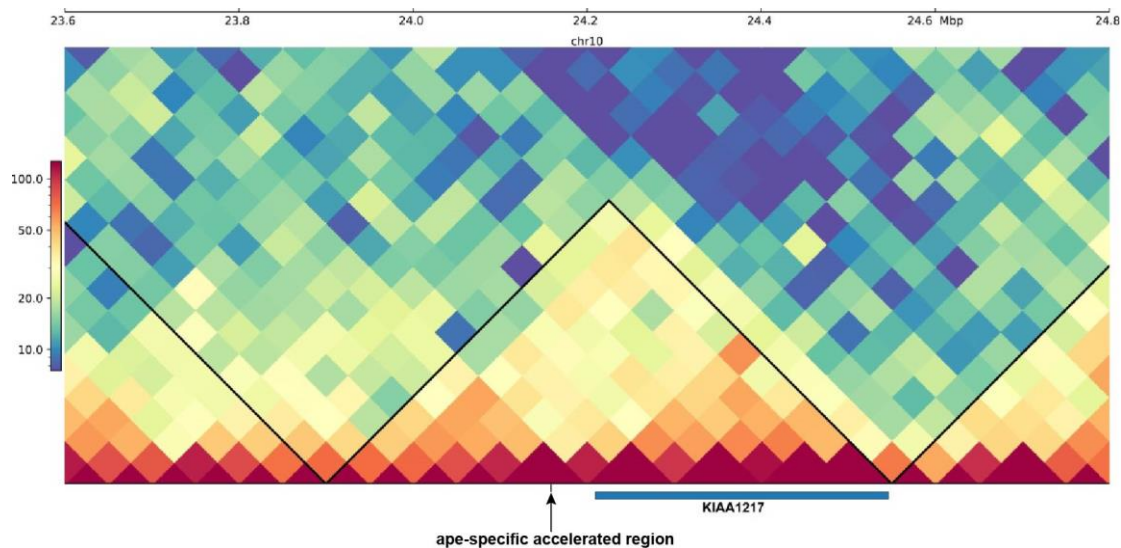


Fig. S33. Sequence alignment analysis of positively selected sites in the *ACADM* gene in the Colobinae ancestral lineage. The Colobinae species are highlighted in red. The multiple sequence alignment is shown across primate species. The human protein sequence (Ensembl protein id: ENSP00000359871) was taken as the reference to determine the sequence order.

75	138	
E Y P V P L I	T F D A C L I	<i>Homo sapiens</i>
E Y P V P L I	T F D A C L I	<i>Pan troglodytes</i>
E Y P V P L I	T F D A C L I	<i>Pan paniscus</i>
E Y P V P L I	T F D A C L I	<i>Gorilla gorilla</i>
E Y P V P I I	T F D A C L I	<i>Pongo abelii</i>
E Y P V P L I	T F D A C L I	<i>Nomascus siki</i>
E Y P V P L I	T F D A C L I	<i>Sympalangus syndactylus</i>
E Y P V P L I	T F D A C L I	<i>Hoolock leuconedys</i>
E Y P V P L I	T F D A C L I	<i>Hylobates pileatus</i>
E Y P V P L I	T F D A C L I	<i>Macaca mulatta</i>
E Y P V P L I	T F D A C L I	<i>Macaca assamensis</i>
E Y P V P L I	T F D A C L I	<i>Macaca nemestrina</i>
E Y P V P L I	T F D A C L I	<i>Macaca silenus</i>
E Y P V P L I	T F D A C L I	<i>Papio hamadryas</i>
E Y P V P L I	T F D A C L I	<i>Papio anubis</i>
E Y P V P L I	T F D A C L I	<i>Lophocebus aterrimus</i>
E Y P V P L I	T F D A C L I	<i>Theropithecus gelada</i>
E Y P V P L I	T F D A C L I	<i>Mandrillus sphinx</i>
E Y P V P L I	T F D A C L I	<i>Mandrillus leucophaeus</i>
E Y P V P L I	T F D A C L I	<i>Cercocebus atys</i>
E Y P V P L I	T F D A C L I	<i>Cercopithecus albogularis</i>
E Y P V P L I	T F D A C L I	<i>Cercopithecus mona</i>
E Y P V P L I	T F D A C L I	<i>Chlorocebus aethiops</i>
E Y P V P L I	T F D A C L I	<i>Chlorocebus sabaeus</i>
E Y P V P L I	T F D A C L I	<i>Erythrocebus patas</i>
E Y P M P L I	T F D C C L I	<i>Trachypithecus crepusculus</i>
E Y P M P L I	T F D C C L I	<i>Pygathrix nigripes</i>
E Y P M P L I	T F D C C L I	<i>Rhinopithecus strykeri</i>
E Y P M P L I	T F D C C L I	<i>Rhinopithecus roxellana</i>
E Y P M P L I	T F D C C L I	<i>Piliocolobus tephrosceles</i>
E Y P M P L I	T F D C C L I	<i>Colobus guereza</i>
E Y P M P L I	T F D C C L I	<i>Colobus angolensis</i>
E Y P V P L I	T F D S C L I	<i>Saguinus midas</i>
E Y P V P L I	T F D A C L I	<i>Aotus nancymaae</i>
E Y P V P L I	T F D A C L I	<i>Sapajus apella</i>
E Y P V P L I	T F D A C L I	<i>Cebus albifrons</i>
E Y P V P L I	T F D A C L I	<i>Ateles geoffroyi</i>
E Y P V P L I	S F D G C L I	<i>Pithecia pithecia</i>
E Y P V P L I	T F D A C L I	<i>Cephalopachus bancanus</i>
E Y P V P L I	T L D A C L I	<i>Daubentonia madagascariensis</i>
E Y P V P L I	T F D A C L I	<i>Microcebus murinus</i>
E Y P V P L I	T L D G C L I	<i>Prolemur simus</i>
E Y P V P L I	T L D G C L I	<i>Lemur catta</i>
E Y P V P L I	T F D A C L I	<i>Loris tardigradus</i>
E Y P V P L I	T F D A C L I	<i>Nycticebus pygmaeus</i>
E Y P V P L I	T F D A C L I	<i>Nycticebus bengalensis</i>
E Y P V P L I	T F D A C L I	<i>Otolemur garnettii</i>
E Y P V P L I	C F D A C L I	<i>Galeopterus variegatus</i>
E Y P V P V I	T F D A C L I	<i>Tupaia belangeri</i>

Fig. S34. Decrease of members of the *OR52A* gene family in Simiiformes compared to Strepsirrhini. The lineages from Simiiformes and Strepsirrhini are highlighted by orange and blue, respectively.

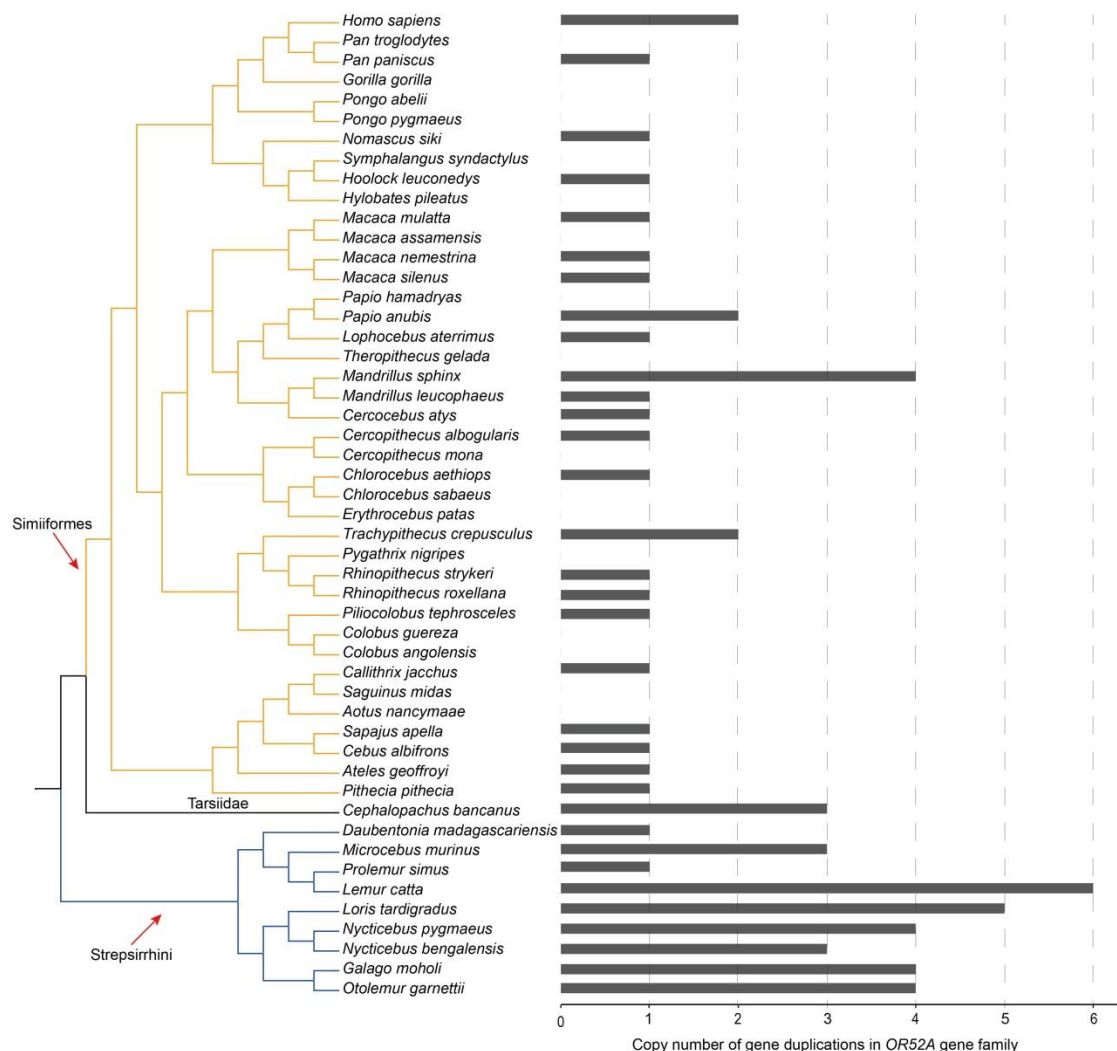


Fig. S35. Decrease of the olfactory receptor gene family *OR52A* in Simiiformes compared to Strepsirrhini. The copy number of each species is shown by point between Strepsirrhini and Simiiformes.

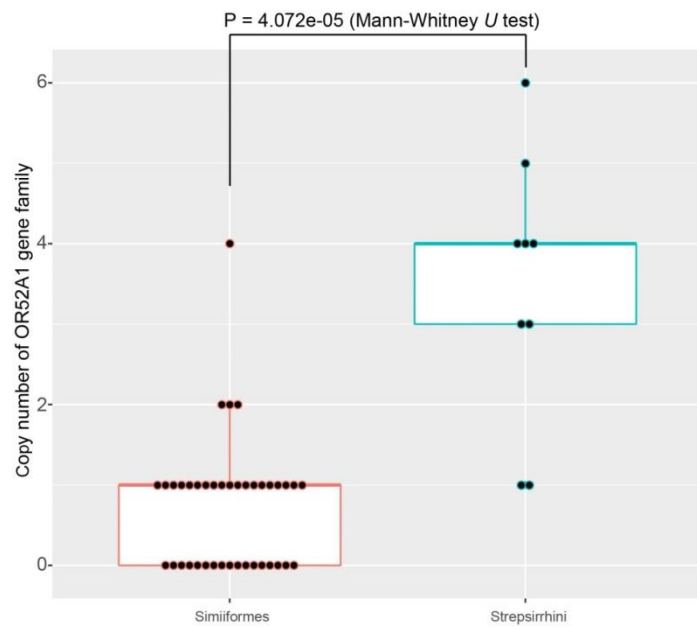
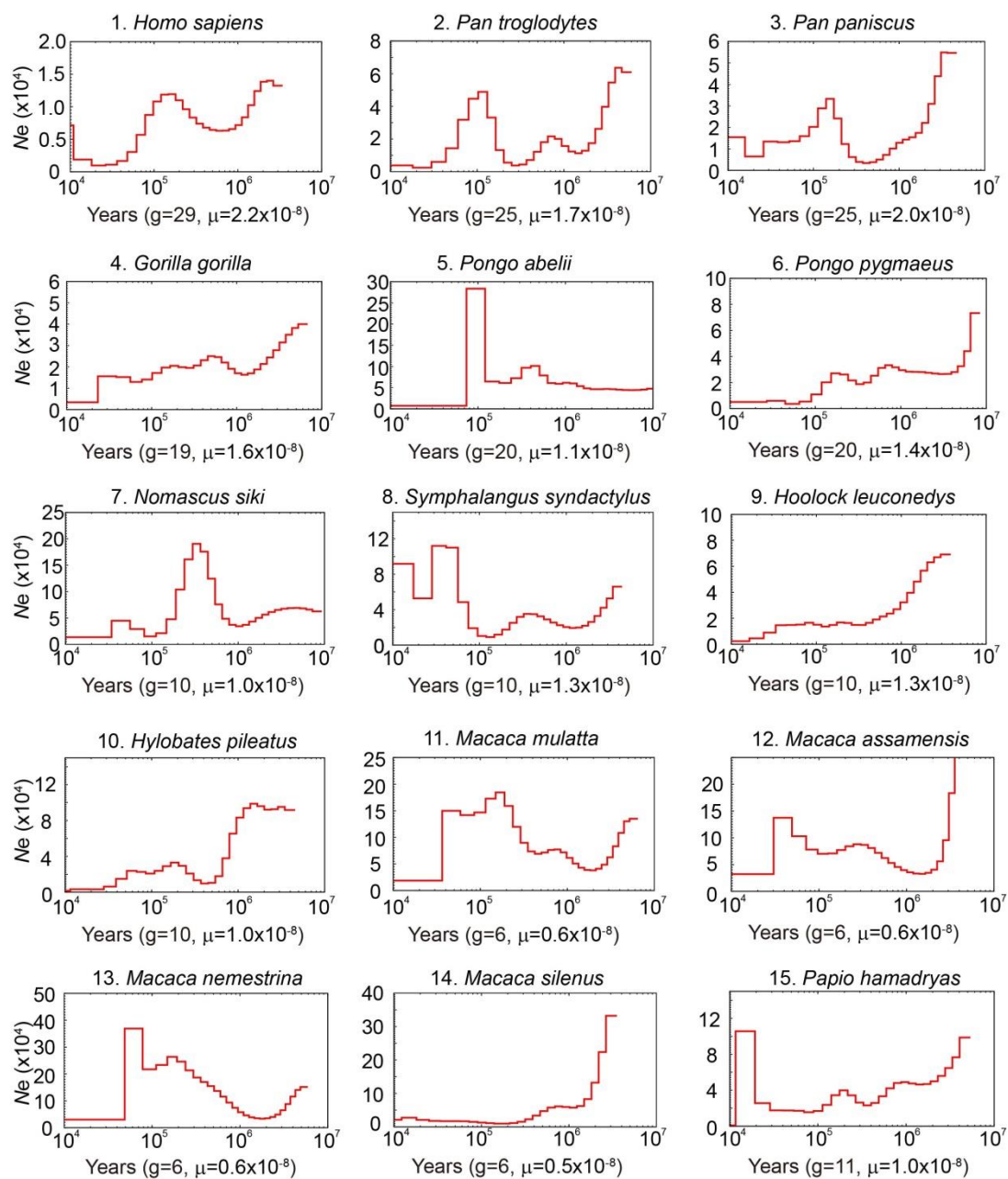
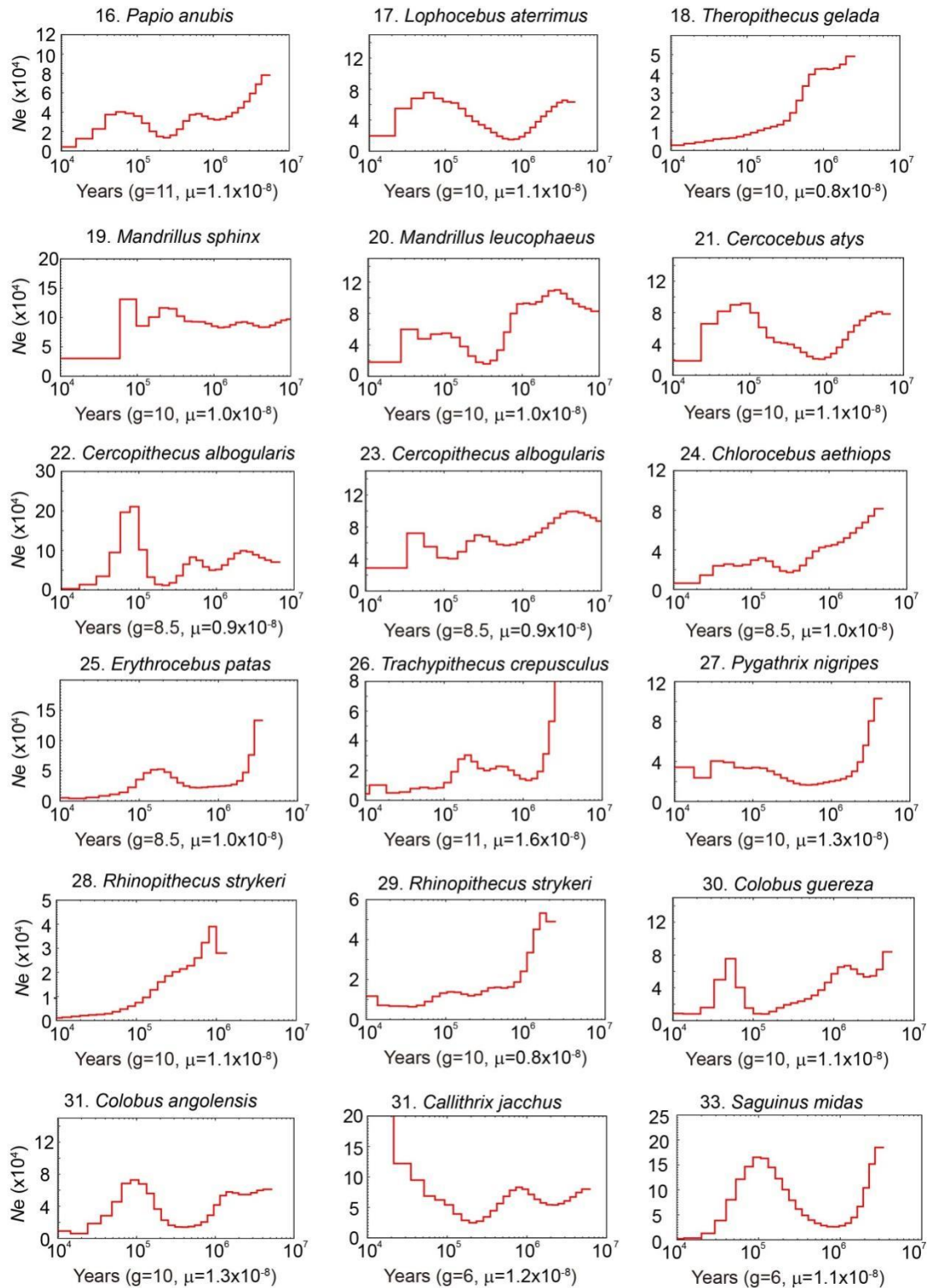


Fig. S36. Population dynamics history of representative primates, including 27 sequenced species and 21 downloaded species, from our primate genome project. The dynamic history of the effective population size (N_e) was visualized by using the PSMC algorithm. The X-axis represents years whereas the Y-axis represents N_e . The “g” parameter shows the generation time for each primate species. The “ μ ” values were inferred from the mutation rate per site per year. These parameters were cited and calculated in table S16 and table S41. The downloaded short-read sequencing data list is given in table S41. *Callithrix jacchus* showed aberrant recent population history dynamics, which may be due to admixture between different subspecies within the same species complex. Two species, namely *Chlorocebus sabaeus* and *Piliocolobus tephrosceles*, were excluded due to the lack of short-read data from the NCBI SRA database.





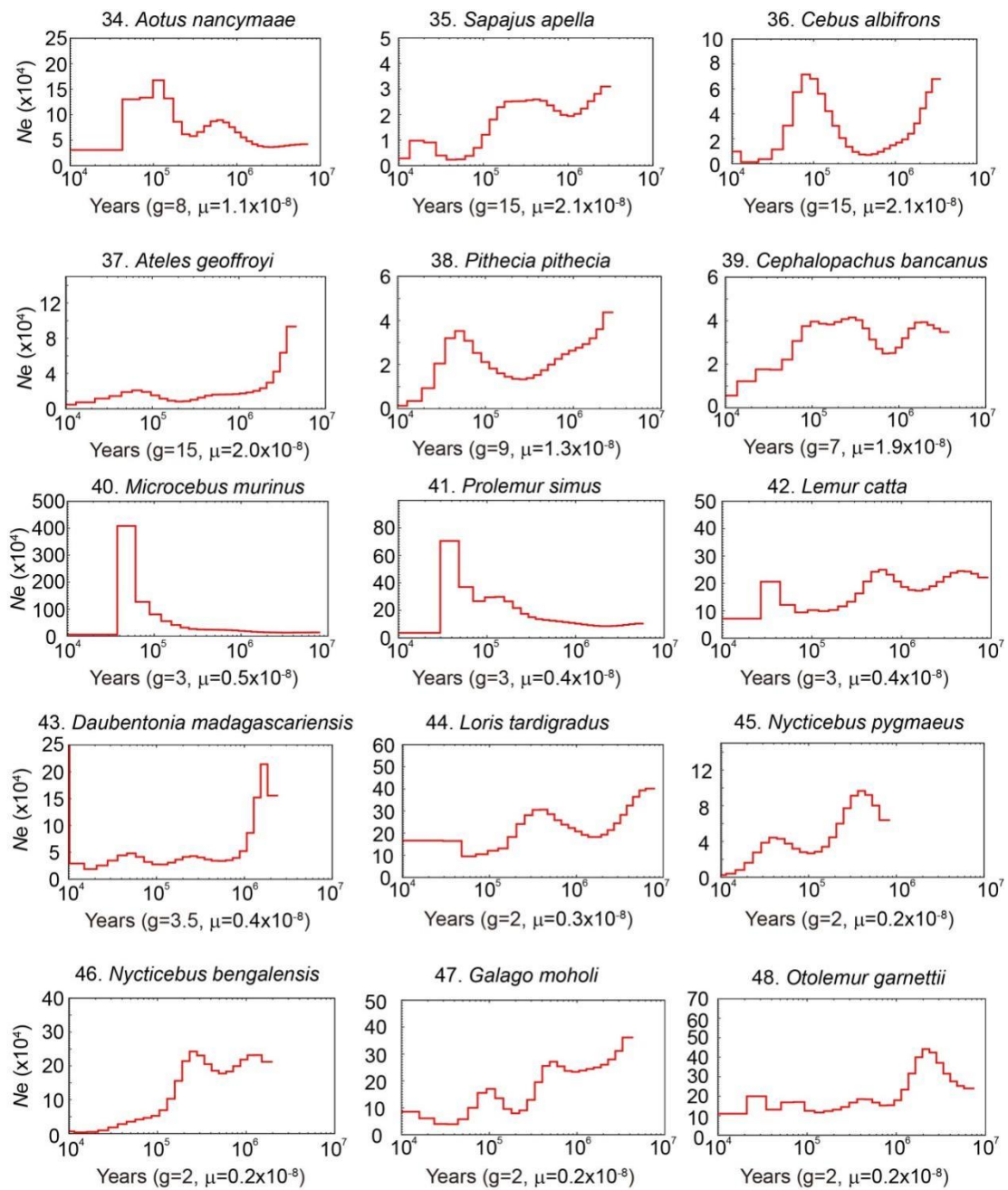


Fig. S37. Demographic history of non-human primates. Demographic history of all non-human primate species was fitted according to the geom_smooth (span=0.1) function in the ggplot2 library of R (v3.5.0). The normalized N_e was inferred by dividing the estimated value of N_e for each species at each time point with its maximum value. *Callithrix jacchus* was removed from this analysis because the genome was from an inbred family. The time including 100,000 and 50,000 years ago is highlighted by the green and black dotted lines, respectively.

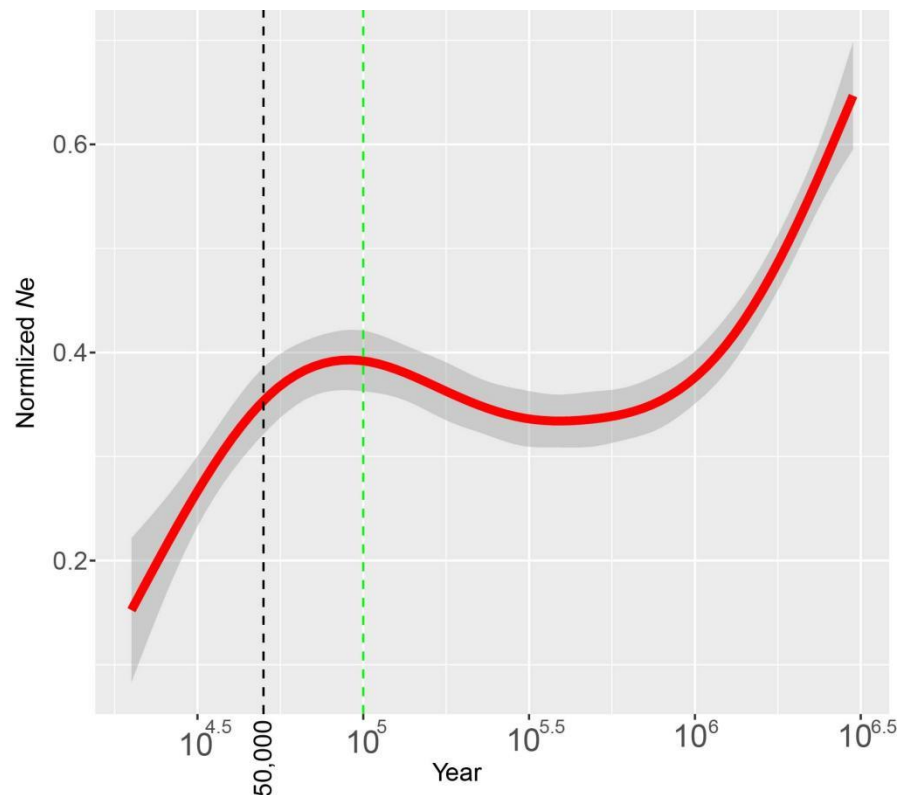


Fig. S38. Comparative analyses of nucleotide diversity in primate species based on IUCN Red List status. The median nucleotide diversity of each primate species was calculated according to a 50-kb non-overlapping sliding window on a whole-genome scale. We downloaded the IUCN Red List status information of each species in this study from THE IUCN RED LIST OF THREATENED SPECIES DATABASE (<https://www.iucnredlist.org/>). LC: Least Concern; NT: Near Threatened; VU: Vulnerable; EN: Endangered; CR: Critically Endangered. Additional information is provided in table S42.

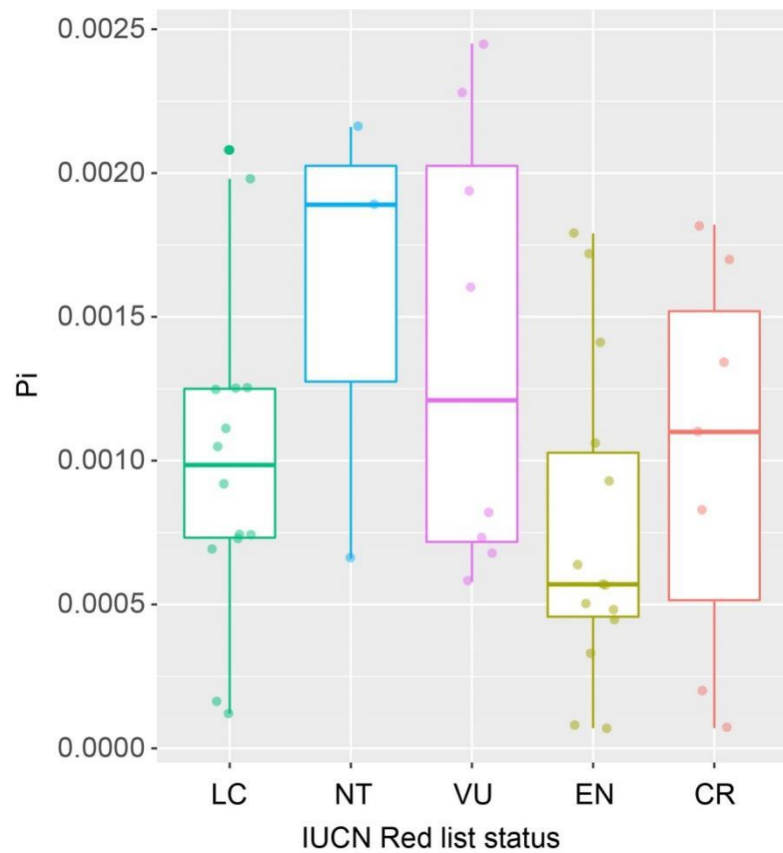


Fig. S39. Population dynamics history of 20 primate species showing a continual decline in N_e . The demographic histories of primate species over the past million years ago were inferred by using the pairwise sequentially Markovian coalescent model (PSMC) (151). We included the IUCN Red List status information for each species. CR=Critically Endangered; EN=Endangered, VU=Vulnerable; NT=Near threatened; LC=Least concern.

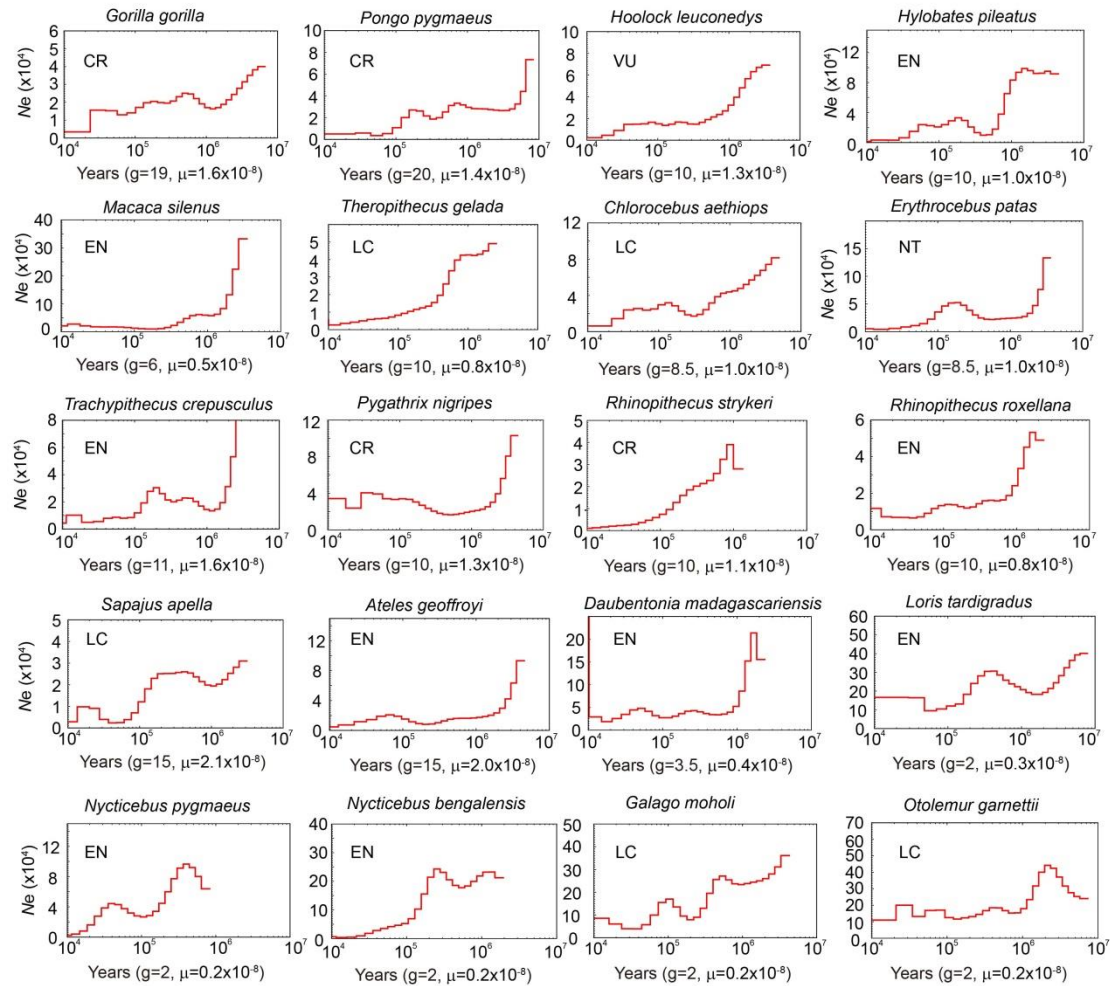


table S1. Single-molecule sequencing raw data statistics for each primate species representing 26 genera from 11 families. Three parameters including long-read sequencing platform, sequencing data and coverage are given.

Family	Genus	Species name	Sequencing platform	Sequencing data (bases)	Coverage (X)
Hominidae	<i>Pongo</i>	<i>Pongo pygmaeus</i>	Pacbio	151,467,742,407	52.85
Hylobatidae	<i>Nomascus</i>	<i>Nomascus siki</i>	Pacbio	149,946,567,298	53.88
Hylobatidae	<i>Sympalangus</i>	<i>Sympalangus syndactylus</i>	Pacbio	159,077,351,518	57.34
Hylobatidae	<i>Hoolock</i>	<i>Hoolock leuconedys</i>	ONT	156,590,185,899	56.22
Hylobatidae	<i>Hylobates</i>	<i>Hylobates pileatus</i>	ONT	150,950,070,274	52.94
Cercopithecidae	<i>Macaca</i>	<i>Macaca assamensis</i>	ONT	156,970,507,529	56.89
Cercopithecidae	<i>Macaca</i>	<i>Macaca silenus</i>	ONT	114,522,534,228	41.21
Cercopithecidae	<i>Papio</i>	<i>Papio hamadryas</i>	ONT	159,646,909,260	52.27
Cercopithecidae	<i>Lophocebus</i>	<i>Lophocebus aterrimus</i>	Pacbio	158,056,630,696	54.44
Cercopithecidae	<i>Mandrillus</i>	<i>Mandrillus sphinx</i>	ONT	165,871,342,996	58.48
Cercopithecidae	<i>Cercopithecus</i>	<i>Cercopithecus albogularis</i>	Pacbio	143,900,291,194	51.52
Cercopithecidae	<i>Chlorocebus</i>	<i>Chlorocebus aethiops</i>	Pacbio	149,295,464,604	52.88
Cercopithecidae	<i>Erythrocebus</i>	<i>Erythrocebus patas</i>	ONT	160,101,247,817	51.70
Cercopithecidae	<i>Trachypithecus</i>	<i>Trachypithecus crepusculus</i>	ONT	143,786,444,630	50.09
Cercopithecidae	<i>Pygathrix</i>	<i>Pygathrix nigripes</i>	ONT	141,205,564,168	48.76
Cercopithecidae	<i>Rhinopithecus</i>	<i>Rhinopithecus strykeri</i>	ONT	154,627,720,964	52.70
Cercopithecidae	<i>Colobus</i>	<i>Colobus guereza</i>	ONT	170,750,537,363	57.62
Callitrichidae	<i>Saguinus</i>	<i>Saguinus midas</i>	ONT	127,496,846,769	42.95
Cebidae	<i>Sapajus</i>	<i>Sapajus apella</i>	Pacbio	90,284,120,654	32.66
Cebidae	<i>Cebus</i>	<i>Cebus albifrons</i>	ONT	132,420,433,893	46.07
Atelidae	<i>Ateles</i>	<i>Ateles geoffroyi</i>	Pacbio	152,574,847,004	56.87
Pitheciidae	<i>Pithecia</i>	<i>Pithecia pithecia</i>	Pacbio	155,739,771,212	57.23
Tarsiidae	<i>Cephalopachus</i>	<i>Cephalopachus bancanus</i>	Pacbio	146,507,320,994	49.83
Daubentoniidae	<i>Daubentonia</i>	<i>Daubentonia madagascariensis</i>	Pacbio	149,520,007,402	61.99
Lorisidae	<i>Loris</i>	<i>Loris tardigradus</i>	Pacbio	154,272,498,770	56.35
Lorisidae	<i>Nycticebus</i>	<i>Nycticebus bengalensis</i>	ONT	144,496,844,856	50.59
Galagidae	<i>Galago</i>	<i>Galago moholi</i>	Pacbio	156,849,070,599	61.66

table S2. Strategies adopted for the *de novo* genome assembly of the long-read sequencing of 27 primate genomes. Four highlighted species in bold (*Hylobates pileatus*, *Colobus guereza*, *Saguinus midas* and *Nycticebus bengalensis*) were assembled at the chromosome level.

Family	Genus	Species name	Phylogenetic group	Assembly strategy
Hominidae	<i>Pongo</i>	<i>Pongo pygmaeus</i>	Hominoidea	Wtdbg2
Hylobatidae	<i>Nomascus</i>	<i>Nomascus siki</i>	Hominoidea	Wtdbg2+scaff10x
Hylobatidae	<i>Sympalangus</i>	<i>Sympalangus syndactylus</i>	Hominoidea	Falcon+scaff10x
Hylobatidae	<i>Hoolock</i>	<i>Hoolock leuconedys</i>	Hominoidea	Wtdbg2
Hylobatidae	<i>Hylobates</i>	<i>Hylobates pileatus</i>	Hominoidea	NextDenovo+3d-dna
Cercopithecidae	<i>Macaca</i>	<i>Macaca assamensis</i>	Old World monkey	NextDenovo
Cercopithecidae	<i>Macaca</i>	<i>Macaca silenus</i>	Old World monkey	NextDenovo
Cercopithecidae	<i>Papio</i>	<i>Papio hamadryas</i>	Old World monkey	NextDenovo
Cercopithecidae	<i>Lophocebus</i>	<i>Lophocebus aterrimus</i>	Old World monkey	Wtdbg2
Cercopithecidae	<i>Mandrillus</i>	<i>Mandrillus sphinx</i>	Old World monkey	NextDenovo
Cercopithecidae	<i>Cercopithecus</i>	<i>Cercopithecus albogularis</i>	Old World monkey	Wtdbg2
Cercopithecidae	<i>Chlorocebus</i>	<i>Chlorocebus aethiops</i>	Old World monkey	Wtdbg2
Cercopithecidae	<i>Erythrocebus</i>	<i>Erythrocebus patas</i>	Old World monkey	NextDenovo
Cercopithecidae	<i>Trachypithecus</i>	<i>Trachypithecus crepusculus</i>	Old World monkey	Wtdbg2
Cercopithecidae	<i>Pygathrix</i>	<i>Pygathrix nigripes</i>	Old World monkey	Wtdbg2
Cercopithecidae	<i>Rhinopithecus</i>	<i>Rhinopithecus strykeri</i>	Old World monkey	Wtdbg2
Cercopithecidae	<i>Colobus</i>	<i>Colobus guereza</i>	Old World monkey	NextDenovo+3d-dna
Callitrichidae	<i>Saguinus</i>	<i>Saguinus midas</i>	New World monkey	NextDenovo+3d-dna
Cebidae	<i>Sapajus</i>	<i>Sapajus apella</i>	New World monkey	NextDenovo
Cebidae	<i>Cebus</i>	<i>Cebus albifrons</i>	New World monkey	NextDenovo
Atelidae	<i>Ateles</i>	<i>Ateles geoffroyi</i>	New World monkey	Wtdbg2+scaffold10x
Pitheciidae	<i>Pithecia</i>	<i>Pithecia pithecia</i>	New World monkey	Falcon+scaffold10x
Tarsidae	<i>Cephalopachus</i>	<i>Cephalopachus bancanus</i>	Tarsier	Wtdbg2
Daubentoniidae	<i>Daubentonia</i>	<i>Daubentonia madagascariensis</i>	Strepsirrhini	Wtdbg2
Lorisidae	<i>Loris</i>	<i>Loris tardigradus</i>	Strepsirrhini	Wtdbg2
Lorisidae	<i>Nycticebus</i>	<i>Nycticebus bengalensis</i>	Strepsirrhini	Wtdbg2+3d-dna
Galagidae	<i>Galago</i>	<i>Galago moholi</i>	Strepsirrhini	Wtdbg2

table S3. Statistics of short-read sequencing data for 27 primate species in this study. Sequencing bases, sequencing depth and mapping ratio are listed.

Family	Genus	Species name	Sequencing bases	Sequencing depth	Mapping ratio (%)
Hominidae	<i>Pongo</i>	<i>Pongo pygmaeus</i>	165,144,953,400	57.62	99.02
Hylobatidae	<i>Nomascus</i>	<i>Nomascus siki</i>	197,205,561,300	70.86	98.75
Hylobatidae	<i>Sympalangus</i>	<i>Sympalangus syndactylus</i>	373,670,997,300	134.70	98.64
Hylobatidae	<i>Hoolock</i>	<i>Hoolock leuconedys</i>	152,500,809,000	54.76	98.80
Hylobatidae	<i>Hylobates</i>	<i>Hylobates pileatus</i>	154,924,394,550	54.33	98.33
Cercopithecidae	<i>Macaca</i>	<i>Macaca assamensis</i>	163,242,183,600	59.16	99.26
Cercopithecidae	<i>Macaca</i>	<i>Macaca silenus</i>	162,518,565,150	58.49	99.06
Cercopithecidae	<i>Papio</i>	<i>Papio hamadryas</i>	163,180,148,400	53.43	99.34
Cercopithecidae	<i>Lophocebus</i>	<i>Lophocebus aterrimus</i>	176,317,463,400	60.73	95.27
Cercopithecidae	<i>Mandrillus</i>	<i>Mandrillus sphinx</i>	203,585,704,800	71.78	98.58
Cercopithecidae	<i>Cercopithecus</i>	<i>Cercopithecus albogularis</i>	181,737,628,950	65.07	98.79
Cercopithecidae	<i>Chlorocebus</i>	<i>Chlorocebus aethiops</i>	170,760,436,650	60.48	99.03
Cercopithecidae	<i>Erythrocebus</i>	<i>Erythrocebus patas</i>	206,236,279,350	66.59	98.73
Cercopithecidae	<i>Trachypithecus</i>	<i>Pygathrix nigripes</i>	177,307,191,000	61.22	98.92
Cercopithecidae	<i>Pygathrix</i>	<i>Trachypithecus crepusculus</i>	174,362,084,550	60.74	98.59
Cercopithecidae	<i>Rhinopithecus</i>	<i>Rhinopithecus strykeri</i>	256,135,731,710	87.29	92.67
Cercopithecidae	<i>Colobus</i>	<i>Colobus guereza</i>	192,735,010,500	65.04	98.44
Callitrichidae	<i>Saguinus</i>	<i>Saguinus midas</i>	138,936,031,800	46.80	98.54
Cebidae	<i>Sapajus</i>	<i>Sapajus apella</i>	170,992,923,300	61.85	99.24
Cebidae	<i>Cebus</i>	<i>Cebus albifrons</i>	150,831,284,850	52.47	99.05
Atelidae	<i>Ateles</i>	<i>Ateles geoffroyi</i>	386,880,162,150	144.20	98.90
Pitheciidae	<i>Pithecia</i>	<i>Pithecia pithecia</i>	400,370,988,600	147.12	99.20
Tarsidae	<i>Cephalopachus</i>	<i>Cephalopachus bancanus</i>	139,605,027,728	47.48	97.40
Daubentoniidae	<i>Daubentonia</i>	<i>Daubentonia madagascariensis</i>	173,969,409,668	72.12	99.00
Lorisidae	<i>Loris</i>	<i>Loris tardigradus</i>	157,028,756,647	57.36	99.18
Lorisidae	<i>Nycticebus</i>	<i>Nycticebus bengalensis</i>	173,774,219,700	60.84	98.56
Galagidae	<i>Galago</i>	<i>Galago moholi</i>	151,403,904,696	59.52	98.58

table S4. Statistics of Hi-C sequencing data for 4 primate species in this study. The four species were *Hylobates pileatus*, *Colobus guereza*, *Saguinus midas* and *Nycticebus bengalensis*.

Family	Genus	Species name	Sequencing data (bases)	Coverage (X)
Hylobatidae	<i>Hylobates</i>	<i>Hylobates pileatus</i>	321,553,728,602	112.77
Cercopithecidae	<i>Colobus</i>	<i>Colobus guereza</i>	285,772,688,923	96.43
Callitrichidae	<i>Saguinus</i>	<i>Saguinus midas</i>	434,754,499,557	146.45
Lorisidae	<i>Nycticebus</i>	<i>Nycticebus bengalensis</i>	288,361,915,627	100.94

table S5. Genome coverage statistics of 27 primate genomes newly assembled in this study. Estimated genome sizes for each primate species were obtained from 17 k-mer-based estimations. The assembled genomes were mostly consistent with the k-mer-based estimations, indicating relatively complete genome coverage for all species.

Family	Genus	Species name	Genome size (bp)	Estimated genome sizes (bp)
Hominidae	<i>Pongo</i>	<i>Pongo pygmaeus</i>	2,866,029,761	3,207,162,863
Hylobatidae	<i>Nomascus</i>	<i>Nomascus siki</i>	2,783,107,017	3,037,418,990
Hylobatidae	<i>Sympalangus</i>	<i>Sympalangus syndactylus</i>	2,774,050,050	3,836,928,248
Hylobatidae	<i>Hoolock</i>	<i>Hoolock leuconedys</i>	2,785,098,935	2,898,596,937
Hylobatidae	<i>Hylobates</i>	<i>Hylobates pileatus</i>	2,851,478,483	2,944,662,251
Cercopithecidae	<i>Macaca</i>	<i>Macaca assamensis</i>	2,759,375,986	2,976,116,000
Cercopithecidae	<i>Macaca</i>	<i>Macaca silenus</i>	2,778,791,713	3,024,651,073
Cercopithecidae	<i>Papio</i>	<i>Papio hamadryas</i>	3,054,335,410	3,036,963,873
Cercopithecidae	<i>Lophocebus</i>	<i>Lophocebus aterrimus</i>	2,903,351,443	3,424,136,245
Cercopithecidae	<i>Mandrillus</i>	<i>Mandrillus sphinx</i>	2,836,346,068	2,981,473,710
Cercopithecidae	<i>Cercopithecus</i>	<i>Cercopithecus albogularis</i>	2,793,076,453	3,382,339,205
Cercopithecidae	<i>Chlorocebus</i>	<i>Chlorocebus aethiops</i>	2,823,243,693	3,316,217,175
Cercopithecidae	<i>Erythrocebus</i>	<i>Erythrocebus patas</i>	3,096,929,461	3,543,033,517
Cercopithecidae	<i>Trachypithecus</i>	<i>Trachypithecus crepusculus</i>	2,870,799,684	3,054,185,533
Cercopithecidae	<i>Pygathrix</i>	<i>Pygathrix nigripes</i>	2,896,210,064	3,167,888,479
Cercopithecidae	<i>Rhinopithecus</i>	<i>Rhinopithecus strykeri</i>	2,934,222,284	3,249,344,642
Cercopithecidae	<i>Colobus</i>	<i>Colobus guereza</i>	2,963,502,603	3,376,011,948
Callitrichidae	<i>Saguinus</i>	<i>Saguinus midas</i>	2,968,712,378	3,354,491,578
Cebidae	<i>Sapajus</i>	<i>Sapajus apella</i>	2,764,443,388	3,394,526,181
Cebidae	<i>Cebus</i>	<i>Cebus albifrons</i>	2,874,442,237	3,368,565,361
Atelidae	<i>Ateles</i>	<i>Ateles geoffroyi</i>	2,683,028,796	3,440,324,378
Pitheciidae	<i>Pithecia</i>	<i>Pithecia pithecia</i>	2,721,439,713	3,506,517,155
Tarsidae	<i>Cephalopachus</i>	<i>Cephalopachus bancanus</i>	2,940,271,818	3,114,266,101
Daubentonidae	<i>Daubentonia</i>	<i>Daubentonia madagascariensis</i>	2,412,055,963	2,589,794,023
Lorisidae	<i>Loris</i>	<i>Loris tardigradus</i>	2,737,734,828	2,921,981,950
Lorisidae	<i>Nycticebus</i>	<i>Nycticebus bengalensis</i>	2,856,368,736	3,302,942,615
Galagidae	<i>Galago</i>	<i>Galago moholi</i>	2,543,922,824	2,759,821,024

table S6. Assembly statistics for genomes from 27 primate species in this study.
 Three assembly parameters (Contig N50, Scaffold N50 and BUSCO) are listed. All the assemblies yielded BUSCO complete scores >92%.

Family	Genus	Species name	Contig N50 (bp)	Scaffold N50 (bp)	BUSCO (%)
Hominidae	<i>Pongo</i>	<i>Pongo pygmaeus</i>	15,810,633	15,810,633	96.3
Hylobatidae	<i>Nomascus</i>	<i>Nomascus siki</i>	8,523,852	19,995,890	95.2
Hylobatidae	<i>Sympalangus</i>	<i>Sympalangus syndactylus</i>	13,408,629	13,408,629	95.5
Hylobatidae	<i>Hoolock</i>	<i>Hoolock leuconedys</i>	22,338,800	22,338,800	95.0
Hylobatidae	<i>Hylobates</i>	<i>Hylobates pileatus</i>	17,385,161	131,825,309	95.5
Cercopithecidae	<i>Macaca</i>	<i>Macaca assamensis</i>	27,348,716	27,348,716	96.6
Cercopithecidae	<i>Macaca</i>	<i>Macaca silenus</i>	25,691,658	25,691,658	96.2
Cercopithecidae	<i>Papio</i>	<i>Papio hamadryas</i>	24,989,958	24,989,958	95.8
Cercopithecidae	<i>Lophocebus</i>	<i>Lophocebus aterrimus</i>	6,802,059	6,802,059	96.5
Cercopithecidae	<i>Mandrillus</i>	<i>Mandrillus sphinx</i>	20,999,372	20,999,372	95.2
Cercopithecidae	<i>Cercopithecus</i>	<i>Cercopithecus albogularis</i>	13,914,891	13,914,891	95.9
Cercopithecidae	<i>Chlorocebus</i>	<i>Chlorocebus aethiops</i>	9,639,656	9,639,656	96.4
Cercopithecidae	<i>Erythrocebus</i>	<i>Erythrocebus patas</i>	18,747,272	18,747,272	96.4
Cercopithecidae	<i>Trachypithecus</i>	<i>Trachypithecus crepusculus</i>	14,781,066	14,781,066	95.0
Cercopithecidae	<i>Pygathrix</i>	<i>Pygathrix nigripes</i>	14,260,291	14,260,291	95.1
Cercopithecidae	<i>Rhinopithecus</i>	<i>Rhinopithecus strykeri</i>	16,766,498	16,766,498	95.2
Cercopithecidae	<i>Colobus</i>	<i>Colobus guereza</i>	15,612,012	145,964,134	96.2
Callitrichidae	<i>Saguinus</i>	<i>Saguinus midas</i>	10,987,047	143,273,090	95.2
Cebidae	<i>Sapajus</i>	<i>Sapajus apella</i>	12,583,278	12,583,278	96.0
Cebidae	<i>Cebus</i>	<i>Cebus albifrons</i>	18,502,463	18,502,463	95.8
Atelidae	<i>Ateles</i>	<i>Ateles geoffroyi</i>	29,212,752	29,212,752	96.5
Pitheciidae	<i>Pithecia</i>	<i>Pithecia pithecia</i>	10,867,430	10,867,430	94.5
Tarsidae	<i>Cephalopachus</i>	<i>Cephalopachus bancanus</i>	5,252,243	5,252,243	94.4
Daubentonidae	<i>Daubentonia</i>	<i>Daubentonia madagascariensis</i>	27,954,151	27,954,151	97.5
Lorisidae	<i>Loris</i>	<i>Loris tardigradus</i>	7,727,436	7,727,436	96.1
Lorisidae	<i>Nycticebus</i>	<i>Nycticebus bengalensis</i>	19,794,679	130,794,859	94.1
Galagidae	<i>Galago</i>	<i>Galago moholi</i>	583,552	583,552	92.0

table S7. Gene predictions of protein-coding genes across sequenced primate species in this study. The gene number, average CDS length and average gene length are given for all species.

Family	Genus	Species name	Gene number	Average CDS length (bp)	Average gene length (bp)
Hominidae	<i>Pongo</i>	<i>Pongo pygmaeus</i>	21,468	1,729	44,298
Hylobatidae	<i>Nomascus</i>	<i>Nomascus siki</i>	20,362	1,704	42,883
Hylobatidae	<i>Sympalangus</i>	<i>Sympalangus syndactylus</i>	21,439	1,624	42,774
Hylobatidae	<i>Hoolock</i>	<i>Hoolock leuconedys</i>	20,942	1,664	44,844
Hylobatidae	<i>Hylobates</i>	<i>Hylobates pileatus</i>	20,656	1,697	40,462
Cercopithecidae	<i>Macaca</i>	<i>Macaca assamensis</i>	20,960	1,740	43,952
Cercopithecidae	<i>Macaca</i>	<i>Macaca silenus</i>	20,689	1,825	46,755
Cercopithecidae	<i>Papio</i>	<i>Papio hamadryas</i>	21,226	1,709	44,802
Cercopithecidae	<i>Lophocebus</i>	<i>Lophocebus aterrimus</i>	21,374	1,746	44,113
Cercopithecidae	<i>Mandrillus</i>	<i>Mandrillus sphinx</i>	20,607	1,785	44,758
Cercopithecidae	<i>Cercopithecus</i>	<i>Cercopithecus albogularis</i>	20,668	1,740	42,051
Cercopithecidae	<i>Chlorocebus</i>	<i>Chlorocebus aethiops</i>	21,038	1,728	42,632
Cercopithecidae	<i>Erythrocebus</i>	<i>Erythrocebus patas</i>	20,967	1,731	41,633
Cercopithecidae	<i>Trachypithecus</i>	<i>Trachypithecus crepusculus</i>	20,368	1,681	44,209
Cercopithecidae	<i>Pygathrix</i>	<i>Pygathrix nigripes</i>	20,667	1,700	41,554
Cercopithecidae	<i>Rhinopithecus</i>	<i>Rhinopithecus strykeri</i>	20,837	1,661	41,159
Cercopithecidae	<i>Colobus</i>	<i>Colobus guereza</i>	20,768	1,676	39,866
Callitrichidae	<i>Saguinus</i>	<i>Saguinus midas</i>	20,303	1,739	42,549
Cebidae	<i>Sapajus</i>	<i>Sapajus apella</i>	20,378	1,801	45,455
Cebidae	<i>Cebus</i>	<i>Cebus albifrons</i>	20,332	1,785	43,566
Atelidae	<i>Ateles</i>	<i>Ateles geoffroyi</i>	20,593	1,786	43,717
Pitheciidae	<i>Pithecia</i>	<i>Pithecia pithecia</i>	20,372	1,600	40,652
Tarsidae	<i>Cephalopachus</i>	<i>Cephalopachus bancanus</i>	20,775	1,566	39,334
Daubentonidae	<i>Daubentonia</i>	<i>Daubentonia madagascariensis</i>	20,066	1,816	39,734
Lorisidae	<i>Loris</i>	<i>Loris tardigradus</i>	20,423	1,784	41,329
Lorisidae	<i>Nycticebus</i>	<i>Nycticebus bengalensis</i>	21,354	1,687	41,245
Galagidae	<i>Galago</i>	<i>Galago moholi</i>	20,789	1,663	32,053

table S8. Downloaded genome version for comparative genomics analysis in this study. Genome version id and associated database origins are given.

Family	Genus	Species Name	Genome version	Origin
Hominidae	<i>Homo</i>	<i>Homo sapiens</i>	GRCh38.p12	ENSEMBL 97
Hominidae	<i>Gorilla</i>	<i>Gorilla gorilla</i>	GCA_900006655.3	NCBI
Hominidae	<i>Pan</i>	<i>Pan paniscus</i>	GCA_000258655.2	NCBI
Hominidae	<i>Pan</i>	<i>Pan troglodytes</i>	GCF_002880755.1	NCBI
Hominidae	<i>Pongo</i>	<i>Pongo abelii</i>	GCA_002880775.3	NCBI
Cercopithecidae	<i>Macaca</i>	<i>Macaca mulatta</i>	GCA_008058575.1	NCBI
Cercopithecidae	<i>Macaca</i>	<i>Macaca nemestrina</i>	GCA_000956065.1	NCBI
Cercopithecidae	<i>Papio</i>	<i>Papio anubis</i>	GCA_000264685.2	NCBI
Cercopithecidae	<i>Theropithecus</i>	<i>Theropithecus gelada</i>	GCA_003255815.1	NCBI
Cercopithecidae	<i>Mandrillus</i>	<i>Mandrillus leucophaeus</i>	PRJNA785018	NCBI
Cercopithecidae	<i>Cercocebus</i>	<i>Cercocebus atys</i>	GCA_000955945.1	NCBI
Cercopithecidae	<i>Chlorocebus</i>	<i>Chlorocebus sabaeus</i>	GCA_000409795.2	NCBI
Cercopithecidae	<i>Cercopithecus</i>	<i>Cercopithecus mona</i>	GCA_014849445.1	NCBI
Cercopithecidae	<i>Piliocolobus</i>	<i>Piliocolobus tephrosceles</i>	GCA_002776525.2	NCBI
Cercopithecidae	<i>Rhinopithecus</i>	<i>Rhinopithecus roxellana</i>	GCA_007565055.1	NCBI
Cercopithecidae	<i>Colobus</i>	<i>Colobus angolensis</i>	GCA_000951035.1	NCBI
Callitrichidae	<i>Callithrix</i>	<i>Callithrix jacchus</i>	GCA_011100535.2	NCBI
Aotidae	<i>Aotus</i>	<i>Aotus nancymaae</i>	GCA_000952055.2	NCBI
Cheirogaleidae	<i>Microcebus</i>	<i>Microcebus murinus</i>	GCA_000165445.3	NCBI
Lemuridae	<i>Prolemur</i>	<i>Prolemur simus</i>	GCA_003258685.1	NCBI
Galagidae	<i>Otolemur</i>	<i>Otolemur garnettii</i>	GCA_000181295.3	NCBI
Lemuridae	<i>Lemur</i>	<i>Lemur catta</i>	PRJNA562215	NCBI
Lorisidae	<i>Nycticebus</i>	<i>Nycticebus pygmaeus</i>	Our accompanying paper (32)	GSA
Cynocephalidae	<i>Galeopterus</i>	<i>Galeopterus variegatus</i>	PRJNA399345	NCBI
Tupaiidae	<i>Tupaia</i>	<i>Tupaia belangeri</i>	TreeshrewDB v2.0: http://www.treeshrewdb.org	GSA

table S9. Aligned length statistics for multiple species genome alignments. The genome size, aligned length and alignment rate are given.

Family	Genus	Species name	Genome size	Aligned length	Alignment rate
Hominidae	<i>Homo</i>	<i>Homo sapiens</i>	3,099,750,718	2,859,711,246	0.92
Hominidae	<i>Pan</i>	<i>Pan troglodytes</i>	3,024,031,013	2,817,711,027	0.93
Hominidae	<i>Pan</i>	<i>Pan paniscus</i>	3,286,643,938	2,747,645,364	0.84
Hominidae	<i>Gorilla</i>	<i>Gorilla gorilla</i>	3,084,595,669	2,794,306,801	0.91
Hominidae	<i>Pongo</i>	<i>Pongo abelii</i>	3,065,035,716	2,752,899,888	0.9
Hominidae	<i>Pongo</i>	<i>Pongo pygmaeus</i>	2,866,029,761	2,714,380,444	0.95
Hylobatidae	<i>Nomascus</i>	<i>Nomascus siki</i>	2,783,107,017	2,603,900,630	0.94
Hylobatidae	<i>Sympalangus</i>	<i>Sympalangus syndactylus</i>	2,774,050,050	2,634,493,348	0.95
Hylobatidae	<i>Hoolock</i>	<i>Hoolock leuconedys</i>	2,785,098,935	2,603,678,188	0.93
Hylobatidae	<i>Hylobates</i>	<i>Hylobates pileatus</i>	2,851,478,483	2,584,499,780	0.91
Cercopithecidae	<i>Macaca</i>	<i>Macaca mulatta</i>	2,955,490,605	2,569,702,476	0.87
Cercopithecidae	<i>Macaca</i>	<i>Macaca assamensis</i>	2,759,375,986	2,557,823,014	0.93
Cercopithecidae	<i>Macaca</i>	<i>Macaca nemestrina</i>	2,948,703,511	2,555,795,260	0.87
Cercopithecidae	<i>Macaca</i>	<i>Macaca silenus</i>	2,778,791,713	2,558,701,946	0.92
Cercopithecidae	<i>Papio</i>	<i>Papio hamadryas</i>	3,054,335,410	2,544,396,386	0.83
Cercopithecidae	<i>Papio</i>	<i>Papio anubis</i>	2,959,356,508	2,565,346,833	0.87
Cercopithecidae	<i>Lophocebus</i>	<i>Lophocebus aterrimus</i>	2,903,351,443	2,568,026,562	0.88
Cercopithecidae	<i>Theropithecus</i>	<i>Theropithecus gelada</i>	2,889,614,139	2,575,616,509	0.89
Cercopithecidae	<i>Mandrillus</i>	<i>Mandrillus sphinx</i>	2,836,346,068	2,527,559,704	0.89
Cercopithecidae	<i>Mandrillus</i>	<i>Mandrillus leucophaeus</i>	2,935,729,887	2,576,476,604	0.88
Cercopithecidae	<i>Cercocebus</i>	<i>Cercocebus atys</i>	2,848,246,356	2,563,099,972	0.9
Cercopithecidae	<i>Cercopithecus</i>	<i>Cercopithecus albogularis</i>	2,793,076,453	2,534,872,735	0.91
Cercopithecidae	<i>Cercopithecus</i>	<i>Cercopithecus mona</i>	2,902,804,697	2,517,749,510	0.87
Cercopithecidae	<i>Chlorocebus</i>	<i>Chlorocebus aethiops</i>	2,823,243,693	2,554,745,799	0.9
Cercopithecidae	<i>Chlorocebus</i>	<i>Chlorocebus sabaeus</i>	2,789,639,778	2,571,549,904	0.92
Cercopithecidae	<i>Erythrocebus</i>	<i>Erythrocebus patas</i>	3,096,929,461	2,528,277,858	0.82
Cercopithecidae	<i>Trachypithecus</i>	<i>Trachypithecus crepusculus</i>	2,870,799,684	2,513,718,414	0.88
Cercopithecidae	<i>Pygathrix</i>	<i>Pygathrix nigripes</i>	2,896,210,064	2,527,627,308	0.87
Cercopithecidae	<i>Rhinopithecus</i>	<i>Rhinopithecus strykeri</i>	2,934,222,284	2,508,236,626	0.85
Cercopithecidae	<i>Rhinopithecus</i>	<i>Rhinopithecus roxellana</i>	3,038,460,517	2,564,419,952	0.84
Cercopithecidae	<i>Piliocolobus</i>	<i>Piliocolobus tephrosceles</i>	3,038,007,327	2,548,107,659	0.84
Cercopithecidae	<i>Colobus</i>	<i>Colobus guereza</i>	2,963,502,603	2,510,173,070	0.85
Cercopithecidae	<i>Colobus</i>	<i>Colobus angolensis</i>	2,970,124,662	2,486,046,307	0.84
Callitrichidae	<i>Callithrix</i>	<i>Callithrix jacchus</i>	2,863,864,636	2,238,835,124	0.78
Callitrichidae	<i>Saguinus</i>	<i>Saguinus midas</i>	2,968,712,378	2,227,242,188	0.75
Aotidae	<i>Aotus</i>	<i>Aotus nancymaae</i>	2,861,668,348	2,253,128,038	0.79
Cebidae	<i>Sapajus</i>	<i>Sapajus apella</i>	2,764,443,388	2,263,802,381	0.82
Cebidae	<i>Cebus</i>	<i>Cebus albifrons</i>	2,874,442,237	2,251,805,898	0.78
Atelidae	<i>Ateles</i>	<i>Ateles geoffroyi</i>	2,683,028,796	2,278,151,074	0.85

Pitheciidae	<i>Pithecia</i>	<i>Pithecia pithecia</i>	2,721,439,713	2,299,935,171	0.85
Tarsidae	<i>Cephalopachus</i>	<i>Cephalopachus bancanus</i>	2,940,271,818	1,828,871,241	0.62
Cheirogaleidae	<i>Microcebus</i>	<i>Microcebus murinus</i>	2,487,392,024	1,722,717,486	0.69
Lemuridae	<i>Prolemur</i>	<i>Prolemur simus</i>	2,411,593,676	1,706,107,078	0.71
Lemuridae	<i>Lemur</i>	<i>Lemur catta</i>	2,122,351,751	1,703,765,223	0.8
Daubentoniiidae	<i>Daubentonii</i>	<i>Daubentonii madagascariensis</i>	2,412,055,963	1,870,779,156	0.78
Lorisidae	<i>Loris</i>	<i>Loris tardigradus</i>	2,737,734,828	1,617,637,987	0.59
Lorisidae	<i>Nycticebus</i>	<i>Nycticebus pygmaeus</i>	2,828,132,058	1,619,133,058	0.57
Lorisidae	<i>Nycticebus</i>	<i>Nycticebus bengalensis</i>	2,856,368,736	1,600,575,412	0.56
Galagidae	<i>Galago</i>	<i>Galago moholi</i>	2,543,922,824	1,602,622,867	0.63
Galagidae	<i>Otolemur</i>	<i>Otolemur garnettii</i>	2,519,724,550	1,590,869,944	0.63
Cynocephalidae	<i>Galeopterus</i>	<i>Galeopterus variegatus</i>	3,349,451,543	1,748,653,931	0.52
Tupaiaidae	<i>Tupaia</i>	<i>Tupaia belangeri</i>	2,667,507,236	1,378,718,279	0.52

table S10. 37 (of 50) representative genomes for the analysis of chromosome evolution and genome rearrangement during primate evolution. Primate genomes with scaffold N50 \geq 13 Mb were retained for this analysis. The outgroup species *Tupaia belangeri* was included in this analysis.

Familiey	Genus	Species name	Genome size (bp)	Contig N50 (bp)	Scaffold N50 (bp)
Hominidae	<i>Homo</i>	<i>Homo sapiens</i>	3,099,750,718	50,761,348	145,138,636
Hominidae	<i>Pan</i>	<i>Pan paniscus</i>	3,286,643,938	61,424	144,709,823
Hominidae	<i>Pan</i>	<i>Pan troglodytes</i>	3,024,031,013	12,421,315	130,995,916
Hominidae	<i>Gorilla</i>	<i>Gorilla gorilla</i>	3,084,595,669	9,406,846	129,679,333
Hominidae	<i>Pongo</i>	<i>Pongo abelii</i>	3,065,035,716	11,074,009	132,178,492
Hominidae	<i>Pongo</i>	<i>Pongo pygmaeus</i>	2,866,029,761	15,810,633	15,810,633
Hylobatidae	<i>Nomascus</i>	<i>Nomascus siki</i>	2,783,107,017	8,523,852	19,995,890
Hylobatidae	<i>Hoolock</i>	<i>Hoolock leuconedys</i>	2,785,098,935	22,338,800	22,338,800
Hylobatidae	<i>Hylobates</i>	<i>Hylobates pileatus</i>	2,851,478,483	17,385,161	131,825,309
Cercopithecidae	<i>Macaca</i>	<i>Macaca mulatta</i>	2,955,490,605	8,353,667	152,195,021
Cercopithecidae	<i>Macaca</i>	<i>Macaca assamensis</i>	2,759,375,986	27,348,716	27,348,716
Cercopithecidae	<i>Macaca</i>	<i>Macaca nemestrina</i>	2,948,703,511	106,822	15,219,753
Cercopithecidae	<i>Papio</i>	<i>Papio hamadryas</i>	3,054,335,410	24,989,958	24,989,958
Cercopithecidae	<i>Papio</i>	<i>Papio anubis</i>	2,959,356,508	138,819	140,346,614
Cercopithecidae	<i>Theropithecus</i>	<i>Theropithecus gelada</i>	2,889,614,139	225,709	130,230,028
Cercopithecidae	<i>Mandrillus</i>	<i>Mandrillus sphinx</i>	2,836,346,068	20,999,372	20,999,372
Cercopithecidae	<i>Mandrillus</i>	<i>Mandrillus leucophaeus</i>	2,935,729,887	124,362	26,881,038
Cercopithecidae	<i>Cercocebus</i>	<i>Cercopithecus albogularis</i>	2,793,076,453	13,914,891	13,914,891
Cercopithecidae	<i>Cercopithecus</i>	<i>Cercopithecus mona</i>	2,902,804,697	22,791,723	22,791,723
Cercopithecidae	<i>Chlorocebus</i>	<i>Chlorocebus sabaeus</i>	2,789,639,778	74,669	101,219,884
Cercopithecidae	<i>Trachypithecus</i>	<i>Trachypithecus crepusculus</i>	2,870,799,684	14,781,066	14,781,066
Cercopithecidae	<i>Pygathrix</i>	<i>Pygathrix nigripes</i>	2,896,210,064	14,260,291	14,260,291
Cercopithecidae	<i>Rhinopithecus</i>	<i>Rhinopithecus strykeri</i>	2,934,222,284	16,766,498	16,766,498
Cercopithecidae	<i>Rhinopithecus</i>	<i>Rhinopithecus roxellana</i>	3,038,460,517	5,723,610	144,559,847
Cercopithecidae	<i>Piliocolobus</i>	<i>Piliocolobus tephrosceles</i>	3,038,007,327	98,446	13,534,873
Cercopithecidae	<i>Colobus</i>	<i>Colobus guereza</i>	2,963,502,603	15,612,012	145,964,134
Callitrichidae	<i>Callithrix</i>	<i>Callithrix jacchus</i>	2,863,864,636	13,255,626	129,995,920
Callitrichidae	<i>Saguinus</i>	<i>Saguinus midas</i>	2,968,712,378	10,987,047	143,273,090
Cebidae	<i>Cebus</i>	<i>Cebus albifrons</i>	2,874,442,237	18,502,463	18,502,463
Atelidae	<i>Ateles</i>	<i>Ateles geoffroyi</i>	2,683,028,796	29,212,752	29,212,752
Cheirogaleidae	<i>Microcebus</i>	<i>Microcebus murinus</i>	2,487,392,024	210,702	108,171,978
Lemuridae	<i>Lemur</i>	<i>Lemur catta</i>	2,233,154,473	25,671,697	25,671,697
Daubentonidae	<i>Daubentonia</i>	<i>Daubentonia madagascariensis</i>	2,412,055,963	27,954,151	27,954,151
Lorisidae	<i>Nycticebus</i>	<i>Nycticebus pygmaeus</i>	2,828,132,058	6,142,509	136,556,743
Lorisidae	<i>Nycticebus</i>	<i>Nycticebus bengalensis</i>	2,856,705,436	19,794,679	130,794,859
Galagidae	<i>Otolemur</i>	<i>Otolemur garnettii</i>	2,519,724,550	27,100	13,852,661
Tupaiidae	<i>Tupaia</i>	<i>Tupaia belangeri</i>	2,667,507,236	3,217,288	104,643,080

table S11. Segmental duplications identified in the genomes of 35 primates and 5 outgroup species in this study. Segmental duplications of $\geq 5\text{kb}$ were retained for downstream comparative genomics analysis. The outgroup species were *Cephalopachus bancanus*, *Tupaia belangeri*, *Mus musculus*, *Felis catus* and *Sus scrofa*.

Species name	number	total_len (bp)	ave_len (bp)	min_len (bp)	max_len (bp)
<i>Pan troglodytes</i>	10,124	103,234,954	11,186	5,001	96,148
<i>Gorilla gorilla</i>	7,386	72,980,326	10,410	5,000	91,694
<i>Pongo abelii</i>	14,154	132,584,212	10,283	5,000	90,792
<i>Pongo pygmaeus</i>	1,384	8,490,743	6,265	5,000	35,146
<i>Hylobates pileatus</i>	3,592	23,856,770	7,030	5,000	45,954
<i>Sympalangus syndactylus</i>	5,023	57,209,090	11,961	5,000	146,164
<i>Hoolock leuconedys</i>	1,154	7,200,734	6,310	5,001	21,258
<i>Nomascus siki</i>	781	4,539,606	5,943	5,000	13,786
<i>Macaca mulatta</i>	10,264	131,917,476	13,904	5,000	149,503
<i>Macaca assamensis</i>	2,674	18,528,014	7,363	5,001	83,638
<i>Macaca silenus</i>	2,383	15,059,924	6,662	5,000	42,550
<i>Mandrillus sphinx</i>	3,809	25,968,581	7,252	5,000	61,387
<i>Papio hamadryas</i>	6,364	41,776,416	6,978	5,000	79,026
<i>Lophocebus aterrimus</i>	2,464	14,451,590	6,368	5,001	35,346
<i>Cercopithecus mona</i>	6,695	45,116,068	7,084	5,000	41,154
<i>Cercopithecus albogularis</i>	1,827	11,136,346	6,347	5,000	26,600
<i>Erythrocebus patas</i>	5,636	39,290,548	7,323	5,000	75,941
<i>Chlorocebus aethiops</i>	1,747	10,190,572	6,224	5,000	24,535
<i>Colobus guereza</i>	7,945	51,372,575	7,328	5,000	102,894
<i>Trachypithecus crepusculus</i>	1,654	9,604,991	5,927	5,001	49,667
<i>Pygathrix nigripes</i>	2,110	12,224,016	5,937	5,001	21,684
<i>Rhinopithecus strykeri</i>	2,922	17,907,851	6,349	5,000	57,979
<i>Rhinopithecus roxellana</i>	13,605	135,025,913	10,724	5,000	96,660
<i>Pithecia pithecia</i>	6,117	66,550,338	11,530	5,001	103,216
<i>Ateles geoffroyi</i>	1,502	10,231,427	7,145	5,001	51,758
<i>Sapajus apella</i>	1,069	6,449,939	6,342	5,001	43,391
<i>Cebus albifrons</i>	5,425	37,464,152	7,349	5,001	43,775
<i>Callithrix jacchus</i>	8,202	85,611,181	11,063	5,001	83,467
<i>Saguinus midas</i>	5,990	40,642,413	7,337	5,000	48,231
<i>Cephalopachus bancanus</i>	6,156	65,449,215	10,988	5,001	78,425
<i>Daubentonia madagascariensis</i>	1,771	10,443,328	6,319	5,000	38,891
<i>Lemur catta</i>	2,475	21,469,237	9,006	5,000	84,638
<i>Nycticebus pygmaeus</i>	4,908	27,522,559	6,038	5,000	25,325
<i>Nycticebus bengalensis</i>	3,688	20,697,751	5,853	5,000	21,119
<i>Loris tardigradus</i>	4,095	24,648,780	6,373	5,000	29,931
<i>Galeopterus variegatus</i>	2,911	19,071,037	6,576	5,001	32,550
<i>Tupaia belangeri</i>	3,938	32,827,464	8,971	5,000	67,521
<i>Mus musculus</i>	21,600	165,071,458	11,111	5,000	528,086
<i>Sus scrofa</i>	6,962	71,755,339	11,320	5,000	164,094
<i>Felis catus</i>	2,991	31,776,404	10,908	5,000	217,003

table S12. Screening criteria for lineage-specific segmental duplications in this study.
 5 outgroup species (*Galeopterus variegatus*, *Tupaia belangeri*, *Mus musculus*, *Felis catus* and *Sus scrofa*) were included in this analysis.

Lineage	Lineage specific species number cutoff
Great apes	3
Hominoidea	Great apes ≥ 3 and Gibbons ≥ 1
Catarrhini	Hominoidea ≥ 4 and OWMs ≥ 4
Simiiformes	Catarrhini ≥ 8 and NWMs ≥ 1
Haplorrhini	Catarrhini ≥ 8 , NWMs ≥ 1 and Tarsiers ≥ 1
Strepsirrhini	2
Primate	Catarrhini ≥ 8 and NWMs ≥ 1 and Strepsirrhini ≥ 1

table S13. 89 genes overlapping lineage-specific segmental duplications in different evolutionary nodes in primates. The ‘NA’ denotes no overlapping genes with primate-specific segmental duplications.

Lineage	Gene name
Great apes	<i>AC013271.1, AC105052.3, ADAMTS11, AL445238.1, AQP7, CA5A, CBWD1, CDK11A, CDK11B, COL4A6, DACH2, DRD5, DUX4, EDA, EFCAB3, FAM227B, FGF7, GYPA, GYPB, HERC2, IARS, IGSF3, IL1RAPL2, INTS4, KLHL2, LIMS1, LIMS3, LRRC69, LRRTM4, METTL2A, METTL2B, MMP23B, MTHFD1L, NIPAL2, NUTM2E, OPHN1, PKD1, PLD5, PLEKHB2, POLR2J, POLR2J2, PRAMEF1, PRKG1, PROS1, PRUNE2, RANBP2, RASA4B, RGPD4, RGPD5, SCAI, SPTLC1, TBX20, TENM1, TLK2, TUSC3, UNC93B1, ZNF827</i>
Hominoidea	<i>ALG10, ALG10B, EVA1C, KRT17, RUNDC3B, SMG1</i>
Catarrhini	<i>AC011330.3, CATSPER2, CCL4, CCL4L2, CSH2, CSHL1, DHRS4, DHRS4L2, GGT1, GGTL2, PDE4DIP, SPANXB1, SPANXC, ZNRF2</i>
Simiiformes	<i>ANKRD18A, ANKRD18B, DEFB131B, FAM95C, GBA, GOLGA6L9, GOLGA8Q, GOLGA8T, GRM5, MTX1, PLEKHB2, SLC9B1, TUBB8</i>
Haplorrhini	NA
Primate	NA

table S14. Biological functions of 47 genes overlapping segmental duplications in different primate lineages. The Human Gene Mutation Database can be searched via the website (<http://www.hgmd.cf.ac.uk/ac/index.php>).

Gene Symbol	Diseases/Phenotype
<i>ADAMTS1</i>	Autism spectrum disorder ? Glaucoma, craniofacial and other systemic features
<i>AQP7</i>	No exercise induced glycerol increase, association Obesity, association with
<i>CA5A</i>	Carbonic anhydrase VA deficiency Hyperammonaemia
<i>CDK11A</i>	Diabetes, type 2, association with Retinal folds, microcephaly & mental retardation ?
	Chronic kidney disease ?
<i>COL4A6</i>	Diffuse leiomyomatosis in Alport syndrome Nonsyndromic hearing loss, X-linked Premature ovarian failure ?
<i>DACH2</i>	Growth retardation, intellectual disability & walking difficulties ?
<i>DRD5</i>	Receptor variant Receptor deficiency Schizophrenia ?
	Ectodermal dysplasia, hypohidrotic Ectodermal dysplasia Tooth agenesis
	Ectodermal dysplasia, hypohidrotic ?
	Ectodermal dysplasia, hypohidrotic & inability to sweat
<i>EDA</i>	Hypodontia Oligodontia Ectodermal dysplasia ? Abnormality of metabolism/homeostasis Autism spectrum disorder with ectodermal dysplasia Hypohidrotic ectodermal dysplasia with bilateral amastia
<i>EFCAB3</i>	Diabetic retinopathy ?
	Blood group variation
	Blood group Erik variant
<i>GYPA</i>	Haemolytic disease of the newborn M blood type variant MNS antigen, absence
	Blood group variation
<i>GYPB</i>	Ss blood group variation
	Autism spectrum disorder Autism spectrum disorder ?
<i>HERC2</i>	Brain abnormalities, transposition of the great arteries, ventricular septal defect, renal anomaly and hearing loss Global developmental delay and autism spectrum disorder Mental retardation, autosomal recessive 38 Neurological disease ?
	Autism spectrum disorder ?
	Nasolacrimal duct obstruction
<i>LRRC69</i>	Altered deoxycarnitine levels Autism spectrum disorder ?
<i>LRRTM4</i>	Autism spectrum disorder
<i>METTL2B</i>	Autism spectrum disorder ?
<i>MMP23B</i>	Epileptic encephalopathy, early onset, with burst suppression ?
<i>MTHFD1L</i>	Neural tube defects, increased risk, association with Neural tube defects, decreased risk, association with
	Mental retardation syndrome, X-linked
<i>OPHN1</i>	Intellectual disability Cerebellar hypoplasia Intellectual disability ?

	Abnormality of the nervous system
	Autism spectrum disorder ?
	Developmental delay
	Epilepsy, syndromic
	Intellectual disability & dysmorphic features
	Intellectual disability & hippocampal alterations
	Intellectual disability, autism & myopathy
	Mental retardation and cerebellar hypoplasia
	Mental retardation and epilepsy
	Mental retardation, motor impairment & seizures ?
	Mental retardation, seizures and tall stature
	Mental retardation, seizures, ataxia, hypotonia
	Mental retardation, seizures, hypoplasia & facial dysmorphisms
	Mental retardation, X-linked
	Schizophrenia, childhood onset ?
	Seizures, intellectual disability & brain malformations
	Speech delay, learning difficulties & behavioural disorders
<i>PKD1</i>	Polycystic kidney disease 1
	Polycystic kidney disease 1 ?
	Intracranial aneurysms ?
	Polycystic kidney disease, autosomal dominant
	Polycystic kidney disease 1, association with
	Phenotype modifier
	Polycystic kidney disease, autosomal dominant, with male infertility
	Phenotype modifier ?
	Polycystic kidney disease, autosomal dominant & cerebral cavernous malformation
<i>PLD5</i>	Polycystic kidney disease, autosomal dominant & testicular germ cell tumour
	Renal cysts ?
	Renal hypoplasia ?
<i>PRAMEF1</i>	Autism spectrum disorder ?
	Autism spectrum disorder ?
<i>PRKG1</i>	Thoracic aortic aneurysms and dissections ?
	Thoracic aortic aneurysms and dissections
<i>PROS1</i>	Protein S deficiency
	Protein S deficiency ?
	Deep vein thrombosis
	Thrombophilia
	Deep vein thrombosis ?
	Protein S deficiency, type I
	Protein S deficiency, type I/III
	Protein S deficiency, type III
	Autism spectrum disorder ?
	Increased plasma Protein S
	Late-onset thrombosis
	Lipodystrophy, familial partial 3
<i>PRUNE2</i>	Protein S deficiency with thrombophilia
	Pulmonary embolism with deep venous thrombosis
	Recurrent miscarriage ?
	Reduced plasma Protein S
	Thrombotic disease
	Autism spectrum disorder ?
	Schizophrenia ?
<i>RANBP2</i>	Encephalopathy, acute necrotising
	Autism spectrum disorder ?
	Neuropathy, hereditary sensory, type I
<i>SPTLC1</i>	Neuropathy, motor and sensory, type 2 ?
	Sensory and autonomic neuropathy ?
	Congenital heart disease
<i>TBX20</i>	Congenital heart disease ?
	Atrial septal defect ?
	Cardiovascular malformations
	Atrial septal defect

	Cardiomyopathy, dilated ? Congenital heart defect, protection against Tetralogy of Fallot ? Atrial septal defects, patent foramen ovale & cardiac valve defec Cardiomyopathy, dilated Noncompaction, left ventricular ? Tetralogy of Fallot/truncus arteriosus Ventricular septal defect
<i>TENM1</i>	Anosmia, general congenital Autism spectrum disorder ? Cerebral palsy ? Schizophrenia ?
<i>TLK2</i>	Neurodevelopmental disorder Autism spectrum disorder ? Intellectual disability ? Neotenic complex syndrome ? Schizophrenia ?
<i>TUSC3</i>	Mental retardation, non-syndromic, autosomal recessive Intellectual disability & autism Intellectual disability, nonsyndromic, autosomal recessive Attention deficit hyperactivity disorder ? Fetal alcohol syndrome, predisposition to ? Intellectual disability ? Intellectual disability and dysmorphic features Intellectual disability with developmental delay Intellectual disability, autosomal recessive ? Intellectual disability, syndromic Mental retardation, non-syndromic, autosomal recessive ? Neurodegenerative disease with blindness
<i>UNC93B1</i>	Herpes simplex encephalitis, UNC93B-deficient
<i>ALG10B</i>	Acquired long QT syndrome Acquired long QT syndrome, protection against, association Fetal alcohol syndrome, predisposition to ?
<i>KRT17</i>	Pachyonychia congenital Steatocystoma multiplex Diabetes, MODY Keratitis-ichthyosis-deafness syndrome, modifier of ? Steatocystoma multiplex ?
<i>RUND3B</i>	Autism spectrum disorder ? Schizophrenia ?
<i>SMG1</i>	Bipolar disorder ?
<i>CATSPER2</i>	Asthenoteratozoospermia & deafness, non-syndromic Oligozoospermia Asthenozoospermia ? Deafness-infertility syndrome
<i>CCL4L2</i>	Haemophilia A, inhibitor development, increased risk HIV/AIDS susceptibility, association with
<i>DHRS4L2</i>	Abdominal pain, association with
<i>GGT1</i>	Glutathionuria
<i>PDE4DIP</i>	Lung squamous cancer ? Schizophrenia ?
<i>SPANXC</i>	Autism spectrum disorder ? Hearing loss ?
<i>ANKRD18A</i>	Thrombocytopaenia ? Gaucher disease Gaucher disease 1 Gaucher disease 2
<i>GBA</i>	Parkinson disease ? Parkinson disease Gaucher disease ? Gaucher disease 3

	Parkinson disease, familial
	Parkinson disease, susceptibility ?
	Lewy body dementia
	Gaucher disease 1 ?
	Gaucher disease 3B ?
	Gaucher disease/Parkinson disease ?
	Parkinson disease, modifier of ?
	Gaucher disease/Parkinson disease
	Lewy body dementia ?
	Lewy body dementia/Alzheimer disease
	Parkinson disease with dementia
	Parkinson disease with dementia ?
	Parkinson disease, familial ?
	Parkinson disease, susceptibility
	Reduced activity ?
	Reduced promoter activity
<i>GRM5</i>	Nasopharyngeal carcinoma, association with
	Schizophrenia ?
	Attention deficit hyperactivity disorder
<i>MTX1</i>	Parkinson disease, GBA-associated, modifier of
<i>TUBB8</i>	Oocyte maturation arrest
	Oocyte meiotic I arrest
	Autism spectrum disorder ?
	Infertility, female

table S15. Transposable element content in the 50 primate genomes. The proportion of each species' genome that comprises transposable elements is given.

Species name	DNA (%)	LINE (%)	SINE (%)	LTR (%)	Other (%)	Unknown (%)	Total (%)
<i>Homo sapiens</i>	3.416312	21.37813	13.21746	8.995259	0	0.024094	51.16242
<i>Pan troglodytes</i>	3.495571	18.79533	12.07351	8.422344	0.000004	0.076046	43.50807
<i>Pan paniscus</i>	2.427124	16.20634	10.43182	6.576004	0.000003	0.210771	34.43042
<i>Gorilla gorilla</i>	4.519278	20.2437	11.86604	7.078511	0.000004	0.659051	39.98748
<i>Pongo abelii</i>	2.67973	23.74067	15.37229	7.337878	0.000006	0.134102	44.32494
<i>Pongo pygmaeus</i>	2.702728	19.41397	13.33098	7.78236	0.000007	2.467336	41.91725
<i>Nomascus siki</i>	4.079089	23.81682	12.69031	7.446399	0.000004	0.199346	41.7907
<i>Symphalangus syndactylus</i>	2.740564	23.24009	12.86542	7.437156	0.000004	0.406352	42.00199
<i>Hoolock leuconedys</i>	2.824069	20.91051	13.77718	7.509741	0.000004	0.801514	42.70155
<i>Hylobates pileatus</i>	2.569771	22.11408	14.06666	7.774654	0.000007	0.066315	43.4856
<i>Macaca mulatta</i>	2.627724	20.36664	13.21097	7.390647	0.000005	0.111009	40.33915
<i>Macaca assamensis</i>	2.697511	22.41217	13.5647	7.825183	0.000009	0.201319	41.9095
<i>Macaca nemestrina</i>	2.768158	19.2794	13.36188	7.242853	0.000005	0.038615	39.80063
<i>Macaca silenus</i>	2.997837	22.08491	13.67432	7.527221	0.000005	0.402573	41.66409
<i>Papio hamadryas</i>	2.652947	19.42902	13.962	7.63461	0.000004	0.529461	42.42333
<i>Papio anubis</i>	2.53303	19.37666	12.65983	7.305972	0.000005	0.9019	39.58893
<i>Lophocebus aterrimus</i>	2.626727	20.08604	13.79541	7.437517	0.000025	0.177457	41.38226
<i>Theropithecus gelada</i>	2.706185	20.36382	13.14712	7.545321	0.000005	0.88258	40.73389
<i>Mandrillus sphinx</i>	2.812574	19.77772	13.71045	7.695317	0	0.73101	41.99178
<i>Mandrillus leucophaeus</i>	2.828926	17.33862	12.47235	8.695023	0.000005	0.743809	39.7174
<i>Cercopithecus atys</i>	2.672215	20.68596	11.63993	7.148165	0	0.674032	39.11317
<i>Cercopithecus albogularis</i>	2.755068	19.71068	13.60433	7.449134	0.000005	0.330782	41.74052
<i>Cercopithecus mona</i>	2.630284	18.48593	13.30515	7.526644	0.000005	2.183436	41.31828
<i>Chlorocebus aethiops</i>	2.599457	20.17746	13.33488	7.469227	0.000005	0.032981	41.27284
<i>Chlorocebus sabaeus</i>	2.837976	21.76352	12.71812	7.921284	0.000005	2.078198	40.18023
<i>Erythrocebus patas</i>	2.559519	20.5166	13.04474	7.116591	0.000004	0.184734	41.47241
<i>Trachypithecus crepusculus</i>	2.882639	22.74601	14.56216	7.387797	0	0.106141	43.86018
<i>Pygathrix nigripes</i>	2.71409	22.37422	13.46232	7.603127	0.000009	0.317145	42.98065
<i>Rhinopithecus strykeri</i>	2.671557	21.29688	13.6758	7.447362	0.000005	0.638443	42.11801
<i>Rhinopithecus roxellana</i>	2.880717	18.84279	12.81576	6.648548	0.000004	0.902558	40.62366
<i>Piliocolobus tephrosceles</i>	2.669056	17.30729	13.03671	7.287504	0.000171	0.366395	39.43253
<i>Colobus guereza</i>	2.535954	21.34616	14.08538	7.676713	0.000005	0.773977	42.91961
<i>Colobus angolensis</i>	2.629353	15.536	12.29748	7.150639	0.000008	1.120888	36.55863
<i>Callithrix jacchus</i>	2.597564	23.24307	12.15885	6.464473	0.000024	3.456594	41.00548
<i>Saguinus midas</i>	2.357737	23.22166	12.59711	6.240792	0.000004	0.751006	43.14452
<i>Aotus nancymaae</i>	2.680732	18.75946	12.22343	6.62525	0.000004	0.161474	37.78009
<i>Sapajus apella</i>	2.640896	18.49049	13.24118	6.420989	0.000004	0.96467	39.29696
<i>Cebus albifrons</i>	2.774134	19.58234	13.58767	6.555068	0.000004	0.223647	41.45974
<i>Ateles geoffroyi</i>	2.805585	18.53016	12.33164	6.749433	0.000016	0.506796	39.19657
<i>Pithecia pithecia</i>	2.715736	20.48659	12.08776	7.162978	0.000011	1.20784	40.45308
<i>Cephalopachus bancanus</i>	2.139191	22.48067	9.421322	5.381964	0	0.281605	39.70475
<i>Microcebus murinus</i>	3.816077	16.34522	7.552485	4.87733	0.000009	0.317364	31.68335
<i>Prolémur simus</i>	4.641324	16.17629	5.492357	5.251497	0.000011	0.760824	30.8309
<i>Lemur catta</i>	4.288137	17.2709	6.044139	5.60213	0.000016	0.516008	32.10227
<i>Daubentonia madagascariensis</i>	4.122496	21.68452	4.5172	6.286112	0.000005	1.126378	36.61008

<i>Loris tardigradus</i>	3.561639	26.23747	9.291736	4.129729	0	2.26674	42.27465
<i>Nycticebus bengalensis</i>	3.336392	27.28023	11.13431	4.050924	0	1.897464	44.32268
<i>Nycticebus pygmaeus</i>	3.097127	30.95835	9.84234	3.990493	0	1.790004	46.74688
<i>Galago moholi</i>	3.704521	22.27339	12.75717	4.777287	0.000004	1.283037	39.00963
<i>Otolemur garnettii</i>	3.733917	16.47771	10.67751	4.376582	0.000004	1.216316	33.63152

table S16. Substitution rates for all primate species. Substitution rates in different lineages were estimated by comparison of the four-fold degenerate sites within coding regions, in units of substitutions per site per million years. OWMs: Old World monkeys. NWMs: New World monkeys.

Common name	Species name	Substitution rate ($\times 10^{-3}$)	Lineages
human	<i>Homo sapiens</i>	0.769360	Human
Chimpanzee	<i>Pan troglodytes</i>	0.690833	great apes
Bonobo	<i>Pan paniscus</i>	0.814966	great apes
Western Gorilla	<i>Gorilla gorilla</i>	0.829426	great apes
Sumatran Orangutan	<i>Pongo abelii</i>	0.553363	great apes
Bornean Orangutan	<i>Pongo pygmaeus</i>	0.716367	great apes
Southern White-cheeked Crested Gibbon	<i>Nomascus siki</i>	1.04689	gibbons
Siamang	<i>Sympalangus syndactylus</i>	1.26521	gibbons
Eastern Hoolock Gibbon	<i>Hoolock leuconedys</i>	1.28001	gibbons
Pileated Gibbon	<i>Hylobates pileatus</i>	1.00582	gibbons
Rhesus Macaque	<i>Macaca mulatta</i>	1.00803	OWMs
Assamese Macaque	<i>Macaca assamensis</i>	1.02882	OWMs
Sunda Pig-tailed Macaque	<i>Macaca nemestrina</i>	0.959020	OWMs
Lion-tailed Macaque	<i>Macaca silenus</i>	0.786217	OWMs
Hamadryas Baboon	<i>Papio hamadryas</i>	0.882062	OWMs
Olive Baboon	<i>Papio anubis</i>	1.02976	OWMs
Northern Black Crested Mangabey	<i>Lophocebus aterrimus</i>	1.14622	OWMs
Gelada	<i>Theropithecus gelada</i>	0.842621	OWMs
Mandrill	<i>Mandrillus sphinx</i>	0.967419	OWMs
Drill	<i>Mandrillus leucophaeus</i>	0.963773	OWMs
Sooty Mangabey	<i>Cercocebus atys</i>	1.10719	OWMs
Syke's Monkey	<i>Cercopithecus albogularis</i>	1.08521	OWMs
Mona Monkey	<i>Cercopithecus mona</i>	1.10985	OWMs
Grivet Monkey	<i>Chlorocebus aethiops</i>	1.18807	OWMs
Green Monkey	<i>Chlorocebus sabaeus</i>	1.16340	OWMs
Patas Monkey	<i>Erythrocebus patas</i>	1.22043	OWMs
Indochinese Gray Langur	<i>Trachypithecus crepusculus</i>	1.43968	OWMs
Black-shanked Douc	<i>Pygathrix nigripes</i>	1.29194	OWMs
Stryker's Snub-nosed Monkey	<i>Rhinopithecus strykeri</i>	1.13282	OWMs
Golden Snub-nosed Monkey	<i>Rhinopithecus roxellana</i>	0.759596	OWMs
Ashy Red Colobus	<i>Piliocolobus tephrosceles</i>	1.25882	OWMs
Guereza	<i>Colobus guereza</i>	1.09806	OWMs
Angolan Colobus	<i>Colobus angolensis</i>	1.34288	OWMs
Common Marmoset	<i>Callithrix jacchus</i>	1.97639	NWMs
Midas Tamarin	<i>Saguinus midas</i>	1.87414	NWMs
Ma's Night Monkey	<i>Aotus nancymaae</i>	1.33320	NWMs
Guianan Brown Capuchin	<i>Sapajus apella</i>	1.40714	NWMs

Humboldt's White-fronted Capuchin	<i>Cebus albifrons</i>	1.37799	NWMs
Central American Spider Monkey	<i>Ateles geoffroyi</i>	1.33453	NWMs
White-faced saki	<i>Pithecia pithecia</i>	1.39319	NWMs
Western Tarsier	<i>Cephalopachus bancanus</i>	2.73656	Tarsiiformes
Aye-aye	<i>Daubentonia madagascariensis</i>	1.01236	Chiromyiformes
Gray Mouse Lemur	<i>Microcebus murinus</i>	1.58555	lemurs (Lemuriformes)
Greater Bamboo Lemur	<i>Prolemur simus</i>	1.17898	lemurs (Lemuriformes)
Ring-tailed Lemur	<i>Lemur catta</i>	1.16764	lemurs (Lemuriformes)
Red Slender Loris	<i>Loris tardigradus</i>	1.26883	lorisoids (Lorisiformes)
Pygmy Slow Loris	<i>Nycticebus pygmaeus</i>	1.10755	lorisoids (Lorisiformes)
Bengal Slow Loris	<i>Nycticebus bengalensis</i>	1.22657	lorisoids (Lorisiformes)
Southern Lesser Galago	<i>Galago moholi</i>	1.22706	lorisoids (Lorisiformes)
Garnett's Greater Galago	<i>Otolemur garnettii</i>	1.08428	lorisoids (Lorisiformes)

table S17. Positively selected genes of the primate ancestor. *P* values were obtained by means of a χ^2 test.

Ensembl Gene ID	Gene Name	2ΔNL	P
ENSG00000168813	ZNF507	194.045838	4.16E-44
ENSG00000112333	NR2E1	114.063966	1.26E-26
ENSG00000177082	WDR73	110.224732	8.75E-26
ENSG00000106012	<i>IQCE</i>	104.365488	1.68E-24
ENSG00000131591	<i>C1orf159</i>	62.681446	2.43E-15
ENSG00000131013	<i>PPIL4</i>	33.652356	6.59E-09
ENSG00000156802	<i>ATAD2</i>	31.562434	1.93E-08
ENSG00000134250	<i>NOTCH2</i>	31.40739	2.09E-08
ENSG00000103064	<i>SLC7A6</i>	29.497584	5.60E-08
ENSG0000042832	<i>TG</i>	22.223052	2.43E-06
ENSG0000064607	<i>SUGP2</i>	17.063862	3.61E-05
ENSG00000138069	<i>RAB1A</i>	14.699082	0.000126108
ENSG00000125831	<i>CSTII</i>	12.242636	0.000467098
ENSG00000105607	<i>GCDH</i>	11.905484	0.000559689
ENSG00000136929	<i>HEMGN</i>	11.5726	0.000669308
ENSG00000128815	<i>WDFY4</i>	11.14847	0.00084101
ENSG00000166105	<i>GLB1L3</i>	10.89862	0.000962359
ENSG00000137076	<i>TLN1</i>	10.56693	0.001151288
ENSG00000135090	<i>TAOK3</i>	10.397474	0.001261878
ENSG0000039560	<i>RAII4</i>	9.699604	0.001843077
ENSG00000259494	<i>MRPL46</i>	9.66599	0.001877106
ENSG00000197694	<i>SPTAN1</i>	9.390208	0.002181475
ENSG00000144306	<i>SCRN3</i>	9.269378	0.002330168
ENSG00000185324	<i>CDK10</i>	9.246788	0.002359088
ENSG00000121749	<i>TBC1D15</i>	9.222914	0.002390048
ENSG00000113716	<i>HMGXB3</i>	9.00032	0.002699323
ENSG00000164190	<i>NIPBL</i>	8.938858	0.002791672
ENSG00000172613	<i>RAD9A</i>	8.55853	0.00343907
ENSG00000108556	<i>CHRNE</i>	8.124474	0.004367165
ENSG00000145777	<i>TSLP</i>	7.998236	0.004682294
ENSG00000100034	<i>PPM1F</i>	7.928984	0.004864911
ENSG00000166257	<i>SCN3B</i>	7.847688	0.005088574
ENSG00000005884	<i>ITGA3</i>	7.730874	0.005428447
ENSG00000134882	<i>UBAC2</i>	7.53235	0.006060081
ENSG00000197858	<i>GPAA1</i>	7.528236	0.006073935
ENSG00000180354	<i>MTURN</i>	7.263946	0.007035254
ENSG0000016602	<i>CLCA4</i>	7.178636	0.007377678
ENSG00000173714	<i>WFIKKN2</i>	7.094918	0.007730283
ENSG00000176974	<i>SHMT1</i>	6.95937	0.008338139
ENSG00000147573	<i>TRIM55</i>	6.875982	0.008736174
ENSG00000084112	<i>SSH1</i>	6.870336	0.008763817
ENSG00000107404	<i>DVL1</i>	6.869678	0.008767045
ENSG00000172269	<i>DPAGT1</i>	6.864626	0.008791865
ENSG00000153774	<i>CFDP1</i>	6.86255	0.008802085
ENSG00000103248	<i>MTHFSD</i>	6.858066	0.008824201

ENSG00000212657	<i>KRTAP16-1</i>	6.843184	0.00889801
ENSG00000203908	<i>KHDC3L</i>	6.809798	0.009065902
ENSG00000109805	<i>NCAPG</i>	6.701512	0.009633119
ENSG00000116824	<i>CD2</i>	6.635904	0.009994346
ENSG00000196535	<i>MYO18A</i>	6.36168	0.011661108
ENSG00000168509	<i>HJV</i>	6.316366	0.011962855
ENSG00000151655	<i>ITIH2</i>	6.287248	0.012160973
ENSG00000128710	<i>HOXD10</i>	6.135984	0.013245781
ENSG00000175003	<i>SLC22A1</i>	5.943742	0.014769629
ENSG00000130413	<i>STK33</i>	5.860434	0.015484975
ENSG00000144635	<i>DYNC1LII</i>	5.84579	0.015614362
ENSG00000135900	<i>MRPL44</i>	5.824368	0.015805646
ENSG00000156172	<i>C8orf37</i>	5.687832	0.017082947
ENSG00000122034	<i>GTF3A</i>	5.559834	0.018377157
ENSG00000167065	<i>DUSP18</i>	5.467248	0.019376113
ENSG00000205442	<i>IZUMO3</i>	5.450048	0.019567789
ENSG00000173157	<i>ADAMTS20</i>	5.449936	0.019569044
ENSG00000164619	<i>BMPER</i>	5.110024	0.023787991
ENSG00000107821	<i>KAZALD1</i>	5.102012	0.023898108
ENSG00000156510	<i>HKDC1</i>	5.064364	0.024422665
ENSG00000148935	<i>GAS2</i>	5.021528	0.025034068
ENSG00000125257	<i>ABCC4</i>	5.013858	0.02514521
ENSG00000102181	<i>CD99L2</i>	4.988836	0.025511364
ENSG00000108576	<i>SLC6A4</i>	4.945932	0.026152135
ENSG00000162623	<i>TYW3</i>	4.724068	0.029743298
ENSG00000168291	<i>PDHB</i>	4.627954	0.031455053
ENSG00000196419	<i>XRCC6</i>	4.49234	0.03404704
ENSG00000177084	<i>POLE</i>	4.456634	0.03476594
ENSG00000066777	<i>ARFGEF1</i>	4.45279	0.034844275
ENSG00000111269	<i>CREBL2</i>	4.358914	0.036815768
ENSG00000103335	<i>PIEZ01</i>	4.349808	0.037013119
ENSG00000186487	<i>MYTIL</i>	4.170962	0.041122444
ENSG00000139597	<i>N4BP2L1</i>	4.133202	0.042049715
ENSG00000117475	<i>BLZF1</i>	4.125438	0.042243084
ENSG00000102125	<i>TAZ</i>	4.027962	0.044751971
ENSG00000132952	<i>USPL1</i>	3.979192	0.046065656
ENSG00000146648	<i>EGFR</i>	3.974956	0.04618166

table S18. Enrichment analyses of tissue-specific expression of positively selected genes in the primate ancestral lineage. *P* value < 0.05 (Modified Fisher's Exact test) are listed. The enrichment analyses were performed by the DAVID Bioinformatics Resources including 8 tissue-specific high expression databases (CGAP_EST_QUARTILE, CGAP_SAGE_QUARTILE, GNF_U133A_QUARTILE, HPA_NORMAL_TISSUE, HPA_NORMAL_TISSUE_CELLTYPE, HPA_RNA_TISSUE, UNIGENE_EST_QUARTILE, and UP_TISSUE).

Category	Term	Count	PValue
UNIGENE_EST_QUARTILE	thymus_normal_3rd	24	0.00226
CGAP_EST_QUARTILE	21853:placenta_normal_3rd	5	0.002702
UNIGENE_EST_QUARTILE	juvenile (< 17 years old)_development_3rd	23	0.0029
CGAP_EST_QUARTILE	38100:bone marrow_neoplasia_3rd	6	0.00602
HPA_NORMAL_TISSUE_CELLTYPE	lung; endothelial cells	10	0.006961
CGAP_EST_QUARTILE	16533:prostate_neoplasia_3rd	4	0.007505
CGAP_EST_QUARTILE	15:colon_neoplasia_3rd	3	0.0087
CGAP_EST_QUARTILE	21544:cerebrum_normal_3rd	3	0.011464
GNF_U133A_QUARTILE	fetal lung_3rd	16	0.011464
HPA_NORMAL_TISSUE_CELLTYPE	esophagus; squamous epithelial cells	38	0.01216
HPA_NORMAL_TISSUE	Esophagus	38	0.01216
HPA_NORMAL_TISSUE_CELLTYPE	pancreas; exocrine glandular cells	39	0.012388
UP_TISSUE	Cervix carcinoma	31	0.012815
HPA_NORMAL_TISSUE_CELLTYPE	endometrium 2; glandular cells	38	0.013619
UNIGENE_EST_QUARTILE	infant (< 3 years old)_development_3rd	17	0.014615
UP_TISSUE	Leukemic T-cell	18	0.016363
GNF_U133A_QUARTILE	salivary gland_3rd	53	0.018462
CGAP_SAGE_QUARTILE	168:uncharacterized tissue_mixture of human cancer cell lines_3rd	14	0.018688
HPA_NORMAL_TISSUE_CELLTYPE	epididymis; glandular cells	40	0.018981
HPA_NORMAL_TISSUE	Epididymis	40	0.018981
CGAP_EST_QUARTILE	20376:testi_neoplasia_3rd	6	0.019915
HPA_NORMAL_TISSUE_CELLTYPE	thyroid gland; glandular cells	39	0.022073
HPA_NORMAL_TISSUE	thyroid gland	39	0.022073
CGAP_SAGE_QUARTILE	406:brain_ependymoma_3rd	13	0.022198
UNIGENE_EST_QUARTILE	esophagus_normal_3rd	17	0.023408
CGAP_EST_QUARTILE	26742:uncharacterized tissue_neoplasia_3rd	5	0.02419
HPA_NORMAL_TISSUE_CELLTYPE	tonsil; squamous epithelial cells	37	0.024632
HPA_NORMAL_TISSUE	endometrium 2	38	0.024734
HPA_NORMAL_TISSUE_CELLTYPE	cervix; squamous epithelial cells	32	0.025071
UP_TISSUE	Erythroleukemia	27	0.025138
CGAP_EST_QUARTILE	40108:cerebrum_normal_3rd	4	0.025647
CGAP_SAGE_QUARTILE	1993:retina_central retina_3rd	11	0.027738
CGAP_SAGE_QUARTILE	1645:brain_null_3rd	13	0.029832
UP_TISSUE	Bone marrow	8	0.030151
CGAP_EST_QUARTILE	28506:brain_normal_3rd	5	0.030792
CGAP_EST_QUARTILE	21737:placenta_normal_3rd	3	0.031485
CGAP_EST_QUARTILE	26745:stomach_neoplasia_3rd	5	0.03229
UNIGENE_EST_QUARTILE	esophageal tumor_disease_3rd	17	0.033583
UNIGENE_EST_QUARTILE	abdominal cavity_normal_3rd	19	0.034186

HPA_NORMAL_TISSUE_CELLTYPE	testis; pachytene spermatocytes	16	0.035055
CGAP_EST_QUARTILE	21455:uncharacterized tissue_neoplasia_3rd	3	0.03533
CGAP_SAGE_QUARTILE	351:brain_anaplastic gradeIII, primary, brain_3rd	12	0.036658
HPA_NORMAL_TISSUE_CELLTYPE	endometrium 1; glandular cells	37	0.038555
CGAP_EST_QUARTILE	38092:uncharacterized tissue_uncharacterized histology_3rd	2	0.038981
HPA_NORMAL_TISSUE_CELLTYPE	heart muscle; cardiomyocytes	35	0.039722
HPA_NORMAL_TISSUE	heart muscle	35	0.039722
HPA_NORMAL_TISSUE_CELLTYPE	seminal vesicle; glandular cells	37	0.040065
HPA_NORMAL_TISSUE	seminal vesicle	37	0.040065
HPA_NORMAL_TISSUE_CELLTYPE	small intestine; glandular cells	38	0.040135
CGAP_SAGE_QUARTILE	1906:retina_Bilateral retinoblastoma, poorly differentiated, left orbit 3rd	13	0.040615
CGAP_SAGE_QUARTILE	1604:stem cell_null_3rd	10	0.040945
CGAP_EST_QUARTILE	16479:uncharacterized tissue_uncharacterized histology_3rd	5	0.042522
HPA_NORMAL_TISSUE_CELLTYPE	stomach 2; glandular cells	40	0.043287
HPA_NORMAL_TISSUE	stomach 2	40	0.043287
CGAP_EST_QUARTILE	38079:muscle_normal_3rd	5	0.044327
CGAP_EST_QUARTILE	19639:lung_normal_3rd	2	0.045906
HPA_NORMAL_TISSUE	Testis	45	0.047504
CGAP_SAGE_QUARTILE	174:mammary gland_breast carcinoma_3rd	13	0.048418
CGAP_EST_QUARTILE	21736:placenta_normal_3rd	3	0.048758
HPA_NORMAL_TISSUE_CELLTYPE	salivary gland; glandular cells	37	0.04889
HPA_NORMAL_TISSUE	salivary gland	37	0.04889
UP_TISSUE	Liver	29	0.049474
HPA_NORMAL_TISSUE	Pancreas	39	0.049964

table S19. 30 positively selected genes along with primate ancestral lineage exhibiting the biased expression in brain. The tissue-biased expression genes were assigned according to eight expression databases including CGAP_EST_QUARTILE, CGAP_SAGE_QUARTILE, GNF_U133A_QUARTILE, HPA_NORMAL_TISSUE, HPA_NORMAL_TISSUE_CELLTYPE, HPA_RNA_TISSUE, UNIGENE_EST_QUARTILE, and UP_TISSUE in the DAVID Bioinformatics Resources (<https://david.ncifcrf.gov/summary.jsp>).

Ensembl Gene ID	Gene Name	Gene Description
ENSG00000186487	<i>MYT1L</i>	myelin transcription factor 1 like
ENSG00000197694	<i>SPTAN1</i>	spectrin alpha, non-erythrocytic 1
ENSG00000180354	<i>MTURN</i>	maturin, neural progenitor differentiation regulator homolog
ENSG00000136929	<i>HEMGN</i>	hemogen
ENSG00000172269	<i>DPAGT1</i>	dolichyl-phosphate N-acetylglucosamineprophosphotransferase 1
ENSG00000132952	<i>USPL1</i>	ubiquitin specific peptidase like 1
ENSG00000106012	<i>IQCE</i>	IQ motif containing E
ENSG00000102181	<i>CD99L2</i>	CD99 molecule like 2
ENSG00000146648	<i>EGFR</i>	epidermal growth factor receptor
ENSG00000135900	<i>MRPL44</i>	mitochondrial ribosomal protein L44
ENSG00000103248	<i>MTHFSD</i>	methenyltetrahydrofolate synthetase domain containing
ENSG00000130413	<i>STK33</i>	serine/threonine kinase 33
ENSG00000168813	<i>ZNF507</i>	zinc finger protein 507
ENSG00000107404	<i>DVL1</i>	dishevelled segment polarity protein 1
ENSG00000166257	<i>SCN3B</i>	sodium voltage-gated channel beta subunit 3
ENSG00000100034	<i>PPM1F</i>	protein phosphatase, Mg ²⁺ /Mn ²⁺ dependent 1F
ENSG00000138069	<i>RAB1A</i>	RAB1A, member RAS oncogene family
ENSG00000196419	<i>XRCC6</i>	X-ray repair cross complementing 6
ENSG00000162623	<i>TYW3</i>	tRNA-γW synthesizing protein 3 homolog
ENSG00000144635	<i>DYNC1LI1</i>	dynein cytoplasmic 1 light intermediate chain 1
ENSG00000131591	<i>C1ORF159</i>	chromosome 1 open reading frame 159
ENSG00000064607	<i>SUGP2</i>	SURP and G-patch domain containing 2
ENSG00000121749	<i>TBC1D15</i>	TBC1 domain family member 15
ENSG00000039560	<i>RAI14</i>	retinoic acid induced 14
ENSG00000109805	<i>NCAPG</i>	non-SMC condensin I complex subunit G
ENSG00000117475	<i>BLZF1</i>	basic leucine zipper nuclear factor 1
ENSG00000145777	<i>TSLP</i>	thymic stromal lymphopoietin
ENSG00000176974	<i>SHMT1</i>	serine hydroxymethyltransferase 1
ENSG00000122034	<i>GTF3A</i>	general transcription factor IIIA
ENSG00000147573	<i>TRIM55</i>	tripartite motif containing 55

table S20. Positively selected genes of the Simiiformes ancestor. Orthologous sequences of 50 primates and two outgroup species (flying lemur and tree shrew) were utilized to obtain positively selected genes in the Simiiformes ancestor lineage using a branch-site model in PAML4. P values were calculated by means of a χ^2 test.

Ensembl Gene ID	Gene Name	2ΔLNL	P
ENSG0000167037	<i>SGSM1</i>	449.3512	9.98E-100
ENSG0000134709	<i>HOOK1</i>	194.746826	2.93E-44
ENSG0000215271	<i>HOMEZ</i>	118.725922	1.20E-27
ENSG0000187955	<i>COL14A1</i>	112.06168	3.46E-26
ENSG0000129521	<i>EGLN3</i>	99.378944	2.09E-23
ENSG0000144674	<i>GOLGA4</i>	90.36033	1.99E-21
ENSG0000144668	<i>ITGA9</i>	85.376384	2.47E-20
ENSG0000075391	<i>RASAL2</i>	85.267824	2.61E-20
ENSG0000243710	<i>CFAP57</i>	80.786632	2.51E-19
ENSG0000188089	<i>PLA2G4E</i>	74.502796	6.06E-18
ENSG0000124743	<i>KLHL31</i>	69.900668	6.24E-17
ENSG0000006715	<i>VPS41</i>	65.227618	6.67E-16
ENSG0000174348	<i>PODN</i>	57.165606	4.01E-14
ENSG0000077254	<i>USP33</i>	45.49202	1.53E-11
ENSG0000094880	<i>CDC23</i>	43.07724	5.26E-11
ENSG0000018189	<i>RUFY3</i>	42.075758	8.78E-11
ENSG0000033100	<i>CHPF2</i>	37.896662	7.46E-10
ENSG0000152382	<i>TADA1</i>	33.028134	9.08E-09
ENSG0000165471	<i>MBL2</i>	29.562052	5.42E-08
ENSG0000102575	<i>ACP5</i>	26.667634	2.42E-07
ENSG0000144550	<i>CPNE9</i>	25.762424	3.86E-07
ENSG0000177606	<i>JUN</i>	25.614606	4.17E-07
ENSG0000090097	<i>PCBP4</i>	22.5868	2.01E-06
ENSG0000175203	<i>DCTN2</i>	19.515158	9.98E-06
ENSG0000176248	<i>ANAPC2</i>	18.61186	1.60E-05
ENSG0000197969	<i>VPS13A</i>	17.867988	2.37E-05
ENSG0000152270	<i>PDE3B</i>	16.856954	4.03E-05
ENSG0000164961	<i>WASHC5</i>	16.086088	6.05E-05
ENSG0000103353	<i>UBFD1</i>	15.883054	6.74E-05
ENSG0000170175	<i>CHRNB1</i>	15.635368	7.68E-05
ENSG0000128652	<i>HOXD3</i>	15.313044	9.11E-05
ENSG0000116337	<i>AMPD2</i>	14.881692	0.000114469
ENSG0000070367	<i>EXOC5</i>	13.781746	0.000205322
ENSG0000163072	<i>NOSTRIN</i>	13.611044	0.000224859
ENSG0000177683	<i>THAP5</i>	12.844554	0.000338463
ENSG0000125656	<i>CLPP</i>	12.652206	0.000375123
ENSG0000113845	<i>TIMMDC1</i>	12.469068	0.000413746
ENSG0000187642	<i>PERM1</i>	12.254928	0.000464031
ENSG0000122679	<i>RAMP3</i>	11.90888	0.00055867
ENSG0000197272	<i>IL27</i>	11.861378	0.000573101
ENSG0000104177	<i>MYEF2</i>	11.73929	0.000611944

ENSG00000173141	<i>MRPL57</i>	11.248472	0.000796886
ENSG00000160712	<i>IL6R</i>	11.228806	0.000805374
ENSG00000183035	<i>CYLC1</i>	11.008464	0.000906968
ENSG00000108344	<i>PSMD3</i>	10.913936	0.000954435
ENSG00000162891	<i>IL20</i>	10.166388	0.001430242
ENSG00000165935	<i>SMCO2</i>	9.922508	0.001632698
ENSG00000243927	<i>MRPS6</i>	9.81793	0.001728187
ENSG00000180878	<i>C11orf42</i>	9.62165	0.001922969
ENSG00000168016	<i>TRANK1</i>	9.534342	0.002016625
ENSG00000196843	<i>ARID5A</i>	9.404968	0.002163983
ENSG00000114942	<i>EEF1B2</i>	9.13835	0.002503067
ENSG00000083307	<i>GRHL2</i>	9.11578	0.002534139
ENSG0000023445	<i>BIRC3</i>	9.071566	0.002596146
ENSG00000237452	<i>BHMG1</i>	8.843928	0.002940656
ENSG00000185974	<i>GRK1</i>	8.689602	0.003200305
ENSG00000111254	<i>AKAP3</i>	8.682594	0.003212634
ENSG00000117505	<i>DR1</i>	8.5147	0.00352289
ENSG00000182150	<i>ERCC6L2</i>	8.508168	0.003535558
ENSG00000170419	<i>VSTM2A</i>	8.439194	0.00367219
ENSG00000141741	<i>MIEN1</i>	8.387434	0.003778239
ENSG00000185909	<i>KLHDC8B</i>	8.159626	0.00428332
ENSG00000154639	<i>CXADR</i>	8.073828	0.004490914
ENSG00000146670	<i>CDCA5</i>	8.045894	0.004560691
ENSG00000188991	<i>SLC15A5</i>	7.997822	0.004683365
ENSG00000242485	<i>MRPL20</i>	7.86438	0.005041811
ENSG00000100867	<i>DHRS2</i>	7.848354	0.0050867
ENSG00000196811	<i>CHRNG</i>	7.813086	0.005186925
ENSG00000162949	<i>CAPN13</i>	7.77842	0.005287402
ENSG00000012171	<i>SEMA3B</i>	7.599362	0.005838896
ENSG00000102904	<i>TSNAXIP1</i>	7.573866	0.005922063
ENSG00000110693	<i>SOX6</i>	7.557326	0.005976661
ENSG00000167656	<i>LY6D</i>	7.551428	0.005996254
ENSG00000176155	<i>CCDC57</i>	7.405518	0.006502412
ENSG00000123243	<i>ITIH5</i>	7.302212	0.006886977
ENSG00000283428	<i>CCDC195</i>	7.298964	0.006899438
ENSG00000148290	<i>SURF1</i>	7.138004	0.007546711
ENSG00000121410	<i>A1BG</i>	7.06324	0.007868157
ENSG00000154252	<i>GAL3ST2</i>	7.038236	0.007978758
ENSG00000178752	<i>ERFE</i>	7.026466	0.008031369
ENSG00000107897	<i>ACBD5</i>	6.976502	0.008258688
ENSG00000153802	<i>TMPRSS11D</i>	6.883142	0.008701247
ENSG00000172167	<i>MTBP</i>	6.784054	0.009197576
ENSG00000165730	<i>STOX1</i>	6.694496	0.0096711
ENSG00000136868	<i>SLC31A1</i>	6.692318	0.009682922
ENSG00000144410	<i>CPO</i>	6.557756	0.010442797
ENSG00000125779	<i>PANK2</i>	6.509746	0.010728483
ENSG00000203872	<i>C6orf163</i>	6.501334	0.010779359
ENSG00000149548	<i>CCDC15</i>	6.43685	0.011177668
ENSG00000131808	<i>FSHB</i>	6.328406	0.011881906

ENSG00000106436	<i>MYL10</i>	6.30312	0.012052566
ENSG00000100023	<i>PPIL2</i>	6.287638	0.012158297
ENSG00000165695	<i>AK8</i>	6.197936	0.012789938
ENSG00000182492	<i>BGN</i>	6.169942	0.012993887
ENSG00000177646	<i>ACAD9</i>	6.148424	0.013152926
ENSG00000133858	<i>ZFC3H1</i>	6.119822	0.013367426
ENSG00000129226	<i>CD68</i>	6.104664	0.013482558
ENSG0000006555	<i>TTC22</i>	6.087322	0.01361553
ENSG00000030066	<i>NUP160</i>	6.069492	0.013753651
ENSG00000171855	<i>IFNB1</i>	6.018916	0.014153337
ENSG0000004799	<i>PDK4</i>	5.983534	0.01444004
ENSG00000155307	<i>SAMSN1</i>	5.980414	0.014465606
ENSG00000120802	<i>TMPO</i>	5.927846	0.014903448
ENSG00000168487	<i>BMP1</i>	5.916176	0.015002485
ENSG00000157884	<i>CIB4</i>	5.909386	0.01506042
ENSG00000123454	<i>DBH</i>	5.8726	0.015378323
ENSG00000139946	<i>PELI2</i>	5.816662	0.015875045
ENSG00000151093	<i>OXSM</i>	5.786518	0.016149546
ENSG00000074964	<i>ARHGEF10L</i>	5.777486	0.016232743
ENSG00000104375	<i>STK3</i>	5.773854	0.016266323
ENSG00000132879	<i>FBXO44</i>	5.722368	0.016750125
ENSG00000142185	<i>TRPM2</i>	5.706242	0.01690469
ENSG00000060140	<i>STYK1</i>	5.686276	0.017098102
ENSG00000168314	<i>MOBP</i>	5.679996	0.017159407
ENSG00000171204	<i>TMEM126B</i>	5.673824	0.017219879
ENSG00000171060	<i>C8orf74</i>	5.628776	0.017667964
ENSG00000162763	<i>LRRC52</i>	5.611454	0.017843451
ENSG00000115368	<i>WDR75</i>	5.605486	0.017904328
ENSG00000155850	<i>SLC26A2</i>	5.59047	0.01805845
ENSG00000100422	<i>CERK</i>	5.523092	0.018767059
ENSG00000110448	<i>CD5</i>	5.436524	0.019719876
ENSG00000187210	<i>GCNT1</i>	5.4056	0.020072248
ENSG00000131697	<i>NPHP4</i>	5.39571	0.020186311
ENSG00000139540	<i>SLC39A5</i>	5.37829	0.020388853
ENSG00000145545	<i>SRD5A1</i>	5.356528	0.020644836
ENSG00000188163	<i>FAM166A</i>	5.34222	0.020814949
ENSG00000204444	<i>APOM</i>	5.323088	0.021044686
ENSG00000168356	<i>SCN11A</i>	5.275364	0.021629265
ENSG00000040487	<i>PQLC2</i>	5.261008	0.021808384
ENSG00000070182	<i>SPTB</i>	5.236584	0.02211666
ENSG00000170854	<i>RIOX2</i>	5.221002	0.022315689
ENSG00000157404	<i>KIT</i>	5.213524	0.022411864
ENSG00000087299	<i>L2HGDH</i>	5.205536	0.022515072
ENSG00000198885	<i>ITPRIPL1</i>	5.200184	0.022584497
ENSG00000183808	<i>RBM12B</i>	5.199092	0.02259869
ENSG00000149658	<i>YTHDF1</i>	5.196914	0.022627025
ENSG00000178828	<i>RNF186</i>	5.195598	0.022644163
ENSG00000104427	<i>ZC2HC1A</i>	5.180342	0.022843827
ENSG00000132600	<i>PRMT7</i>	5.170256	0.02297683

ENSG00000188389	<i>PDCD1</i>	5.169508	0.022986725
ENSG00000181418	<i>DDN</i>	5.153974	0.023193234
ENSG00000159261	<i>CLDN14</i>	5.144154	0.023324773
ENSG00000149308	<i>NPAT</i>	5.133838	0.023463789
ENSG00000105664	<i>COMP</i>	5.083712	0.02415161
ENSG0000008838	<i>MED24</i>	5.073708	0.024291369
ENSG00000119318	<i>RAD23B</i>	5.071646	0.02432028
ENSG00000123496	<i>IL13RA2</i>	5.067454	0.024379165
ENSG00000162738	<i>VANGL2</i>	5.036854	0.024813514
ENSG00000131773	<i>KHDRBS3</i>	4.973408	0.025739882
ENSG00000126218	<i>F10</i>	4.931624	0.026369525
ENSG00000164236	<i>ANKRD33B</i>	4.88775	0.027047914
ENSG00000144791	<i>LIMD1</i>	4.885796	0.027078546
ENSG00000173662	<i>TASIR1</i>	4.842906	0.027760077
ENSG00000137831	<i>UACA</i>	4.817134	0.028178161
ENSG00000115841	<i>RMDN2</i>	4.710282	0.029982733
ENSG00000068650	<i>ATP11A</i>	4.659032	0.030890602
ENSG00000139496	<i>NUP58</i>	4.626058	0.031489835
ENSG00000100249	<i>C22orf31</i>	4.618984	0.031619962
ENSG00000197323	<i>TRIM33</i>	4.58952	0.032168022
ENSG00000132854	<i>KANK4</i>	4.572368	0.032491623
ENSG00000188313	<i>PLSCR1</i>	4.570416	0.032528665
ENSG00000004455	<i>AK2</i>	4.5162	0.033575326
ENSG00000166260	<i>COX11</i>	4.511038	0.033676798
ENSG00000116151	<i>MORN1</i>	4.485256	0.034188426
ENSG00000113296	<i>THBS4</i>	4.472648	0.034441575
ENSG00000183665	<i>TRMT12</i>	4.443008	0.035044451
ENSG00000115363	<i>EVA1A</i>	4.422854	0.035460678
ENSG00000039523	<i>RIPOR1</i>	4.394094	0.036063616
ENSG00000174943	<i>KCTD13</i>	4.284406	0.03846352
ENSG00000115091	<i>ACTR3</i>	4.27827	0.03860262
ENSG00000108244	<i>KRT23</i>	4.24545	0.039355639
ENSG00000113810	<i>SMC4</i>	4.241152	0.039455386
ENSG00000064933	<i>PMS1</i>	4.188884	0.040689875
ENSG00000078081	<i>LAMP3</i>	4.183464	0.040820187
ENSG00000185880	<i>TRIM69</i>	4.115186	0.042499852
ENSG00000055732	<i>MCOLN3</i>	4.092196	0.043081634
ENSG00000164405	<i>UQCRO</i>	4.091046	0.043110955
ENSG00000180263	<i>FGD6</i>	4.082468	0.043330326
ENSG00000166582	<i>CENPV</i>	4.081766	0.04334833
ENSG00000127184	<i>COX7C</i>	4.076508	0.043483436
ENSG00000183161	<i>FANCF</i>	4.04233	0.044372518
ENSG00000106477	<i>CEP41</i>	4.024186	0.044852259
ENSG00000167775	<i>CD320</i>	4.022642	0.044893335
ENSG00000143436	<i>MRPL9</i>	4.014564	0.045108885
ENSG00000076344	<i>RGS11</i>	3.980968	0.046017111
ENSG00000140950	<i>MEAK7</i>	3.974056	0.046206346
ENSG00000151092	<i>NGLY1</i>	3.956014	0.046704172
ENSG00000164171	<i>ITGA2</i>	3.944738	0.047018175

ENSG00000143578	<i>CREB3L4</i>	3.939496	0.047164906
ENSG00000108826	<i>MRPL27</i>	3.922366	0.047647777
ENSG00000157593	<i>SLC35B2</i>	3.920568	0.047698762
ENSG00000133069	<i>TMCC2</i>	3.918826	0.047748214
ENSG00000126787	<i>DLGAP5</i>	3.918074	0.047769578
ENSG00000166860	<i>ZBTB39</i>	3.854156	0.049622887

The following supplementary table is presented as a separate Excel file, as the table is very large.

table S21 (as a separate Excel file). Identification of lineage-specific accelerated regions along with the Simiiformes branch. Lineage-specific accelerated regions significance was determined by $FDR \leq 0.05$. Nearest genes were obtained by reference to the distance to the lineage-specific accelerated regions in 500kbp.

The following supplementary table is presented as a separate Excel file, as the table is very large.

table S22 (as a separate Excel file). Significantly expanded gene families in the Simiiformes lineage in contrast to all other primate species. Unpaired t test P values were adjusted by Benjamini-Hochberg *FDR* ($FDR < 0.05$). Gene copy numbers in each species are listed. Red represents copy numbers in the Simiiformes species, whereas black represents copy numbers in other primate species. The species names (see Fig. 1) are shown by first three letter abbreviations of the Latin names. Here, human gene names of expanded gene families with at least one copy in human are used.

table S23. Functional enrichment analysis of the gene-set including positively selected genes, genes associated with lineage-specific accelerated regions, and expanded gene families in the Simiiformes lineage. Categories with P value < 0.05 (Modified Fisher's Exact test) are listed.

Category	Term	Count	P
GOTERM_CC_DIRECT	GO:0005829~cytosol	181	2.65E-08
GOTERM_CC_DIRECT	GO:0005654~nucleoplasm	131	5.31E-06
UP_SEQ_FEATURE	COMPBIAS:Basic and acidic residues	179	1.56E-05
UP_SEQ_FEATURE	COMPBIAS:Polar residues	210	3.51E-05
GOTERM_CC_DIRECT	GO:0005911~cell-cell junction	15	0.000151
GOTERM_MF_DIRECT	GO:0005515~protein binding	343	0.000184
KEGG_PATHWAY	hsa04510:Focal adhesion	16	0.000237
GOTERM_BP_DIRECT	GO:0001736~establishment of planar polarity	5	0.000404
GOTERM_MF_DIRECT	GO:0003712~transcription cofactor activity	12	0.000664
GOTERM_BP_DIRECT	GO:0008360~regulation of cell shape	12	0.00094
GOTERM_CC_DIRECT	GO:0016020~membrane	83	0.000943
UP_SEQ_FEATURE	REGION:Disordered	363	0.001003
GOTERM_CC_DIRECT	GO:0014069~postsynaptic density	16	0.001398
GOTERM_CC_DIRECT	GO:0005856~cytoskeleton	25	0.00177
KEGG_PATHWAY	hsa04151:PI3K-Akt signaling pathway	20	0.002232
GOTERM_BP_DIRECT	GO:0045944~positive regulation of transcription from RNA polymerase II promoter	44	0.002714
UP_KW_CELLULAR_COMPONENT	KW-0539~Nucleus	168	0.003355
UP_KW_CELLULAR_COMPONENT	KW-0965~Cell junction	36	0.003462
UP_SEQ_FEATURE	REPEAT:ANK 5	11	0.003769
GOTERM_MF_DIRECT	GO:0017056~structural constituent of nuclear pore	5	0.005163
GOTERM_CC_DIRECT	GO:0005769~early endosome	16	0.00539
GOTERM_CC_DIRECT	GO:0005635~nuclear envelope	12	0.005437
UP_KW_BIOLOGICAL_PROCESS	KW-0804~Transcription	83	0.006561
UP_KW_BIOLOGICAL_PROCESS	KW-0805~Transcription regulation	81	0.006565
GOTERM_BP_DIRECT	GO:0030335~positive regulation of cell migration	14	0.006585
GOTERM_MF_DIRECT	GO:0030165~PDZ domain binding	8	0.006932
GOTERM_BP_DIRECT	GO:0060011~Sertoli cell proliferation	3	0.00745
GOTERM_BP_DIRECT	GO:0048193~Golgi vesicle transport	4	0.007631
UP_KW_CELLULAR_COMPONENT	KW-0770~Synapse	23	0.007874
UP_KW_CELLULAR_COMPONENT	KW-0206~Cytoskeleton	48	0.00823
GOTERM_BP_DIRECT	GO:0006897~endocytosis	12	0.008965
GOTERM_BP_DIRECT	GO:0016477~cell migration	14	0.009474
GOTERM_MF_DIRECT	GO:0051015~actin filament binding	13	0.009621
GOTERM_BP_DIRECT	GO:0030036~actin cytoskeleton organization	11	0.009653
UP_SEQ_FEATURE	REPEAT:ANK 1	14	0.010011
UP_SEQ_FEATURE	REPEAT:ANK 2	14	0.010325
GOTERM_CC_DIRECT	GO:0005796~Golgi lumen	8	0.011297
GOTERM_BP_DIRECT	GO:0007160~cell-matrix adhesion	8	0.011839
UP_SEQ_FEATURE	REPEAT:ANK 6	8	0.012984
GOTERM_CC_DIRECT	GO:0009986~cell surface	25	0.013084
UP_SEQ_FEATURE	REPEAT:ANK 4	11	0.013947
GOTERM_BP_DIRECT	GO:0045184~establishment of protein localization	5	0.014301

UP_KW_BIOLOGICAL_PROCESS	KW-0221~Differentiation	31	0.014739
GOTERM_BP_DIRECT	GO:0051220~cytoplasmic sequestering of protein	3	0.017081
UP_SEQ_FEATURE	REPEAT:ANK 3	12	0.017689
UP_SEQ_FEATURE	MOTIF:LXXLL motif 1	4	0.017692
UP_SEQ_FEATURE	MOTIF:LXXLL motif 2	4	0.017692
GOTERM_CC_DIRECT	GO:0034451~centriolar satellite	8	0.018591
GOTERM_MF_DIRECT	GO:0001540~beta-amyloid binding	7	0.018829
UP_SEQ_FEATURE	DOMAIN:GAGE	3	0.019016
GOTERM_BP_DIRECT	GO:0060976~coronary vasculature development	4	0.019107
GOTERM_BP_DIRECT	GO:0090090~negative regulation of canonical Wnt signaling pathway	9	0.019124
GOTERM_CC_DIRECT	GO:0005634~nucleus	158	0.020576
UP_SEQ_FEATURE	REPEAT:TPR 7	6	0.020953
UP_KW_CELLULAR_COMPONENT	KW-0963~Cytoplasm	157	0.021229
GOTERM_BP_DIRECT	GO:0048661~positive regulation of smooth muscle cell proliferation	6	0.022482
UP_SEQ_FEATURE	DOMAIN:DAD	3	0.023391
GOTERM_MF_DIRECT	GO:1990247~N6-methyladenosine-containing RNA binding	3	0.023579
UP_SEQ_FEATURE	REPEAT:Spectrin 2	4	0.02462
UP_SEQ_FEATURE	REPEAT:TPR 10	4	0.02462
UP_SEQ_FEATURE	REPEAT:Spectrin 1	4	0.02462
GOTERM_BP_DIRECT	GO:0046037~GMP metabolic process	3	0.025316
GOTERM_MF_DIRECT	GO:0005518~collagen binding	6	0.025332
UP_SEQ_FEATURE	REPEAT:TPR 3	9	0.025777
GOTERM_BP_DIRECT	GO:0050673~epithelial cell proliferation	5	0.025947
UP_KW_MOLECULAR_FUNCTION	KW-0009~Actin-binding	14	0.026433
GOTERM_BP_DIRECT	GO:0051649~establishment of localization in cell	7	0.026785
KEGG_PATHWAY	hsa04512:ECM-receptor interaction	7	0.027221
KEGG_PATHWAY	hsa04810:Regulation of actin cytoskeleton	12	0.027247
GOTERM_MF_DIRECT	GO:0008139~nuclear localization sequence binding	4	0.027507
UP_KW_MOLECULAR_FUNCTION	KW-0010~Activator	27	0.027996
UP_SEQ_FEATURE	DOMAIN:GBD/FH3	3	0.028134
GOTERM_BP_DIRECT	GO:0051897~positive regulation of protein kinase B signaling	8	0.02865
UP_KW_BIOLOGICAL_PROCESS	KW-0833~Ubl conjugation pathway	29	0.028823
GOTERM_BP_DIRECT	GO:0010628~positive regulation of gene expression	20	0.02906
GOTERM_BP_DIRECT	GO:0046718~viral entry into host cell	7	0.029176
GOTERM_CC_DIRECT	GO:0001726~ruffle	7	0.029204
KEGG_PATHWAY	hsa04024:cAMP signaling pathway	12	0.029634
KEGG_PATHWAY	hsa05132:Salmonella infection	13	0.029753
GOTERM_BP_DIRECT	GO:0009101~glycoprotein biosynthetic process	3	0.029924
GOTERM_BP_DIRECT	GO:0038180~nerve growth factor signaling pathway	3	0.029924
GOTERM_BP_DIRECT	GO:0045842~positive regulation of mitotic metaphase/anaphase transition	3	0.029924
GOTERM_CC_DIRECT	GO:0043005~neuron projection	16	0.030172
GOTERM_BP_DIRECT	GO:0010592~positive regulation of lamellipodium assembly	4	0.031011
GOTERM_BP_DIRECT	GO:0070979~protein K11-linked ubiquitination	4	0.031011
GOTERM_CC_DIRECT	GO:0005814~centriole	9	0.031031
GOTERM_BP_DIRECT	GO:0051301~cell division	16	0.031381
GOTERM_BP_DIRECT	GO:0043410~positive regulation of MAPK cascade	9	0.031991
GOTERM_BP_DIRECT	GO:0001525~angiogenesis	12	0.032259
GOTERM_BP_DIRECT	GO:0043484~regulation of RNA splicing	6	0.033858
UP_KW_CELLULAR_COMPONENT	KW-0628~Postsynaptic cell membrane	9	0.03396

GOTERM_BP_DIRECT	GO:0010468~regulation of gene expression	12	0.0343
GOTERM_BP_DIRECT	GO:0071872~cellular response to epinephrine stimulus	3	0.034835
UP_SEQ_FEATURE	DNA_BIND:HMG box	5	0.035308
UP_KW_CELLULAR_COMPONENT	KW-0906~Nuclear pore complex	5	0.035323
GOTERM_MF_DIRECT	GO:0005102~receptor binding	17	0.035456
UP_SEQ_FEATURE	REPEAT:TPR 4	7	0.035457
GOTERM_CC_DIRECT	GO:0005737~cytoplasm	147	0.03582
GOTERM_CC_DIRECT	GO:0032991~macromolecular complex	25	0.036309
GOTERM_CC_DIRECT	GO:0015629~actin cytoskeleton	12	0.0372
GOTERM_CC_DIRECT	GO:0005925~focal adhesion	17	0.037435
UP_SEQ_FEATURE	REPEAT:TPR 6	6	0.037836
GOTERM_BP_DIRECT	GO:0019228~neuronal action potential	4	0.039636
GOTERM_BP_DIRECT	GO:0043388~positive regulation of DNA binding	4	0.039636
GOTERM_BP_DIRECT	GO:0006515~misfolded or incompletely synthesized protein catabolic process	3	0.040033
GOTERM_BP_DIRECT	GO:0060996~dendritic spine development	3	0.040033
GOTERM_CC_DIRECT	GO:0043240~Fanconi anaemia nuclear complex	3	0.04004
GOTERM_BP_DIRECT	GO:0007015~actin filament organization	8	0.040568
UP_SEQ_FEATURE	REPEAT:TPR 2	9	0.041128
UP_SEQ_FEATURE	REPEAT:TPR 1	9	0.041128
GOTERM_CC_DIRECT	GO:0005762~mitochondrial large ribosomal subunit	5	0.042015
GOTERM_MF_DIRECT	GO:0015276~ligand-gated ion channel activity	4	0.042676
GOTERM_CC_DIRECT	GO:0046658~anchored component of plasma membrane	4	0.042768
UP_SEQ_FEATURE	DOMAIN:L27	3	0.044372
UP_SEQ_FEATURE	REPEAT:Spectrin 7	3	0.044372
UP_SEQ_FEATURE	REPEAT:Spectrin 8	3	0.044372
UP_SEQ_FEATURE	REPEAT:Spectrin 9	3	0.044372
GOTERM_CC_DIRECT	GO:0012505~endomembrane system	8	0.044737
KEGG_PATHWAY	hsa04145:Phagosome	9	0.045402
GOTERM_BP_DIRECT	GO:0032707~negative regulation of interleukin-23 production	2	0.045484
GOTERM_BP_DIRECT	GO:0003210~cardiac atrium formation	2	0.045484
GOTERM_BP_DIRECT	GO:0006895~Golgi to endosome transport	3	0.045503
GOTERM_BP_DIRECT	GO:0006904~vesicle docking involved in exocytosis	4	0.04599
GOTERM_BP_DIRECT	GO:0031532~actin cytoskeleton reorganization	5	0.046711
GOTERM_MF_DIRECT	GO:0005200~structural constituent of cytoskeleton	7	0.047567
GOTERM_BP_DIRECT	GO:0007010~cytoskeleton organization	8	0.047582
UP_SEQ_FEATURE	REPEAT:TPR 5	6	0.047637
UP_SEQ_FEATURE	REGION:Cisternal side	2	0.048103
UP_SEQ_FEATURE	REGION:Required for targeting to the nucleus and nuclear pore complex	2	0.048103
UP_SEQ_FEATURE	REGION:Pore side	2	0.048103
GOTERM_MF_DIRECT	GO:0031267~small GTPase binding	13	0.0482
GOTERM_MF_DIRECT	GO:0038177~death receptor agonist activity	2	0.048311
UP_KW_MOLECULAR_FUNCTION	KW-9996~Developmental protein	34	0.048854
UP_KW_MOLECULAR_FUNCTION	KW-0217~Developmental protein	34	0.048854
UP_KW_CELLULAR_COMPONENT	KW-0967~Endosome	24	0.049146
GOTERM_BP_DIRECT	GO:0022900~electron transport chain	5	0.049176
GOTERM_CC_DIRECT	GO:0016235~aggresome	4	0.04936
GOTERM_CC_DIRECT	GO:0005912~adherens junction	9	0.049855

table S24. Tissue-specific expression enrichment analysis of the genes including positively selected genes, genes associated with lineage-specific accelerated regions, and expanded gene families in the Simiiformes lineage. Categories with P value < 0.05 (Modified Fisher's Exact test) are listed.

Category	Term	Count	P
CGAP_EST_QUARTILE	33578:brain_neoplasia_3rd	23	3.85E-06
CGAP_EST_QUARTILE	21078:genitourinary_neoplasia_3rd	11	1.10E-05
UP_TISSUE	Testis	166	1.43E-04
GNF_U133A_QUARTILE	Prostate_3rd	268	1.44E-04
CGAP_EST_QUARTILE	20008:placenta_normal_3rd	8	3.14E-04
CGAP_EST_QUARTILE	16366:cerebrum_normal_3rd	13	4.88E-04
UP_TISSUE	Brain	250	5.50E-04
GNF_U133A_QUARTILE	Cerebellum_3rd	292	5.97E-04
GNF_U133A_QUARTILE	fetalliver_3rd	112	6.01E-04
CGAP_EST_QUARTILE	21766:placenta_normal_3rd	11	6.81E-04
CGAP_EST_QUARTILE	379:heart_normal_3rd	19	7.28E-04
CGAP_SAGE_QUARTILE	656:brain_null_3rd	49	7.30E-04
GNF_U133A_QUARTILE	Smooth Muscle_3rd	134	7.73E-04
CGAP_EST_QUARTILE	10713:lymph_node_normal_3rd	14	8.30E-04
CGAP_EST_QUARTILE	6372:uncharacterized_tissue_uncharacterized_histology_3rd	6	8.90E-04
CGAP_EST_QUARTILE	23995:uncharacterized_tissue_uncharacterized_histology_3rd	15	0.001453
CGAP_EST_QUARTILE	10749:colon_neoplasia_3rd	5	0.001656
GNF_U133A_QUARTILE	TONGUE_3rd	117	0.001681
UNIGENE_EST_QUARTILE	vascular_normal_3rd	100	0.001932
CGAP_EST_QUARTILE	10956:colon_neoplasia_3rd	8	0.002047
HPA_NORMAL_TISSUE_CELLTYPE	caudate; neuronal cells	201	0.002237
GNF_U133A_QUARTILE	BM-CD105+Endothelial_3rd	130	0.002368
CGAP_EST_QUARTILE	19994:placenta_normal_3rd	11	0.002648
CGAP_EST_QUARTILE	20249:colon_neoplasia_3rd	7	0.002745
CGAP_SAGE_QUARTILE	410:cerebellum_medulloblastoma_3rd	66	0.002865
CGAP_EST_QUARTILE	674:placenta_normal_3rd	9	0.003423
GNF_U133A_QUARTILE	WHOLE BLOOD_3rd	141	0.003478
CGAP_EST_QUARTILE	20574:placenta_normal_3rd	8	0.003642
CGAP_EST_QUARTILE	16016:uteru_uncharacterized_histology_3rd	13	0.003682
CGAP_EST_QUARTILE	16593:mammary_gland_normal_3rd	14	0.003731
HPA_NORMAL_TISSUE_CELLTYPE	cerebellum; cells in molecular layer	151	0.003883
GNF_U133A_QUARTILE	Uterus_3rd	90	0.003951
HPA_NORMAL_TISSUE_CELLTYPE	cerebral cortex; neuropil	167	0.003966
CGAP_EST_QUARTILE	19998:placenta_normal_3rd	10	0.003969
UNIGENE_EST_QUARTILE	laryngeal_cancer_disease_3rd	99	0.003986
HPA_NORMAL_TISSUE	caudate	221	0.004434
HPA_NORMAL_TISSUE_CELLTYPE	caudate; glial cells	154	0.004439
HPA_NORMAL_TISSUE	hippocampus	217	0.004893
CGAP_SAGE_QUARTILE	359:brain_Glioblastoma_3rd	47	0.004929
CGAP_EST_QUARTILE	19268:cerebrum_normal_3rd	3	0.005406
UNIGENE_EST_QUARTILE	larynx_normal_3rd	96	0.006266
CGAP_SAGE_QUARTILE	144:brain_astrocytoma_grade_II_3rd	48	0.006305
CGAP_EST_QUARTILE	20280:placenta_normal_3rd	7	0.006422

CGAP_EST_QUARTILE	13801:colon_normal_3rd	4	0.007133
CGAP_EST_QUARTILE	11116:head and neck_neoplasia_3rd	3	0.007982
CGAP_EST_QUARTILE	19377:placenta_normal_3rd	9	0.008055
UNIGENE_EST_QUARTILE	muscle_normal_3rd	119	0.00834
HPA_NORMAL_TISSUE_CELLTYPE	lymph node; non-germinal center cells	194	0.008416
HPA_NORMAL_TISSUE_CELLTYPE	cerebral cortex; glial cells	162	0.008569
GNF_U133A_QUARTILE	Occipital Lobe_3rd	84	0.008877
CGAP_EST_QUARTILE	23547:placenta_normal_3rd	8	0.008973
CGAP_EST_QUARTILE	21477:uncharacterized tissue_neoplasia_3rd	6	0.009119
CGAP_EST_QUARTILE	492:thymu_normal_3rd	11	0.009715
HPA_NORMAL_TISSUE_CELLTYPE	placenta; trophoblastic cells	202	0.009798
UNIGENE_EST_QUARTILE	pituitary gland_normal_3rd	97	0.00989
CGAP_EST_QUARTILE	16884:mammary gland_neoplasia_3rd	5	0.010265
CGAP_EST_QUARTILE	11260:head and neck_neoplasia_3rd	6	0.010599
CGAP_SAGE_QUARTILE	655:vascular_normal liver_3rd	34	0.01094
CGAP_EST_QUARTILE	25:uncharacterized tissue_uncharacterized histology_3rd	9	0.011146
CGAP_EST_QUARTILE	19520:uncharacterized tissue_normal_3rd	5	0.011298
UNIGENE_EST_QUARTILE	pharynx_normal_3rd	63	0.011311
UNIGENE_EST_QUARTILE	ear_normal_3rd	81	0.012223
CGAP_EST_QUARTILE	20729:genitourinary_neoplasia_3rd	6	0.012235
CGAP_EST_QUARTILE	19072:colon_neoplasia_3rd	6	0.012235
CGAP_SAGE_QUARTILE	283:brain_anaplastic astrocytoma grade III_3rd	47	0.01236
HPA_NORMAL_TISSUE_CELLTYPE	hippocampus; glial cells	138	0.012769
UNIGENE_EST_QUARTILE	mammary gland_normal_3rd	128	0.012795
CGAP_EST_QUARTILE	40265:synovium_uncharacterized histology_3rd	12	0.013012
HPA_NORMAL_TISSUE_CELLTYPE	lung; alveolar cells type II	59	0.013192
HPA_NORMAL_TISSUE_CELLTYPE	parathyroid gland; glandular cells	188	0.013221
HPA_NORMAL_TISSUE	parathyroid gland	188	0.013221
CGAP_EST_QUARTILE	21531:cerebrum_normal_3rd	5	0.013558
CGAP_EST_QUARTILE	16631:mammary gland_normal_3rd	3	0.014436
CGAP_EST_QUARTILE	6259:mammary gland_neoplasia_3rd	3	0.014436
GNF_U133A_QUARTILE	PLACENTA_3rd	298	0.014903
CGAP_SAGE_QUARTILE	430:brain_null_3rd	57	0.015094
GNF_U133A_QUARTILE	Olfactory Bulb_3rd	74	0.015513
CGAP_EST_QUARTILE	686:cervix_neoplasia_3rd	11	0.015939
CGAP_EST_QUARTILE	23545:placenta_normal_3rd	7	0.015942
UNIGENE_EST_QUARTILE	juvenile (< 17 years old)_development_3rd	100	0.016062
CGAP_EST_QUARTILE	553:mammary gland_normal_3rd	8	0.016234
HPA_NORMAL_TISSUE_CELLTYPE	cerebellum; cells in granular layer	149	0.016828
HPA_NORMAL_TISSUE	placenta	232	0.01687
CGAP_EST_QUARTILE	26805:placenta_normal_3rd	16	0.017197
HPA_NORMAL_TISSUE_CELLTYPE	spleen; cells in red pulp	171	0.017318
HPA_NORMAL_TISSUE_CELLTYPE	lung; alveolar cells type I	44	0.017664
CGAP_SAGE_QUARTILE	604:cartilage_chondrosarcoma grade 2._3rd	32	0.017788
CGAP_EST_QUARTILE	16373:cerebrum_normal_3rd	6	0.018147
CGAP_EST_QUARTILE	32281:liver_normal_3rd	5	0.018892
HPA_NORMAL_TISSUE	cerebellum	223	0.019729
CGAP_EST_QUARTILE	16695:mammary gland_normal_3rd	9	0.019827
HPA_NORMAL_TISSUE_CELLTYPE	hippocampus; neuronal cells	196	0.019859

UNIGENE_EST_QUARTILE	tongue_normal_3rd	108	0.020126
CGAP_EST_QUARTILE	21106:genitourinary_neoplasia_3rd	8	0.020232
UP_TISSUE	Erythroleukemia	137	0.020339
HPA_NORMAL_TISSUE_CELLTYPE	soft tissue 2; fibroblasts	136	0.020461
CGAP_EST_QUARTILE	16290:cerebrum_normal_3rd	6	0.020473
CGAP_EST_QUARTILE	11528:stomach_neoplasia_3rd	6	0.020473
CGAP_EST_QUARTILE	20739:genitourinary_neoplasia_3rd	7	0.020578
CGAP_EST_QUARTILE	16329:cerebrum_normal_3rd	7	0.020578
HPA_NORMAL_TISSUE	fallopian tube	230	0.020632
CGAP_EST_QUARTILE	22090:nervou_normal_3rd	15	0.020775
HPA_NORMAL_TISSUE	lymph node	204	0.021038
GNF_U133A_QUARTILE	Pons_3rd	173	0.021359
CGAP_EST_QUARTILE	21491:uncharacterized_tissue_neoplasia_3rd	10	0.021618
HPA_NORMAL_TISSUE	spleen	186	0.022012
GNF_U133A_QUARTILE	skin_3rd	57	0.022243
CGAP_EST_QUARTILE	19178:head_and_neck_neoplasia_3rd	3	0.022482
CGAP_SAGE_QUARTILE	646:mammary_gland_invasive_breast_cancer_ER+, PR+, Her2-, grade II_3rd	26	0.023385
HPA_NORMAL_TISSUE_CELLTYPE	endometrium 2; glandular cells	209	0.023539
CGAP_EST_QUARTILE	20591:uteru_neoplasia_3rd	5	0.023637
HPA_NORMAL_TISSUE_CELLTYPE	skin 1; eccrine_glands	14	0.023766
CGAP_EST_QUARTILE	21747:placenta_normal_3rd	6	0.024314
CGAP_EST_QUARTILE	20571:placenta_normal_3rd	9	0.024726
HPA_NORMAL_TISSUE_CELLTYPE	cerebellum; Purkinje cells	177	0.025691
HPA_NORMAL_TISSUE	endometrium 2	214	0.025773
CGAP_SAGE_QUARTILE	1443:stomach_Adenocarcinoma_3rd	35	0.026107
CGAP_EST_QUARTILE	11470:stomach_neoplasia_3rd	8	0.026913
CGAP_EST_QUARTILE	20003:placenta_normal_3rd	3	0.027051
CGAP_EST_QUARTILE	1528:cerebrum_uncharacterized_histology_3rd	9	0.027469
HPA_NORMAL_TISSUE	soft_tissue 2	166	0.028199
CGAP_SAGE_QUARTILE	645:mammary_gland_invasive_breast_cancer_ER+, PR+, Her-, grade II_3rd	28	0.028264
CGAP_EST_QUARTILE	13843:uncharacterized_tissue_neoplasia_3rd	9	0.028429
HPA_NORMAL_TISSUE_CELLTYPE	endometrium 1; glandular cells	211	0.028445
CGAP_EST_QUARTILE	20062:uncharacterized_tissue_neoplasia_3rd	7	0.028489
UP_TISSUE	Hippocampus	29	0.028881
CGAP_SAGE_QUARTILE	70:prostate_carcinoma_3rd	63	0.029364
CGAP_EST_QUARTILE	21725:placenta_normal_3rd	6	0.030115
CGAP_EST_QUARTILE	16496:lung_normal_3rd	6	0.030115
CGAP_EST_QUARTILE	11090:kidney_uncharacterized_histology_3rd	8	0.030189
HPA_NORMAL_TISSUE_CELLTYPE	cerebral_cortex; neuronal_cells	208	0.030341
CGAP_EST_QUARTILE	21863:placenta_normal_3rd	7	0.031072
UP_TISSUE	Leukemic_T-cell	79	0.031074
CGAP_EST_QUARTILE	32:colon_neoplasia_3rd	14	0.031094
GNF_U133A_QUARTILE	Appendix_3rd	118	0.031112
HPA_NORMAL_TISSUE_CELLTYPE	tonsil; non-germinal_center_cells	191	0.031126
CGAP_EST_QUARTILE	20123:uteru_neoplasia_3rd	6	0.031169
CGAP_EST_QUARTILE	16321:cerebrum_normal_3rd	3	0.031957
CGAP_EST_QUARTILE	23453:colon_neoplasia_3rd	3	0.031957
HPA_NORMAL_TISSUE_CELLTYPE	salivary_gland; glandular_cells	213	0.031974

HPA_NORMAL_TISSUE	salivary gland	213	0.031974
HPA_NORMAL_TISSUE_CELLTYPE	epididymis; glandular cells	225	0.032156
HPA_NORMAL_TISSUE	epididymis	225	0.032156
CGAP_EST_QUARTILE	20721:uncharacterized tissue_normal_3rd	10	0.032573
CGAP_EST_QUARTILE	937:gastrointestinal tract_normal_3rd	13	0.03349
CGAP_SAGE_QUARTILE	1906:retina_Bilateral retinoblastoma, poorly differentiated, left orbit_3rd	58	0.033925
CGAP_EST_QUARTILE	847:ovary_normal_3rd	15	0.034755
CGAP_EST_QUARTILE	21720:placenta_normal_3rd	5	0.035125
CGAP_EST_QUARTILE	21715:placenta_normal_3rd	9	0.035798
CGAP_SAGE_QUARTILE	263:cerebellum_medulloblastoma_3rd	57	0.036652
CGAP_EST_QUARTILE	21451:uncharacterized tissue_neoplasia_3rd	7	0.036684
CGAP_EST_QUARTILE	23731:genitourinary_normal_3rd	3	0.037182
CGAP_SAGE_QUARTILE	1649:brain_3rd	52	0.038069
CGAP_EST_QUARTILE	19862:testi_normal_3rd	10	0.038089
CGAP_SAGE_QUARTILE	420:mammary gland_normal breast tissue from a breast cancer patient (corresponding to IDC7)_3rd	39	0.038165
CGAP_EST_QUARTILE	23542:placenta_normal_3rd	6	0.038498
CGAP_EST_QUARTILE	40304:thymu_uncharacterized histology_3rd	8	0.038848
HPA_NORMAL_TISSUE_CELLTYPE	adipose tissue; adipocytes	128	0.039208
HPA_NORMAL_TISSUE	adipose tissue	128	0.039208
UNIGENE_EST_QUARTILE	uterine tumor_disease_3rd	121	0.039307
GNF_U133A_QUARTILE	spinalcord_3rd	69	0.039772
CGAP_SAGE_QUARTILE	1883:retina_Bilateral retinoblastoma, poorly differentiated, left orbit_3rd	48	0.039968
GNF_U133A_QUARTILE	TemporalLobe_3rd	93	0.040124
CGAP_EST_QUARTILE	32326:eye_normal_3rd	16	0.040321
CGAP_EST_QUARTILE	852:nervou_normal_3rd	14	0.040775
CGAP_SAGE_QUARTILE	350:brain_anaplastic gradIII, primary, brain_3rd	46	0.040778
HPA_NORMAL_TISSUE	cerebral cortex	245	0.041106
HPA_NORMAL_TISSUE_CELLTYPE	skin 1; cells in basal layer	35	0.041643
CGAP_EST_QUARTILE	6163:mammary gland_neoplasia_3rd	3	0.042708
CGAP_EST_QUARTILE	40588:endocrine_uncharacterized histology_3rd	7	0.042907
CGAP_EST_QUARTILE	673:nervou_normal_3rd	8	0.04301
HPA_NORMAL_TISSUE	endometrium 1	216	0.0432
HPA_NORMAL_TISSUE_CELLTYPE	pancreas; exocrine glandular cells	213	0.04373
HPA_NORMAL_TISSUE	liver	195	0.04389
CGAP_SAGE_QUARTILE	356:brain_Glioblastoma_3rd	35	0.044292
UNIGENE_EST_QUARTILE	lymph node_normal_3rd	123	0.045889
HPA_RNA_TISSUE	testis	61	0.047302
CGAP_SAGE_QUARTILE	124:cerebellum_medulloblastoma, cerebellum_3rd	56	0.047322
CGAP_EST_QUARTILE	27218:ovary_neoplasia_3rd	7	0.047985
CGAP_EST_QUARTILE	21525:cerebrum_normal_3rd	10	0.04834
CGAP_EST_QUARTILE	16821:mammary gland_neoplasia_3rd	10	0.04834
CGAP_EST_QUARTILE	10715:lymph node_normal_3rd	10	0.04834
CGAP_EST_QUARTILE	20006:placenta_normal_3rd	3	0.048517
CGAP_EST_QUARTILE	19196:head and neck_neoplasia_3rd	3	0.048517
CGAP_SAGE_QUARTILE	506:white blood cells_invasive breast tumor (~2 cm), extensive high-grade comedo DCIS (~4 cm), positive lymph nodes_3rd	50	0.049104
CGAP_SAGE_QUARTILE	607:cartilage_Dedifferentiated chondrosarcoma lung metastasis_3rd	37	0.049192
CGAP_EST_QUARTILE	21660:brain_neoplasia_3rd	5	0.049339

CGAP_SAGE_QUARTILE	362:pancreas_null_3rd	35	0.049509
CGAP_SAGE_QUARTILE	647:mammary gland_normal breast tissue from a breast cancer patient (corresponding to IDC7)_3rd	24	0.049887

table S25. Five candidate genes including four genes associated with lineage-specific accelerated regions and one positively selected gene in the Simiiformes ancestral lineage in the pathway ‘axon guidance’ with the high expression in the human brain. The 5 candidates were identified as highly expressed genes in brain by the DAVID Tissue_Expression database (<https://david.ncifcrf.gov/home.jsp>). The positively selected gene is displayed in bold font.

Ensembl Gene ID	Gene Name	Tissue Category
ENSG00000044524	<i>EPHA3</i>	Cerebellum_3rd/brain_anaplastic gradeIII, primary, brain_3rd cerebral cortex; neuropil/hippocampus/brain_astrocytoma grade II_3rd/ brain_anaplastic astrocytoma grade III_3rd/ hippocampus; glial cells/ cerebellum_meningioma_3rd/ brain_3rd/ brain_anaplastic gradeIII, primary, brain_3rd/ cerebral cortex/ brain_Glioblastoma_3rd/ brain_neoplasia_3rd
ENSG00000136238	<i>RAC1</i>	
ENSG00000196358	<i>NTNG2</i>	Brain
ENSG0000012171	<i>SEMA3B</i>	Brain/ Cerebellum_3rd
ENSG00000153993	<i>SEMA3D</i>	Cerebellum_3rd/ brain_anaplastic gradeIII, primary, brain_3rd

table S26. Positively selected genes involved in brain development from the primate common ancestor leading to the human lineage. 772 genes involved in ‘GO:0007420~brain development’ were retrieved from g:Profiler (104v) (<https://biit.cs.ut.ee/gprofiler/gost>). 772 genes overlapped positively selected genes from the primate ancestral lineage leading to the human lineage in order to identify PSGs involved in ‘brain development’ in each crucial node.

Lineage	Positively selected genes involved in ‘brain development’ (GO:0007420)
Primate ancestor	<i>SLC6A4, NR2E1, NIPBL, XRCC6</i>
Haplorrhini ancestor	<i>ATAT1, FRS2, PFKFB3, TCTN1</i>
Simiiformes ancestor	<i>GRHL2, SRD5A1, UQCRCO, AK8</i>
Catarrhini ancestor	<i>KDM1A, UBA6, SEMA3A, NCOA1, XRN2, PPP3CA, GDF7, CDK5</i>
Hominoidea ancestor	<i>DPYSL2, MAST1, SCYL2</i>
Great ape ancestor	<i>DUOX2</i>
Homininae ancestor	<i>SUN2, CDH22, RBPJ, LDB1</i>
Hominini ancestor	<i>TNR, TTC21B, CRH</i>
Human	<i>NRPI, NIN, ROBO1</i>

table S27. Positively selected gene involved in ‘Microcephaly’ from the Primate ancestor leading to the human lineage. 1,133 genes putatively involved in microcephaly (HP:0000252) were obtained from g:Profiler (v104) (<https://biit.cs.ut.ee/gprofiler/gost>).

Lineage	PSGs involved in ‘Microcephaly’ (HP:0000252)
Primate ancestor	<i>ITGA3, NIPBL, DPAGT1, WDR73, POLE, CDK10, MYTIL, SPTAN1</i>
Haplorrhini ancestor	<i>HCCS, UPB1, MOCSI, THOC6, SLC5A6, LINS1, GTPBP2, DALRD3, SIX6</i>
Simiiformes ancestor	<i>ACBD5, TIMMDC1, AMPD2, CLPP, PRMT7, NGLY1, KIT, TMEM126B, ERCC6L2, FANCF, CHRNG</i>
Catarrhini ancestor	<i>PNKP, ERCC8, SNAP29, ESS2, DOCK8, TDP2, DNMT3A, PAX3, PPP3CA, PEX10, CDK5, TP53RK, NDUFA6, PI4KA</i>
Hominoidea ancestor	<i>SALL4, RPL5, AGT, SCYL2, JMJD1C, BLM</i>
Great ape ancestor	<i>SLC18A2, IFT140</i>
Homininae ancestor	<i>POLR1A, TMEM165, XPR1, CPT2, RBPJ, LARP7, RUSC2</i>
Hominini ancestor	<i>KMT2E, MTFMT</i>
Human	<i>TRIT1, NIN, FARSB, GATA6, SMAD4, PISD</i>

The following supplementary table is presented as a separate Excel file, as the table is very large.

table S28 (as a separate Excel file). Identification of lineage-specific accelerated regions along the Catarrhini branch. Lineage-specific accelerated regions significance was determined by FDR \leq 0.05. Nearest genes were obtained by reference to the distance to the lineage-specific accelerated regions in 500kbp.

The following supplementary table is presented as a separate Excel file, as the table is very large.

table S29 (as a separate Excel file). Identification of lineage-specific accelerated regions along the great ape (Hominidae) branch. Lineage-specific accelerated regions significance was determined by FDR \leq 0.05. Nearest genes were obtained by reference to the distance to the lineage-specific accelerated regions in 500kbp.

The following supplementary table is presented as a separate Excel file, as the table is very large.

table S30 (as a separate Excel file). Identification of lineage-specific accelerated regions along the human branch. Lineage-specific accelerated regions significance was determined by FDR \leq 0.05. Nearest genes were obtained by reference to the distance to the lineage-specific accelerated regions in 500kbp.

table S31. 15 genes associated with lineage-specific accelerated regions with a high level of expression in fetal brain for the great ape ancestral lineage. The 15 candidate genes were identified as being highly expressed in fetal brain by the DAVID Tissue_Expression database (UP_TISSUE) (<https://david.ncifcrf.gov/home.jsp>).

Ensembl Gene ID	Gene Name	Gene Description	UP_TISSUE
ENSG00000081189	<i>MEF2C</i>	myocyte enhancer factor 2C	Fetal brain
ENSG0000072315	<i>TRPC5</i>	transient receptor potential cation channel subfamily C member 5	Fetal brain
ENSG00000182985	<i>CADM1</i>	cell adhesion molecule 1	Fetal brain
ENSG00000163590	<i>PPM1L</i>	protein phosphatase, Mg ²⁺ /Mn ²⁺ dependent 1L	Fetal brain
ENSG00000113645	<i>WWC1</i>	WW and C2 domain containing 1	Fetal brain
ENSG00000187905	<i>LRRK74B</i>	leucine rich repeat containing 74B	Fetal brain
ENSG00000058668	<i>ATP2B4</i>	ATPase plasma membrane Ca ²⁺ transporting 4	Fetal brain
ENSG00000258818	<i>RNASE4</i>	ribonuclease A family member 4	Fetal brain
ENSG00000164742	<i>ADCY1</i>	adenylate cyclase 1	Fetal brain
ENSG00000170502	<i>NUDT9</i>	nudix hydrolase 9	Fetal brain
ENSG00000090776	<i>EFNB1</i>	ephrin B1	Fetal brain
ENSG00000126858	<i>RHOT1</i>	ras homolog family member T1	Fetal brain
ENSG00000089091	<i>DZANK1</i>	double zinc ribbon and ankyrin repeat domains	Fetal brain
ENSG00000151208	<i>DLG5</i>	discs large MAGUK scaffold protein 5	Fetal brain
ENSG00000147162	<i>OGT</i>	O-linked N-acetylglucosamine (GlcNAc) transferase	Fetal brain

table S32. 5 positively selected genes and 33 genes associated with lineage-specific accelerated regions showing a high level of expression in the human brain along with primate ancestral lineage leading to the human lineage. Candidate genes were identified as being highly expressed in the human brain-related tissues by the DAVID Tissue_Expression database (UP_TISSUE) (<https://david.ncifcrf.gov/home.jsp>).

Category	Gene Symbol
positively selected genes	<i>PPP3CA, ADCY2, SLC1A6, SLC18A2, SLC6A4</i>
genes associated with lineage-specific accelerated regions	<i>GRIA2, APP, CHRM3, GABRB1, CHRNA3, MAOB, GRIK4, HTR2C, CACNA1D, GRIK2, HTR4, RIMS1, GRIN2A, GRM7, GNG4, GRIA3, GRIA4, KCNJ3, UNC13C, SYT1, PPP2R5A, SLC6A11, KCNJ18, HTR5A, STX1B, ADCY9, GNAQ, GNAS, KRAS, KCNQ5, GRIK3, ADCY1, JAK2</i>

The following supplementary table is presented as a separate Excel file, as the table is very large.

table S33 (as a separate Excel file). Identification of lineage-specific accelerated regions along the ape (Hominoidea) branch. Lineage-specific accelerated regions significance was determined by FDR \leq 0.05. Nearest genes were obtained by reference to the distance to the lineage-specific accelerated regions in 500kbp.

table S34. Positively selected genes of the gibbon ancestral lineage. Identification of positively selected genes in the gibbon ancestral lineage was used the branch-site model in PAML4. *P* values were calculated by means of a χ^2 test. Four positively selected genes (*LONP1*, *BRCA2*, *NEK1* and *SLC25A24*) were involved in abnormal upper limb bone morphology (HP:0040070) according to Human Phenotype Ontology in the g:Profiler database (<https://biit.cs.ut.ee/gprofiler/gost>).

Ensembl Gene ID	Gene Name	2ΔNLN	P
ENSG00000137501	<i>SYTL2</i>	364.154914	3.51E-81
ENSG00000136542	<i>GALNT5</i>	266.771874	5.73E-60
ENSG00000130724	<i>CHMP2A</i>	235.329284	4.10E-53
ENSG00000164323	<i>CFAP97</i>	153.6108	2.82E-35
ENSG00000125107	<i>CNOT1</i>	107.103322	4.23E-25
ENSG00000124074	<i>ENKD1</i>	64.818516	8.21E-16
ENSG00000135378	<i>PRRG4</i>	64.717368	8.64E-16
ENSG00000172426	<i>RSPH9</i>	58.023872	2.59E-14
ENSG00000162300	<i>ZFPL1</i>	38.868894	4.53E-10
ENSG00000175785	<i>PRIMA1</i>	37.141416	1.10E-09
ENSG00000123307	<i>NEUROD4</i>	35.959902	2.01E-09
ENSG00000134369	<i>NAVI</i>	35.94184	2.03E-09
ENSG00000148985	<i>PGAP2</i>	31.912158	1.61E-08
ENSG00000196365	<i>LONP1</i>	25.110698	5.41E-07
ENSG00000180628	<i>PCGF5</i>	23.928804	1.00E-06
ENSG00000106290	<i>TAF6</i>	20.806838	5.08E-06
ENSG00000180739	<i>S1PR5</i>	20.433454	6.17E-06
ENSG00000157551	<i>KCNJ15</i>	19.417698	1.05E-05
ENSG00000070748	<i>CHAT</i>	19.300442	1.12E-05
ENSG00000139618	<i>BRCA2</i>	19.080764	1.25E-05
ENSG00000160867	<i>FGFR4</i>	18.803404	1.45E-05
ENSG00000057019	<i>DCBLD2</i>	18.073392	2.13E-05
ENSG00000105697	<i>HAMP</i>	17.98844	2.22E-05
ENSG00000170242	<i>USP47</i>	17.331206	3.14E-05
ENSG00000175556	<i>LONRF3</i>	16.491402	4.89E-05
ENSG00000173040	<i>EVC2</i>	16.239878	5.58E-05
ENSG00000133119	<i>RFC3</i>	14.55125	0.000136398
ENSG00000065675	<i>PRKCQ</i>	14.399382	0.000147851
ENSG00000115318	<i>LOXL3</i>	13.674512	0.000217385
ENSG00000143171	<i>RXRG</i>	13.632332	0.000222324
ENSG00000187848	<i>P2RX2</i>	12.302396	0.000452377
ENSG00000173020	<i>GRK2</i>	12.150848	0.000490656
ENSG00000081026	<i>MAGI3</i>	12.121408	0.000498463
ENSG00000110841	<i>PPFIBP1</i>	12.112154	0.000500942
ENSG00000089558	<i>KCNH4</i>	11.692894	0.000627392
ENSG00000284862	<i>CCDC39</i>	11.184462	0.000824852
ENSG00000077684	<i>JADE1</i>	11.026462	0.000898204
ENSG00000187772	<i>LIN28B</i>	10.743642	0.001046382
ENSG00000147548	<i>NSD3</i>	10.61213	0.001123482
ENSG00000076356	<i>PLXNA2</i>	10.572942	0.00114755

ENSG00000139151	<i>PLCZ1</i>	10.561626	0.001154596
ENSG00000254470	<i>AP5B1</i>	10.188478	0.001413209
ENSG00000162073	<i>PAQR4</i>	9.863488	0.001685912
ENSG00000167543	<i>TP53I13</i>	9.73626	0.001806681
ENSG00000162869	<i>PPP1R21</i>	9.673682	0.001869263
ENSG00000102383	<i>ZDHHC15</i>	9.395724	0.002174921
ENSG00000162344	<i>FGF19</i>	9.359302	0.002218566
ENSG00000104549	<i>SQLE</i>	8.93113	0.002803508
ENSG00000137672	<i>TRPC6</i>	8.86454	0.002907635
ENSG00000186795	<i>KCNK18</i>	8.768724	0.003064398
ENSG00000213722	<i>DDAH2</i>	8.71389	0.003157946
ENSG00000156414	<i>TDRD9</i>	8.564324	0.003428142
ENSG00000132740	<i>IGHMBP2</i>	8.500424	0.003550637
ENSG00000142599	<i>RERE</i>	8.47771	0.003595244
ENSG00000155761	<i>SPAG17</i>	8.391164	0.003770494
ENSG00000115361	<i>ACADL</i>	8.375528	0.003803071
ENSG00000168268	<i>NT5DC2</i>	8.227782	0.004125392
ENSG00000172197	<i>MBOAT1</i>	8.164908	0.004270864
ENSG00000136270	<i>TBRG4</i>	8.145464	0.004316901
ENSG00000108669	<i>CYTH1</i>	8.064678	0.00451365
ENSG00000274523	<i>RCC1L</i>	7.784724	0.005268984
ENSG00000127445	<i>PIN1</i>	7.684184	0.005570686
ENSG00000169605	<i>GKNI</i>	7.678632	0.005587851
ENSG00000135636	<i>DYSF</i>	7.665486	0.00562871
ENSG00000184436	<i>THAP7</i>	7.65978	0.005646539
ENSG00000165688	<i>PMPCA</i>	7.549944	0.006001194
ENSG00000213949	<i>ITGA1</i>	7.516216	0.006114599
ENSG00000113492	<i>AGXT2</i>	7.435096	0.006396395
ENSG00000135018	<i>UBQLN1</i>	7.409268	0.006488872
ENSG00000126216	<i>TUBGCP3</i>	7.38097	0.006591761
ENSG00000147255	<i>IGSF1</i>	7.303328	0.006882701
ENSG00000160472	<i>TMEM190</i>	7.190066	0.007330828
ENSG00000139410	<i>SDSL</i>	7.150844	0.007492872
ENSG00000079337	<i>RAPGEF3</i>	7.110632	0.007662809
ENSG00000105894	<i>PTN</i>	7.108974	0.0076699
ENSG00000163630	<i>SYNPR</i>	7.008828	0.008110876
ENSG00000153029	<i>MR1</i>	6.909976	0.008571614
ENSG00000140379	<i>BCL2A1</i>	6.838598	0.008920883
ENSG00000100416	<i>TRMU</i>	6.82763	0.008975829
ENSG00000096063	<i>SRPK1</i>	6.80745	0.009077831
ENSG00000137601	<i>NEK1</i>	6.568646	0.010379088
ENSG00000150782	<i>IL18</i>	6.52527	0.01063524
ENSG00000187806	<i>TMEM202</i>	6.42877	0.011228631
ENSG00000109674	<i>NEIL3</i>	6.42795	0.011233816
ENSG00000117280	<i>RAB29</i>	6.373028	0.011586772
ENSG00000131480	<i>AOC2</i>	6.264768	0.01231623
ENSG00000237441	<i>RGL2</i>	6.250534	0.012415587
ENSG00000169994	<i>MYO7B</i>	6.210048	0.012702719
ENSG00000151304	<i>SRFBP1</i>	6.139516	0.013219349

ENSG00000160094	<i>ZNF362</i>	6.073346	0.013723674
ENSG00000138483	<i>CCDC54</i>	6.047518	0.013925859
ENSG00000104312	<i>RIPK2</i>	5.973464	0.014522725
ENSG00000151779	<i>NBAS</i>	5.913754	0.015023124
ENSG00000089048	<i>ESF1</i>	5.738964	0.016592577
ENSG00000136546	<i>SCN7A</i>	5.73693	0.016611803
ENSG00000103994	<i>ZNF106</i>	5.669664	0.017260762
ENSG00000153446	<i>C16orf89</i>	5.449654	0.019572203
ENSG00000147570	<i>DNAJC5B</i>	5.400272	0.020133614
ENSG00000167861	<i>HID1</i>	5.375732	0.020418771
ENSG00000132359	<i>RAP1GAP2</i>	5.368004	0.020509434
ENSG00000166035	<i>LIPC</i>	5.273922	0.021647188
ENSG00000164532	<i>TBX20</i>	5.199398	0.022594712
ENSG00000182400	<i>TRAPP C6B</i>	5.124974	0.023583924
ENSG00000214376	<i>VSTM5</i>	5.119642	0.023656497
ENSG00000168769	<i>TET2</i>	5.110472	0.023781849
ENSG00000136573	<i>BLK</i>	5.04416	0.024709085
ENSG00000124785	<i>NRN1</i>	4.997492	0.025384076
ENSG00000138867	<i>GUCD1</i>	4.978124	0.025669805
ENSG00000164037	<i>SLC9B1</i>	4.90694	0.026748989
ENSG00000134917	<i>ADAMTS8</i>	4.837132	0.027853181
ENSG00000171840	<i>NINJ2</i>	4.793242	0.0285716
ENSG00000152464	<i>RPP38</i>	4.75275	0.029251512
ENSG00000134905	<i>CARS2</i>	4.750132	0.029296047
ENSG00000138944	<i>SHISAL1</i>	4.629372	0.031429066
ENSG00000012983	<i>MAP4K5</i>	4.613724	0.031717084
ENSG00000100418	<i>DESI1</i>	4.48855	0.034122608
ENSG00000102189	<i>EEA1</i>	4.483832	0.03421692
ENSG00000112031	<i>MTRF1L</i>	4.478106	0.034331747
ENSG00000183559	<i>C10orf120</i>	4.433806	0.035233856
ENSG00000128482	<i>RNF112</i>	4.433124	0.035247936
ENSG00000174485	<i>DENND4A</i>	4.431694	0.035277478
ENSG00000174827	<i>PDZK1</i>	4.407648	0.035778138
ENSG00000088682	<i>COQ9</i>	4.313376	0.037813848
ENSG00000116667	<i>C1orf21</i>	4.240852	0.039462359
ENSG00000092421	<i>SEMA6A</i>	4.06231	0.043850475
ENSG00000121270	<i>ABCC11</i>	4.00205	0.045444959
ENSG00000166479	<i>TMX3</i>	3.987282	0.045844961
ENSG00000074696	<i>HACD3</i>	3.98035	0.046033997
ENSG00000085491	<i>SLC25A24</i>	3.938498	0.047192896

table S35. Positively selected genes of the great ape ancestral lineage. Identification of positively selected genes in the Hominidae ancestral lineage was used by the branch-site model in PAML4. *P* values were calculated by means of a χ^2 test.

Ensembl Gene ID	Gene Name	2ΔNL	P
ENSG0000104237	<i>RP1</i>	1365.451372	6.76E-299
ENSG0000137106	<i>GRHPR</i>	140.016026	2.64E-32
ENSG0000181744	<i>DIPK2A</i>	54.241744	1.77E-13
ENSG0000036530	<i>CYP46A1</i>	49.068068	2.47E-12
ENSG0000179271	<i>GADD45GIP1</i>	46.22338	1.06E-11
ENSG0000179388	<i>EGR3</i>	38.939902	4.37E-10
ENSG0000048540	<i>LMO3</i>	27.891554	1.28E-07
ENSG0000025770	<i>NCAPH2</i>	23.456698	1.28E-06
ENSG0000177728	<i>TMEM94</i>	20.592338	5.68E-06
ENSG0000137500	<i>CCDC90B</i>	17.90543	2.32E-05
ENSG0000075415	<i>SLC25A3</i>	16.973928	3.79E-05
ENSG0000182836	<i>PLCXD3</i>	16.031252	6.23E-05
ENSG0000187535	<i>IFT140</i>	15.164406	9.85E-05
ENSG0000105143	<i>SLC1A6</i>	12.455108	0.00041685
ENSG0000107902	<i>LHPP</i>	11.046678	0.000888463
ENSG0000157330	<i>C1orf158</i>	9.895464	0.001656867
ENSG0000058056	<i>USP13</i>	9.594442	0.001951672
ENSG0000164080	<i>RAD54L2</i>	8.653064	0.003265118
ENSG0000006747	<i>SCIN</i>	8.30123	0.003961824
ENSG0000198911	<i>SREBF2</i>	8.190026	0.004212132
ENSG0000171551	<i>ECEL1</i>	8.059504	0.004526557
ENSG0000125755	<i>SYMPK</i>	8.053118	0.004542541
ENSG0000097021	<i>ACOT7</i>	7.768796	0.005315647
ENSG0000096696	<i>DSP</i>	7.41257	0.006476974
ENSG0000137693	<i>YAPI</i>	6.402814	0.011393963
ENSG0000125744	<i>RTN2</i>	6.097962	0.013533788
ENSG0000166833	<i>NAV2</i>	6.007836	0.014242484
ENSG0000150756	<i>ATPSCKMT</i>	5.989346	0.014392538
ENSG0000064692	<i>SNCAIP</i>	5.845306	0.015618658
ENSG0000083097	<i>DOPIA</i>	5.815804	0.015882791
ENSG0000140279	<i>DUOX2</i>	5.607628	0.017882454
ENSG0000148143	<i>ZNF462</i>	5.420178	0.019905331
ENSG0000136279	<i>DBNL</i>	5.252712	0.021912593
ENSG0000165646	<i>SLC18A2</i>	5.197328	0.022621636
ENSG0000155158	<i>TTC39B</i>	4.791232	0.02860496
ENSG0000214595	<i>EML6</i>	4.558784	0.032750318
ENSG0000137504	<i>CREBZF</i>	4.526448	0.033374821
ENSG0000020577	<i>SAMD4A</i>	4.305688	0.037985128
ENSG0000145868	<i>FBXO38</i>	4.20396	0.040329697
ENSG0000154269	<i>ENPP3</i>	4.18356	0.040817875
ENSG0000166532	<i>RIMKLB</i>	3.970096	0.046315132
ENSG0000070915	<i>SLC12A3</i>	3.951398	0.046832446

table S36. KEGG pathway enrichment analysis of combined genes including positively selected genes and genes associated with lineage-specific accelerated regions in the great ape ancestral lineage. KEGG pathways with *P* values < 0.05 (Modified Fisher's Exact test) are given.

Category	Term	Count	P
KEGG_PATHWAY	hsa00534:Glycosaminoglycan biosynthesis - heparan sulfate / heparin	3	0.031987
KEGG_PATHWAY	hsa04740:Olfactory transduction	11	0.033139
KEGG_PATHWAY	hsa04392:Hippo signaling pathway - multiple species	3	0.045311

table S37. Positively selected genes of the Colobinae ancestral lineage. Identification of positively selected genes in the Colobinae ancestral lineage was used by the branch-site model in PAML4. *P* values were calculated by means of a χ^2 test.

Ensembl Gene ID	Gene Name	2ΔLNL	P
ENSG00000269964	<i>MEI4</i>	98.581512	3.12E-23
ENSG00000162999	<i>DUSP19</i>	97.283538	6.01E-23
ENSG00000188493	<i>C19orf54</i>	72.684878	1.52E-17
ENSG00000215187	<i>FAM166B</i>	59.811832	1.04E-14
ENSG00000133398	<i>MED10</i>	57.399812	3.56E-14
ENSG00000133740	<i>E2F5</i>	50.895054	9.74E-13
ENSG00000007952	<i>NOX1</i>	49.21334	2.30E-12
ENSG00000198836	<i>OPA1</i>	34.717522	3.81E-09
ENSG00000107262	<i>BAG1</i>	32.455514	1.22E-08
ENSG00000008405	<i>CRY1</i>	29.17048	6.63E-08
ENSG00000120094	<i>HOXB1</i>	25.433198	4.58E-07
ENSG00000135457	<i>TFCP2</i>	24.350108	8.03E-07
ENSG00000145362	<i>ANK2</i>	22.669638	1.92E-06
ENSG00000108846	<i>ABCC3</i>	20.402486	6.27E-06
ENSG00000233436	<i>BTB18</i>	17.441824	2.96E-05
ENSG00000183476	<i>SH2D7</i>	16.985252	3.77E-05
ENSG00000188816	<i>HMX2</i>	16.70217	4.37E-05
ENSG00000117054	<i>ACADM</i>	16.521876	4.81E-05
ENSG00000179361	<i>ARID3B</i>	16.081094	6.07E-05
ENSG00000159131	<i>GART</i>	15.052248	0.000104576
ENSG00000149476	<i>TKFC</i>	14.187868	0.000165434
ENSG00000103148	<i>NPRL3</i>	13.985484	0.000184227
ENSG00000105851	<i>PIK3CG</i>	11.857502	0.000574295
ENSG00000117425	<i>PTCH2</i>	11.455252	0.000712922
ENSG00000128191	<i>DGCR8</i>	11.433356	0.000721373
ENSG00000122965	<i>RBM19</i>	11.401142	0.00073399
ENSG00000173166	<i>RAPH1</i>	11.13651	0.00084645
ENSG00000170955	<i>CAVIN3</i>	11.131152	0.000848899
ENSG00000079156	<i>OSBPL6</i>	10.936678	0.000942791
ENSG00000119711	<i>ALDH6A1</i>	10.55033	0.001161673
ENSG00000174948	<i>GPR149</i>	10.491368	0.001199335
ENSG00000137507	<i>LRRC32</i>	9.601798	0.001943869
ENSG00000196091	<i>MYBPC1</i>	8.749114	0.003097525
ENSG00000126790	<i>L3HYPDH</i>	7.977488	0.004736262
ENSG00000181722	<i>ZBTB20</i>	7.866442	0.005036065
ENSG00000140807	<i>NKDI</i>	7.696486	0.005532844
ENSG00000126749	<i>EMG1</i>	7.393782	0.006544973
ENSG00000117643	<i>MANIC1</i>	7.37091	0.006628738
ENSG00000112378	<i>PERP</i>	7.28951	0.006935839
ENSG00000141425	<i>RPRD1A</i>	7.274298	0.006994822
ENSG00000175104	<i>TRAF6</i>	7.23014	0.007168962
ENSG00000151379	<i>MSGN1</i>	6.539992	0.010547582
ENSG00000186417	<i>GLDN</i>	6.4298	0.011222121
ENSG00000283654	<i>LMLN2</i>	6.388102	0.011488781

ENSG00000100364	<i>KIAA0930</i>	6.337098	0.011823817
ENSG0000074211	<i>PPP2R2C</i>	5.754212	0.016449172
ENSG0000166510	<i>CCDC68</i>	5.5596	0.018379613
ENSG0000197548	<i>ATG7</i>	5.443194	0.019644715
ENSG0000198171	<i>DDRGK1</i>	5.393746	0.020209042
ENSG0000127334	<i>DYRK2</i>	5.26192	0.02179696
ENSG0000114062	<i>UBE3A</i>	5.020984	0.025041934
ENSG0000151322	<i>NPAS3</i>	4.892078	0.026980194
ENSG0000186919	<i>ZACN</i>	4.870608	0.027317874
ENSG0000204574	<i>ABCF1</i>	4.394166	0.036062093
ENSG0000148516	<i>ZEB1</i>	4.32845	0.037480362
ENSG0000204186	<i>ZDBF2</i>	4.287796	0.038386896
ENSG0000170271	<i>FAXDC2</i>	4.233564	0.039632136
ENSG0000102580	<i>DNAJC3</i>	4.140248	0.041875034
ENSG0000162852	<i>CNST</i>	4.098982	0.042909042
ENSG0000077984	<i>CST7</i>	4.02863	0.044734254

table S38. Positively selected genes and genes associated with lineage-specific accelerated regions in the ancestral lineage of the Colobinae with a high expression level in the stomach, colon, pancreas and small intestine. These genes were identified as highly expressed genes in digestive organs by the DAVID Tissue_Expression database (UP_TISSUE) (<https://david.ncifcrf.gov/home.jsp>).

Highly Expressed Tissue	Gene Name	Gene Category
Pancreas	<i>MYBPC1, PERP, PIK3CG</i>	positively selected genes
Small intestine	<i>ZBTB20</i>	positively selected genes
Colon	<i>ABCC3, ZBTB20, ACADM, GLDN, NOX1</i>	positively selected genes
Stomach	<i>BCHE</i>	genes associated with lineage-specific accelerated regions
Pancreas	<i>CASZ1, RNASE4, SLC4A4, ZPBP</i>	genes associated with lineage-specific accelerated regions
Small intestine	<i>AHI1, THEMIS, EIF4E</i>	genes associated with lineage-specific accelerated regions
Colon	<i>SHF, TMEM267, CYP4A11, MTMR8, PEX26, SOD1, PAFAH1B1</i>	genes associated with lineage-specific accelerated regions

The following supplementary table is presented as a separate Excel file, as the table is very large.

table S39 (as a separate Excel file). Identification of lineage-specific accelerated regions along the Colobinae ancestral lineage. Lineage-specific accelerated regions significance was determined by $FDR \leq 0.05$. Nearest genes were obtained by reference to the distance to the lineage-specific accelerated regions in 500kbp.

table S40. Positively selected genes in the Strepsirrhini ancestor lineage.
 Identification of positively selected genes in the Strepsirrhini ancestral lineage was used by the branch-site model in PAML4. *P* values were calculated by means of a χ^2 test.

Ensembl Gene ID	Gene Name	2ΔNL	P
ENSG00000114735	<i>HEMK1</i>	141.525484	1.23E-32
ENSG00000186765	<i>FSCN2</i>	85.299248	2.56E-20
ENSG00000100284	<i>TOM1</i>	82.569186	1.02E-19
ENSG00000198399	<i>ITSN2</i>	49.740946	1.75E-12
ENSG00000090686	<i>USP48</i>	32.245068	1.36E-08
ENSG00000165209	<i>STRBP</i>	29.629326	5.23E-08
ENSG00000157827	<i>FMNL2</i>	29.403862	5.88E-08
ENSG00000139865	<i>TTC6</i>	28.990602	7.27E-08
ENSG00000166886	<i>NAB2</i>	26.219928	3.05E-07
ENSG00000168101	<i>NUDT16L1</i>	26.110156	3.22E-07
ENSG00000197217	<i>ENTPD4</i>	25.511488	4.40E-07
ENSG00000123213	<i>NLN</i>	24.750996	6.52E-07
ENSG00000116984	<i>MTR</i>	23.905984	1.01E-06
ENSG00000177302	<i>TOP3A</i>	23.256428	1.42E-06
ENSG00000213347	<i>MXD3</i>	19.99643	7.76E-06
ENSG00000170871	<i>KIAA0232</i>	19.589466	9.60E-06
ENSG00000171823	<i>FBXL14</i>	18.506026	1.69E-05
ENSG00000083635	<i>NUFIP1</i>	17.981726	2.23E-05
ENSG00000018408	<i>WWTR1</i>	17.627836	2.69E-05
ENSG00000164031	<i>DNAJB14</i>	17.343768	3.12E-05
ENSG00000133895	<i>MEN1</i>	15.685886	7.48E-05
ENSG00000106829	<i>TLE4</i>	14.923122	0.000111982
ENSG00000072041	<i>SLC6A15</i>	14.71282	0.000125192
ENSG00000127311	<i>HELB</i>	13.738278	0.000210128
ENSG00000184345	<i>IQCF2</i>	13.651138	0.000220108
ENSG00000143190	<i>POU2F1</i>	13.56612	0.000230305
ENSG00000143442	<i>POGZ</i>	13.484488	0.000240544
ENSG00000103710	<i>RASL12</i>	13.23324	0.000275028
ENSG00000136518	<i>ACTL6A</i>	13.13785	0.00028939
ENSG00000152359	<i>POC5</i>	13.12923	0.000290724
ENSG00000038219	<i>BOD1L1</i>	11.95479	0.000545071
ENSG00000164056	<i>SPRY1</i>	11.789776	0.000595569
ENSG00000157060	<i>SHCBP1L</i>	11.703302	0.000623893
ENSG00000089101	<i>CFAP61</i>	11.238458	0.000801197
ENSG00000148248	<i>SURF4</i>	10.809582	0.001009761
ENSG00000055813	<i>CCDC85A</i>	10.757528	0.00103856
ENSG00000155100	<i>OTUD6B</i>	10.638918	0.001107324
ENSG00000160714	<i>UBE2Q1</i>	10.517752	0.001182332
ENSG00000050730	<i>TNIP3</i>	10.318172	0.001317267
ENSG00000112282	<i>MED23</i>	10.00073	0.001564782
ENSG00000113441	<i>LNPEP</i>	9.954804	0.001604302
ENSG00000186009	<i>ATP4B</i>	9.69278	0.001849934
ENSG00000088888	<i>MAVS</i>	9.681742	0.001861081
ENSG00000188676	<i>IDO2</i>	9.587644	0.001958911

ENSG00000127083	<i>OMD</i>	9.547224	0.00200252
ENSG00000132321	<i>IQCA1</i>	9.513708	0.002039426
ENSG0000044459	<i>CNTLN</i>	9.432446	0.002131798
ENSG00000112996	<i>MRPS30</i>	9.13207	0.002511674
ENSG00000143970	<i>ASXL2</i>	8.953982	0.002768654
ENSG00000126870	<i>WDR60</i>	8.74762	0.003100064
ENSG00000169499	<i>PLEKHA2</i>	8.550788	0.003453727
ENSG00000112149	<i>CD83</i>	8.530206	0.003493002
ENSG0000072778	<i>ACADVL</i>	8.507412	0.003537028
ENSG00000198162	<i>MANIA2</i>	8.482844	0.003585112
ENSG00000197563	<i>PIGN</i>	8.477702	0.00359526
ENSG00000105982	<i>RNF32</i>	8.463044	0.003624348
ENSG00000162621	<i>LRRC53</i>	8.370052	0.003814547
ENSG00000186827	<i>TNFRSF4</i>	8.299018	0.003966652
ENSG00000130584	<i>ZBTB46</i>	8.264992	0.004041684
ENSG00000085365	<i>SCAMP1</i>	8.163744	0.004273606
ENSG00000005893	<i>LAMP2</i>	7.965534	0.004767642
ENSG00000105856	<i>HBPI</i>	7.91357	0.004906535
ENSG00000158488	<i>CD1E</i>	7.664748	0.005631012
ENSG00000117500	<i>TMED5</i>	7.470494	0.006271834
ENSG00000184281	<i>TSSC4</i>	7.3731	0.00662067
ENSG00000173588	<i>CEP83</i>	7.363026	0.006657865
ENSG00000108349	<i>CASC3</i>	7.32772	0.006789913
ENSG00000112893	<i>MAN2A1</i>	7.246276	0.007104821
ENSG00000186834	<i>HEXIM1</i>	7.12267	0.007611527
ENSG00000130643	<i>CALY</i>	7.099018	0.00771262
ENSG00000107742	<i>SPOCK2</i>	7.08294	0.007782123
ENSG00000146530	<i>VWDE</i>	7.040056	0.007970654
ENSG00000134013	<i>LOXL2</i>	6.997842	0.008160804
ENSG00000237524	<i>TEX51</i>	6.884606	0.008694123
ENSG00000182185	<i>RAD51B</i>	6.711616	0.009578688
ENSG00000175806	<i>MSRA</i>	6.646118	0.00993721
ENSG00000171522	<i>PTGER4</i>	6.586174	0.010277381
ENSG00000103174	<i>NAGPA</i>	6.566768	0.010390047
ENSG00000172803	<i>SNX32</i>	6.55571	0.010454811
ENSG00000239779	<i>WBP1</i>	6.549898	0.010489017
ENSG00000127952	<i>STYXL1</i>	6.547634	0.010502373
ENSG00000141579	<i>ZNF750</i>	6.522076	0.010654356
ENSG00000104731	<i>KLHDC4</i>	6.46091	0.011027316
ENSG00000187097	<i>ENTPD5</i>	6.437372	0.011174384
ENSG00000198870	<i>STKLD1</i>	6.404706	0.011381827
ENSG00000162711	<i>NLRP3</i>	6.339114	0.011810386
ENSG00000137563	<i>GGH</i>	6.310662	0.012001402
ENSG00000143740	<i>SNAP47</i>	6.283776	0.01218482
ENSG00000154342	<i>WNT3A</i>	6.21876	0.012640361
ENSG00000115425	<i>PECR</i>	6.193688	0.012820673
ENSG00000127720	<i>METTL25</i>	6.054942	0.013867431
ENSG00000129636	<i>ITFG1</i>	6.02319	0.014119104
ENSG00000131389	<i>SLC6A6</i>	5.910126	0.015054095

ENSG00000177238	<i>TRIM72</i>	5.891954	0.015210214
ENSG00000140057	<i>AK7</i>	5.84708	0.01560292
ENSG00000214842	<i>RAD51AP2</i>	5.825848	0.015792353
ENSG00000227729	<i>RD3L</i>	5.767494	0.016325298
ENSG00000154734	<i>ADAMTS1</i>	5.683774	0.017122499
ENSG00000127419	<i>TMEM175</i>	5.657242	0.017383438
ENSG00000155833	<i>CYLC2</i>	5.621062	0.017745893
ENSG00000189079	<i>ARID2</i>	5.562164	0.018352715
ENSG00000197024	<i>ZNF398</i>	5.466428	0.019385207
ENSG00000137860	<i>SLC28A2</i>	5.407258	0.020053191
ENSG00000166503	<i>HDGFL3</i>	5.387556	0.020280857
ENSG00000147113	<i>DIPK2B</i>	5.309378	0.021210928
ENSG00000095321	<i>CRAT</i>	5.278032	0.021596145
ENSG00000136933	<i>RABEPK</i>	5.238302	0.022094829
ENSG00000107651	<i>SEC23IP</i>	5.221372	0.022310942
ENSG00000115548	<i>KDM3A</i>	5.150958	0.023233552
ENSG00000080572	<i>PIH1D3</i>	5.1201	0.023650254
ENSG00000135124	<i>P2RX4</i>	5.098456	0.02394715
ENSG00000011566	<i>MAP4K3</i>	5.09675	0.023970716
ENSG00000116981	<i>NT5C1A</i>	5.056098	0.024539429
ENSG00000226763	<i>SRRM5</i>	5.015044	0.025127991
ENSG00000147853	<i>AK3</i>	5.010198	0.025198425
ENSG00000115966	<i>ATF2</i>	4.985442	0.025561454
ENSG00000078900	<i>TP73</i>	4.91436	0.026634329
ENSG00000131148	<i>EMC8</i>	4.885066	0.027089999
ENSG00000240021	<i>TEX35</i>	4.876474	0.02722518
ENSG00000008283	<i>CYB56I</i>	4.832564	0.027927069
ENSG00000006116	<i>CACNG3</i>	4.787818	0.028661713
ENSG00000275342	<i>PRAG1</i>	4.759668	0.029134167
ENSG00000219545	<i>UMAD1</i>	4.75676	0.029183433
ENSG00000113594	<i>LIFR</i>	4.740496	0.029460576
ENSG00000143278	<i>F13B</i>	4.674916	0.0306062
ENSG00000127863	<i>TNFRSF19</i>	4.633296	0.031357269
ENSG00000174173	<i>TRMT10C</i>	4.629904	0.031419322
ENSG00000106689	<i>LHX2</i>	4.613796	0.031715753
ENSG00000114757	<i>PEX5L</i>	4.60436	0.031890755
ENSG00000214954	<i>LRRC69</i>	4.591566	0.032129646
ENSG00000135374	<i>ELF5</i>	4.504958	0.033796726
ENSG00000170915	<i>PAQR8</i>	4.470852	0.034477795
ENSG00000189280	<i>GJB5</i>	4.391888	0.036110305
ENSG00000124574	<i>ABCC10</i>	4.363386	0.036719252
ENSG0000011600	<i>TYROBP</i>	4.360382	0.036784056
ENSG00000132530	<i>XAF1</i>	4.347404	0.037065404
ENSG00000136425	<i>CIB2</i>	4.262288	0.038967404
ENSG00000129925	<i>TMEM8A</i>	4.248942	0.039274791
ENSG00000105926	<i>MPP6</i>	4.226916	0.039787674
ENSG00000204099	<i>NEU4</i>	4.179098	0.040925477
ENSG00000147896	<i>IFNK</i>	4.174898	0.041027032
ENSG00000091127	<i>PUS7</i>	4.164328	0.041283787

ENSG00000176915	<i>ANKLE2</i>	4.129522	0.042141253
ENSG00000102683	<i>SGCG</i>	4.12693	0.042205852
ENSG00000162522	<i>KIAA1522</i>	4.073226	0.043567992
ENSG00000124243	<i>BCAS4</i>	4.050164	0.044167054
ENSG00000163638	<i>ADAMTS9</i>	4.035122	0.044562453
ENSG00000112297	<i>CRYBG1</i>	4.00633	0.04532972
ENSG00000118412	<i>CASP8AP2</i>	3.9742	0.046202396
ENSG00000119686	<i>FLVCR2</i>	3.961318	0.046557237
ENSG00000088970	<i>KIZ</i>	3.924582	0.047585019

table S41. Generation times and short-read data from each primate species according to previous studies. ‘NA’ indicates that the data were not obtained from prior studies and that in this study we used the generation times of their mostly related species based on our species tree as succedanea.

Family	Genus	Species name	Generation time (year)	Illumina short-read data (NCBI sra/EBI database)
Hominidae	<i>Homo</i>	<i>Homo sapiens</i>	29 (215)	ERR004098-ERR004577; ERR004580; ERR004582; ERR004584-ERR004621; ERR004623-ERR004640; ERR004643-ERR004811
Hominidae	<i>Pan</i>	<i>Pan troglodytes</i>	25 (215)	SRX8439961
Hominidae	<i>Pan</i>	<i>Pan paniscus</i>	25 (216)	SRX242681, SRX242682
Hominidae	<i>Gorilla</i>	<i>Gorilla gorilla</i>	19 (215)	SRX243505
Hominidae	<i>Pongo</i>	<i>Pongo abelii</i>	20 (217)	SRX243481, SRX243482
Hominidae	<i>Pongo</i>	<i>Pongo pygmaeus</i>	20 (218)	In this study
Hylobatidae	<i>Nomascus</i>	<i>Nomascus siki</i>	10 (24, 219)	In this study
Hylobatidae	<i>Sympalangus</i>	<i>Sympalangus syndactylus</i>	10 (24, 219)	In this study
Hylobatidae	<i>Hoolock</i>	<i>Hoolock leuconedys</i>	10 (24, 219)	In this study
Hylobatidae	<i>Hylobates</i>	<i>Hylobates pileatus</i>	10 (24, 219)	In this study
Cercopithecidae	<i>Macaca</i>	<i>Macaca mulatta</i>	6 (220)	SRX6606578
Cercopithecidae	<i>Macaca</i>	<i>Macaca assamensis</i>	6 (220, 221)	In this study
Cercopithecidae	<i>Macaca</i>	<i>Macaca nemestrina</i>	NA	SRX3106039
Cercopithecidae	<i>Macaca</i>	<i>Macaca silenus</i>	6 (220, 221)	In this study
Cercopithecidae	<i>Papio</i>	<i>Papio hamadryas</i>	11 (222)	In this study
Cercopithecidae	<i>Papio</i>	<i>Papio anubis</i>	11 (222)	SRX4503011, SRX4503012, SRX4503015
Cercopithecidae	<i>Lophocebus</i>	<i>Lophocebus aterrimus</i>	10 (223)	In this study
Cercopithecidae	<i>Theropithecus</i>	<i>Theropithecus gelada</i>	10 (224)	SRX2521053, SRX2521054
Cercopithecidae	<i>Mandrillus</i>	<i>Mandrillus sphinx</i>	10 (225)	In this study
Cercopithecidae	<i>Mandrillus</i>	<i>Mandrillus leucophaeus</i>	10 (226)	SRX794703—SRX794706
Cercopithecidae	<i>Cercocebus</i>	<i>Cercocebus atys</i>	NA	SRX790327—SRX790334
Cercopithecidae	<i>Cercopithecus</i>	<i>Cercopithecus albogularis</i>	NA	In this study
Cercopithecidae	<i>Cercopithecus</i>	<i>Cercopithecus mona</i>	7 (227)	SRX7990421
Cercopithecidae	<i>Chlorocebus</i>	<i>Chlorocebus aethiops</i>	8.5 (228)	In this study
Cercopithecidae	<i>Chlorocebus</i>	<i>Chlorocebus sabaeus</i>	8.5 (228)	NA
Cercopithecidae	<i>Erythrocebus</i>	<i>Erythrocebus patas</i>	NA	In this study
Cercopithecidae	<i>Trachypithecus</i>	<i>Trachypithecus crepusculus</i>	11 (229)	In this study
Cercopithecidae	<i>Pygathrix</i>	<i>Pygathrix nigripes</i>	NA	In this study
Cercopithecidae	<i>Rhinopithecus</i>	<i>Rhinopithecus strykeri</i>	10 (26)	In this study
Cercopithecidae	<i>Rhinopithecus</i>	<i>Rhinopithecus roxellana</i>	10 (26)	SRX828307
Cercopithecidae	<i>Piliocolobus</i>	<i>Piliocolobus tephrosceles</i>	5 (230, 231)	NA
Cercopithecidae	<i>Colobus</i>	<i>Colobus guereza</i>	5 (230, 231)	In this study
Cercopithecidae	<i>Colobus</i>	<i>Colobus angolensis</i>	5 (230, 231)	SRX792356—SRX792361
Callitrichidae	<i>Callithrix</i>	<i>Callithrix jacchus</i>	6 (232)	In this study
Callitrichidae	<i>Saguinus</i>	<i>Saguinus midas</i>	6 (215)	In this study
Aotidae	<i>Aotus</i>	<i>Aotus nancymaae</i>	8 (215)	SRX4473017

Cebidae	<i>Sapajus</i>	<i>Sapajus apella</i>	15 (215)	In this study
Cebidae	<i>Cebus</i>	<i>Cebus albifrons</i>	15 (215)	In this study
Atelidae	<i>Ateles</i>	<i>Ateles geoffroyi</i>	15 (215)	In this study
Pitheciidae	<i>Pithecia</i>	<i>Pithecia pithecia</i>	9 (215)	In this study
Tarsidae	<i>Cephalopachus</i>	<i>Cephalopachus bancanus</i>	7 (62)	In this study
Cheirogaleidae	<i>Microcebus</i>	<i>Microcebus murinus</i>	3 (233)	SRX670567
Lemuridae	<i>Prolemur</i>	<i>Prolemur simus</i>	3.5 (234)	SRX4465422
Lemuridae	<i>Lemur</i>	<i>Lemur catta</i>	3 (235)	In this study
Daubentonidae	<i>Daubentonnia</i>	<i>Daubentonnia madagascariensis</i>	3.5 (236)	In this study
Lorisidae	<i>Loris</i>	<i>Loris tardigradus</i>	NA	In this study
Lorisidae	<i>Nycticebus</i>	<i>Nycticebus pygmaeus</i>	2 (237)	In this study
Lorisidae	<i>Nycticebus</i>	<i>Nycticebus bengalensis</i>	2 (237)	In this study
Galagidae	<i>Galago</i>	<i>Galago moholi</i>	NA	In this study
Galagidae	<i>Otolemur</i>	<i>Otolemur garnettii</i>	NA	SRX4465433

table S42. Summary information of conservation genetics for primate species. In total, 46 non-human primate species were analyzed in this analysis. The species *Chlorocebus sabaeus* and *Piliocolobus tephrosceles* were excluded because the high coverage short-read data are missing in the NCBI SRA database (<https://www.ncbi.nlm.nih.gov/>). *Callithrix jacchus* was removed from this analysis because the genome was from an inbred individual. The IUCN Red List species status was obtained from the website (<https://www.iucnredlist.org/>).

Species name	Π_{median}	IUCN Red List status	N_e ($\times 10^4$ in 20,000 years ago)
<i>Pan troglodytes</i>	0.00057	EN	0.241449682
<i>Pan paniscus</i>	0.00057	EN	0.648794739
<i>Gorilla gorilla</i>	0.00083	CR	1.559425526
<i>Pongo abelii</i>	0.00182	CR	0.717874511
<i>Pongo pygmaeus</i>	0.0011	CR	0.503474723
<i>Nomascus siki</i>	0.0017	CR	1.359667189
<i>Sympalangus syndactylus</i>	0.00106	EN	5.274632286
<i>Hoolock leuconedys</i>	0.00058	VU	0.450462482
<i>Hylobates pileatus</i>	0.0005	EN	0.310245424
<i>Macaca mulatta</i>	0.00208	LC	1.868278975
<i>Macaca assamensis</i>	0.00216	NT	3.208116315
<i>Macaca nemestrina</i>	0.00194	VU	3.009434564
<i>Macaca silenus</i>	0.00045	EN	2.07890067
<i>Papio hamadryas</i>	0.00074	LC	2.564670298
<i>Papio anubis</i>	0.00012	LC	1.263479978
<i>Lophocebus aterrimus</i>	0.0016	VU	5.499862681
<i>Theropithecus gelada</i>	0.00016	LC	0.420439062
<i>Mandrillus sphinx</i>	0.00245	VU	3.028259057
<i>Mandrillus leucophaeus</i>	0.00064	EN	1.811095063
<i>Cercopithecus atys</i>	0.00073	VU	6.567033139
<i>Cercopithecus albogularis</i>	0.00125	LC	1.363557634
<i>Cercopithecus mona</i>	0.00189	NT	2.888423855
<i>Chlorocebus aethiops</i>	0.00111	LC	1.435820132
<i>Erythrocebus patas</i>	0.00066	NT	0.602580514
<i>Trachypithecus crepusculus</i>	0.00093	EN	0.499043814
<i>Pygathrix nigripes</i>	0.00134	CR	2.380222025

<i>Rhinopithecus strykeri</i>	0.00007	CR	0.202554603
<i>Rhinopithecus roxellana</i>	0.00033	EN	0.675578962
<i>Colobus guereza</i>	0.00073	LC	1.594377736
<i>Colobus angolensis</i>	0.00082	VU	0.607909735
<i>Saguinus midas</i>	0.00125	LC	1.289943937
<i>Aotus nancymaae</i>	0.00068	VU	3.061421186
<i>Sapajus apella</i>	0.00074	LC	0.905683755
<i>Cebus albifrons</i>	0.00092	LC	0.366957549
<i>Ateles geoffroyi</i>	0.00141	EN	1.163167684
<i>Pithecia pithecia</i>	0.00105	LC	0.931025333
<i>Cephalopachus bancanus</i>	0.00228	VU	1.766781487
<i>Daubentonia madagascariensis</i>	0.00048	EN	2.551512884
<i>Microcebus murinus</i>	0.00198	LC	5.354912039
<i>Prolemur simus</i>	0.0002	CR	3.599630087
<i>Lemur catta</i>	0.00172	EN	7.150895406
<i>Loris tardigradus</i>	0.00179	EN	16.62657852
<i>Nycticebus pygmaeus</i>	0.00007	EN	1.608037778
<i>Nycticebus bengalensis</i>	0.00008	EN	0.949696297
<i>Galago moholi</i>	0.00069	LC	6.055302869
<i>Otolemur garnettii</i>	0.00125	LC	19.97383041

References and Notes

1. A. Estrada, P. A. Garber, A. B. Rylands, C. Roos, E. Fernandez-Duque, A. Di Fiore, K. A. Nekaris, V. Nijman, E. W. Heymann, J. E. Lambert, F. Rovero, C. Barelli, J. M. Setchell, T. R. Gillespie, R. A. Mittermeier, L. V. Arregoitia, M. de Guinea, S. Gouveia, R. Dobrovolski, S. Shanee, N. Shanee, S. A. Boyle, A. Fuentes, K. C. MacKinnon, K. R. Amato, A. L. Meyer, S. Wich, R. W. Sussman, R. Pan, I. Kone, B. Li, Impending extinction crisis of the world's primates: Why primates matter. *Sci. Adv.* **3**, e1600946 (2017).
[doi:10.1126/sciadv.1600946](https://doi.org/10.1126/sciadv.1600946) [Medline](#)
2. C. Roos, K. M. Helgen, R. P. Miguez, N. M. L. Thant, N. Lwin, A. K. Lin, A. Lin, K. M. Yi, P. Soe, Z. M. Hein, M. N. N. Myint, T. Ahmed, D. Chetry, M. Urh, E. G. Veatch, N. Duncan, P. Kamminga, M. A. H. Chua, L. Yao, C. Matauscheck, D. Meyer, Z. J. Liu, M. Li, T. Nadler, P. F. Fan, L. K. Quyet, M. Hofreiter, D. Zinner, F. Momberg, Mitogenomic phylogeny of the Asian colobine genus *Trachypithecus* with special focus on *Trachypithecus phayrei* (Blyth, 1847) and description of a new species. *Zool. Res.* **41**, 656–669 (2020).
[doi:10.24272/j.issn.2095-8137.2020.254](https://doi.org/10.24272/j.issn.2095-8137.2020.254) [Medline](#)
3. A. Nater, M. P. Mattle-Greminger, A. Nurcahyo, M. G. Nowak, M. de Manuel, T. Desai, C. Groves, M. Pybus, T. B. Sonay, C. Roos, A. R. Lameira, S. A. Wich, J. Askew, M. Davila-Ross, G. Fredriksson, G. de Valles, F. Casals, J. Prado-Martinez, B. Goossens, E. J. Verschoor, K. S. Warren, I. Singleton, D. A. Marques, J. Pamungkas, D. Perwitasari-Farajallah, P. Rianti, A. Tuuga, I. G. Gut, M. Gut, P. Orozco-terWengel, C. P. van Schaik, J. Bertranpetti, M. Anisimova, A. Scally, T. Marques-Bonet, E. Meijaard, M. Krützen, Morphometric, behavioral, and genomic evidence for a new orangutan species. *Curr. Biol.* **27**, 3487–3498.e10 (2017). [doi:10.1016/j.cub.2017.09.047](https://doi.org/10.1016/j.cub.2017.09.047) [Medline](#)
4. P. F. Fan, K. He, X. Chen, A. Ortiz, B. Zhang, C. Zhao, Y. Q. Li, H. B. Zhang, C. Kimock, W. Z. Wang, C. Groves, S. T. Turvey, C. Roos, K. M. Helgen, X. L. Jiang, Description of a new species of *Hoolock* gibbon (Primates: Hylobatidae) based on integrative taxonomy. *Am. J. Primatol.* **79**, e22631 (2017). [doi:10.1002/ajp.22631](https://doi.org/10.1002/ajp.22631) [Medline](#)
5. C. Li, C. Zhao, P. F. Fan, White-cheeked macaque (*Macaca leucogenys*): A new macaque species from Medog, southeastern Tibet. *Am. J. Primatol.* **77**, 753–766 (2015). [doi:10.1002/ajp.22394](https://doi.org/10.1002/ajp.22394) [Medline](#)
6. J. Rogers, R. A. Gibbs, Comparative primate genomics: Emerging patterns of genome content and dynamics. *Nat. Rev. Genet.* **15**, 347–359 (2014).
[doi:10.1038/nrg3707](https://doi.org/10.1038/nrg3707) [Medline](#)

7. B. Rockx, T. Kuiken, S. Herfst, T. Bestebroer, M. M. Lamers, B. B. Oude Munnink, D. de Meulder, G. van Amerongen, J. van den Brand, N. M. A. Okba, D. Schipper, P. van Run, L. Leijten, R. Sikkema, E. Verschoor, B. Verstrepen, W. Bogers, J. Langermans, C. Drosten, M. Fentener van Vlissingen, R. Fouchier, R. de Swart, M. Koopmans, B. L. Haagmans, Comparative pathogenesis of COVID-19, MERS, and SARS in a nonhuman primate model. *Science* **368**, 1012–1015 (2020). [doi:10.1126/science.abb7314](https://doi.org/10.1126/science.abb7314) [Medline](#)
8. A. Chandrashekhar, J. Liu, A. J. Martinot, K. McMahan, N. B. Mercado, L. Peter, L. H. Tostanoski, J. Yu, Z. Maliga, M. Nekorchuk, K. Busman-Sahay, M. Terry, L. M. Wrijil, S. Ducat, D. R. Martinez, C. Atyeo, S. Fischinger, J. S. Burke, M. D. Slein, L. Pessaint, A. Van Ry, J. Greenhouse, T. Taylor, K. Blade, A. Cook, B. Finneyfrock, R. Brown, E. Teow, J. Velasco, R. Zahn, F. Wegmann, P. Abbink, E. A. Bondzie, G. Dagotto, M. S. Gebre, X. He, C. Jacob-Dolan, N. Kordana, Z. Li, M. A. Lifton, S. H. Mahrokhian, L. F. Maxfield, R. Nityanandam, J. P. Nkolola, A. G. Schmidt, A. D. Miller, R. S. Baric, G. Alter, P. K. Sorger, J. D. Estes, H. Andersen, M. G. Lewis, D. H. Barouch, SARS-CoV-2 infection protects against rechallenge in rhesus macaques. *Science* **369**, 812–817 (2020). [doi:10.1126/science.abc4776](https://doi.org/10.1126/science.abc4776) [Medline](#)
9. Q. Gao, L. Bao, H. Mao, L. Wang, K. Xu, M. Yang, Y. Li, L. Zhu, N. Wang, Z. Lv, H. Gao, X. Ge, B. Kan, Y. Hu, J. Liu, F. Cai, D. Jiang, Y. Yin, C. Qin, J. Li, X. Gong, X. Lou, W. Shi, D. Wu, H. Zhang, L. Zhu, W. Deng, Y. Li, J. Lu, C. Li, X. Wang, W. Yin, Y. Zhang, C. Qin, Development of an inactivated vaccine candidate for SARS-CoV-2. *Science* **369**, 77–81 (2020). [doi:10.1126/science.abc1932](https://doi.org/10.1126/science.abc1932) [Medline](#)
10. J. Yu, L. H. Tostanoski, L. Peter, N. B. Mercado, K. McMahan, S. H. Mahrokhian, J. P. Nkolola, J. Liu, Z. Li, A. Chandrashekhar, D. R. Martinez, C. Loos, C. Atyeo, S. Fischinger, J. S. Burke, M. D. Slein, Y. Chen, A. Zuiani, F. J. N. Lelis, M. Travers, S. Habibi, L. Pessaint, A. Van Ry, K. Blade, R. Brown, A. Cook, B. Finneyfrock, A. Dodson, E. Teow, J. Velasco, R. Zahn, F. Wegmann, E. A. Bondzie, G. Dagotto, M. S. Gebre, X. He, C. Jacob-Dolan, M. Kirilova, N. Kordana, Z. Lin, L. F. Maxfield, F. Nampanya, R. Nityanandam, J. D. Ventura, H. Wan, Y. Cai, B. Chen, A. G. Schmidt, D. R. Wesemann, R. S. Baric, G. Alter, H. Andersen, M. G. Lewis, D. H. Barouch, DNA vaccine protection against SARS-CoV-2 in rhesus macaques. *Science* **369**, 806–811 (2020). [doi:10.1126/science.abc6284](https://doi.org/10.1126/science.abc6284) [Medline](#)
11. V. J. Munster, F. Feldmann, B. N. Williamson, N. van Doremalen, L. Pérez-Pérez, J. Schulz, K. Meade-White, A. Okumura, J. Callison, B. Brumbaugh, V. A. Avanzato, R. Rosenke, P. W. Hanley, G. Saturday, D. Scott, E. R. Fischer, E. de Wit, Respiratory disease in rhesus macaques inoculated with SARS-CoV-2. *Nature* **585**, 268–272 (2020). [doi:10.1038/s41586-020-2324-7](https://doi.org/10.1038/s41586-020-2324-7) [Medline](#)

12. N. B. Mercado, R. Zahn, F. Wegmann, C. Loos, A. Chandrashekhar, J. Yu, J. Liu, L. Peter, K. McMahan, L. H. Tostanoski, X. He, D. R. Martinez, L. Rutten, R. Bos, D. van Manen, J. Vellinga, J. Custers, J. P. Langedijk, T. Kwaks, M. J. G. Bakkers, D. Zuidgeest, S. K. Rosendahl Huber, C. Atyeo, S. Fischinger, J. S. Burke, J. Feldman, B. M. Hauser, T. M. Caradonna, E. A. Bondzie, G. Dagotto, M. S. Gebre, E. Hoffman, C. Jacob-Dolan, M. Kirilova, Z. Li, Z. Lin, S. H. Mahrokhan, L. F. Maxfield, F. Nampanya, R. Nityanandam, J. P. Nkolola, S. Patel, J. D. Ventura, K. Verrington, H. Wan, L. Pessant, A. Van Ry, K. Blade, A. Strasbaugh, M. Cabus, R. Brown, A. Cook, S. Zouantchangadou, E. Teow, H. Andersen, M. G. Lewis, Y. Cai, B. Chen, A. G. Schmidt, R. K. Reeves, R. S. Baric, D. A. Lauffenburger, G. Alter, P. Stoffels, M. Mammen, J. Van Hoof, H. Schuitemaker, D. H. Barouch, Single-shot Ad26 vaccine protects against SARS-CoV-2 in rhesus macaques. *Nature* **586**, 583–588 (2020). [doi:10.1038/s41586-020-2607-z](https://doi.org/10.1038/s41586-020-2607-z) [Medline](#)
13. K. S. Corbett, B. Flynn, K. E. Foulds, J. R. Francica, S. Boyoglu-Barnum, A. P. Werner, B. Flach, S. O'Connell, K. W. Bock, M. Minai, B. M. Nagata, H. Andersen, D. R. Martinez, A. T. Noe, N. Douek, M. M. Donaldson, N. N. Nji, G. S. Alvarado, D. K. Edwards, D. R. Flebbe, E. Lamb, N. A. Doria-Rose, B. C. Lin, M. K. Louder, S. O'Dell, S. D. Schmidt, E. Phung, L. A. Chang, C. Yap, J. M. Todd, L. Pessant, A. Van Ry, S. Browne, J. Greenhouse, T. Putman-Taylor, A. Strasbaugh, T. A. Campbell, A. Cook, A. Dodson, K. Steingrebe, W. Shi, Y. Zhang, O. M. Abiona, L. Wang, A. Pegu, E. S. Yang, K. Leung, T. Zhou, I. T. Teng, A. Widge, I. Gordon, L. Novik, R. A. Gillespie, R. J. Loomis, J. I. Moliva, G. Stewart-Jones, S. Himansu, W. P. Kong, M. C. Nason, K. M. Morabito, T. J. Ruckwardt, J. E. Ledgerwood, M. R. Gaudinski, P. D. Kwong, J. R. Mascola, A. Carfi, M. G. Lewis, R. S. Baric, A. McDermott, I. N. Moore, N. J. Sullivan, M. Roederer, R. A. Seder, B. S. Graham, Evaluation of the mRNA-1273 Vaccine against SARS-CoV-2 in nonhuman primates. *N. Engl. J. Med.* **383**, 1544–1555 (2020). [doi:10.1056/NEJMoa2024671](https://doi.org/10.1056/NEJMoa2024671) [Medline](#)
14. N. van Doremalen, T. Lambe, A. Spencer, S. Belij-Rammerstorfer, J. N. Purushotham, J. R. Port, V. A. Avanzato, T. Bushmaker, A. Flaxman, M. Ulaszewska, F. Feldmann, E. R. Allen, H. Sharpe, J. Schulz, M. Holbrook, A. Okumura, K. Meade-White, L. Pérez-Pérez, N. J. Edwards, D. Wright, C. Bissett, C. Gilbride, B. N. Williamson, R. Rosenke, D. Long, A. Ishwarbhai, R. Kailath, L. Rose, S. Morris, C. Powers, J. Lovaglio, P. W. Hanley, D. Scott, G. Saturday, E. de Wit, S. C. Gilbert, V. J. Munster, ChAdOx1 nCoV-19 vaccine prevents SARS-CoV-2 pneumonia in rhesus macaques. *Nature* **586**, 578–582 (2020). [doi:10.1038/s41586-020-2608-y](https://doi.org/10.1038/s41586-020-2608-y) [Medline](#)
15. B. N. Williamson, F. Feldmann, B. Schwarz, K. Meade-White, D. P. Porter, J. Schulz, N. van Doremalen, I. Leighton, C. K. Yinda, L. Pérez-Pérez, A.

- Okumura, J. Lovaglio, P. W. Hanley, G. Saturday, C. M. Bosio, S. Anzick, K. Barbian, T. Cihlar, C. Martens, D. P. Scott, V. J. Munster, E. de Wit, Clinical benefit of remdesivir in rhesus macaques infected with SARS-CoV-2. *Nature* **585**, 273–276 (2020). [doi:10.1038/s41586-020-2423-5](https://doi.org/10.1038/s41586-020-2423-5) [Medline](#)
16. T. Z. Song, H. Y. Zheng, J. B. Han, L. Jin, X. Yang, F. L. Liu, R. H. Luo, R. R. Tian, H. R. Cai, X. L. Feng, C. Liu, M. H. Li, Y. T. Zheng, Delayed severe cytokine storm and immune cell infiltration in SARS-CoV-2-infected aged Chinese rhesus macaques. *Zool. Res.* **41**, 503–516 (2020). [doi:10.24272/j.issn.2095-8137.2020.202](https://doi.org/10.24272/j.issn.2095-8137.2020.202) [Medline](#)
17. W. Enard, S. Pääbo, Comparative primate genomics. *Annu. Rev. Genomics Hum. Genet.* **5**, 351–378 (2004). [doi:10.1146/annurev.genom.5.061903.180040](https://doi.org/10.1146/annurev.genom.5.061903.180040) [Medline](#)
18. Z. N. Kronenberg, I. T. Fiddes, D. Gordon, S. Murali, S. Cantsilieris, O. S. Meyerson, J. G. Underwood, B. J. Nelson, M. J. P. Chaisson, M. L. Dougherty, K. M. Munson, A. R. Hastie, M. Diekhans, F. Hormozdiari, N. Lorusso, K. Hoekzema, R. Qiu, K. Clark, A. Raja, A. E. Welch, M. Sorensen, C. Baker, R. S. Fulton, J. Armstrong, T. A. Graves-Lindsay, A. M. Denli, E. R. Hoppe, P. Hsieh, C. M. Hill, A. W. C. Pang, J. Lee, E. T. Lam, S. K. Dutcher, F. H. Gage, W. C. Warren, J. Shendure, D. Haussler, V. A. Schneider, H. Cao, M. Ventura, R. K. Wilson, B. Paten, A. Pollen, E. E. Eichler, High-resolution comparative analysis of great ape genomes. *Science* **360**, eaar6343 (2018). [doi:10.1126/science.aar6343](https://doi.org/10.1126/science.aar6343) [Medline](#)
19. Chimpanzee Sequencing and Analysis Consortium, Initial sequence of the chimpanzee genome and comparison with the human genome. *Nature* **437**, 69–87 (2005). [doi:10.1038/nature04072](https://doi.org/10.1038/nature04072) [Medline](#)
20. R. A. Gibbs, J. Rogers, M. G. Katze, R. Bumgarner, G. M. Weinstock, E. R. Mardis, K. A. Remington, R. L. Strausberg, J. C. Venter, R. K. Wilson, M. A. Batzer, C. D. Bustamante, E. E. Eichler, M. W. Hahn, R. C. Hardison, K. D. Makova, W. Miller, A. Milosavljevic, R. E. Palermo, A. Siepel, J. M. Sikela, T. Attaway, S. Bell, K. E. Bernard, C. J. Buhay, M. N. Chandrabose, M. Dao, C. Davis, K. D. Delehaunty, Y. Ding, H. H. Dinh, S. Dugan-Rocha, L. A. Fulton, R. A. Gabisi, T. T. Garner, J. Godfrey, A. C. Hawes, J. Hernandez, S. Hines, M. Holder, J. Hume, S. N. Jhangiani, V. Joshi, Z. M. Khan, E. F. Kirkness, A. Cree, R. G. Fowler, S. Lee, L. R. Lewis, Z. Li, Y. S. Liu, S. M. Moore, D. Muzny, L. V. Nazareth, D. N. Ngo, G. O. Okwuonu, G. Pai, D. Parker, H. A. Paul, C. Pfannkoch, C. S. Pohl, Y. H. Rogers, S. J. Ruiz, A. Sabo, J. Santibanez, B. W. Schneider, S. M. Smith, E. Sodergren, A. F. Svatek, T. R. Utterback, S. Vattathil, W. Warren, C. S. White, A. T. Chinwalla, Y. Feng, A. L. Halpern, L. W. Hillier, X. Huang, P. Minx, J. O. Nelson, K. H. Pepin, X. Qin, G. G. Sutton, E. Venter, B. P. Walenz, J. W. Wallis, K. C. Worley, S. P. Yang, S. M. Jones, M. A. Marra, M. Rocchi, J. E.

Schein, R. Baertsch, L. Clarke, M. Csürös, J. Glasscock, R. A. Harris, P. Havlak, A. R. Jackson, H. Jiang, Y. Liu, D. N. Messina, Y. Shen, H. X. Song, T. Wylie, L. Zhang, E. Birney, K. Han, M. K. Konkel, J. Lee, A. F. Smit, B. Ullmer, H. Wang, J. Xing, R. Burhans, Z. Cheng, J. E. Karro, J. Ma, B. Raney, X. She, M. J. Cox, J. P. Demuth, L. J. Dumas, S. G. Han, J. Hopkins, A. Karimpour-Fard, Y. H. Kim, J. R. Pollack, T. Vinar, C. Addo-Quaye, J. Degenhardt, A. Denby, M. J. Hubisz, A. Indap, C. Kosiol, B. T. Lahn, H. A. Lawson, A. Marklein, R. Nielsen, E. J. Vallender, A. G. Clark, B. Ferguson, R. D. Hernandez, K. Hirani, H. Kehrer-Sawatzki, J. Kolb, S. Patil, L. L. Pu, Y. Ren, D. G. Smith, D. A. Wheeler, I. Schenck, E. V. Ball, R. Chen, D. N. Cooper, B. Giardine, F. Hsu, W. J. Kent, A. Lesk, D. L. Nelson, W. E. O'Brien, K. Prüfer, P. D. Stenson, J. C. Wallace, H. Ke, X. M. Liu, P. Wang, A. P. Xiang, F. Yang, G. P. Barber, D. Haussler, D. Karolchik, A. D. Kern, R. M. Kuhn, K. E. Smith, A. S. Zwig; Rhesus Macaque Genome Sequencing and Analysis Consortium, Evolutionary and biomedical insights from the rhesus macaque genome. *Science* **316**, 222–234 (2007).
[doi:10.1126/science.1139247](https://doi.org/10.1126/science.1139247) [Medline](#)

21. A. Scally, J. Y. Dutheil, L. W. Hillier, G. E. Jordan, I. Goodhead, J. Herrero, A. Hobolth, T. Lappalainen, T. Mailund, T. Marques-Bonet, S. McCarthy, S. H. Montgomery, P. C. Schwalie, Y. A. Tang, M. C. Ward, Y. Xue, B. Yngvadottir, C. Alkan, L. N. Andersen, Q. Ayub, E. V. Ball, K. Beal, B. J. Bradley, Y. Chen, C. M. Cleo, S. Fitzgerald, T. A. Graves, Y. Gu, P. Heath, A. Heger, E. Karakoc, A. Kolb-Kokocinski, G. K. Laird, G. Lunter, S. Meader, M. Mort, J. C. Mullikin, K. Munch, T. D. O'Connor, A. D. Phillips, J. Prado-Martinez, A. S. Rogers, S. Sajadian, D. Schmidt, K. Shaw, J. T. Simpson, P. D. Stenson, D. J. Turner, L. Vigilant, A. J. Vilella, W. Whitener, B. Zhu, D. N. Cooper, P. de Jong, E. T. Dermitzakis, E. E. Eichler, P. Flücke, N. Goldman, N. I. Mundy, Z. Ning, D. T. Odom, C. P. Ponting, M. A. Quail, O. A. Ryder, S. M. Searle, W. C. Warren, R. K. Wilson, M. H. Schierup, J. Rogers, C. Tyler-Smith, R. Durbin, Insights into hominid evolution from the gorilla genome sequence. *Nature* **483**, 169–175 (2012). [doi:10.1038/nature10842](https://doi.org/10.1038/nature10842) [Medline](#)
22. Marmoset Genome Sequencing and Analysis Consortium, The common marmoset genome provides insight into primate biology and evolution. *Nat. Genet.* **46**, 850–857 (2014). [doi:10.1038/ng.3042](https://doi.org/10.1038/ng.3042) [Medline](#)
23. D. P. Locke, L. W. Hillier, W. C. Warren, K. C. Worley, L. V. Nazareth, D. M. Muzny, S. P. Yang, Z. Wang, A. T. Chinwalla, P. Minx, M. Mitreva, L. Cook, K. D. Delehaunty, C. Fronick, H. Schmidt, L. A. Fulton, R. S. Fulton, J. O. Nelson, V. Magrini, C. Pohl, T. A. Graves, C. Markovic, A. Cree, H. H. Dinh, J. Hume, C. L. Kovar, G. R. Fowler, G. Lunter, S. Meader, A. Heger, C. P. Ponting, T. Marques-Bonet, C. Alkan, L. Chen, Z. Cheng, J. M. Kidd, E. E.

- Eichler, S. White, S. Searle, A. J. Vilella, Y. Chen, P. Fliceck, J. Ma, B. Raney, B. Suh, R. Burhans, J. Herrero, D. Haussler, R. Faria, O. Fernando, F. Darré, D. Farré, E. Gazave, M. Oliva, A. Navarro, R. Roberto, O. Capozzi, N. Archidiacono, G. Della Valle, S. Purgato, M. Rocchi, M. K. Konkel, J. A. Walker, B. Ullmer, M. A. Batzer, A. F. Smit, R. Hubley, C. Casola, D. R. Schrider, M. W. Hahn, V. Quesada, X. S. Puente, G. R. Ordoñez, C. López-Otín, T. Vinar, B. Brejova, A. Ratan, R. S. Harris, W. Miller, C. Kosiol, H. A. Lawson, V. Taliwal, A. L. Martins, A. Siepel, A. Roychoudhury, X. Ma, J. Degenhardt, C. D. Bustamante, R. N. Gutenkunst, T. Mailund, J. Y. Dutheil, A. Hobolth, M. H. Schierup, O. A. Ryder, Y. Yoshinaga, P. J. de Jong, G. M. Weinstock, J. Rogers, E. R. Mardis, R. A. Gibbs, R. K. Wilson, Comparative and demographic analysis of orang-utan genomes. *Nature* **469**, 529–533 (2011). [doi:10.1038/nature09687](https://doi.org/10.1038/nature09687) [Medline](#)
24. L. Carbone, R. A. Harris, S. Gnerre, K. R. Veeramah, B. Lorente-Galdos, J. Huddleston, T. J. Meyer, J. Herrero, C. Roos, B. Aken, F. Anacletio, N. Archidiacono, C. Baker, D. Barrell, M. A. Batzer, K. Beal, A. Blancher, C. L. Bohrson, M. Brameier, M. S. Campbell, O. Capozzi, C. Casola, G. Chiatante, A. Cree, A. Damert, P. J. de Jong, L. Dumas, M. Fernandez-Callejo, P. Fliceck, N. V. Fuchs, I. Gut, M. Gut, M. W. Hahn, J. Hernandez-Rodriguez, L. W. Hillier, R. Hubley, B. Ianc, Z. Izsvák, N. G. Jablonski, L. M. Johnstone, A. Karimpour-Fard, M. K. Konkel, D. Kostka, N. H. Lazar, S. L. Lee, L. R. Lewis, Y. Liu, D. P. Locke, S. Mallick, F. L. Mendez, M. Muffato, L. V. Nazareth, K. A. Neponen, M. O’Blenness, C. Ochis, D. T. Odom, K. S. Pollard, J. Quilez, D. Reich, M. Rocchi, G. G. Schumann, S. Searle, J. M. Sikela, G. Skollar, A. Smit, K. Sonmez, B. ten Hallers, E. Terhune, G. W. Thomas, B. Ullmer, M. Ventura, J. A. Walker, J. D. Wall, L. Walter, M. C. Ward, S. J. Wheelan, C. W. Whelan, S. White, L. J. Wilhelm, A. E. Woerner, M. Yandell, B. Zhu, M. F. Hammer, T. Marques-Bonet, E. E. Eichler, L. Fulton, C. Fronick, D. M. Muzny, W. C. Warren, K. C. Worley, J. Rogers, R. K. Wilson, R. A. Gibbs, Gibbon genome and the fast karyotype evolution of small apes. *Nature* **513**, 195–201 (2014). [doi:10.1038/nature13679](https://doi.org/10.1038/nature13679) [Medline](#)
25. L. Yu, G. D. Wang, J. Ruan, Y. B. Chen, C. P. Yang, X. Cao, H. Wu, Y. H. Liu, Z. L. Du, X. P. Wang, J. Yang, S. C. Cheng, L. Zhong, L. Wang, X. Wang, J. Y. Hu, L. Fang, B. Bai, K. L. Wang, N. Yuan, S. F. Wu, B. G. Li, J. G. Zhang, Y. Q. Yang, C. L. Zhang, Y. C. Long, H. S. Li, J. Y. Yang, D. M. Irwin, O. A. Ryder, Y. Li, C. I. Wu, Y. P. Zhang, Genomic analysis of snub-nosed monkeys (*Rhinopithecus*) identifies genes and processes related to high-altitude adaptation. *Nat. Genet.* **48**, 947–952 (2016). [doi:10.1038/ng.3615](https://doi.org/10.1038/ng.3615) [Medline](#)
26. X. Zhou, B. Wang, Q. Pan, J. Zhang, S. Kumar, X. Sun, Z. Liu, H. Pan, Y. Lin, G. Liu, W. Zhan, M. Li, B. Ren, X. Ma, H. Ruan, C. Cheng, D. Wang, F. Shi, Y.

- Hui, Y. Tao, C. Zhang, P. Zhu, Z. Xiang, W. Jiang, J. Chang, H. Wang, Z. Cao, Z. Jiang, B. Li, G. Yang, C. Roos, P. A. Garber, M. W. Bruford, R. Li, M. Li, Whole-genome sequencing of the snub-nosed monkey provides insights into folivory and evolutionary history. *Nat. Genet.* **46**, 1303–1310 (2014). [doi:10.1038/ng.3137](https://doi.org/10.1038/ng.3137) [Medline](#)
27. A. O. Ayoola, B. L. Zhang, R. P. Meisel, L. M. Nneji, Y. Shao, O. B. Morenikeji, A. C. Adeola, S. I. Ng’ang’a, B. G. Ogunjemite, A. O. Okeyoyin, C. Roos, D. D. Wu, Population genomics reveals incipient speciation, introgression, and adaptation in the African mico monkey (*Cercopithecus mona*). *Mol. Biol. Evol.* **38**, 876–890 (2021). [doi:10.1093/molbev/msaa248](https://doi.org/10.1093/molbev/msaa248) [Medline](#)
28. D. M. Bickhart, B. D. Rosen, S. Koren, B. L. Sayre, A. R. Hastie, S. Chan, J. Lee, E. T. Lam, I. Liachko, S. T. Sullivan, J. N. Burton, H. J. Huson, J. C. Nystrom, C. M. Kelley, J. L. Hutchison, Y. Zhou, J. Sun, A. Crisà, F. A. Ponce de León, J. C. Schwartz, J. A. Hammond, G. C. Waldbieser, S. G. Schroeder, G. E. Liu, M. J. Dunham, J. Shendure, T. S. Sonstegard, A. M. Phillippe, C. P. Van Tassell, T. P. Smith, Single-molecule sequencing and chromatin conformation capture enable *de novo* reference assembly of the domestic goat genome. *Nat. Genet.* **49**, 643–650 (2017). [doi:10.1038/ng.3802](https://doi.org/10.1038/ng.3802) [Medline](#)
29. B.-L. Zhang, W. Chen, Z. Wang, W. Pang, M.-T. Luo, S. Wang, Y. Shao, W.-Q. He, Y. Deng, L. Zhou, J. Chen, M. Yang, Y. Wu, L. Wang, H. Fernandez, S. Molloy, H. Meunier, F. Wanert, L. Kuderna, T. Marques-Bonet, C. Roos, X. Qi, M. Li, Z.-J. Liu, M. H. Schierup, D. N. Cooper, J. Liu, Y.-T. Zheng, G. Zhang, D.-D. Wu, Comparative genomics reveals the hybrid origin of a macaque group. *Sci. Adv.* **9**, eadd3580 (2023). [doi:10.1126/sciadv.abn7153](https://doi.org/10.1126/sciadv.abn7153)
30. H. Wu, Z. Wang, Y. Zhang, L. Frantz, C. Roos, D. M. Irwin, C. Zhang, X. Liu, D. Wu, S. Huang, T. Gu, J. Liu, L. Yu, Hybrid origin of a primate, the gray snub-nosed monkey. *Science* **380**, eabl4997 (2023) [doi:10.1126/science.abl4997](https://doi.org/10.1126/science.abl4997).
31. X.-G. Qi, J. Wu, L. Zhao, L. Wang, X. Guang, P. A. Garber, C. Opie, Y. Yuan, R. Diao, G. Li, K. Wang, R. Pan, W. Ji, H. Sun, Z.-P. Huang, C. Xu, A. B. Witarto, R. Jia, C. Zhang, C. Deng, Q. Qiu, G. Zhang, C. C. Grueter, D. Wu, B. Li, Adaptations to a cold climate promoted social evolution in Asian colobine primates. *Science* **380**, eabl8621 (2023). [doi:10.1126/science.abl8621](https://doi.org/10.1126/science.abl8621)
32. M.-L. Li, S. Wang, P. Xu, H.-Y. Tian, M. Bai, Y.-P. Zhang, Y. Shao, Z.-J. Xiong, X.-G. Qi, D. N. Cooper, G. Zhang, H. H. Zhu, D.-D. Wu, Functional genomics analysis reveals the evolutionary adaptation and demographic history of pygmy lorises. *Proc. Natl. Acad. Sci. U. S. A.* **119**, e2123030119 (2022). [doi:10.1073/pnas.2123030119](https://doi.org/10.1073/pnas.2123030119) [Medline](#)
33. M. S. Ye, J. Y. Zhang, D. D. Yu, M. Xu, L. Xu, L. B. Lv, Q. Y. Zhu, Y. Fan, Y. G. Yao, Comprehensive annotation of the Chinese tree shrew genome by

- large-scale RNA sequencing and long-read isoform sequencing. *Zool. Res.* **42**, 692–709 (2021). [doi:10.24272/j.issn.2095-8137.2021.272](https://doi.org/10.24272/j.issn.2095-8137.2021.272) [Medline](#)
34. A. M. Kozlov, A. J. Aberer, A. Stamatakis, ExaML version 3: A tool for phylogenomic analyses on supercomputers. *Bioinformatics* **31**, 2577–2579 (2015). [doi:10.1093/bioinformatics/btv184](https://doi.org/10.1093/bioinformatics/btv184) [Medline](#)
35. P. Perelman, W. E. Johnson, C. Roos, H. N. Seuánez, J. E. Horvath, M. A. Moreira, B. Kessing, J. Pontius, M. Roelke, Y. Rumpler, M. P. Schneider, A. Silva, S. J. O'Brien, J. Pecon-Slattery, A molecular phylogeny of living primates. *PLOS Genet.* **7**, e1001342 (2011). [doi:10.1371/journal.pgen.1001342](https://doi.org/10.1371/journal.pgen.1001342) [Medline](#)
36. C. M. Shi, Z. Yang, Coalescent-based analyses of genomic sequence data provide a robust resolution of phylogenetic relationships among major groups of gibbons. *Mol. Biol. Evol.* **35**, 159–179 (2018). [doi:10.1093/molbev/msx277](https://doi.org/10.1093/molbev/msx277) [Medline](#)
37. A. Hobolth, O. F. Christensen, T. Mailund, M. H. Schierup, Genomic relationships and speciation times of human, chimpanzee, and gorilla inferred from a coalescent hidden Markov model. *PLOS Genet.* **3**, e7 (2007). [doi:10.1371/journal.pgen.0030007](https://doi.org/10.1371/journal.pgen.0030007) [Medline](#)
38. I. Rivas-González, M. Rousselle, F. Li, L. Zhou, J. Y. Dutheil, K. Munch, Y. Shao, D. Wu, M. H. Schierup, G. Zhang, Pervasive incomplete lineage sorting illuminates speciation and selection processes in primates. *Science* **380**, eabn4409 (2022). [doi:10.1126/science.abn4409](https://doi.org/10.1126/science.abn4409)
39. D. Vanderpool, B. Q. Minh, R. Lanfear, D. Hughes, S. Murali, R. A. Harris, M. Raveendran, D. M. Muzny, M. S. Hibbins, R. J. Williamson, R. A. Gibbs, K. C. Worley, J. Rogers, M. W. Hahn, Primate phylogenomics uncovers multiple rapid radiations and ancient interspecific introgression. *PLOS Biol.* **18**, e3000954 (2020). [doi:10.1371/journal.pbio.3000954](https://doi.org/10.1371/journal.pbio.3000954) [Medline](#)
40. Z. Yang, PAML 4: Phylogenetic analysis by maximum likelihood. *Mol. Biol. Evol.* **24**, 1586–1591 (2007). [doi:10.1093/molbev/msm088](https://doi.org/10.1093/molbev/msm088) [Medline](#)
41. S. Álvarez-Carretero, A. U. Tamuri, M. Battini, F. F. Nascimento, E. Carlisle, R. J. Asher, Z. Yang, P. C. J. Donoghue, M. Dos Reis, A species-level timeline of mammal evolution integrating phylogenomic data. *Nature* **602**, 263–267 (2022). [doi:10.1038/s41586-021-04341-1](https://doi.org/10.1038/s41586-021-04341-1) [Medline](#)
42. C. Liu, J. Gao, X. Cui, Z. Li, L. Chen, Y. Yuan, Y. Zhang, L. Mei, L. Zhao, D. Cai, M. Hu, B. Zhou, Z. Li, T. Qin, H. Si, G. Li, Z. Lin, Y. Xu, C. Zhu, Y. Yin, C. Zhang, W. Xu, Q. Li, K. Wang, M. T. P. Gilbert, R. Heller, W. Wang, J. Huang, Q. Qiu, A towering genome: Experimentally validated adaptations to high blood pressure and extreme stature in the giraffe. *Sci. Adv.* **7**, eabe9459 (2021). [doi:10.1126/sciadv.abe9459](https://doi.org/10.1126/sciadv.abe9459) [Medline](#)

43. E. E. Eichler, D. Sankoff, Structural dynamics of eukaryotic chromosome evolution. *Science* **301**, 793–797 (2003). [doi:10.1126/science.1086132](https://doi.org/10.1126/science.1086132) [Medline](#)
44. Y. Yin, H. Fan, B. Zhou, Y. Hu, G. Fan, J. Wang, F. Zhou, W. Nie, C. Zhang, L. Liu, Z. Zhong, W. Zhu, G. Liu, Z. Lin, C. Liu, J. Zhou, G. Huang, Z. Li, J. Yu, Y. Zhang, Y. Yang, B. Zhuo, B. Zhang, J. Chang, H. Qian, Y. Peng, X. Chen, L. Chen, Z. Li, Q. Zhou, W. Wang, F. Wei, Molecular mechanisms and topological consequences of drastic chromosomal rearrangements of muntjac deer. *Nat. Commun.* **12**, 6858 (2021). [doi:10.1038/s41467-021-27091-0](https://doi.org/10.1038/s41467-021-27091-0) [Medline](#)
45. R. Stanyon, M. Rocchi, O. Capozzi, R. Roberto, D. Misceo, M. Ventura, M. F. Cardone, F. Bigoni, N. Archidiacono, Primate chromosome evolution: Ancestral karyotypes, marker order and neocentromeres. *Chromosome Res.* **16**, 17–39 (2008). [doi:10.1007/s10577-007-1209-z](https://doi.org/10.1007/s10577-007-1209-z) [Medline](#)
46. T. Marques-Bonet, J. M. Kidd, M. Ventura, T. A. Graves, Z. Cheng, L. W. Hillier, Z. Jiang, C. Baker, R. Malfavon-Borja, L. A. Fulton, C. Alkan, G. Aksay, S. Girirajan, P. Siswara, L. Chen, M. F. Cardone, A. Navarro, E. R. Mardis, R. K. Wilson, E. E. Eichler, A burst of segmental duplications in the genome of the African great ape ancestor. *Nature* **457**, 877–881 (2009). [doi:10.1038/nature07744](https://doi.org/10.1038/nature07744) [Medline](#)
47. P. D. Stenson, M. Mort, E. V. Ball, M. Chapman, K. Evans, L. Azevedo, M. Hayden, S. Heywood, D. S. Millar, A. D. Phillips, D. N. Cooper, The Human Gene Mutation Database (HGMD®): Optimizing its use in a clinical diagnostic or research setting. *Hum. Genet.* **139**, 1197–1207 (2020). [doi:10.1007/s00439-020-02199-3](https://doi.org/10.1007/s00439-020-02199-3) [Medline](#)
48. L. Chen, Q. Qiu, Y. Jiang, K. Wang, Z. Lin, Z. Li, F. Bibi, Y. Yang, J. Wang, W. Nie, W. Su, G. Liu, Q. Li, W. Fu, X. Pan, C. Liu, J. Yang, C. Zhang, Y. Yin, Y. Wang, Y. Zhao, C. Zhang, Z. Wang, Y. Qin, W. Liu, B. Wang, Y. Ren, R. Zhang, Y. Zeng, R. R. da Fonseca, B. Wei, R. Li, W. Wan, R. Zhao, W. Zhu, Y. Wang, S. Duan, Y. Gao, Y. E. Zhang, C. Chen, C. Hvilsom, C. W. Epps, L. G. Chemnick, Y. Dong, S. Mirarab, H. R. Siegismund, O. A. Ryder, M. T. P. Gilbert, H. A. Lewin, G. Zhang, R. Heller, W. Wang, Large-scale ruminant genome sequencing provides insights into their evolution and distinct traits. *Science* **364**, eaav6202 (2019). [doi:10.1126/science.aav6202](https://doi.org/10.1126/science.aav6202) [Medline](#)
49. J. D. Smith, J. W. Bickham, T. R. Gregory, Patterns of genome size diversity in bats (order Chiroptera). *Genome* **56**, 457–472 (2013). [doi:10.1139/gen-2013-0046](https://doi.org/10.1139/gen-2013-0046) [Medline](#)
50. S. Shen, L. Lin, J. J. Cai, P. Jiang, E. J. Kenkel, M. R. Stroik, S. Sato, B. L. Davidson, Y. Xing, Widespread establishment and regulatory impact of Alu

- exons in human genes. *Proc. Natl. Acad. Sci. U.S.A.* **108**, 2837–2842 (2011). [doi:10.1073/pnas.1012834108](https://doi.org/10.1073/pnas.1012834108) [Medline](#)
51. G. E. Liu, C. Alkan, L. Jiang, S. Zhao, E. E. Eichler, Comparative analysis of Alu repeats in primate genomes. *Genome Res.* **19**, 876–885 (2009). [doi:10.1101/gr.083972.108](https://doi.org/10.1101/gr.083972.108) [Medline](#)
52. T. Hayakawa, Y. Satta, P. Gagneux, A. Varki, N. Takahata, Alu-mediated inactivation of the human CMP-*N*-acetylneuraminic acid hydroxylase gene. *Proc. Natl. Acad. Sci. U.S.A.* **98**, 11399–11404 (2001). [doi:10.1073/pnas.191268198](https://doi.org/10.1073/pnas.191268198) [Medline](#)
53. P. Kuehnen, M. Mischke, S. Wiegand, C. Sers, B. Horsthemke, S. Lau, T. Keil, Y. A. Lee, A. Grueters, H. Krude, An Alu element-associated hypermethylation variant of the *POMC* gene is associated with childhood obesity. *PLOS Genet.* **8**, e1002543 (2012). [doi:10.1371/journal.pgen.1002543](https://doi.org/10.1371/journal.pgen.1002543) [Medline](#)
54. J. Jurka, Evolutionary impact of human Alu repetitive elements. *Curr. Opin. Genet. Dev.* **14**, 603–608 (2004). [doi:10.1016/j.gde.2004.08.008](https://doi.org/10.1016/j.gde.2004.08.008) [Medline](#)
55. G. Zhang, C. Li, Q. Li, B. Li, D. M. Larkin, C. Lee, J. F. Storz, A. Antunes, M. J. Greenwald, R. W. Meredith, A. Ödeen, J. Cui, Q. Zhou, L. Xu, H. Pan, Z. Wang, L. Jin, P. Zhang, H. Hu, W. Yang, J. Hu, J. Xiao, Z. Yang, Y. Liu, Q. Xie, H. Yu, J. Lian, P. Wen, F. Zhang, H. Li, Y. Zeng, Z. Xiong, S. Liu, L. Zhou, Z. Huang, N. An, J. Wang, Q. Zheng, Y. Xiong, G. Wang, B. Wang, J. Wang, Y. Fan, R. R. da Fonseca, A. Alfaro-Núñez, M. Schubert, L. Orlando, T. Mourier, J. T. Howard, G. Ganapathy, A. Pfenning, O. Whitney, M. V. Rivas, E. Hara, J. Smith, M. Farré, J. Narayan, G. Slavov, M. N. Romanov, R. Borges, J. P. Machado, I. Khan, M. S. Springer, J. Gatesy, F. G. Hoffmann, J. C. Opazo, O. Håstad, R. H. Sawyer, H. Kim, K. W. Kim, H. J. Kim, S. Cho, N. Li, Y. Huang, M. W. Bruford, X. Zhan, A. Dixon, M. F. Bertelsen, E. Derryberry, W. Warren, R. K. Wilson, S. Li, D. A. Ray, R. E. Green, S. J. O'Brien, D. Griffin, W. E. Johnson, D. Haussler, O. A. Ryder, E. Willerslev, G. R. Graves, P. Alström, J. Fjeldså, D. P. Mindell, S. V. Edwards, E. L. Braun, C. Rahbek, D. W. Burt, P. Houde, Y. Zhang, H. Yang, J. Wang, E. D. Jarvis, M. T. Gilbert, J. Wang; Avian Genome Consortium, Comparative genomics reveals insights into avian genome evolution and adaptation. *Science* **346**, 1311–1320 (2014). [doi:10.1126/science.1251385](https://doi.org/10.1126/science.1251385) [Medline](#)
56. P. Moorjani, C. E. Amorim, P. F. Arndt, M. Przeworski, Variation in the molecular clock of primates. *Proc. Natl. Acad. Sci. U.S.A.* **113**, 10607–10612 (2016). [doi:10.1073/pnas.1600374113](https://doi.org/10.1073/pnas.1600374113) [Medline](#)
57. E. Fontanillas, J. J. Welch, J. A. Thomas, L. Bromham, The influence of body size and net diversification rate on molecular evolution during the radiation of animal phyla. *BMC Evol. Biol.* **7**, 95 (2007). [doi:10.1186/1471-2148-7-95](https://doi.org/10.1186/1471-2148-7-95) [Medline](#)

58. A. Wong, Covariance between testes size and substitution rates in primates. *Mol. Biol. Evol.* **31**, 1432–1436 (2014). [doi:10.1093/molbev/msu091](https://doi.org/10.1093/molbev/msu091) [Medline](#)
59. W. H. Li, M. Tanimura, The molecular clock runs more slowly in man than in apes and monkeys. *Nature* **326**, 93–96 (1987). [doi:10.1038/326093a0](https://doi.org/10.1038/326093a0) [Medline](#)
60. M. E. Steiper, N. M. Young, Primate molecular divergence dates. *Mol. Phylogenet. Evol.* **41**, 384–394 (2006). [doi:10.1016/j.ympev.2006.05.021](https://doi.org/10.1016/j.ympev.2006.05.021) [Medline](#)
61. S. H. Kim, N. Elango, C. Warden, E. Vigoda, S. V. Yi, Heterogeneous genomic molecular clocks in primates. *PLOS Genet.* **2**, e163 (2006). [doi:10.1371/journal.pgen.0020163](https://doi.org/10.1371/journal.pgen.0020163) [Medline](#)
62. J. Schmitz, A. Noll, C. A. Raabe, G. Churakov, R. Voss, M. Kiefmann, T. Rozhdestvensky, J. Brosius, R. Baertsch, H. Clawson, C. Roos, A. Zimin, P. Minx, M. J. Montague, R. K. Wilson, W. C. Warren, Genome sequence of the basal haplorrhine primate *Tarsius syrichta* reveals unusual insertions. *Nat. Commun.* **7**, 12997 (2016). [doi:10.1038/ncomms12997](https://doi.org/10.1038/ncomms12997) [Medline](#)
63. L. Fang, W. Cai, S. Liu, O. Canela-Xandri, Y. Gao, J. Jiang, K. Rawlik, B. Li, S. G. Schroeder, B. D. Rosen, C. J. Li, T. S. Sonstegard, L. J. Alexander, C. P. Van Tassell, P. M. VanRaden, J. B. Cole, Y. Yu, S. Zhang, A. Tenesa, L. Ma, G. E. Liu, Comprehensive analyses of 723 transcriptomes enhance genetic and biological interpretations for complex traits in cattle. *Genome Res.* **30**, 790–801 (2020). [doi:10.1101/gr.250704.119](https://doi.org/10.1101/gr.250704.119) [Medline](#)
64. B. Y. Liao, J. Zhang, Low rates of expression profile divergence in highly expressed genes and tissue-specific genes during mammalian evolution. *Mol. Biol. Evol.* **23**, 1119–1128 (2006). [doi:10.1093/molbev/msj119](https://doi.org/10.1093/molbev/msj119) [Medline](#)
65. G. J. Wyckoff, W. Wang, C. I. Wu, Rapid evolution of male reproductive genes in the descent of man. *Nature* **403**, 304–309 (2000). [doi:10.1038/35002070](https://doi.org/10.1038/35002070) [Medline](#)
66. T. Boehm, Evolution of vertebrate immunity. *Curr. Biol.* **22**, R722–R732 (2012). [doi:10.1016/j.cub.2012.07.003](https://doi.org/10.1016/j.cub.2012.07.003) [Medline](#)
67. H. Y. Wang, H. C. Chien, N. Osada, K. Hashimoto, S. Sugano, T. Gojobori, C. K. Chou, S. F. Tsai, C. I. Wu, C. K. Shen, Rate of evolution in brain-expressed genes in humans and other primates. *PLOS Biol.* **5**, e13 (2007). [doi:10.1371/journal.pbio.0050013](https://doi.org/10.1371/journal.pbio.0050013) [Medline](#)
68. Materials and methods are available as supplementary materials.
69. J. Tohyama, M. Nakashima, S. Nabatame, C. Gaik-Siew, R. Miyata, Z. Rener-Primec, M. Kato, N. Matsumoto, H. Saitsu, *SPTAN1* encephalopathy: Distinct phenotypes and genotypes. *J. Hum. Genet.* **60**, 167–173 (2015). [doi:10.1038/jhg.2015.5](https://doi.org/10.1038/jhg.2015.5) [Medline](#)

70. P. Mansfield, J. N. Constantino, D. Baldridge, *MYTIL*: A systematic review of genetic variation encompassing schizophrenia and autism. *Am. J. Med. Genet. B. Neuropsychiatr. Genet.* **183**, 227–233 (2020). [doi:10.1002/ajmg.b.32781](https://doi.org/10.1002/ajmg.b.32781) [Medline](#)
71. M. Maekawa, T. Ohnishi, K. Hashimoto, A. Watanabe, Y. Iwayama, H. Ohba, E. Hattori, K. Yamada, T. Yoshikawa, Analysis of strain-dependent prepulse inhibition points to a role for Shmt1 (*SHMT1*) in mice and in schizophrenia. *J. Neurochem.* **115**, 1374–1385 (2010). [doi:10.1111/j.1471-4159.2010.07039.x](https://doi.org/10.1111/j.1471-4159.2010.07039.x) [Medline](#)
72. X. Bi, L. Zhou, J.-J. Zhang, S. Feng, M. Hu, D. N. Cooper, J. Lin, J. Li, D.-D. Wu, G. Zhang, Lineage-specific accelerated sequences underlying primate evolution. *Sci. Adv.* 10.1126/sciadv.adc9507 (2023).
73. J. K. Rilling, T. R. Insel, Differential expansion of neural projection systems in primate brain evolution. *Neuroreport* **10**, 1453–1459 (1999).
[doi:10.1097/00001756-199905140-00012](https://doi.org/10.1097/00001756-199905140-00012) [Medline](#)
74. K. Isler, E. Christopher Kirk, J. M. Miller, G. A. Albrecht, B. R. Gelvin, R. D. Martin, Endocranial volumes of primate species: Scaling analyses using a comprehensive and reliable data set. *J. Hum. Evol.* **55**, 967–978 (2008).
[doi:10.1016/j.jhevol.2008.08.004](https://doi.org/10.1016/j.jhevol.2008.08.004) [Medline](#)
75. C. Plachez, L. J. Richards, Mechanisms of axon guidance in the developing nervous system. *Curr. Top. Dev. Biol.* **69**, 267–346 (2005).
[doi:10.1016/S0070-2153\(05\)69010-2](https://doi.org/10.1016/S0070-2153(05)69010-2) [Medline](#)
76. M. A. Robichaux, C. W. Cowan, Signaling mechanisms of axon guidance and early synaptogenesis. *Curr. Top. Behav. Neurosci.* **16**, 19–48 (2014).
[doi:10.1007/978-3-662-45758-0_255](https://doi.org/10.1007/978-3-662-45758-0_255) [Medline](#)
77. J. Falk, A. Bechara, R. Fiore, H. Nawabi, H. Zhou, C. Hoyo-Becerra, M. Bozon, G. Rougon, M. Grumet, A. W. Püschel, J. R. Sanes, V. Castellani, Dual functional activity of semaphorin 3B is required for positioning the anterior commissure. *Neuron* **48**, 63–75 (2005). [doi:10.1016/j.neuron.2005.10.024](https://doi.org/10.1016/j.neuron.2005.10.024) [Medline](#)
78. M. A. Wolman, Y. Liu, H. Tawarayama, W. Shoji, M. C. Halloran, Repulsion and attraction of axons by semaphorin3D are mediated by different neuropilins in vivo. *J. Neurosci.* **24**, 8428–8435 (2004). [doi:10.1523/JNEUROSCI.2349-04.2004](https://doi.org/10.1523/JNEUROSCI.2349-04.2004) [Medline](#)
79. C. Kudo, I. Ajioka, Y. Hirata, K. Nakajima, Expression profiles of *EphA3* at both the RNA and protein level in the developing mammalian forebrain. *J. Comp. Neurol.* **487**, 255–269 (2005). [doi:10.1002/cne.20551](https://doi.org/10.1002/cne.20551) [Medline](#)
80. M. V. Tejada-Simon, Modulation of actin dynamics by *Rac1* to target cognitive function. *J. Neurochem.* **133**, 767–779 (2015). [doi:10.1111/jnc.13100](https://doi.org/10.1111/jnc.13100) [Medline](#)

81. S. L. Eastwood, P. J. Harrison, Decreased mRNA expression of netrin-G1 and netrin-G2 in the temporal lobe in schizophrenia and bipolar disorder. *Neuropsychopharmacology* **33**, 933–945 (2008). [doi:10.1038/sj.npp.1301457](https://doi.org/10.1038/sj.npp.1301457) [Medline](#)
82. D. Pan, Hippo signaling in organ size control. *Genes Dev.* **21**, 886–897 (2007). [doi:10.1101/gad.1536007](https://doi.org/10.1101/gad.1536007) [Medline](#)
83. S. H. Patel, F. D. Camargo, D. Yimlamai, Hippo signaling in the liver regulates organ size, cell fate, and carcinogenesis. *Gastroenterology* **152**, 533–545 (2017). [doi:10.1053/j.gastro.2016.10.047](https://doi.org/10.1053/j.gastro.2016.10.047) [Medline](#)
84. R. H. Gokhale, A. W. Shingleton, Size control: The developmental physiology of body and organ size regulation. *Wiley Interdiscip. Rev. Dev. Biol.* **4**, 335–356 (2015). [doi:10.1002/wdev.181](https://doi.org/10.1002/wdev.181) [Medline](#)
85. E. C. Kirk, Comparative morphology of the eye in primates. *Anat. Rec. A Discov. Mol. Cell. Evol. Biol.* **281**, 1095–1103 (2004). [doi:10.1002/ar.a.20115](https://doi.org/10.1002/ar.a.20115) [Medline](#)
86. A. C. Wiik, C. Wade, T. Biagi, E. O. Ropstad, E. Bjerkås, K. Lindblad-Toh, F. Lingaas, A deletion in nephronophthisis 4 (*NPHP4*) is associated with recessive cone-rod dystrophy in standard wire-haired dachshund. *Genome Res.* **18**, 1415–1421 (2008). [doi:10.1101/gr.074302.107](https://doi.org/10.1101/gr.074302.107) [Medline](#)
87. P. Liskova, L. Dudakova, C. J. Evans, K. E. Rojas Lopez, N. Pontikos, D. Athanasiou, H. Jama, J. Sach, P. Skalicka, V. Stranecky, S. Kmoch, C. Thaung, M. Filipec, M. E. Cheetham, A. E. Davidson, S. J. Tuft, A. J. Hardcastle, Ectopic *GRHL2* expression due to non-coding mutations promotes cell state transition and causes posterior polymorphous corneal dystrophy 4. *Am. J. Hum. Genet.* **102**, 447–459 (2018). [doi:10.1016/j.ajhg.2018.02.002](https://doi.org/10.1016/j.ajhg.2018.02.002) [Medline](#)
88. Y. Toda, T. Hayakawa, A. Itoigawa, Y. Kurihara, T. Nakagita, M. Hayashi, R. Ashino, A. D. Melin, Y. Ishimaru, S. Kawamura, H. Imai, T. Misaka, Evolution of the primate glutamate taste sensor from a nucleotide sensor. *Curr. Biol.* **31**, 4641–4649.e5 (2021). [doi:10.1016/j.cub.2021.08.002](https://doi.org/10.1016/j.cub.2021.08.002) [Medline](#)
89. J. M. Kamilar, B. J. Bradley, Interspecific variation in primate coat colour supports Gloger's rule. *J. Biogeogr.* **38**, 2270–2277 (2011). [doi:10.1111/j.1365-2699.2011.02587.x](https://doi.org/10.1111/j.1365-2699.2011.02587.x)
90. S. Hu, Y. Chen, B. Zhao, N. Yang, S. Chen, J. Shen, G. Bao, X. Wu, *KIT* is involved in melanocyte proliferation, apoptosis and melanogenesis in the Rex Rabbit. *PeerJ* **8**, e9402 (2020). [doi:10.7717/peerj.9402](https://doi.org/10.7717/peerj.9402) [Medline](#)
91. M. C. Garrido, B. C. Bastian, *KIT* as a therapeutic target in melanoma. *J. Invest. Dermatol.* **130**, 20–27 (2010). [doi:10.1038/jid.2009.334](https://doi.org/10.1038/jid.2009.334) [Medline](#)

92. J. M. Grichnik, Kit and melanocyte migration. *J. Invest. Dermatol.* **126**, 945–947 (2006). [doi:10.1038/sj.jid.5700164](https://doi.org/10.1038/sj.jid.5700164) [Medline](#)
93. Y. Mizutani, N. Hayashi, M. Kawashima, G. Imokawa, A single UVB exposure increases the expression of functional *KIT* in human melanocytes by up-regulating *MITF* expression through the phosphorylation of p38/CREB. *Arch. Dermatol. Res.* **302**, 283–294 (2010). [doi:10.1007/s00403-009-1007-x](https://doi.org/10.1007/s00403-009-1007-x) [Medline](#)
94. R. Kitamura, K. Tsukamoto, K. Harada, A. Shimizu, S. Shimada, T. Kobayashi, G. Imokawa, Mechanisms underlying the dysfunction of melanocytes in vitiligo epidermis: Role of SCF/KIT protein interactions and the downstream effector, MITF-M. *J. Pathol.* **202**, 463–475 (2004). [doi:10.1002/path.1538](https://doi.org/10.1002/path.1538) [Medline](#)
95. B. Wen, Y. Chen, H. Li, J. Wang, J. Shen, A. Ma, J. Qu, K. Bismuth, J. Debbache, H. Arnheiter, L. Hou, Allele-specific genetic interactions between Mitf and Kit affect melanocyte development. *Pigment Cell Melanoma Res.* **23**, 441–447 (2010). [doi:10.1111/j.1755-148X.2010.00699.x](https://doi.org/10.1111/j.1755-148X.2010.00699.x) [Medline](#)
96. D. L. C. van den Berg, R. Azzarelli, K. Oishi, B. Martynoga, N. Urbán, D. H. W. Dekkers, J. A. Demmers, F. Guillemot, *NIPBL* interacts with *ZFP609* and the integrator complex to regulate cortical neuron migration. *Neuron* **93**, 348–361 (2017). [doi:10.1016/j.neuron.2016.11.047](https://doi.org/10.1016/j.neuron.2016.11.047) [Medline](#)
97. G. H. Mochida, C. A. Walsh, Molecular genetics of human microcephaly. *Curr. Opin. Neurol.* **14**, 151–156 (2001). [doi:10.1097/00019052-200104000-00003](https://doi.org/10.1097/00019052-200104000-00003) [Medline](#)
98. S. H. Montgomery, I. Capellini, C. Venditti, R. A. Barton, N. I. Mundy, Adaptive evolution of four microcephaly genes and the evolution of brain size in anthropoid primates. *Mol. Biol. Evol.* **28**, 625–638 (2011). [doi:10.1093/molbev/msq237](https://doi.org/10.1093/molbev/msq237) [Medline](#)
99. L. Shi, M. Li, Q. Lin, X. Qi, B. Su, Functional divergence of the brain-size regulating gene *MCPH1* during primate evolution and the origin of humans. *BMC Biol.* **11**, 62 (2013). [doi:10.1186/1741-7007-11-62](https://doi.org/10.1186/1741-7007-11-62) [Medline](#)
100. L. Shi, B. Su, A transgenic monkey model for the study of human brain evolution. *Zool. Res.* **40**, 236–238 (2019). [doi:10.24272/j.issn.2095-8137.2019.031](https://doi.org/10.24272/j.issn.2095-8137.2019.031) [Medline](#)
101. J. Rogers, P. Kochunov, K. Zilles, W. Shelledy, J. Lancaster, P. Thompson, R. Duggirala, J. Blangero, P. T. Fox, D. C. Glahn, On the genetic architecture of cortical folding and brain volume in primates. *Neuroimage* **53**, 1103–1108 (2010). [doi:10.1016/j.neuroimage.2010.02.020](https://doi.org/10.1016/j.neuroimage.2010.02.020) [Medline](#)
102. S. V. Puram, A. Riccio, S. Koirala, Y. Ikeuchi, A. H. Kim, G. Corfas, A. Bonni, A TRPC5-regulated calcium signaling pathway controls dendrite patterning in

- the mammalian brain. *Genes Dev.* **25**, 2659–2673 (2011).
[doi:10.1101/gad.174060.111](https://doi.org/10.1101/gad.174060.111) [Medline](#)
103. A. Yamada, E. Inoue, M. Deguchi-Tawarada, C. Matsui, A. Togawa, T. Nakatani, Y. Ono, Y. Takai, *Necl-2/CADM1* interacts with *ErbB4* and regulates its activity in GABAergic neurons. *Mol. Cell. Neurosci.* **56**, 234–243 (2013). [doi:10.1016/j.mcn.2013.06.003](https://doi.org/10.1016/j.mcn.2013.06.003) [Medline](#)
104. R. Kusano, K. Fujita, Y. Shinoda, Y. Nagaura, H. Kiyonari, T. Abe, T. Watanabe, Y. Matsui, M. Fukaya, H. Sakagami, T. Sato, J. I. Funahashi, M. Ohnishi, S. Tamura, T. Kobayashi, Targeted disruption of the mouse protein phosphatase *ppm1l* gene leads to structural abnormalities in the brain. *FEBS Lett.* **590**, 3606–3615 (2016). [doi:10.1002/1873-3468.12429](https://doi.org/10.1002/1873-3468.12429) [Medline](#)
105. M. Talarowska, J. Szemraj, M. Kowalczyk, P. Gałecki, Serum *KIBRA* mRNA and protein expression and cognitive functions in depression. *Med. Sci. Monit.* **22**, 152–160 (2016). [doi:10.12659/MSM.895200](https://doi.org/10.12659/MSM.895200) [Medline](#)
106. A. K. Pandey, L. Lu, X. Wang, R. Homayouni, R. W. Williams, Functionally enigmatic genes: A case study of the brain ignorome. *PLOS ONE* **9**, e88889 (2014). [doi:10.1371/journal.pone.0088889](https://doi.org/10.1371/journal.pone.0088889) [Medline](#)
107. A. Graziano, G. Foffani, E. B. Knudsen, J. Shumsky, K. A. Moxon, Passive exercise of the hind limbs after complete thoracic transection of the spinal cord promotes cortical reorganization. *PLOS ONE* **8**, e54350 (2013).
[doi:10.1371/journal.pone.0054350](https://doi.org/10.1371/journal.pone.0054350) [Medline](#)
108. H. Li, J. C. Radford, M. J. Ragusa, K. L. Shea, S. R. McKercher, J. D. Zaremba, W. Soussou, Z. Nie, Y. J. Kang, N. Nakanishi, S. Okamoto, A. J. Roberts, J. J. Schwarz, S. A. Lipton, Transcription factor *MEF2C* influences neural stem/progenitor cell differentiation and maturation *in vivo*. *Proc. Natl. Acad. Sci. U.S.A.* **105**, 9397–9402 (2008). [doi:10.1073/pnas.0802876105](https://doi.org/10.1073/pnas.0802876105) [Medline](#)
109. Y. Chang, O. Klezovitch, R. S. Walikonis, V. Vasioukhin, J. J. LoTurco, Discs large 5 is required for polarization of citron kinase in mitotic neural precursors. *Cell Cycle* **9**, 1990–1997 (2010). [doi:10.4161/cc.9.10.11730](https://doi.org/10.4161/cc.9.10.11730) [Medline](#)
110. M. R. Sarkisian, Discs large 5: a new regulator of Citron kinase localization in developing neocortex: comment on: Chang Y, et al. Cell Cycle 2010; 9:1990–7. *Cell Cycle* **9**, 1876 (2010). [doi:10.4161/cc.9.10.11923](https://doi.org/10.4161/cc.9.10.11923) [Medline](#)
111. D. A. Berg, L. Belnoue, H. Song, A. Simon, Neurotransmitter-mediated control of neurogenesis in the adult vertebrate brain. *Development* **140**, 2548–2561 (2013). [doi:10.1242/dev.088005](https://doi.org/10.1242/dev.088005) [Medline](#)
112. P. Levitt, J. A. Harvey, E. Friedman, K. Simansky, E. H. Murphy, New evidence for neurotransmitter influences on brain development. *Trends Neurosci.* **20**, 269–274 (1997). [doi:10.1016/S0166-2236\(96\)01028-4](https://doi.org/10.1016/S0166-2236(96)01028-4) [Medline](#)

113. L. Wang, X. You, S. Lotinun, L. Zhang, N. Wu, W. Zou, Mechanical sensing protein PIEZO1 regulates bone homeostasis via osteoblast-osteoclast crosstalk. *Nat. Commun.* **11**, 282 (2020). [doi:10.1038/s41467-019-14146-6](https://doi.org/10.1038/s41467-019-14146-6) [Medline](#)
114. M. Linder, M. Hecking, E. Glitzner, K. Zwerina, M. Holcmann, L. Bakiri, M. G. Ruocco, J. Tuckermann, G. Schett, E. F. Wagner, M. Sibilia, *EGFR* controls bone development by negatively regulating mTOR-signaling during osteoblast differentiation. *Cell Death Differ.* **25**, 1094–1106 (2018). [doi:10.1038/s41418-017-0054-7](https://doi.org/10.1038/s41418-017-0054-7) [Medline](#)
115. F. Xiao, C. Wang, C. Wang, Y. Gao, X. Zhang, X. Chen, *BMPER* enhances bone formation by promoting the osteogenesis-angiogenesis coupling process in mesenchymal stem cells. *Cell. Physiol. Biochem.* **45**, 1927–1939 (2018). [doi:10.1159/000487969](https://doi.org/10.1159/000487969) [Medline](#)
116. S. Zanotti, E. Canalis, *Notch1* and *Notch2* expression in osteoblast precursors regulates femoral microarchitecture. *Bone* **62**, 22–28 (2014). [doi:10.1016/j.bone.2014.01.023](https://doi.org/10.1016/j.bone.2014.01.023) [Medline](#)
117. J. M. Kim, C. Lin, Z. Stavre, M. B. Greenblatt, J. H. Shim, Osteoblast-osteoclast communication and bone homeostasis. *Cells* **9**, 2073 (2020). [doi:10.3390/cells9092073](https://doi.org/10.3390/cells9092073) [Medline](#)
118. S. Zanotti, E. Canalis, Notch signaling and the skeleton. *Endocr. Rev.* **37**, 223–253 (2016). [doi:10.1210/er.2016-1002](https://doi.org/10.1210/er.2016-1002) [Medline](#)
119. M. Schmidt, Locomotion and postural behaviour. *Adv. Sci. Res.* **5**, 23–39 (2011). [doi:10.5194/asr-5-23-2010](https://doi.org/10.5194/asr-5-23-2010)
120. Y. He, X. Luo, B. Zhou, T. Hu, X. Meng, P. A. Audano, Z. N. Kronenberg, E. E. Eichler, J. Jin, Y. Guo, Y. Yang, X. Qi, B. Su, Long-read assembly of the Chinese rhesus macaque genome and identification of ape-specific structural variants. *Nat. Commun.* **10**, 4233 (2019). [doi:10.1038/s41467-019-12174-w](https://doi.org/10.1038/s41467-019-12174-w) [Medline](#)
121. S. A. Williams, G. A. Russo, Evolution of the hominoid vertebral column: The long and the short of it. *Evol. Anthropol.* **24**, 15–32 (2015). [doi:10.1002/evan.21437](https://doi.org/10.1002/evan.21437) [Medline](#)
122. K. Semba, K. Araki, Z. Li, K. Matsumoto, M. Suzuki, N. Nakagata, K. Takagi, M. Takeya, K. Yoshinobu, M. Araki, K. Imai, K. Abe, K. Yamamura, A novel murine gene, Sickle tail, linked to the Danforth's short tail locus, is required for normal development of the intervertebral disc. *Genetics* **172**, 445–456 (2006). [doi:10.1534/genetics.105.048934](https://doi.org/10.1534/genetics.105.048934) [Medline](#)
123. N. Al Dhaheri, N. Wu, S. Zhao, Z. Wu, R. D. Blank, J. Zhang, C. Raggio, M. Halanski, J. Shen, K. Noonan, G. Qiu, B. Nemeth, S. Sund, S. L. Dunwoodie, G. Chapman, I. Glurich, R. D. Steiner, E. Wohler, R. Martin, N. L. Sobreira,

- P. F. Giampietro, *KIAA1217*: A novel candidate gene associated with isolated and syndromic vertebral malformations. *Am. J. Med. Genet. A.* **182**, 1664–1672 (2020). [doi:10.1002/ajmg.a.61607](https://doi.org/10.1002/ajmg.a.61607) [Medline](#)
124. J. R. Usherwood, J. E. Bertram, Understanding brachiation: Insight from a collisional perspective. *J. Exp. Biol.* **206**, 1631–1642 (2003). [doi:10.1242/jeb.00306](https://doi.org/10.1242/jeb.00306) [Medline](#)
125. J. R. Usherwood, S. G. Larson, J. E. Bertram, Mechanisms of force and power production in unsteady ricochet brachiation. *Am. J. Phys. Anthropol.* **120**, 364–372 (2003). [doi:10.1002/ajpa.10133](https://doi.org/10.1002/ajpa.10133) [Medline](#)
126. S. M. Cheyne, “Gibbon locomotion research in the field: Problems, possibilities, and benefits for conservation,” in *Primate Locomotion: Linking Field and Laboratory Research*, K. D’Août, E. E. Vereecke, Eds. (Springer, NY, 2011), pp. 201–213.
127. C. Thiel, K. Kessler, A. Giessl, A. Dimmler, S. A. Shalev, S. von der Haar, M. Zenker, D. Zahnleiter, H. Stöss, E. Beinder, R. Abou Jamra, A. B. Ekici, N. Schröder-Kress, T. Aigner, T. Kirchner, A. Reis, J. H. Brandstätter, A. Rauch, *NEK1* mutations cause short-rib polydactyly syndrome type majewski. *Am. J. Hum. Genet.* **88**, 106–114 (2011). [doi:10.1016/j.ajhg.2010.12.004](https://doi.org/10.1016/j.ajhg.2010.12.004) [Medline](#)
128. J. El Hokayem, C. Huber, A. Couvé, J. Aziza, G. Baujat, R. Bouvier, D. P. Cavalcanti, F. A. Collins, M.-P. Cordier, A.-L. Delezoide, M. Gonzales, D. Johnson, M. Le Merrer, A. Levy-Mozziconacci, P. Loget, D. Martin-Coignard, J. Martinovic, G. R. Mortier, M.-J. Perez, J. Roume, G. Scarano, A. Munnich, V. Cormier-Daire, *NEK1* and *DYNC2H1* are both involved in short rib polydactyly Majewski type but not in Beemer Langer cases. *J. Med. Genet.* **49**, 227–233 (2012). [doi:10.1136/jmedgenet-2011-100717](https://doi.org/10.1136/jmedgenet-2011-100717) [Medline](#)
129. J. M. Vazquez, V. J. Lynch, Pervasive duplication of tumor suppressors in Afrotherians during the evolution of large bodies and reduced cancer risk. *eLife* **10**, e65041 (2021). [doi:10.7554/eLife.65041](https://doi.org/10.7554/eLife.65041) [Medline](#)
130. J. G. M. Thewissen, L. N. Cooper, J. C. George, S. Bajpai, From land to water: The origin of whales, dolphins, and porpoises. *Evolution (N. Y.)* **2**, 272–288 (2009). [doi:10.1007/s12052-009-0135-2](https://doi.org/10.1007/s12052-009-0135-2)
131. W. L. Junger, “Body size and scaling of limb proportions in primates,” in *Size and Scaling in Primate Biology*, W. L. Junger, Ed. (Springer, 1985), pp. 345–381.
132. A. M. Rudolf, Q. Wu, L. Li, J. Wang, Y. Huang, J. Togo, C. Liechti, M. Li, C. Niu, Y. Nie, F. Wei, J. R. Speakman, A single nucleotide mutation in the dual-oxidase 2 (*DUOX2*) gene causes some of the panda’s unique metabolic phenotypes. *Natl. Sci. Rev.* **9**, nwab125 (2021). [doi:10.1093/nsr/nwab125](https://doi.org/10.1093/nsr/nwab125) [Medline](#)

133. K. R. Johnson, C. C. Marden, P. Ward-Bailey, L. H. Gagnon, R. T. Bronson, L. R. Donahue, Congenital hypothyroidism, dwarfism, and hearing impairment caused by a missense mutation in the mouse dual oxidase 2 gene, *Duo2*. *Mol. Endocrinol.* **21**, 1593–1602 (2007). [doi:10.1210/me.2007-0085](https://doi.org/10.1210/me.2007-0085) [Medline](#)
134. J. G. Fleagle, *Primate Adaptation and Evolution* (Academic, 2013).
135. K. Milton, Physiological ecology of howlers (*Alouatta*): Energetic and digestive considerations and comparison with the Colobinae. *Int. J. Primatol.* **19**, 513–548 (1998). [doi:10.1023/A:1020364523213](https://doi.org/10.1023/A:1020364523213)
136. I. Matsuda, C. A. Chapman, M. Clauss, Colobine forestomach anatomy and diet. *J. Morphol.* **280**, 1608–1616 (2019). [doi:10.1002/jmor.21052](https://doi.org/10.1002/jmor.21052) [Medline](#)
137. M. C. Janiak, Digestive enzymes of human and nonhuman primates. *Evol. Anthropol.* **25**, 253–266 (2016). [doi:10.1002/evan.21498](https://doi.org/10.1002/evan.21498) [Medline](#)
138. J. J. Kim, R. Miura, Acyl-CoA dehydrogenases and acyl-CoA oxidases. Structural basis for mechanistic similarities and differences. *Eur. J. Biochem.* **271**, 483–493 (2004). [doi:10.1046/j.1432-1033.2003.03948.x](https://doi.org/10.1046/j.1432-1033.2003.03948.x) [Medline](#)
139. C. Matziouridou, S. D. C. Rocha, O. A. Haabeth, K. Rudi, H. Carlsen, A. Kielland, iNOS- and NOX1-dependent ROS production maintains bacterial homeostasis in the ileum of mice. *Mucosal Immunol.* **11**, 774–784 (2018). [doi:10.1038/mi.2017.106](https://doi.org/10.1038/mi.2017.106) [Medline](#)
140. C.-J. Li, R. W. Li, R. L. Baldwin Vi, Assembly and analysis of changes in transcriptomes of dairy cattle rumen epithelia during lactation and dry periods. *Agric. Sci.* **9**, 619–638 (2018).
141. M. C. Janiak, A. S. Burrell, J. D. Orkin, T. R. Disotell, Duplication and parallel evolution of the pancreatic ribonuclease gene (*RNASE1*) in folivorous non-colobine primates, the howler monkeys (*Alouatta spp.*). *Sci. Rep.* **9**, 20366 (2019). [doi:10.1038/s41598-019-56941-7](https://doi.org/10.1038/s41598-019-56941-7) [Medline](#)
142. P. Pontarotti, *Evolutionary Biology: Mechanisms and Trends* (Springer, 2012).
143. N. J. Dominy, P. W. Lucas, Ecological importance of trichromatic vision to primates. *Nature* **410**, 363–366 (2001). [doi:10.1038/35066567](https://doi.org/10.1038/35066567) [Medline](#)
144. N. G. Caine, N. I. Mundy, Demonstration of a foraging advantage for trichromatic marmosets (*Callithrix geoffroyi*) dependent on food colour. *Proc. Biol. Sci.* **267**, 439–444 (2000). [doi:10.1098/rspb.2000.1019](https://doi.org/10.1098/rspb.2000.1019) [Medline](#)
145. A. C. Smith, H. M. Buchanan-Smith, A. K. Surridge, D. Osorio, N. I. Mundy, The effect of colour vision status on the detection and selection of fruits by tamarins (*Saguinus spp.*). *J. Exp. Biol.* **206**, 3159–3165 (2003). [doi:10.1242/jeb.00536](https://doi.org/10.1242/jeb.00536) [Medline](#)
146. S. Heritage, Modeling olfactory bulb evolution through primate phylogeny. *PLOS ONE* **9**, e113904 (2014). [doi:10.1371/journal.pone.0113904](https://doi.org/10.1371/journal.pone.0113904) [Medline](#)

147. A. Matsui, Y. Go, Y. Niimura, Degeneration of olfactory receptor gene repertoires in primates: No direct link to full trichromatic vision. *Mol. Biol. Evol.* **27**, 1192–1200 (2010). [doi:10.1093/molbev/msq003](https://doi.org/10.1093/molbev/msq003) [Medline](#)
148. T. D. Smith, K. P. Bhatnagar, Microsmotic primates: Reconsidering how and when size matters. *Anat. Rec. B New Anat.* **279**, 24–31 (2004). [doi:10.1002/ar.b.20026](https://doi.org/10.1002/ar.b.20026) [Medline](#)
149. A. Berghard, A. C. Hägglund, S. Bohm, L. Carlsson, *Lhx2*-dependent specification of olfactory sensory neurons is required for successful integration of olfactory, vomeronasal, and GnRH neurons. *FASEB J.* **26**, 3464–3472 (2012). [doi:10.1096/fj.12-206193](https://doi.org/10.1096/fj.12-206193) [Medline](#)
150. J. Hirota, P. Mombaerts, The LIM-homeodomain protein *Lhx2* is required for complete development of mouse olfactory sensory neurons. *Proc. Natl. Acad. Sci. U.S.A.* **101**, 8751–8755 (2004). [doi:10.1073/pnas.0400940101](https://doi.org/10.1073/pnas.0400940101) [Medline](#)
151. H. Li, R. Durbin, Inference of human population history from individual whole-genome sequences. *Nature* **475**, 493–496 (2011). [doi:10.1038/nature10231](https://doi.org/10.1038/nature10231) [Medline](#)
152. A. D. Barnosky, P. L. Koch, R. S. Feranec, S. L. Wing, A. B. Shabel, Assessing the causes of late Pleistocene extinctions on the continents. *Science* **306**, 70–75 (2004). [doi:10.1126/science.1101476](https://doi.org/10.1126/science.1101476) [Medline](#)
153. X. Luo, Y. Liu, D. Dang, T. Hu, Y. Hou, X. Meng, F. Zhang, T. Li, C. Wang, M. Li, H. Wu, Q. Shen, Y. Hu, X. Zeng, X. He, L. Yan, S. Zhang, C. Li, B. Su 3rd, 3D Genome of macaque fetal brain reveals evolutionary innovations during primate corticogenesis. *Cell* **184**, 723–740.e21 (2021). [doi:10.1016/j.cell.2021.01.001](https://doi.org/10.1016/j.cell.2021.01.001) [Medline](#)
154. C. Yang, Y. Zhou, S. Marcus, G. Formenti, L. A. Bergeron, Z. Song, X. Bi, J. Bergman, M. M. C. Rousselle, C. Zhou, L. Zhou, Y. Deng, M. Fang, D. Xie, Y. Zhu, S. Tan, J. Mountcastle, B. Haase, J. Balacco, J. Wood, W. Chow, A. Rhy, M. Pippel, M. M. Fabiszak, S. Koren, O. Fedrigo, W. A. Freiwald, K. Howe, H. Yang, A. M. Phillippy, M. H. Schierup, E. D. Jarvis, G. Zhang, Evolutionary and biomedical insights from a marmoset diploid genome assembly. *Nature* **594**, 227–233 (2021). [doi:10.1038/s41586-021-03535-x](https://doi.org/10.1038/s41586-021-03535-x) [Medline](#)
155. G. Dumas, S. Malesys, T. Bourgeron, Systematic detection of brain protein-coding genes under positive selection during primate evolution and their roles in cognition. *Genome Res.* **31**, 484–496 (2021). [doi:10.1101/gr.262113.120](https://doi.org/10.1101/gr.262113.120) [Medline](#)
156. J. K. Rilling, Human and nonhuman primate brains: Are they allometrically scaled versions of the same design? *Evol. Anthropol.* **15**, 65–77 (2006). [doi:10.1002/evan.20095](https://doi.org/10.1002/evan.20095)

157. H. Stephan, H. Frahm, G. Baron, New and revised data on volumes of brain structures in insectivores and primates. *Folia Primatol. (Basel)* **35**, 1–29 (1981). [doi:10.1159/000155963](https://doi.org/10.1159/000155963) [Medline](#)
158. Genome annotation GFF files at Mendeley Data for: Y. Shao, L. Zhou, F. Li, L. Zhao, B.-L. Zhang, F. Shao, J.-W. Chen, C.-Y. Chen, X.-P. Bi, X.-L. Zhuang, H.-L. Zhu, J. Hu, Z. Sun, X. Li, D. Wang, I. Rivas-González, S. Wang, Y.-M. Wang, W. Chen, G. Li, H.-M. Lu, Y. Liu, L. F. K. Kuderna, K. K.-H. Farh, P.-F. Fan, L. Yu, M. Li, Z.-J. Liu, G. P. Tiley, A. D. Yoder, C. Roos, T. Hayakawa, T. Marques-Bonet, J. Rogers, P. D. Stenson, D. N. Cooper, M. H. Schierup, Y.-G. Yao, Y.-P. Zhang, W. Wang, X.-G. Qi, G. Zhang, D.-D. Wu, Phylogenomic analyses provide insights into primate evolution, Mendeley (2023); <https://doi.org/10.17632/87bh23zxj2.1>.
159. Genome annotation GFF files at Figshare for: Y. Shao, L. Zhou, F. Li, L. Zhao, B.-L. Zhang, F. Shao, J.-W. Chen, C.-Y. Chen, X.-P. Bi, X.-L. Zhuang, H.-L. Zhu, J. Hu, Z. Sun, X. Li, D. Wang, I. Rivas-González, S. Wang, Y.-M. Wang, W. Chen, G. Li, H.-M. Lu, Y. Liu, L. F. K. Kuderna, K. K.-H. Farh, P.-F. Fan, L. Yu, M. Li, Z.-J. Liu, G. P. Tiley, A. D. Yoder, C. Roos, T. Hayakawa, T. Marques-Bonet, J. Rogers, P. D. Stenson, D. N. Cooper, M. H. Schierup, Y.-G. Yao, Y.-P. Zhang, W. Wang, X.-G. Qi, G. Zhang, D.-D. Wu, Phylogenomic analyses provide insights into primate evolution, Figshare (2023); <https://doi.org/10.6084/m9.figshare.21692894.v1>.
160. Gene sequences for: Y. Shao, L. Zhou, F. Li, L. Zhao, B.-L. Zhang, F. Shao, J.-W. Chen, C.-Y. Chen, X.-P. Bi, X.-L. Zhuang, H.-L. Zhu, J. Hu, Z. Sun, X. Li, D. Wang, I. Rivas-González, S. Wang, Y.-M. Wang, W. Chen, G. Li, H.-M. Lu, Y. Liu, L. F. K. Kuderna, K. K.-H. Farh, P.-F. Fan, L. Yu, M. Li, Z.-J. Liu, G. P. Tiley, A. D. Yoder, C. Roos, T. Hayakawa, T. Marques-Bonet, J. Rogers, P. D. Stenson, D. N. Cooper, M. H. Schierup, Y.-G. Yao, Y.-P. Zhang, W. Wang, X.-G. Qi, G. Zhang, D.-D. Wu, Phylogenomic analyses provide insights into primate evolution, Dryad (2023); <https://doi.org/10.5061/dryad.8w9ghx3qj>.
161. J. Ruan, H. Li, Fast and accurate long-read assembly with wtdbg2. *Nat. Methods* **17**, 155–158 (2020). [doi:10.1038/s41592-019-0669-3](https://doi.org/10.1038/s41592-019-0669-3) [Medline](#)
162. C.-S. Chin, P. Peluso, F. J. Sedlazeck, M. Nattestad, G. T. Concepcion, A. Clum, C. Dunn, R. O’Malley, R. Figueroa-Balderas, A. Morales-Cruz, G. R. Cramer, M. Delledonne, C. Luo, J. R. Ecker, D. Cantu, D. R. Rank, M. C. Schatz, Phased diploid genome assembly with single-molecule real-time sequencing. *Nat. Methods* **13**, 1050–1054 (2016). [doi:10.1038/nmeth.4035](https://doi.org/10.1038/nmeth.4035) [Medline](#)
163. H. Li, R. Durbin, Fast and accurate short read alignment with Burrows-Wheeler transform. *Bioinformatics* **25**, 1754–1760 (2009). [doi:10.1093/bioinformatics/btp324](https://doi.org/10.1093/bioinformatics/btp324) [Medline](#)

164. F. A. Simão, R. M. Waterhouse, P. Ioannidis, E. V. Kriventseva, E. M. Zdobnov, BUSCO: Assessing genome assembly and annotation completeness with single-copy orthologs. *Bioinformatics* **31**, 3210–3212 (2015). [doi:10.1093/bioinformatics/btv351](https://doi.org/10.1093/bioinformatics/btv351) [Medline](#)
165. G. Benson, Tandem repeats finder: A program to analyze DNA sequences. *Nucleic Acids Res.* **27**, 573–580 (1999). [doi:10.1093/nar/27.2.573](https://doi.org/10.1093/nar/27.2.573) [Medline](#)
166. J. Ye, S. McGinnis, T. L. Madden, BLAST: Improvements for better sequence analysis. *Nucleic Acids Res.* **34**, W6–W9 (2006). [doi:10.1093/nar/gkl164](https://doi.org/10.1093/nar/gkl164) [Medline](#)
167. R. She, J. S. Chu, K. Wang, J. Pei, N. Chen, GenBlastA: Enabling BLAST to identify homologous gene sequences. *Genome Res.* **19**, 143–149 (2009). [doi:10.1101/gr.082081.108](https://doi.org/10.1101/gr.082081.108) [Medline](#)
168. E. Birney, M. Clamp, R. Durbin, GeneWise and Genomewise. *Genome Res.* **14**, 988–995 (2004). [doi:10.1101/gr.1865504](https://doi.org/10.1101/gr.1865504) [Medline](#)
169. M. Stanke, S. Waack, Gene prediction with a hidden Markov model and a new intron submodel. *Bioinformatics* **19**, ii215–ii225 (2003). [doi:10.1093/bioinformatics/btg1080](https://doi.org/10.1093/bioinformatics/btg1080) [Medline](#)
170. S. Hunter, R. Apweiler, T. K. Attwood, A. Bairoch, A. Bateman, D. Binns, P. Bork, U. Das, L. Daugherty, L. Duquenne, R. D. Finn, J. Gough, D. Haft, N. Hulo, D. Kahn, E. Kelly, A. Laugraud, I. Letunic, D. Lonsdale, R. Lopez, M. Madera, J. Maslen, C. McAnulla, J. McDowall, J. Mistry, A. Mitchell, N. Mulder, D. Natale, C. Orengo, A. F. Quinn, J. D. Selengut, C. J. A. Sigrist, M. Thimma, P. D. Thomas, F. Valentin, D. Wilson, C. H. Wu, C. Yeats, InterPro: The integrative protein signature database. *Nucleic Acids Res.* **37**, D211–D215 (2009). [doi:10.1093/nar/gkn785](https://doi.org/10.1093/nar/gkn785) [Medline](#)
171. M. Blanchette, W. J. Kent, C. Riemer, L. Elnitski, A. F. Smit, K. M. Roskin, R. Baertsch, K. Rosenbloom, H. Clawson, E. D. Green, D. Haussler, W. Miller, Aligning multiple genomic sequences with the threaded blockset aligner. *Genome Res.* **14**, 708–715 (2004). [doi:10.1101/gr.1933104](https://doi.org/10.1101/gr.1933104) [Medline](#)
172. J. Gatesy, R. H. Baker, Hidden likelihood support in genomic data: Can forty-five wrongs make a right? *Syst. Biol.* **54**, 483–492 (2005). [doi:10.1080/10635150590945368](https://doi.org/10.1080/10635150590945368) [Medline](#)
173. L. S. Kubatko, J. H. Degnan, Inconsistency of phylogenetic estimates from concatenated data under coalescence. *Syst. Biol.* **56**, 17–24 (2007). [doi:10.1080/10635150601146041](https://doi.org/10.1080/10635150601146041) [Medline](#)
174. C. Zhang, M. Rabiee, E. Sayyari, S. Mirarab, ASTRAL-III: Polynomial time species tree reconstruction from partially resolved gene trees. *BMC Bioinformatics* **19**, 153 (2018). [doi:10.1186/s12859-018-2129-y](https://doi.org/10.1186/s12859-018-2129-y) [Medline](#)

175. Y. Fan, M. S. Ye, J. Y. Zhang, L. Xu, D. D. Yu, T. L. Gu, Y. L. Yao, J. Q. Chen, L. B. Lv, P. Zheng, D. D. Wu, G. J. Zhang, Y. G. Yao, Chromosomal level assembly and population sequencing of the Chinese tree shrew genome. *Zool. Res.* **40**, 506–521 (2019). [doi:10.24272/j.issn.2095-8137.2019.063](https://doi.org/10.24272/j.issn.2095-8137.2019.063) [Medline](#)
176. A. Stamatakis, RAxML version 8: A tool for phylogenetic analysis and post-analysis of large phylogenies. *Bioinformatics* **30**, 1312–1313 (2014). [doi:10.1093/bioinformatics/btu033](https://doi.org/10.1093/bioinformatics/btu033) [Medline](#)
177. M. J. Hubisz, K. S. Pollard, A. Siepel, PHAST and RPHAST: Phylogenetic analysis with space/time models. *Brief. Bioinform.* **12**, 41–51 (2011). [doi:10.1093/bib/bbq072](https://doi.org/10.1093/bib/bbq072) [Medline](#)
178. R. S. Harris, “Improved pairwise alignment of genomic DNA,” The Pennsylvania State University, University Park, PA (2007).
179. B. R. Jones, A. Rajaraman, E. Tannier, C. Chauve, ANGES: Reconstructing ANcestral GEnomeS maps. *Bioinformatics* **28**, 2388–2390 (2012). [doi:10.1093/bioinformatics/bts457](https://doi.org/10.1093/bioinformatics/bts457) [Medline](#)
180. G. Tesler, GRIMM: Genome rearrangements web server. *Bioinformatics* **18**, 492–493 (2002). [doi:10.1093/bioinformatics/18.3.492](https://doi.org/10.1093/bioinformatics/18.3.492) [Medline](#)
181. B. S. Emanuel, T. H. Shaikh, Segmental duplications: An ‘expanding’ role in genomic instability and disease. *Nat. Rev. Genet.* **2**, 791–800 (2001). [doi:10.1038/35093500](https://doi.org/10.1038/35093500) [Medline](#)
182. R. V. Samonte, E. E. Eichler, Segmental duplications and the evolution of the primate genome. *Nat. Rev. Genet.* **3**, 65–72 (2002). [doi:10.1038/nrg705](https://doi.org/10.1038/nrg705) [Medline](#)
183. J. A. Bailey, Z. Gu, R. A. Clark, K. Reinert, R. V. Samonte, S. Schwartz, M. D. Adams, E. W. Myers, P. W. Li, E. E. Eichler, Recent segmental duplications in the human genome. *Science* **297**, 1003–1007 (2002). [doi:10.1126/science.1072047](https://doi.org/10.1126/science.1072047) [Medline](#)
184. F. Delehelle, S. Cussat-Blanc, J. M. Alliot, H. Luga, P. Balaresque, ASGART: Fast and parallel genome scale segmental duplications mapping. *Bioinformatics* **34**, 2708–2714 (2018). [doi:10.1093/bioinformatics/bty172](https://doi.org/10.1093/bioinformatics/bty172) [Medline](#)
185. E. B. Chuong, N. C. Elde, C. Feschotte, Regulatory activities of transposable elements: From conflicts to benefits. *Nat. Rev. Genet.* **18**, 71–86 (2017). [doi:10.1038/nrg.2016.139](https://doi.org/10.1038/nrg.2016.139) [Medline](#)
186. S. J. Thomson, F. G. Goh, H. Banks, T. Krausgruber, S. V. Kotenko, B. M. Foxwell, I. A. Udalova, The role of transposable elements in the regulation of IFN-lambda1 gene expression. *Proc. Natl. Acad. Sci. U.S.A.* **106**, 11564–11569 (2009). [doi:10.1073/pnas.0904477106](https://doi.org/10.1073/pnas.0904477106) [Medline](#)

187. P. É. Jacques, J. Jeyakani, G. Bourque, The majority of primate-specific regulatory sequences are derived from transposable elements. *PLOS Genet.* **9**, e1003504 (2013). [doi:10.1371/journal.pgen.1003504](https://doi.org/10.1371/journal.pgen.1003504) [Medline](#)
188. Y. Huang, B. Niu, Y. Gao, L. Fu, W. Li, CD-HIT Suite: A web server for clustering and comparing biological sequences. *Bioinformatics* **26**, 680–682 (2010). [doi:10.1093/bioinformatics/btq003](https://doi.org/10.1093/bioinformatics/btq003) [Medline](#)
189. GTEx Consortium, The genotype-tissue expression (GTEx) project. *Nat. Genet.* **45**, 580–585 (2013). [doi:10.1038/ng.2653](https://doi.org/10.1038/ng.2653) [Medline](#)
190. R. C. Edgar, MUSCLE: Multiple sequence alignment with high accuracy and high throughput. *Nucleic Acids Res.* **32**, 1792–1797 (2004). [doi:10.1093/nar/gkh340](https://doi.org/10.1093/nar/gkh340) [Medline](#)
191. J. Castresana, Selection of conserved blocks from multiple alignments for their use in phylogenetic analysis. *Mol. Biol. Evol.* **17**, 540–552 (2000). [doi:10.1093/oxfordjournals.molbev.a026334](https://doi.org/10.1093/oxfordjournals.molbev.a026334) [Medline](#)
192. G. Talavera, J. Castresana, Improvement of phylogenies after removing divergent and ambiguously aligned blocks from protein sequence alignments. *Syst. Biol.* **56**, 564–577 (2007). [doi:10.1080/10635150701472164](https://doi.org/10.1080/10635150701472164) [Medline](#)
193. H. Li, A. Coghlan, J. Ruan, L. J. Coin, J. K. Hériché, L. Osmotherly, R. Li, T. Liu, Z. Zhang, L. Bolund, G. K. Wong, W. Zheng, P. Dehal, J. Wang, R. Durbin, TreeFam: A curated database of phylogenetic trees of animal gene families. *Nucleic Acids Res.* **34**, D572–D580 (2006). [doi:10.1093/nar/gkj118](https://doi.org/10.1093/nar/gkj118) [Medline](#)
194. E. B. Kim, X. Fang, A. A. Fushan, Z. Huang, A. V. Lobanov, L. Han, S. M. Marino, X. Sun, A. A. Turanov, P. Yang, S. H. Yim, X. Zhao, M. V. Kasaikina, N. Stoletzki, C. Peng, P. Polak, Z. Xiong, A. Kiezun, Y. Zhu, Y. Chen, G. V. Kryukov, Q. Zhang, L. Peshkin, L. Yang, R. T. Bronson, R. Buffenstein, B. Wang, C. Han, Q. Li, L. Chen, W. Zhao, S. R. Sunyaev, T. J. Park, G. Zhang, J. Wang, V. N. Gladyshev, Genome sequencing reveals insights into physiology and longevity of the naked mole rat. *Nature* **479**, 223–227 (2011). [doi:10.1038/nature10533](https://doi.org/10.1038/nature10533) [Medline](#)
195. T. De Bie, N. Cristianini, J. P. Demuth, M. W. Hahn, CAFE: A computational tool for the study of gene family evolution. *Bioinformatics* **22**, 1269–1271 (2006). [doi:10.1093/bioinformatics/btl097](https://doi.org/10.1093/bioinformatics/btl097) [Medline](#)
196. Y. Benjamini, Y. Hochberg, Controlling the false discovery rate: A practical and powerful approach to multiple testing. *J. R. Stat. Soc. B* **57**, 289–300 (1995). [doi:10.1111/j.2517-6161.1995.tb02031.x](https://doi.org/10.1111/j.2517-6161.1995.tb02031.x)
197. X. Jiao, B. T. Sherman, W. Huang, R. Stephens, M. W. Baseler, H. C. Lane, R. A. Lempicki, DAVID-WS: A stateful web service to facilitate gene/protein list

- analysis. *Bioinformatics* **28**, 1805–1806 (2012).
[doi:10.1093/bioinformatics/bts251](https://doi.org/10.1093/bioinformatics/bts251) [Medline](#)
198. W. Huang, B. T. Sherman, R. A. Lempicki, Systematic and integrative analysis of large gene lists using DAVID bioinformatics resources. *Nat. Protoc.* **4**, 44–57 (2009). [doi:10.1038/nprot.2008.211](https://doi.org/10.1038/nprot.2008.211) [Medline](#)
199. W. Huang, B. T. Sherman, R. A. Lempicki, Bioinformatics enrichment tools: Paths toward the comprehensive functional analysis of large gene lists. *Nucleic Acids Res.* **37**, 1–13 (2009). [doi:10.1093/nar/gkn923](https://doi.org/10.1093/nar/gkn923) [Medline](#)
200. W. Huang, B. T. Sherman, X. Zheng, J. Yang, T. Imamichi, R. Stephens, R. A. Lempicki, Extracting biological meaning from large gene lists with DAVID. *Curr. Protoc. Bioinformatics Chapter 13*, Unit 13.11 (2009).
[doi:10.1002/0471250953.bi1311s27](https://doi.org/10.1002/0471250953.bi1311s27) [Medline](#)
201. W. Huang, B. T. Sherman, R. Stephens, M. W. Baseler, H. C. Lane, R. A. Lempicki, DAVID gene ID conversion tool. *Bioinformation* **2**, 428–430 (2008). [doi:10.6026/97320630002428](https://doi.org/10.6026/97320630002428) [Medline](#)
202. B. T. Sherman, W. Huang, Q. Tan, Y. Guo, S. Bour, D. Liu, R. Stephens, M. W. Baseler, H. C. Lane, R. A. Lempicki, DAVID Knowledgebase: A gene-centered database integrating heterogeneous gene annotation resources to facilitate high-throughput gene functional analysis. *BMC Bioinformatics* **8**, 426 (2007). [doi:10.1186/1471-2105-8-426](https://doi.org/10.1186/1471-2105-8-426) [Medline](#)
203. G. Dennis Jr., B. T. Sherman, D. A. Hosack, J. Yang, W. Gao, H. C. Lane, R. A. Lempicki, DAVID: Database for annotation, visualization, and integrated discovery. *Genome Biol.* **4**, P3 (2003). [doi:10.1186/gb-2003-4-5-p3](https://doi.org/10.1186/gb-2003-4-5-p3) [Medline](#)
204. D. A. Hosack, G. Dennis Jr., B. T. Sherman, H. C. Lane, R. A. Lempicki, Identifying biological themes within lists of genes with EASE. *Genome Biol.* **4**, R70 (2003). [doi:10.1186/gb-2003-4-10-r70](https://doi.org/10.1186/gb-2003-4-10-r70) [Medline](#)
205. H. Li, Aligning sequence reads, clone sequences and assembly contigs with BWA-MEM. [arXiv:1303.3997](https://arxiv.org/abs/1303.3997) [q-bio.GN] (2013).
206. H. Li, A statistical framework for SNP calling, mutation discovery, association mapping and population genetical parameter estimation from sequencing data. *Bioinformatics* **27**, 2987–2993 (2011). [doi:10.1093/bioinformatics/btr509](https://doi.org/10.1093/bioinformatics/btr509) [Medline](#)
207. M. A. DePristo, E. Banks, R. Poplin, K. V. Garimella, J. R. Maguire, C. Hartl, A. Philippakis, G. del Angel, M. A. Rivas, M. Hanna, A. McKenna, T. J. Fennell, A. M. Kernytsky, A. Y. Sivachenko, K. Cibulskis, S. B. Gabriel, D. Altshuler, M. J. Daly, A framework for variation discovery and genotyping using next-generation DNA sequencing data. *Nat. Genet.* **43**, 491–498 (2011). [doi:10.1038/ng.806](https://doi.org/10.1038/ng.806) [Medline](#)

208. A. R. Quinlan, I. M. Hall, BEDTools: A flexible suite of utilities for comparing genomic features. *Bioinformatics* **26**, 841–842 (2010).
[doi:10.1093/bioinformatics/btq033](https://doi.org/10.1093/bioinformatics/btq033) [Medline](#)
209. P. Danecek, A. Auton, G. Abecasis, C. A. Albers, E. Banks, M. A. DePristo, R. E. Handsaker, G. Lunter, G. T. Marth, S. T. Sherry, G. McVean, R. Durbin; 1000 Genomes Project Analysis Group, The variant call format and VCFtools. *Bioinformatics* **27**, 2156–2158 (2011). [doi:10.1093/bioinformatics/btr330](https://doi.org/10.1093/bioinformatics/btr330) [Medline](#)
210. M. Hasegawa, H. Kishino, T. Yano, Dating of the human-ape splitting by a molecular clock of mitochondrial DNA. *J. Mol. Evol.* **22**, 160–174 (1985).
[doi:10.1007/BF02101694](https://doi.org/10.1007/BF02101694) [Medline](#)
211. S. Kumar, G. Stecher, K. Tamura, MEGA7: Molecular evolutionary genetics analysis version 7.0 for bigger datasets. *Mol. Biol. Evol.* **33**, 1870–1874 (2016). [doi:10.1093/molbev/msw054](https://doi.org/10.1093/molbev/msw054) [Medline](#)
212. N. C. Durand, M. S. Shamim, I. Machol, S. S. Rao, M. H. Huntley, E. S. Lander, E. L. Aiden, Juicer provides a one-click system for analyzing loop-resolution Hi-C experiments. *Cell Syst.* **3**, 95–98 (2016). [doi:10.1016/j.cels.2016.07.002](https://doi.org/10.1016/j.cels.2016.07.002) [Medline](#)
213. N. Abdennur, L. A. Mirny, Cooler: Scalable storage for Hi-C data and other genomically labeled arrays. *Bioinformatics* **36**, 311–316 (2020).
[doi:10.1093/bioinformatics/btz540](https://doi.org/10.1093/bioinformatics/btz540) [Medline](#)
214. F. Ramírez, V. Bhardwaj, L. Arrigoni, K. C. Lam, B. A. Grüning, J. Villaveces, B. Habermann, A. Akhtar, T. Manke, High-resolution TADs reveal DNA sequences underlying genome organization in flies. *Nat. Commun.* **9**, 189 (2018). [doi:10.1038/s41467-017-02525-w](https://doi.org/10.1038/s41467-017-02525-w) [Medline](#)
215. S. I. Perez, M. F. Tejedor, N. M. Novo, L. Aristide, Divergence times and the evolutionary radiation of New World monkeys (Platyrrhini, Primates): An analysis of fossil and molecular data. *PLOS ONE* **8**, e68029 (2013).
[doi:10.1371/journal.pone.0068029](https://doi.org/10.1371/journal.pone.0068029) [Medline](#)
216. J. Eriksson, H. Siedel, D. Lukas, M. Kayser, A. Erler, C. Hashimoto, G. Hohmann, C. Boesch, L. Vigilant, Y-chromosome analysis confirms highly sex-biased dispersal and suggests a low male effective population size in bonobos (*Pan paniscus*). *Mol. Ecol.* **15**, 939–949 (2006). [doi:10.1111/j.1365-294X.2006.02845.x](https://doi.org/10.1111/j.1365-294X.2006.02845.x) [Medline](#)
217. M. E. Steiper, Population history, biogeography, and taxonomy of orangutans (Genus: *Pongo*) based on a population genetic meta-analysis of multiple loci. *J. Hum. Evol.* **50**, 509–522 (2006). [doi:10.1016/j.jhevol.2005.12.005](https://doi.org/10.1016/j.jhevol.2005.12.005) [Medline](#)

218. Y. Zhang, O. A. Ryder, Y. Zhang, Genetic divergence of orangutan subspecies (*Pongo pygmaeus*). *J. Mol. Evol.* **52**, 516–526 (2001).
[doi:10.1007/s002390010182](https://doi.org/10.1007/s002390010182) [Medline](#)
219. S. K. Kim, L. Carbone, C. Becquet, A. R. Mootnick, D. J. Li, P. J. de Jong, J. D. Wall, Patterns of genetic variation within and between Gibbon species. *Mol. Biol. Evol.* **28**, 2211–2218 (2011). [doi:10.1093/molbev/msr033](https://doi.org/10.1093/molbev/msr033) [Medline](#)
220. Z. Fan, G. Zhao, P. Li, N. Osada, J. Xing, Y. Yi, L. Du, P. Silva, H. Wang, R. Sakate, X. Zhang, H. Xu, B. Yue, J. Li, Whole-genome sequencing of tibetan macaque (*Macaca Thibetana*) provides new insight into the macaque evolutionary history. *Mol. Biol. Evol.* **31**, 1475–1489 (2014).
[doi:10.1093/molbev/msu104](https://doi.org/10.1093/molbev/msu104) [Medline](#)
221. X. Zhang, Q. Zhang, B. Su, Emergence and evolution of inter-specific segregating retrocopies in cynomolgus monkey (*Macaca fascicularis*) and rhesus macaque (*Macaca mulatta*). *Sci. Rep.* **6**, 32598 (2016).
[doi:10.1038/srep32598](https://doi.org/10.1038/srep32598) [Medline](#)
222. J. Rogers, M. Raveendran, R. A. Harris, T. Mailund, K. Leppälä, G. Athanasiadis, M. H. Schierup, J. Cheng, K. Munch, J. A. Walker, M. K. Konkel, V. Jordan, C. J. Steely, T. O. Beckstrom, C. Bergey, A. Burrell, D. Schrempf, A. Noll, M. Kothe, G. H. Kopp, Y. Liu, S. Murali, K. Billis, F. J. Martin, M. Muffato, L. Cox, J. Else, T. Disotell, D. M. Muzny, J. Phillips-Conroy, B. Aken, E. E. Eichler, T. Marques-Bonet, C. Kosiol, M. A. Batzer, M. W. Hahn, J. Tung, D. Zinner, C. Roos, C. J. Jolly, R. A. Gibbs, K. C. Worley; Baboon Genome Analysis Consortium, The comparative genomics and complex population history of *Papio* baboons. *Sci. Adv.* **5**, eaau6947 (2019). [doi:10.1126/sciadv.aau6947](https://doi.org/10.1126/sciadv.aau6947) [Medline](#)
223. S. K. Patterson, A. A. Sandel, J. A. Miller, J. C. Mitani, Data quality and the comparative method: The case of primate group size. *Int. J. Primatol.* **35**, 990–1003 (2014). [doi:10.1007/s10764-014-9777-1](https://doi.org/10.1007/s10764-014-9777-1)
224. D. Zinner, A. Atickem, J. C. Bebehner, A. Bekele, T. J. Bergman, R. Burke, S. Dolotovskaya, P. J. Fashing, S. Gippoliti, S. Knauf, Y. Knauf, A. Mekonnen, A. Moges, N. Nguyen, N. C. Stenseth, C. Roos, Phylogeography, mitochondrial DNA diversity, and demographic history of geladas (*Theropithecus gelada*). *PLOS ONE* **13**, e0202303 (2018).
[doi:10.1371/journal.pone.0202303](https://doi.org/10.1371/journal.pone.0202303) [Medline](#)
225. Y. Yin, T. Yang, H. Liu, Z. Huang, Y. Zhang, Y. Song, W. Wang, X. Guang, S. K. Sahu, K. Kristiansen, The draft genome of mandrill (*Mandrillus sphinx*): An Old World monkey. *Sci. Rep.* **10**, 2431 (2020). [doi:10.1038/s41598-020-59110-3](https://doi.org/10.1038/s41598-020-59110-3) [Medline](#)

226. N. Ting, C. Astaras, G. Hearn, S. Honarvar, J. Corush, A. S. Burrell, N. Phillips, B. J. Morgan, E. L. Gadsby, R. Raaum, C. Roos, Genetic signatures of a demographic collapse in a large-bodied forest dwelling primate (*Mandrillus leucophaeus*). *Ecol. Evol.* **2**, 550–561 (2012). [doi:10.1002/ece3.98](https://doi.org/10.1002/ece3.98) [Medline](#)
227. K. M. Detwiler, Mitochondrial DNA analyses of *Cercopithecus* monkeys reveal a localized hybrid origin for *C. mitis doggetti* in Gombe National Park, Tanzania. *Int. J. Primatol.* **40**, 28–52 (2019). [doi:10.1007/s10764-018-0029-7](https://doi.org/10.1007/s10764-018-0029-7)
228. W. C. Warren, A. J. Jasinska, R. García-Pérez, H. Svardal, C. Tomlinson, M. Rocchi, N. Archidiacono, O. Capozzi, P. Minx, M. J. Montague, K. Kyung, L. W. Hillier, M. Kremitzki, T. Graves, C. Chiang, J. Hughes, N. Tran, Y. Huang, V. Ramensky, O. W. Choi, Y. J. Jung, C. A. Schmitt, N. Juretic, J. Wasserscheid, T. R. Turner, R. W. Wiseman, J. J. Tuscher, J. A. Karl, J. E. Schmitz, R. Zahn, D. H. O'Connor, E. Redmond, A. Nisbett, B. Jacquelin, M. C. Müller-Trutwin, J. M. Brenchley, M. Dione, M. Antonio, G. P. Schroth, J. R. Kaplan, M. J. Jorgensen, G. W. Thomas, M. W. Hahn, B. J. Raney, B. Aken, R. Nag, J. Schmitz, G. Churakov, A. Noll, R. Stanyon, D. Webb, F. Thibaud-Nissen, M. Nordborg, T. Marques-Bonet, K. Dewar, G. M. Weinstock, R. K. Wilson, N. B. Freimer, The genome of the vervet (*Chlorocebus aethiops sabaeus*). *Genome Res.* **25**, 1921–1933 (2015). [doi:10.1101/gr.192922.115](https://doi.org/10.1101/gr.192922.115) [Medline](#)
229. C. Roos, R. Liedigk, V. N. Thinh, T. Nadler, D. Zinner, The hybrid origin of the Indochinese gray langur *Trachypithecus crepusculus*. *Int. J. Primatol.* **40**, 9–27 (2019). [doi:10.1007/s10764-017-0008-4](https://doi.org/10.1007/s10764-017-0008-4)
230. T. Minhós, L. Chikhi, C. Sousa, L. M. Vicente, M. Ferreira da Silva, R. Heller, C. Casanova, M. W. Bruford, Genetic consequences of human forest exploitation in two *Colobus* monkeys in Guinea Bissau. *Biol. Conserv.* **194**, 194–208 (2016). [doi:10.1016/j.biocon.2015.12.019](https://doi.org/10.1016/j.biocon.2015.12.019)
231. J. M. Allen, M. M. Miyamoto, C.-H. Wu, T. E Carter, J. Ungvari-Martin, K. Magrini, C. A. Chapman, Primate DNA suggests long-term stability of an African rainforest. *Ecol. Evol.* **2**, 2829–2842 (2012). [doi:10.1002/ece3.395](https://doi.org/10.1002/ece3.395) [Medline](#)
232. M. K. Konkel, B. Ullmer, E. L. Arceneaux, S. Sanampudi, S. A. Brantley, R. Hubley, A. F. Smit, M. A. Batzer, Discovery of a new repeat family in the *Callithrix jacchus* genome. *Genome Res.* **26**, 649–659 (2016). [doi:10.1101/gr.199075.115](https://doi.org/10.1101/gr.199075.115) [Medline](#)
233. U. Radespiel, H. Lutermann, B. Schmelting, E. Zimmermann, An empirical estimate of the generation time of mouse lemurs. *Am. J. Primatol.* **81**, e23062 (2019). [doi:10.1002/ajp.23062](https://doi.org/10.1002/ajp.23062) [Medline](#)

234. C. L. Frasier, J.-N. Rakotonirina, L. G. Razanajatovo, T. S. Nasolonjanahary, S. B. Rasolonileniraka, J. F. Mamaritiana, E. E. Ramarolahy, Louis Jr., Expanding knowledge on life history traits and infant development in the greater bamboo lemur (*Prolemur simus*): Contributions from Kianjavato, Madagascar. *Primate Conserv.* **2015**, 75–86 (2015). [doi:10.1896/052.029.0110](https://doi.org/10.1896/052.029.0110)
235. M. J. E. Charpentier, C. V. Williams, C. M. Drea, Inbreeding depression in ring-tailed lemurs (*Lemur catta*): Genetic diversity predicts parasitism, immunocompetence, and survivorship. *Conserv. Genet.* **9**, 1605–1615 (2008). [doi:10.1007/s10592-007-9499-4](https://doi.org/10.1007/s10592-007-9499-4)
236. G. H. Perry, D. Reeves, P. Melsted, A. Ratan, W. Miller, K. Michelini, E. E. Louis Jr., J. K. Pritchard, C. E. Mason, Y. Gilad, A genome sequence resource for the aye-aye (*Daubentonia madagascariensis*), a nocturnal lemur from Madagascar. *Genome Biol. Evol.* **4**, 126–135 (2012). [doi:10.1093/gbe/evr132](https://doi.org/10.1093/gbe/evr132) [Medline](#)
237. D. Pan, J.-H. Chen, C. Groves, Y.-X. Wang, E. Narushima, H. Fitch-Snyder, P. Crow, X. Jinggong, V. N. Thanh, O. Ryder, L. Chemnick, H.-W. Zhang, Y.-X. Fu, Y.-P. Zhang, Mitochondrial control region and population genetic patterns of *Nycticebus bengalensis* and *N. pygmaeus*. *Int. J. Primatol.* **28**, 791–799 (2007). [doi:10.1007/s10764-007-9157-1](https://doi.org/10.1007/s10764-007-9157-1)